Toxic Effects and Exposure of Per- and Polyfluoroalkyl Substances in Cell-based Bioassays

Dissertation

der Mathematisch-Naturwissenschaftlichen Fakultät

der Eberhard Karls Universität Tübingen

zur Erlangung des Grades eines

Doktors der Naturwissenschaften

(Dr. rer. nat.)

vorgelegt von

M.Sc. Weiping Qin

aus Guangxi, China

Tübingen

2024

Gedruckt mit Genehmigung der Mathematisch-Naturwissenschaftlichen Fakultät der Eberhard Karls Universität Tübingen.

Tag der mündlichen Qualifikation:	28.05.2024
Dekan:	Prof. Dr. Thilo Stehle
1. Berichterstatterin:	Prof. Dr. Beate I. Escher
2. Berichterstatter:	Prof. Dr. Christian Zwiener

Contents

Abbreviations

Full name	Abbreviations
New approach methodologies	NAMs
High-throughput screening	HTS
Quantitative *in vitro* to *in vivo* extrapolation	QIVIVE
Adverse outcome pathways	AOPs
- molecular initiating events	MIEs
- key events	KEs
- key event relationships	KERs
- adverse outcomes	AOs
Experimental methods	
Solid phase microextraction	SPME
Polydimethylsiloxane	PDMS
Divinylbenzene	DVB
Carboxen	CAR
Liquid chromatography coupled with mass spectrometer	LCMS
Gas chromatography coupled with mass spectrometry	GCMS
Bioassays	
Concentration-response curves	CRC
Free concentration	C_{free}
Nominal (i.e. dosed) concentration	C_{nom}
Nominal inhibitory concentrations of the chemicals that caused 10% cytotoxicity	$IC_{10,nom}$
Nominal effect concentrations of the chemicals that caused 10% cellular response of defined targets	$EC_{10,nom}$
Peroxisome proliferator-activated receptor	PPAR
Aryl hydrocarbon receptor	AhR
Oxidative stress response	ARE
Estrogen receptor	ER
Baseline toxicity	
Membrane concentration of baseline toxicants that caused 10% cytotoxicity	$IC_{10,membrane,baseline}$
Free concentrations of baseline toxicants that caused 10% cytotoxicity	$IC_{10,free,baseline}$
Nominal concentrations of baseline toxicants that caused 10% cytotoxicity	$IC_{10,nom,baseline}$
Toxic ratio	TR
Specificity ratio	SR
Mass balance model	

Distribution between lipid and water	$D_{lipid/w}$
Distribution between liposome and water	$D_{lip/w}$
Distribution between olive oil and water	$D_{oil/w}$
Distribution between protein and water	$D_{protein/w}$
Distribution between bovine serum albumin and water	$D_{BSA/w}$
Distribution between structure protein and water	$D_{SP/w}$
Distribution between plasma and water	$D_{plasma/w}$
Distribution between medium and water	$D_{medium/w}$
Distribution between cell and water	$D_{cell/w}$

Summary

Per- and polyfluoroalkyl substance (PFAS) are man-made chemicals that are widely used in commercial, industrial and military products. PFAS are ubiquitously found in environmental media and organisms including human beings due to their persistence and bioaccumulation potential. Many studies have shown the correlation of PFAS exposure and diseases. There are more than 14,000 PFAS chemicals in the CompTox Chemicals Dashboard but only fraction of them have toxicological information. Cell-based high-throughput screening (HTS) bioassays may inform risk assessment of large numbers of PFAS provided that quantitative *in vitro* to *in vivo* extrapolation (QIVIVE) can be developed. Challenges of QIVIVE lie in the predictive accuracy of the bioavailability of PFAS, species difference, as well as the specificity of cellular responses that may lead to potential adverse outcomes.

This thesis aimed to evaluate the toxic effects and exposure of PFAS in cell-based bioassays to facilitate the use of *in vitro* bioassay data for risk assessment. **The first objective** was to measure *in vitro* exposure and determine the binding constants to plasma proteins of different species. The bioavailability of PFAS can be presented as the free concentrations (C_{free}) in bioassays and plasma. PFAS bound to proteins and lipids usually result in lower C_{free} compared to their nominal (i.e. dosed) concentrations (C_{nom}). Solid-phase microextraction (SPME) combined with liquid chromatography mass spectrometry (LCMS) was used to measure the C_{free} of PFAS among biomaterials, including bioassay media, cell homogenates and blood plasmas. The binding constants were derived from different binding models. Binding isotherms of 16 PFAS with human and trout (fish) plasmas were compared. Anionic PFAS showed higher binding affinities to human plasma in the low concentration ranges compared to the trout plasma, because there were more proteins in human plasma, which led to very strong and specific binding of PFAS with proteins. Partitioning of PFAS to plasma was also predicted correctly by mass balance models (MBMs) that were parameterized with the protein-water and lipid-water binding constants (chemical characteristics) as well as the protein and lipid contents of the plasma (species characteristics). **The second objective** was to inform risk assessment with a simple form of QIVIVE, which is the ratio of *in vivo* human plasma concentrations (C_{plasma}) and *in vitro* cell-based effect concentrations (EC), either based on

nominal or free concentrations. The C_{free} can be measured experimentally or predicted by validated MBMs. $C_{nom,plasma}$ of PFAS were collected from literature and $C_{free,plasma}$ were predicted by the MBMs parameterized with plasma binding constants. A cell-based reporter gene assays targeting peroxisome proliferator-activated receptor gamma (PPARγ) was selected to measure the effect concentrations EC_{nom} or EC_{free} of PFAS, because PPARs have been shown to be specific targets of PFAS. $QIVIVE_{free}$ ratios, which are the ratios between freely dissolved concentration of PFAS in blood and their EC_{free}, of some hydrophobic PFAS were up to 1000 times lower than their corresponding $QIVIVE_{nom}$ ratios. This was caused by a strong affinity to proteins and human plasma contained 50 times more proteins than in the bioassay medium, leading highly specific binding at low PFAS concentrations in human plasma, contrasted by nonspecific partitioning to proteins at high concentrations that were required to trigger an effect in bioassays. The proteins and lipids in plasma may act as reservoirs of PFAS in human bodies that pose a risk of chronic exposure. The case study using PPARγ is a demonstration of the importance of using C_{free} for the QIVIVE ratios, but for a comprehensive risk assessment, a large set of specific responsive *in vitro* cell-based bioassays needs to be applied. **The third objective** was to identify the specific from nonspecific effects among different cell-based HTS bioassays, where baseline toxicity can be a reference. Baseline toxicity is the minimal toxicity that is caused by nonspecific accumulation of chemicals in the cellular membranes. Exceedance of the critical membrane burden leads to cell death. Separate baseline toxicity prediction models were developed for anionic PFAS and neutral chemicals, which were used to define the specificity of cell response of 30 PFAS on six target effects (activation of PPARγ, aryl hydrocarbon receptor, oxidative stress response, and neurotoxicity in own experiments, and literature data for activation of several PPARs and the estrogen receptor). HFPO-DA showed high specificity for PPARs, while the majority of PFAS acted as baseline toxicants. This implicates a heightened need for the risk assessment of PFAS mixtures, because nonspecific effects, i.e., baseline toxicity, behave concentration-additive in mixtures.

In brief, QIVIVE is suggested to consider the bioavailability using C_{free}. It will not always be necessary to measure C_{free} of PFAS but existing data of plasma concentration and bioassay effect based on C_{nom} can be converted to C_{free} by using MBMs. The differences of plasma binding can be predicted by amounts of proteins and lipids in

plasmas, which is influenced by many factors not only between species but also between individuals, and also depends on the concentration range because specific binding at low concentrations is very strong while nonspecific binding at higher concentration has lower binding constants. The baseline toxicity prediction model may be able to re-evaluate the specificity of existing bioassay results, as well as provide a testing strategy in future studies. The identification of high specificity of targets may advance the development of adverse outcome pathways related to single PFAS, which may also be applied for PFAS mixtures. The combined assessment *in vitro* cellular responses of PFAS and organism exposure levels (e.g. human and fish plasma) can facilitate the comprehensive human and environmental risk assessment of PFAS in the near future.

Zusammenfassung

Per- und Polyfluoralkylsubstanzen (PFAS) sind nicht natürlich vorkommende Chemikalien, die häufig in kommerziellen, industriellen und militärischen Produkten verwendet werden. PFAS sind aufgrund ihrer Persistenz und Bioakkumulation allgegenwärtig in der Umwelt und in Organismen, einschließlich des Menschen. Viele Studien haben in den vergangenen Jahrzehnten den Zusammenhang zwischen PFAS-Exposition und Krankheiten gezeigt. Es gibt mehr als 14.000 PFAS-Chemikalien in der CompTox Datenbank der US-Umweltbehörde, von denen aber nur wenige über toxikologische Informationen verfügen. Zellbasierter Hochdurchsatz-Screening (HTS) Biotests kann zur Risikobewertung einer großen Anzahl von PFAS beitragen, sofern eine quantitative *In-vitro* zu *In-vivo* Extrapolation (QIVIVE) entwickelt werden kann. Die Herausforderungen bei der QIVIVE liegen in der Vorhersagegenauigkeit der Bioverfügbarkeit von PFAS, den Unterschieden zwischen verschiedenen Spezies sowie der Spezifität zellulärer Antworten, welche möglicherweise auf unerwünschte Effekte hinweisen.

Ziel dieser Arbeit war es, die toxischen Effekte und die Exposition von PFAS in zellbasierten Biotests zu bewerten, damit diese für die Risikobewertung eingesetzt werden können. **Das erste Ziel bestand darin**, die *In-vitro*-Exposition zu messen und die Bindungskonstanten von Plasmaproteinen zwischen den Arten zu bestimmen. Die Bioverfügbarkeit von PFAS kann als freie Konzentration (C_{free}) in Biotests und Blutplasma dargestellt werden. Die Bindung von PFAS an Proteine und Lipide führt häufig dazu, dass C_{free} deutlich unterhalb der nominalen (d. h. dosierten) Konzentrationen (C_{nom}) liegt. Festphasenmikroextraktion (SPME) kombiniert mit Flüssigchromatographie-Massenspektrometrie (LCMS) wurde verwendet, um C_{free} von PFAS in Biomaterialien, einschließlich Biotestmedien, Zellhomogenaten und Blutplasma zu messen. Außerdem wurden die Verteilungs- und Bindungskonstanten mit verschiedenen Modellen abgeleitet. Bindungsisothermen von 16 PFAS im Plasma von Menschen und Forellen (Fischen) verglichen. Anionische PFAS zeigten in den niedrigen Konzentrationsbereichen höhere Bindungsaffinität für menschliches Plasma im Vergleich zum Forellenplasma, da im menschlichen Plasma mehr Proteine vorhanden waren, was zu einer sehr starken und spezifischen Bindung von PFAS führte. Die Verteilung von PFAS in Plasma konnte auch

mit einem Massenbilanzmodelle (MBM) vorhergesagt werden, welches mit den Protein-Wasser- und Lipid-Wasser-Bindungskonstanten (chemische Eigenschaften) sowie den Protein- und Lipidgehalten des Plasmas (Arteigenschaften) parametrisiert wurde. **Das zweite Ziel bestand darin**, eine fundierte Risikobewertung mit einer vereinfachten Form von QIVIVE verwendet, welche das Verhältnis von menschlichen *In-vivo*-Plasmakonzentrationen (C_{Plasma}) und zellbasierten *In-vitro*-Effektkonzentrationen (EC) nutzt, entweder basierend auf C_{nom} oder C_{free}. Die C_{free} kann experimentell gemessen oder durch validierte MBMs vorhergesagt werden. Literaturwerte für $C_{nom,Plasma}$ der PFAS wurden gesammelt und $C_{free,Plasma}$ wurde mit Hilfe des mit Plasmabindungskonstanten parametrisierten MBM berechnet. Zur Ermittlung der Effektkonzentrationen EC der PFAS wurde ein zellbasierter Reportergentest ausgewählt, der die Aktivierung oder Hemmung des Peroxisom-Proliferator-aktivierten Rezeptors Gamma (PPARγ) anzeigt, da sich PPARs als spezifische Angriffspunkte für PFAS erwiesen haben. $QIVIVE_{free}$-Verhältnisse sind die Verhältnisse zwischen der frei gelösten PFAS-Konzentration im Blut und ihrem EC_{free}. Die $QIVIVE_{free}$-Verhältnisse einiger hydrophober PFAS waren bis zu 1000-mal niedriger als ihren $QIVIVE_{nom}$-Verhältnissen. Die Unterschiede wurden erklärt durch eine starke Affinität der PFAS für Proteine im menschlichem Blut, da Blut 50 mal mehr Protein enthielt als das Biotestmedium, was zu einer hochspezifischen Bindung bei niedrigen PFAS-Konzentrationen im menschlichen Plasma führte, im Gegensatz zu einer unspezifischen Verteilung an Proteine bei hohen Konzentrationen, die zur Auslösung erforderlich waren ein Effekt in Biotests. Die Proteine und Lipide im Plasma können im menschlichen Körper als PFAS-Reservoir fungieren, was zu einer chronischen Exposition führen kann. Dies ist ein Beleg dafür, dass C_{free} für die QIVIVE verwendet werden sollte. Für eine umfassende Risikobewertung müsste jedoch eine große Anzahl zellbasierter *in-vitro* Biotests mit verschiedenen toxikologischen Endpunkten angewendet werden. **Das dritte Ziel bestand darin**, die spezifischen von unspezifischen Wirkungen von PFAS in verschiedenen zellbasierten HTS-Biotests zu identifizieren, wobei die Basislinientoxizität (kurz Basistoxizität) als Referenz dienen sollte. Als Basistoxizität bezeichnet man die minimale Toxizität, die durch unspezifische Anreicherung von Chemikalien in den zellulären Membranen verursacht wird. Wird die kritische Membrankonzentration überschritten, führt dies zum Zelltod. Für anionische PFAS und neutrale Chemikalien wurden separate Modelle zur Vorhersage der Basistoxizität entwickelt, die anschließend

zur Berechnung des Spezifitätsgrades der Effekte von 30 PFAS auf sechs Zieleffekte (Aktivierung von PPARγ, Aryl-Kohlenwasserstoff-Rezeptor, Reaktion auf oxidativen Stress und Neurotoxizität in eigenen Experimenten, sowie Literaturdaten zur Aktivierung mehrerer PPARs und des Östrogenrezeptors) genutzt wurden. HFPO-DA zeigte eine hohe Spezifität für PPARs, während die meisten PFAS nur unspezifische Effekte, d.h. Basistoxizität, zeigten. Dies impliziert, dass für die Risikobewertung Mischungen von PFAS besonders wichtig sind, da sich unspezifische Effekte in Mischungen konzentrationsadditiv verhalten.

Zusammenfassend wird für die QIVIVE von PFAS empfohlen, die Bioverfügbarkeit, also C_{free}, zu berücksichtigen. Es ist dabei nicht immer notwendig, C_{free} der PFAS zu messen, denn bereits gemessene Plasmakonzentrationen und Effektkonzentrationen aus zellbasierten Biotests, basierend auf C_{nom}, können mithilfe von MBMs in C_{free} umgerechnet werden. Die Unterschiede der Plasmabindung können ebenfalls vorhergesagt werden, wenn Protein- und Lipidgehalt des Plasmas und Konzentrationsbereiche der PFAS bekannt sind. Der Gehalt an Proteinen und Lipiden im Plasma unterscheidet sich nicht nur zwischen Arten, sondern auf Grund verschiedener Faktoren auch zwischen Individuen. Die spezifische Bindung ist bei niedrigen Konzentrationen sehr stark, während die unspezifische Bindung bei höheren Konzentrationen niedrigere Bindungskonstanten aufweist. Das Modell zur Vorhersage der Basistoxizität kann möglicherweise die Spezifität der Effekte von bestehender Biotestergebnisse neu bewerten und Bereitstellung einer Teststrategie für weitere Studien. Die Identifizierung einer hohen Spezifität von zellulären Reaktionen kann die Entwicklung von AOPs („adverse outcome pathways“) im Zusammenhang mit einzelnen PFAS vorantreiben, die auch auf PFAS-Mischungen angewendet werden können. Die kombinierte Betrachtung von zellulären Reaktionen, die durch PFAS hervorgerufen werden und Expositionskonzentrationen von Organismen (z. B. in humanem und Fischplasma) kann in naher Zukunft die umfassende Risikobewertung von PFAS in Bezug auf die menschliche Gesundheit und die Umwelt voranbringen.

Acknowledgements

Pursuing a PhD in Germany is one of the most pivotal decisions in my life! I still clearly remember the trepidation by unfamiliar surroundings when I stood alone with three suitcases in a chilly and rainy morning three years ago, but tonight I am already writing the last part of my dissertation adeptly. Throughout the past years, I have not only acquired academic knowledge to continuously explore my research interests and career paths, but also nurtured resilience through various challenges. I would appreciate everyone who make my life of studying abroad so precious and memorable.

I would like to express my deepest gratitude to my supervisor Beate Escher. Thank you for your patience in giving me guidance, your generous praise when I progressed and your prompt critique when I erred. Over 90 times of one-on-one mentoring sessions, you consistently provide me with great inspirations and supports, enabling me to advance the project with the highest efficiency. I had never imagined I would receive such meticulous guidance from a super busy professor. Your dedication to scientific rigor, intense focus at work and enthusiasm for life have been influencing on me during the period we spend together, motivating me to approach future endeavors with optimism and eagerness.

I would like to say a big thank to Luise Henneberger for your invaluable assistance in discussing experiments, analyzing data and providing suggestions when I was frustrated with failures. I would also like to thank Julia Huchthausen for guiding me through independent experiments in the lab during the initial stages and always providing timely helps with both work and personal matters. My sincere thanks to all CELLTOX members, especially Maria König, Jungeun Lee, Niklas Wojtysiak and Georg Braun for your instrumental supports in experimental designs and executions, as well as Vanessa Srebny, Jenny Braasch, Christin Kühnert, Anke Petermann. It is the excellent teamwork that facilitates the smooth completion of my dissertation.

I would like to extend special thanks to all members in Office 105 who have created such a harmonious atmosphere that surpasses the boundary of typical workplace. We celebrate each person's birthday with homemade cakes, do routine sports after work and hold gatherings in holidays. The moments that we share about experiences and emotions make us not just colleagues but also very close friends. All of you make my life in Germany

vibrant and heartwarming. Thank you, Anna Goellner, Inga Haalck, Isaac Tanui, Kathrin Sigl, Elena Hommel, Alain Hoyek, Allan dos Santos Argolo.

I would like to give heartfelt thanks to my family. Thanks to my parents for regularly sending packages from our hometown with mystery gifts and hidden delights. Thanks to my brother who takes the responsibility to take care of our parents but encourages me to explore new world. Thanks to my beloved Kun Ma who has accompanied me through my entire twenties, offering unwavering supports for all my decisions. I never feel lonely as our daily calls over the past three years have become our cherished habit. Thanks to my family for caring about me all the time and willing to grant me the freedom for my goals.

1. Introduction

1.1 PFAS in environment and their health risks

PFAS are manufactured chemicals that are widely used in commercial, industrial and military products because of their unique properties of waterproofing, grease- and heat-resistance (Gluge et al. 2020) . The Organization for Economic Co-operation and Development (OECD) broadened the definition of PFAS to at least one perfluorinated carbon (Wang et al. 2021), implying more than 14,000 PFAS in the Comptox Chemicals Dashboard (Richard et al. 2023).

PFAS are highly persistent and have been termed “forever chemicals”. PFAS are found in many environmental media, such as glaciers, water, soils and air-dust particles (Evich et al. 2022), and their polluted concentrations are generally at nanomolar levels. The bioaccumulation of PFAS in aquatic, terrestrial and aerial organisms is more alarming (Ankley et al. 2021; Fenton et al. 2021). PFAS were detected at nanomolar levels in general populations according to national surveys (Cakmak et al. 2022; Gockener et al. 2020; Petriello et al. 2022; Yu et al. 2020), while PFAS were higher up to micromolar levels in workers and residents living near fluorochemical plants (Bao et al. 2022; Gao et al. 2015; Peng et al. 2021; Rotander et al. 2015).

Epidemiological investigations suggested associations between exposure to PFAS and human diseases caused by endocrine disruption (Mokra 2021), neurotoxicity (Mariussen 2012), immunotoxicity (DeWitt et al. 2009), reproductive (Calvert et al. 2021) and developmental toxicity (Rappazzo et al. 2017). Toxicological studies also revealed some toxic mechanisms. PFAS show high affinities to proteins and the interactions of PFAS with functional proteins dominate their molecular initiating events (MIEs) and key events (KEs) in the adverse outcome pathways (AOPs), including activations of receptor-mediated signaling pathways (Behr et al. 2020), interference of activities and functions of enzymes (Liu et al. 2020; Wang et al. 2014), and competitive binding with transport-proteins (Ren et al. 2016). The potential health impacts of PFAS have been a great concern to society.

1.2 New approach methodologies for risk assessments

Traditional toxicological methods using animals in the experiments are time-consuming and ethically problematic, which is inadequate to generate biological safety information for thousands of commercial PFAS. New approach methodologies (NAMs) refer to innovative methods to replace the use of animals, improve the efficiency of testing, and provide more accurate and human-relevant data, including *in vitro* testing, organ-on-a-chip testing, high-throughput screening, as well as computer-based mimicking, modeling and predicting.

1.2.1 Cell-based high-throughput screening (HTS)

Cell-based high-throughput screening (HTS) provides early warning of bioactivations and also enables rapid detection of a large number of samples with robots automatically. Tox21 and ToxCast, proposed by the U.S. Environmental Protection Agency (EPA) and the National Toxicology Program (Patlewicz et al. 2019), are conducting large-scale testing of PFAS in cell-based HTS. Currently, 430 PFAS (https://comptox.epa.gov/dashboard/chemical-lists/EPAPFASINV) have been selected for a serial bioassay test involving hundreds of endpoints (Carstens et al. 2023; Franzosa et al. 2021; Houck et al. 2023; Houck et al. 2021; Stoker et al. 2023; Villeneuve et al. 2023), such as transcription factors related receptor-mediated signaling pathways, biomarkers related to immune system, sodium iodide symporter for thyroid function, neurite outgrowth for neurotoxicity, cell proliferator, apoptosis and others.

1.2.2 Quantitative *in vitro* to *in vivo* extrapolation (QIVIVE)

Cell-based HTS has the potential to inform risk assessments of PFAS, provided that the *in vitro* experimental data obtained from cell-based bioassays can predict the *in vivo* responses in living organisms, namely quantitative *in vitro* to *in vivo* extrapolation (QIVIVE). QIVIVE is a computer-based model to translate the concentration-response curves (CRC) from cell-based bioassays into equivalent *in vivo* concentrations in plasma considering a physiological process of absorption, distribution, metabolism and excretion of chemicals (Loizou et al. 2021; Worley et al. 2015). However, the challenges of QIVIVE lie in the predictive accuracy of the bioavailability of PFAS in cell-based bioassays and plasmas, as well as variations between different species for human and ecological risk.

PFAS may bind to components in bioassay medium and plasma, such as lipids and proteins, resulting in the free concentration (C_{free}) is usually lower than the nominal (i.e. dosed) concentration (C_{nom}) (Henneberger et al. 2019). As the C_{free} is more relevant to the bioavailability, the development of CRC with C_{free} is crucial for QIVIVE (Henneberger et al. 2021). The prediction of C_{free} in plasma also needs to consider the species differences if the extrapolation is applicable for different organisms.

The C_{free} can be measured experimentally with solid phase microextraction (SPME) using fiber coated with C18 particles or polydimethylsiloxane (PDMS) that have been used for charged and neutral pharmaceuticals in previous studies (Henneberger et al. 2019; 2020). The fluorinated-carbon chain of PFAS can interact with the hydrocarbon chain of C18 particles via van der Waals interactions, which provides an opportunity to measure the C_{free} of PFAS from complex biomaterials with C18-coated fiber combined with liquid chromatography mass spectrometry (LCMS). It may be able to inform risk assessment with QIVIVE using the C_{free} of PFAS in both human plasma and bioassays.

1.2.3 Adverse outcome pathways (AOPs)

Cell-based HTS can provide large-scale data on how PFAS interact with cellular targets (Carstens et al. 2023; Houck et al. 2023; Houck et al. 2021; Stoker et al. 2023), which can be used to identify MIEs and KEs in AOPs. The information about the specificity degree of PFAS on selected targets and the biomedical connections among targets will facilitate the understanding of AOPs related to PFAS. Once PFAS-relevant AOPs are established, the verifications of MIEs and KEs at the cellular level can help to figure out possible pathways leading to adverse outcomes (AOs) for risk assessment. The challenge of integrating cell-based HTS data with AOP lies in the definition of the specificity degree of cellular responses. MIEs and KEs with higher specificity are more likely to occur at low exposure concentrations of PFAS.

It is difficult to identify the specific from the nonspecific effects in large dataset of cellular response because there may be inconsistent results caused by artifacts. Cellular responses of PFAS on selected targets may be inferred by cytotoxicity burst when cells are close to death (Judson et al. 2016). Cytotoxicity (cell death) can hence be a reference for the definition of specificity (Escher et al. 2020). The loss of cell membrane integrity is a critical event in the process of cell death. A common mechanism of nonspecific

accumulation of chemicals on the cell membrane may disrupt the membrane function and even destroy the membrane integrity, so-called baseline toxicity, the minimum (cy)toxicity (Escher et al. 2002). Baseline toxicity can serve as an anchor to distinguish the specific from the nonspecific effects of chemicals in cell-based bioassays.

1.3 Baseline toxicity in cell-based bioassays

Baseline toxicity, also known as narcosis, is a nonspecific effect when chemicals accumulate in the cell membrane exceeding the critical membrane burdens. Escher et al. (2019) derived the critical membrane concentration of baseline toxicants that caused 10% cytotoxicity ($IC_{10,membrane,baseline}$) as a mean value of 69 mmol/L_{lip} from eight cell lines. The cell membrane is primarily composed of the phospholipid bilayer. $IC_{10,membrane,baseline}$ is related to the arrangement and stability of phospholipid molecules, and hence independent of cell lines and constant for all organic chemicals. That means the concept of baseline toxicity can serve as a universal anchor to assess the minimum (cy)toxicity of individual chemicals or mixtures in different cell-based bioassays.

As most CRCs in cell-based HTS bioassay are established with C_{nom} of chemicals in the bioassay medium, one needs to link the membrane concentrations ($IC_{10,membrane,baseline}$) and free concentrations ($IC_{10,free,baseline}$) to nominal concentrations ($IC_{10,nom,baseline}$) by a mass balance model (MBM), so that we can apply this anchor for cell-based HTS data. While $IC_{10,membrane,baseline}$ is constant, $IC_{10,free,baseline}$ is dependent on the binding affinity of chemicals to membrane lipid layer, and $IC_{10,nom,baseline}$ is determined by the experimental conditions and binding affinities of chemicals to proteins and lipids in the medium and cells. A relationship of different metrics related to baseline toxicity can be found in Figure 1.

Cellular baseline toxicity is predictable if the chemicals bound to proteins and lipids of bioassay medium and cells are quantified. Since the lipid partitioning of chemicals to cellular membrane is the major cause of baseline toxicity, the lipid binding constant ($D_{lip/w}$) of individual chemicals is an important parameter to present the potent of baseline toxicity. A linear relationship between protein binding constants ($D_{protein/w}$) and $D_{lip/w}$ can be derived and used to predict the baseline toxicity of individual chemicals, resulting $D_{lip/w}$ as the only input parameters for the baseline toxicity prediction model. Escher et al. (2020) and Lee

et al.(2021) developed such models to predict $IC_{10,nom,baseline}$ dependent on the $D_{lip/w}$, which serve well for neutral and cationic species but have some limitations for anionic species. This may be caused by a strong protein binding of anionic chemicals. There are numerous neutral and anionic PFAS due to the wide range of chemical structures and functional groups. Short- and middle-chain length of carboxylic and sulfonic acids are common degradation products of PFAS, which present as anionic species at physiological conditions (pH=7.4). Hence, the linear relationship of protein and lipid bindings needs to be updated for anionic chemicals, leading to separate models for neutral and anionic PFAS.

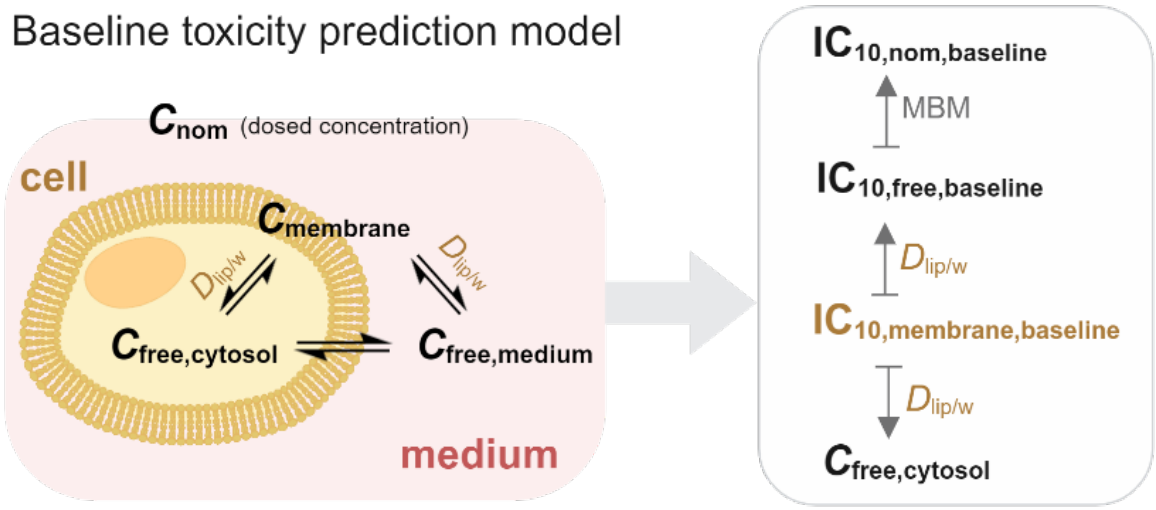

Figure 1. Concept of baseline toxicity applied in the cell-based bioassays. C_{nom}=nominal concentration, C_{free}=free concentration, $D_{lip/w}$=binding constants between liposome and water, MBM=mass balance model, IC=inhibitory concentration.

1.4 Aims and approaches of this thesis

This thesis aims to evaluate the toxic effects and exposures of PFAS in cell-based bioassays for risk assessment. This includes three subprojects that are numbered according to the publication time. In *Publication 1*, four anionic PFAS were selected as case study to demonstrate the importance and impact of using C_{free} from both *in vivo*

human plasma and *in vitro* cell-based bioassays on QIVIVE for risk assessment. In *Publication 2*, the baseline toxicity prediction models were developed separately for neutral and anionic PFAS, which were further used to define the specificity degree of 24 PFAS on selected targets in our cell-based HTS, as well as the specificity degree of 16 PFAS with literature data. In *Publication 3*, plasma bindings of 16 PFAS between human and trout (fish) were compared to investigate species differences, which were explained by the MBMs that are parameterized with the affinities and distributions of PFAS to plasma proteins and lipids.

The information about the experimental methods, models, results and implications from three papers is integrated and restructured to present the whole story in this thesis. Brief introductions of three papers and a framework of this thesis is shown as Figure 2. 24 PFAS were used for experiments and detailed information can be found in Table 1. There are 6 extra PFAS that were taken from literature only for data re-evaluations. Structure information of 30 PFAS are in Table 2.

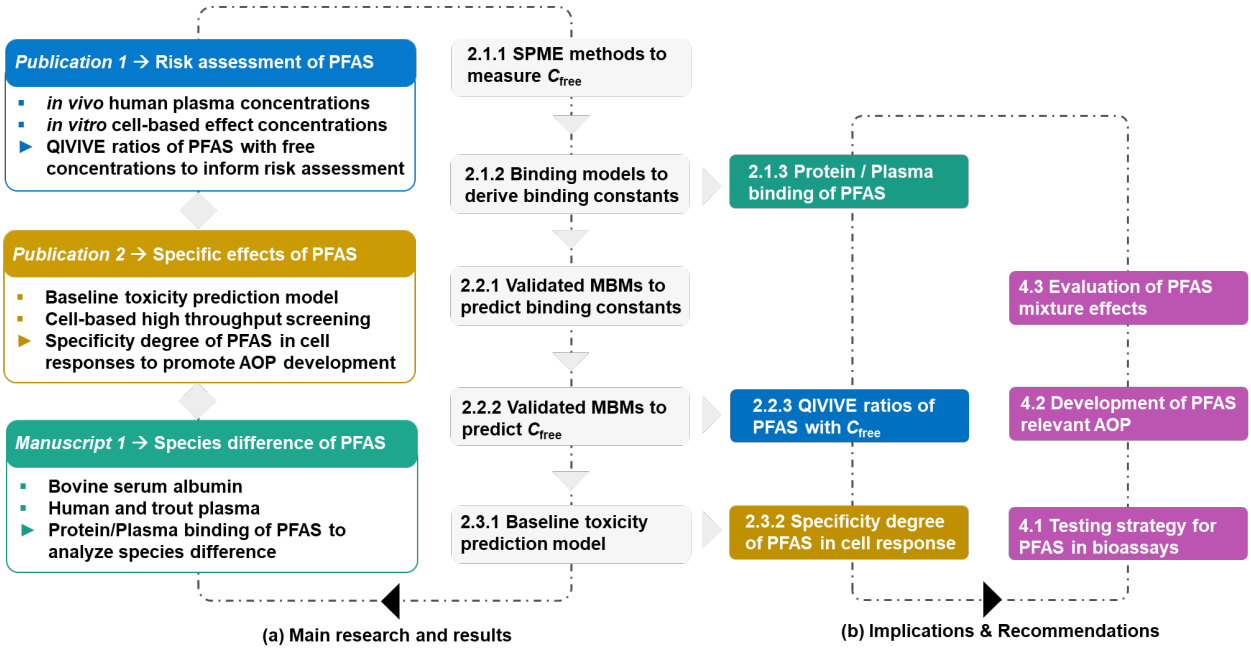

Figure 2. Framework of the thesis. (a) Main research and results from three papers are restructured (chapter 2). (b) Implications of findings (chapter 3) and recommendations for future studies (chapter 4).

Different SPME methods were developed for PFAS according to their physicochemical properties (2.1.1). These methods are further used to study the binding of PFAS with different biomaterials. The binding constants of PFAS with these biomaterials were derived from different binding models based on their binding behaviors (2.1.2). The binding isotherms from human plasma and trout (fish) plasma are compared to analyze the species difference (2.1.3).

The binding constants of PFAS between plasma and water ($D_{plasma/w}$), medium and water ($D_{medium/w}$), and cell and water ($D_{cell/w}$) can be derived experimentally and predicted by the MBMs, assuming that proteins and lipids are major sorption phases (2.2.1). These binding constants were used to predict the C_{free} in human plasma and in bioassays. A comparison of experimental and predicted C_{free} can help to validate the accuracy of MBMs (2.2.2). A ratio of either free or nominal concentrations in human plasma and in bioassays are defined as QIVIVE ratio for risk assessments (2.2.3).

Baseline toxicity prediction models are derived from the validated MBMs that linked the $IC_{10,membrane,baseline}$ of 69 mmol/L_{lip} to $IC_{10,nom,baseline}$ of PFAS in different cell-based bioassays, considering both experimental conditions and affinities of PFAS to protein and lipids in the assay medium and cells (2.3.1). Baseline toxicity prediction models were used to evaluate the specificity of 24 PFAS in four cell-based HTS, including three reporter gene assays and one imaging-based neurotoxicity assay. We also demonstrated the applicability of these models to other cell-based bioassays from literature (2.3.2).

All key findings are demonstrated for an overview of this thesis (3.1). Implications of results from three papers are discussed in details, including species difference of plasma binding (3.2), risk assessment with QIVIVE ratio (3.3) and the application of baseline toxicity prediction models (3.4). Based on these existing researches, some recommendations are proposed for future studies of PFAS, including a test strategy of PFAS in cell-based HTS (4.1), development of PFAS-relevant AOP (4.2) and evaluation of PFAS mixture effects (4.3).

Table 1. Information of PFAS and their application for different experimental purposes in this thesis and literature.

	CASRN	Full name	Abbreviation	QIVIVE ratio (4)	SPME method (16)	Baseline toxicity prediction (11)	Cell-based HTS (24)	Literature (16)
1	422-64-0	Perfluoropropanoic acid	PFPrA				Yes	
2	375-22-4	Perfluorobutanoic acid	PFBA	Yes	Yes	Yes	Yes	
3	2706-90-3	Perfluoropentanoic acid	PFPeA				Yes	
4	307-24-4	Perfluorohexanoic acid	PFHxA		Yes	Yes	Yes	Yes
5	375-85-9	Perfluoroheptanoic acid	PFHpA		Yes	Yes	Yes	
6	335-67-1	Perfluorooctanoic acid	PFOA	Yes	Yes	Yes	Yes	Yes
7	375-95-1	Perfluorononanoic acid	PFNA		Yes	Yes	Yes	Yes
8	2058-94-8	Perfluoroundecanoic acid	PFUnA		Yes	Yes	Yes	
9	307-55-1	Perfluorododecanoic acid	PFDoDA				Yes	
10	678-45-5	Perfluorooctanedioic acid	PFOdA				Yes	
11	13252-13-6	Perfluoro-2-methyl-3-oxahexanoic acid	HFPO-DA		Yes	Yes	Yes	Yes
12	1493-13-6	Trifluoromethanesulfonic acid	TfOH				Yes	
13	3871-99-6	Potassium perfluorohexanesulfonate	PFHxS	Yes	Yes	Yes	Yes	Yes
14	2795-39-3	Potassium perfluorooctanesulfonate	PFOS	Yes	Yes	Yes	Yes	Yes
15	27619-97-2	6:2 Fluorotelomer sulfonic acid	6:2 FTSA		Yes	Yes	Yes	
16	754-91-6	Perfluorooctanesulfonamide	PFOSA		Yes	Yes	Yes	Yes
17	4151-50-2	N-Ethylperfluorooctanesulfonamide	nEt-PFOSA				Yes	Yes
18	1691-99-2	N-Ethyl-N-(2-hydroxyethyl) perfluorooctane sulfonamide	nEt-PFOSE				Yes	
19	647-42-7	2-(Perfluorohexyl)ethanol	6:2 FTOH		Yes		Yes	Yes
20	678-39-7	2-(Perfluorooctyl)ethanol	8:2 FTOH		Yes		Yes	Yes
21	865-86-1	2-(Perfluorodecyl)ethanol	10:2 FTOH		Yes		Yes	
22	86479-06-3	Hexaflumuron	Hexaflumuron		Yes		Yes	
23	103055-07-8	Lufenuron	Lufenuron				Yes	
24	272451-65-7	Flubendiamide	Flubendiamide		Yes		Yes	
25	335-76-2	Perfluorodecanoic acid	PFDA					Yes
26	21837-98-9	2,2-Difluoro-2-(trifluoromethoxy)acetate sodium salt	PFMOAA					Yes
27	62037-80-3	Ammonium perfluoro-2-methyl-3-oxahexanoate	HFPO-DA-AS					Yes
28	375-73-5	Perfluorobutanesulfonic acid	PFBS					Yes
29	749836-20-2	5-(1,2,2,2-Tetrafluoro)ethoxy-perfluoro-3-oxa-4-methylpentanesulfonic acid	NBP2					Yes
30	2043-47-2	4:2 Fluorotelomer alcohol	4:2 FTOH					Yes

Table 2. Structure information of PFAS

	Abbreviation	Molecular formula	Structure		Abbreviation	Molecular formula	Structure
1	PFPrA	$C_3HF_5O_2$	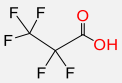	**16**	PFOSA	$C_8H_2F_{17}NO_2S$	
2	PFBA	$C_4HF_7O_2$	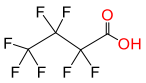	**17**	nEt-PFOSA	$C_{10}H_6F_{17}NO_2S$	
3	PFPeA	$C_5HF_9O_2$		**18**	nEt-PFOSE	$C_{12}H_{10}F_{17}NO_3S$	
4	PFHxA	$C_6HF_{11}O_2$	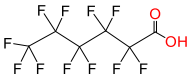	**19**	6:2 FTOH	$C_8H_5F_{13}O$	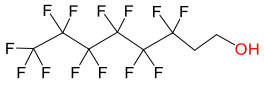
5	PFHpA	$C_7HF_{13}O_2$		**20**	8:2 FTOH	$C_{10}H_5F_{17}O$	
6	PFOA	$C_8HF_{15}O_2$	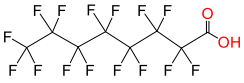	**21**	10:2 FTOH	$C_{12}H_5F_{21}O$	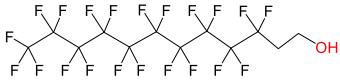
7	PFNA	$C_9HF_{17}O_2$		**22**	Hexaflumuron	$C_{16}H_8Cl_2F_6N_2O_3$	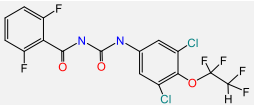
8	PFUnA	$C_{11}HF_{21}O_2$	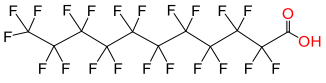	**23**	Lufenuron	$C_{17}H_8Cl_2F_8N_2O_3$	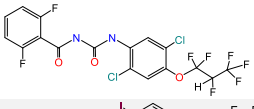
9	PFDoDA	$C_{12}HF_{23}O_2$	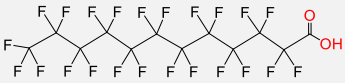	**24**	Flubendiamide	$C_{23}H_{22}F_7IN_2O_4S$	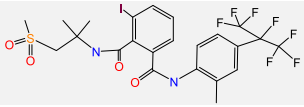
10	PFOdA	$C_8H_2F_{12}O_4$	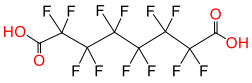	**25**	PFDA	$C_{10}HF_{19}O_2$	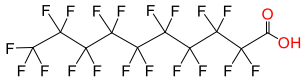
11	HFPO-DA	$C_6HF_{11}O_3$	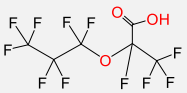	**26**	PFMOAA	$C_3F_5NaO_3$	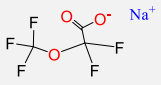
12	TfOH	CHF_3O_3S		**27**	HFPO-DA-AS	$C_6H_4F_{11}NO_3$	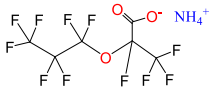
13	PFHxS	$C_6F_{13}KO_3S$	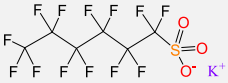	**28**	PFBS	$C_4HF_9O_3S$	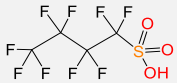
14	PFOS	$C_8F_{17}KO_3S$	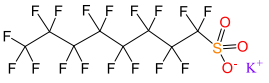	**29**	NBP2	$C_7H_2F_{14}O_5S$	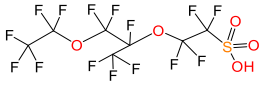
15	6:2 FTSA	$C_8H_5F_{13}O_3S$		**30**	4:2 FTOH	$C_6H_5F_9O$	

2. Main research and results

In this chapter, an overview of doctoral study is presented as the storyline depicted in Figure 2 (a) with main results from three papers. Detailed information of experimental methods, prediction models and results are introduced here to demonstrate the progression of the research contents, but extensive explanations and more discussion are in the original publications attached at the end of this thesis.

2.1 SPME combined binding models to derive binding constants of PFAS with biomaterials

SPME is a sample preparation technique prior to chemical analysis by instrument (e.g., liquid chromatograph-LC, gas chromatograph-GC and mass spectrometer-MS). In SPME fibers, a small amount of a stationary phase (e.g. C18 particles, polydimethylsiloxane-PDMS or divinylbenzene-DVB) is coated onto a solid support. There are four steps in the SPME process: extraction, equilibration, desorption and quantification. The SPME fiber is inserted into the sample to extract the chemicals from biomatrix. After equilibration of the assay system, the SPME fiber is introduced into desorption solvent or analytical instrument to release the chemicals for further quantification by LCMS or GCMS.

The method development of SPME involves optimization such as extraction time, temperature, shaking speed, desorption solvent and the volume of the sample to ensure that the extraction process removes certain amount of chemicals from the sample matrix. The concentrations of chemicals in water and fiber should be within the measurable ranges of analytical instruments. These concentrations are used in the MBMs and binding models to derive the binding isotherms and binding constants of PFAS with different biomaterials. Applications of three SPME methods and three binding models are the foundations in *Publication 1, 2* and *3*.

16 PFAS were selected to demonstrate the method development process of SPME (Table 1), include 13 non-volatile PFAS (PFBA, PFHxA, PFHpA, PFOA, PFNA, PFUnA, HFPO-DA, PFHxS, PFOS, 6:2 FTSA, PFOSA, hexaflumuron and Flubendiamide) and 3 semi-volatile FTOH (6:2, 8:2 and 10:2 FTOH). Their binding constants were derived from different binding models based on their binding behaviors among biomaterials, including bovine serum albumin (BSA), structural protein (SP), bioassay medium, cell homogenates

and plasmas. Plasma bindings of 16 PFAS between human and trout (fish) were compared for species analysis. Detailed description for the chemical selection and method development can be found in *Publication 3.*

2.1.1 Method developments of solid phase microextraction

Three methods of SPME (Figure 3) were developed according to the properties of 16 PFAS. 13 non-volatile PFAS were extracted by C18-particle coated fibers from the aqueous phase and then quantified by LCMS after the desorption of PFAS from the fibers. 3 semi-volatile FTOH were extracted by an assembly divinylbenzene-carboxen-polydimethylsiloxane (DVB-CAR-PDMS) fiber from the gaseous phase in the headspace of the vial in a closed system and then quantified by GCMS after the desorption of FTOH from the fibers. The sample volumes and operations are different according to the experimental conditions.

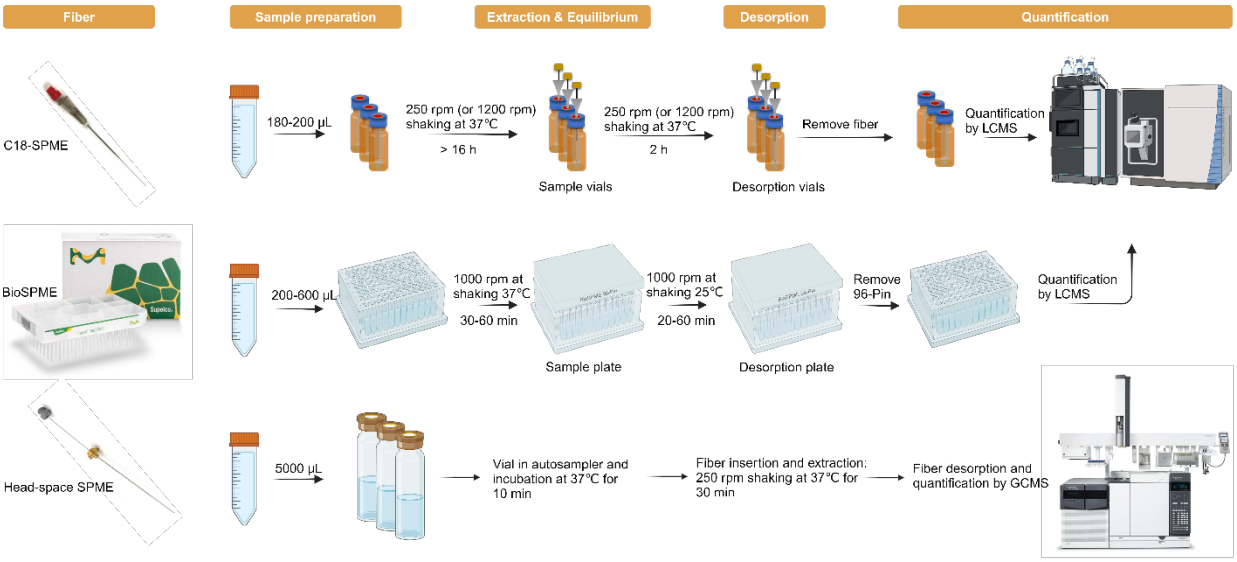

Figure 3. Experimental workflows of three methods of solid phase microextraction (SPME). C18-SPME with signal fibers and BioSPME 96-Pin Devices combined with liquid chromatography mass spectrometry (LCMS) are used for non-volatile PFAS. Head-space SPME combined with gas chromatography mass spectrometry is used for semi-volatile FTOH.

(1) C18-SPME and BioSPME

There are two kinds of C18-particles coated fibers for 13 non-volatile PFAS used in different assays. C18-SPME using single fiber (57281-U, Sigma-Aldrich) is made of metal alloy coated with 173 or 520 nL C18 particles. The coating volumes of C18 particles were decided according to the affinities of PFAS to fibers. The advantage of C18-SPME using single fibers is that samples were prepared in 1.5 mL HPLC vials and the experimental conditions can be optimized individually. BioSPME 96-Pin Device (59683-U, Sigma-Aldrich) has 96 polypropylene pins coated with 80 nL C18 particles. The advantage of BioSPME 96-Pin Device is that 96 samples are prepared in a 96-well plate and can be measured automatedly by a robot. The whole process can be completed in a short period (< 2h). Detailed information for C18-SPME using single fibers can be found in *Publication 1* and for BioSPME 96-Pin Device can be found in *Publication 3*.

As shown in Figure 4, the uptake kinetics were measured to determine the time required to reach 95% equilibrium ($t_{0.95}$) of PFAS between fiber and water phases. The $t_{0.95}$ is determined by several factors. The coating volume and thickness of C18 particles are different for two methods, leading the equilibrium times of C18-SPME using single fibers (Figure 4a-d) and BioSPME 96-Pin Device (Figure 4e-h) vary from hours to minutes. Hydrophilic PFBA reached equilibrium within a very short time, while more hydrophobic ones needed longer time. The $t_{0.95}$ of PFOS in Figure 4d was 1.65 h – shorter than that of PFOA (Figure 4b) and PFHxS (Figure 4c), because the small coating volume of 173 nL and high shaking speed of 1200 rpm for PFOS extraction, while large coating volume of 520 nL and low shaking speed of 250 rpm for PFOA and PFHxS extractions.

Both C18-SPME and BioSPME can be used to study the binding of PFAS to BSA, medium and plasma (*Publication 1, 2 and 3*). The binding of PFAS to cell homogenates and structural protein were only measured by C18-SPME using single fibers (*Publication 1 and 2*), because the binding affinities of PFAS to cells and structural proteins are considered weak, and a larger volume (173 or 520 nL) of C18 particle and a longer equilibrium time (> 16 h) in vials can guarantee of the quality of SPME. The recoveries of 13 PFAS in two methods were around 90-120%. These results demonstrated that two methods are validated to study the binding of PFAS with complex biomaterials.

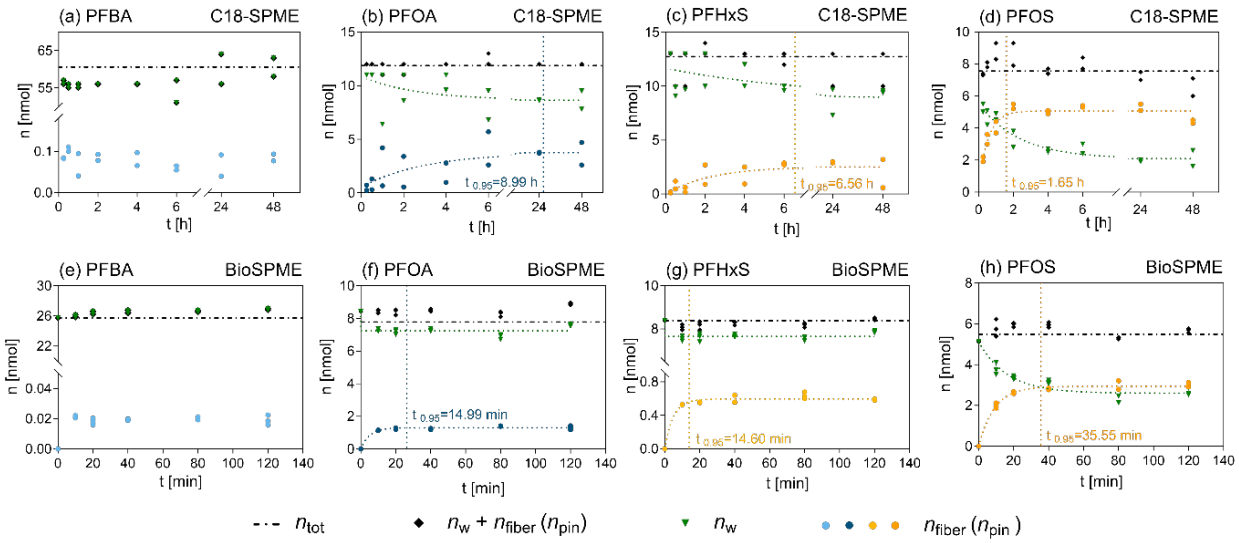

Figure 4. Sorption kinetic of PFAS to **(a-d)** C18-SPME with individual fibers and **(e-h)** BioSPME 96-Pin Device. The black dashed horizontal line is the total amount of chemical (n_{tot}) used in the samples. n_w and n_{fiber} (n_{pin}) were the measured molar amount of chemicals in water phase and fiber (pin). The sum of n_w and n_{fiber} (n_{pin}) were compared with n_{tot} to derive the mass balance. $t_{0.95}$ is the time to reach 95% equilibrium and is indicated by dotted vertical line. Detailed information of (a-d) can be found in *Publication 1* and (e-h) can be found in *Publication 3*.

(2) Head-space SPME

A SPME fiber assembly with DVB-CAR-PDMS (57345-U, Sigma-Aldrich) was used for 3 semi-volatile FTOH in the protein and plasma binding assays. Samples were prepared individually in a 20 mL head-space vial with single FTOH dissolved in biomaterials. The advantages of head-space SPME are that the whole process of SPME and the measurement can be completed automatedly with an autosampler, and the experimental conditions can be optimized individually. Detailed information for head-space SPME can be found in *Publication 3*.

As shown in Figure 5, good linear regressions of the measured GC peak areas (A) and the total concentrations (C_{tot}) of FTOH were obtained ($R^2 > 0.98$) after optimizations of experimental conditions, including sample volume, shaking speed, equilibrium time and temperature, as well as instrument parameters. Head-space SPME was used to study the binding of FTOH with proteins and plasmas.

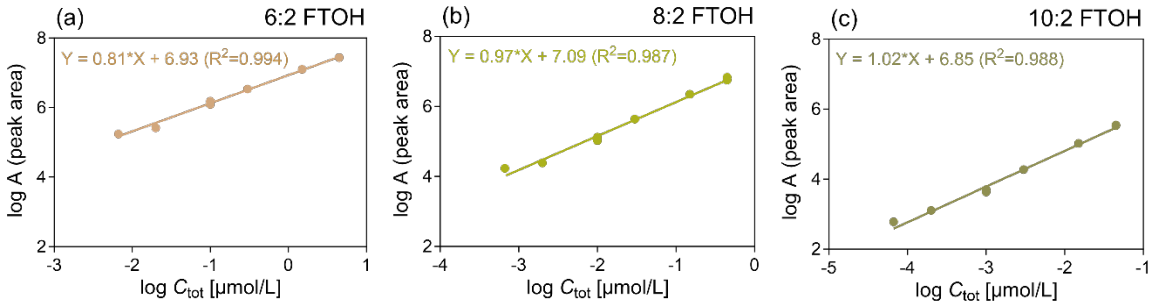

Figure 5. Linear detector response for the measured GC peak areas (A) and the total concentrations of FTOH (C_{tot}). Detailed information can be found in *Publication 3*.

2.1.2 Binding models for binding isotherms and constants

Neutral chemicals bind to proteins mainly with non-covalent bonds via hydrophobicity, van der Waals interaction and hydrogen bonds. Ionizable chemicals have different charged forms at physiological pH=7.4, indicating an additional electrostatic interaction may occur between charged ions and charged amino residues in the protein

binding pockets, which influence the affinities of ionizable chemicals to protein and even produce specific binding.

16 PFAS include fully charged anionic PFBA, PFHxA, PFHpA, PFOA, PFNA, PFUnA, HFPO-DA, PFHxS, PFOS and 6:2 FTSA, and partially charged PFOSA, hexaflumuron and Flubendiamide, as well as neutral 6:2, 8:2 and 10:2 FTOH. To better understand their binding mechanisms, the protein binding assays were performed over 3-4 orders of magnitude in concentrations, where the specific and nonspecific binding constants can be differentiated by following models.

(1) Freundlich-type model

Freundlich isotherm model (eq 1) is an empirical model to describe the binding behavior of chemicals to the sorption phase i (i = BSA, plasma, medium).

$$C_{bound,i}=K_{Fr}\times (C_w)^{n_{Fr}} \quad (1)$$

K_{Fr} and n_{Fr} are Freundlich constant and exponent, which can be deduced from experimental data by the logarithmic form of eq 1, namely Freundlich-type model (eq 2). Inserting eq 3 into eq 2, the binding constants log $D_{i/w}$ can be present by K_{Fr} and n_{Fr} (eq 4).

$$\log C_{bound,i} = n_{Fr}\times \log C_w + \log K_{Fr} \quad (2)$$

$$D_{i/w}=\frac{C_{bound,i}}{C_w} \quad (3)$$

$$\log D_{i/w} = (n_{Fr}-1)\times \log C_w + \log K_{Fr} \quad (4)$$

The average value of log $D_{i/w}$ is approximately equal to log K_{Fr}, if the n_{Fr} is close to 1, suggesting the bindings of PFAS to BSA, plasma or medium are independent of concentration. In contrast, $n_{Fr} < 1$ suggests a concentration-dependent binding isotherm.

(2) Combined binding/partitioning model

The binding isotherms of some anionic PFAS were concentration-dependent, which can be fitted nonlinearly with a combined binding/partitioning model (eq 5). The specific binding is consistent with saturation kinetics and the nonspecific partitioning is proportional to ligand concentrations.

$$C_{\text{bound, total}} = \frac{C_{\max} \cdot C_w}{K_d + C_w} + D_{\text{nonspecific}} \times C_w \quad (5)$$

It is assumed there is only one specific ligand binding site in the protein. In an ideal saturable binding, the molar ratio of bound PFAS and protein, v [mol_{PFAS} / $\text{mol}_{\text{protein}}$] is close to 1. Hence, the $v \leq 1$ is used to identify the saturable binding range with eq 6. D_{specific} can be derived by eq 7 with a maximum bound concentration ($C_{\max}$) and dissociation constant (K_d). The nonspecific binding constant, $D_{\text{nonspecific}}$ is derived from total binding by eq 5 with the fixed values of $C_{\max}$ and K_d from eq 6.

$$C_{\text{bound, specific}} = \frac{C_{\max} \cdot C_w}{K_d + C_w} \quad (6)$$

$$D_{\text{specific}} = \frac{C_{\max}}{2 \times K_d} \quad (7)$$

This mechanistic model can also be used for plasma binding, assuming that plasma protein binding is highly specific at one binding site, while the nonspecific binding is relevant for plasma proteins and lipids at high concentrations. Therefore, the plasma binding isotherm is fitted by eq 8 with an extra volume fraction of proteins for specific binding.

$$C_{\text{bound, total}}\ (\text{plasma}) = \frac{C_{\max} \cdot C_w}{K_d + C_w} \times \frac{V_{\text{protein,plasma}}}{V_{\text{protein+lipid,plasma}}} + D_{\text{nonspecific}} \times C_w \quad (8)$$

As shown in Figure 6, the binding isotherm of HFPO-DA was fitted firstly with Freundlich-type model resulting $n_{Fr} < 1$ (eq 2, Figure 6a), which suggested a concentration-dependent log $D_{BSA/w}$ (eq 4, Figure 6b). The isotherm was then fitted with mechanistic model (eq 5, Figure 6c) and a saturable binding was identified in the low concentration range ($v < 1$, eq 6, Figure 6d). The specific (eq 7) and nonspecific protein binding constants (eq 5) of HFPO-DA can be derived. Although the $n_{Fr} \neq 1$ of PFNA was found (eq 2, Figure 6e), there is no saturable binding in Figure 6h that means the specific binding cannot be distinguished from the nonspecific binding. The average log $D_{BSA/w}$ of PFNA was derived with Freundlich-type model (eq 4) by setting $n_{Fr} = 1$.

All the binding constants of PFAS with BSA and plasmas were analyzed with the same criterion and listed in Table 3. The values of log $D_{BSA/w}$ increase as the numbers of perfluorinated carbons increase. Both specific and nonspecific log $D_{BSA/w}$ of PFBA, PFHxA,

PFHpA, PFOA, HFPO-DA, PFHxS and PFOS can be identified, while only average values of nonspecific protein binding for long-chain PFUnA, 6:2 FTSA and PFOSA were obtained.

Binding constants of some PFAS measured by traditional dialysis previously (Allendorf et al. 2019; Xia et al. 2013) were compared with the BSA binding isotherms measured in this thesis (Figure 6). Literature data, which looked initially inconsistent, were located in different regions of the binding isotherms, suggesting results from different methods are comparable. The binding isotherms derived in this thesis depict a broader view of binding behavior of these PFAS. The specific and nonspecific binding constants were calculated for anionic PFAS that bind to proteins concentration-dependently.

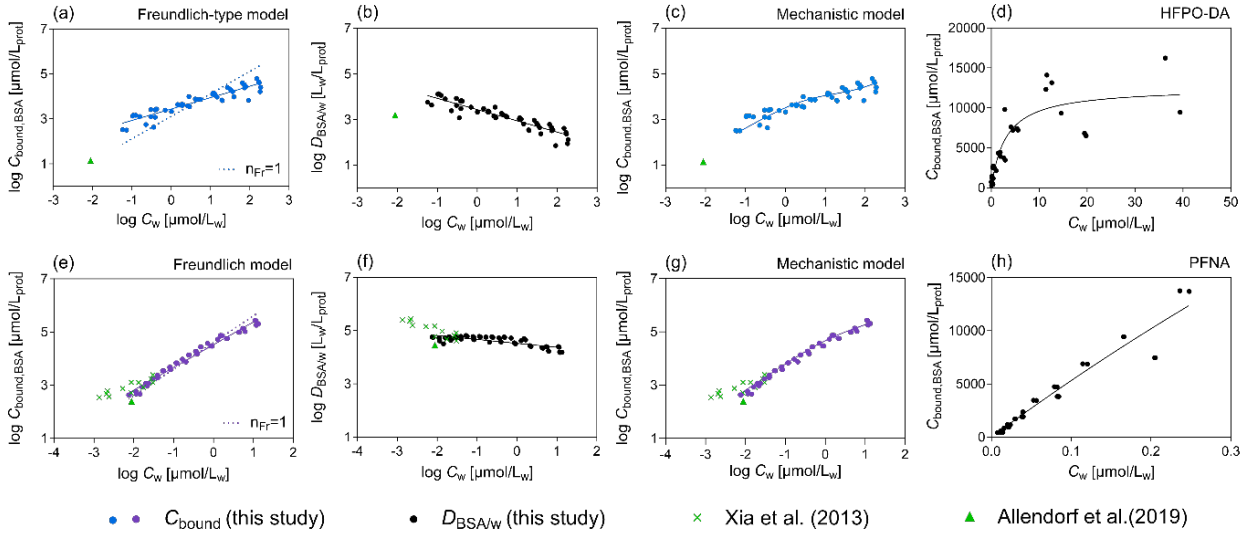

Figure 6. Bovine serum albumin (BSA) binding of **(a-d)** HFPO-DA and **(e-h)** PFNA. **(a, e)** Data points were fitted linearly with the empirical Freundlich-type model (eq 2) and **(b, f)** the concentration-dependent distribution ratios between BSA and water, log $D_{BSA/w}$ were fitted linearly (eq 4). **(c, g)** Experimental data points were fitted nonlinearly with the mechanistic combined binding/partition model (eq 5) and **(d, h)** the saturable specific binding in the low concentration rage was derived with eq 6. Results of this study were compared with literature data (green triangles and crosses) (Allendorf et al. 2019; Xia et al. 2013). Detailed information can be found in *Publication 3*.

Table 3. Binding constants of 16 PFAS with proteins and plasmas. Binding constants between bovine serum albumin and water (log $D_{BSA/w}$), between human or trout plasma and water (log $D_{plasma/w}$) were measured in this study. Average log $D_{i/w}$ were calculated with Freundlich-type model (eqs 4, 13). log $D_{i/w}$ of specific and nonspecific binding were derived with combined binding/partitioning model (eqs 5, 7, 8). In parentheses are the 95% confidence intervals.

	number of C-F	BSA: log $D_{BSA/w}$ [L_w/L_{prot}]		Human plasma: log $D_{plasma/w}$ [$L_w/L_{prot+lip}$]		Trout plasma: log $D_{plasma/w}$ [$L_w/L_{prot+lip}$]	
		Specific	Nonspecific or average *	Specific	Nonspecific or average *	Specific	Nonspecific or average *
PFBA	3	2.44 (2.10-2.63)	1.97 (1.90-2.04)	2.20 (0.87-2.49)	1.35 (1.23-1.44)	n/a	1.43 * (1.28-1.58)
PFHxA	5	3.26 (2.98-3.42)	2.69 (2.66-2.72)	3.19 (3.01-3.31)	2.61 (2.56-2.66)	n/a	2.49 * (2.41-2.57)
PFHpA	6	4.12 (3.87-4.27)	3.47 (3.42-3.52)	4.10 (3.98-4.20)	3.20 (3.15-3.24)	n/a	3.32 * (3.25-3.39)
PFOA	7	4.58 (4.47-4.67)	3.88 (3.86-3.90)	4.45 (4.34-4.54)	3.65 (3.59-3.70)	n/a	4.18 * (4.14-4.21)
PFNA	8	n/a	4.61* (4.56-4.65)	n/a	4.19 * (4.14-4.24)	n/a	4.71 * (4.65-4.76)
PFUnA	10	n/a	4.75 * (4.71-4.80)	n/a	4.54 * (4.49-4.59)	n/a	4.99 * (4.96-5.03)
HFPO-DA	5	3.31 (2.95-3.50)	2.17 (2.05-2.26)	3.35 (2.77-3.58)	1.99 (1.93-2.04)	3.56 (3.08-3.78)	1.89 (1.67-2.04)
PFHxS	6	5.02 (4.90-5.11)	3.58 (3.50-3.64)	4.98 (4.80-5.11)	2.92 (2.78-3.03)	n/a	4.00 * (3.91-4.10)
PFOS	8	5.27 (4.84-5.48)	4.17 (4.14-4.20)	4.82 (4.41-5.03)	4.07 (4.04-4.11)	5.49 (4.88-5.74)	4.57 (4.54-4.60)
6:2 FTSA	6	n/a	3.87 * (3.84-3.90)	n/a	3.67 * (3.63-3.70)	n/a	4.11 * (4.04-4.19)
PFOSA	8	n/a	4.32 * (4.28-4.37)	n/a	3.90 * (3.86-3.93)	n/a	4.33 * (4.27-4.40)
Hexaflumuron	2	n/a	3.96 * (3.93-4.00)	n/a	4.29 * (4.24-4.35)	n/a	4.61 * (4.53-4.69)
Flubendiamide	3	n/a	3.98 * (3.93-4.02)	n/a	3.88 * (3.85-3.91)	n/a	4.46 * (4.42-4.50)
6:2 FTOH	6	n/a	2.67 * (2.54-2.77)	n/a	2.73 * (2.49-2.89)	n/a	2.77 * (2.49-2.94)
8:2 FTOH	8	n/a	4.61* (4.48-4.72)	n/a	4.55 * (4.49-4.61)	n/a	5.01 * (4.90-5.10)
10:2 FTOH	10	n/a	6.72 * (6.44-6.89)	n/a	6.21 * (6.11-6.28)	n/a	6.86 * (6.68-6.99)

n/a: not available

(3) Mass balance model to derive binding constants of semi-volatile PFAS with peak areas

Neutral chemicals bind to protein mainly with non-covalent bonds, which is considered as nonspecific binding and independent of concentrations. The binding constants of neutral FTOHs can be derived with the simple MBMs. Partition constants of FTOHs between air and water ($K_{air/w}$) (Arp et al. 2006), wet glass surface and air ($K_{glass/air}$) (Goss et al. 2006), and biomaterials and water ($D_{i/w}$, i=BSA, plasma) were used in the MBMs to derive the concentration of FTOH in the aqueous phase of the PBS samples as control, C_w (eq 9), as well as the aqueous phase of BSA and plasma samples, $C_{w,i}$ (eq 10).

$$C_w = \frac{n_{tot}}{V_w + K_{air/w} \times V_{air} + K_{air/w} \times K_{glass/air} \times S_{glass}} \quad (9)$$

$$C_{w,i} = \frac{n_{tot}}{V_w + K_{air/w} \times V_{air} + K_{air/w} \times K_{glass/air} \times S_{glass} + D_{i/w} \times V_i} \quad (10)$$

Given a linear detector response (Figure 5), the GC peak areas of the FTOHs from the control samples (A_w, eq 11), and BSA or plasma samples ($A_{w,i}$, eq 12) can be assumed to be linearly related to the concentration of the FTOH in the aqueous phases.

$$A_w = \text{slope} \times C_w \quad (11)$$

$$A_{w,\ i} = \text{slope} \times C_{w,i} \quad (12)$$

The slope is the response factor of the GC measurement, which cancels out if a ratio of peak areas ($A_w/A_{w,i}$) is calculated. Insertion of eq 9 to eq 11 and eq 10 to eq 12 also cancels out the n_{tot} for control samples, BSA and plasma samples. $D_{i/w}$ was moved to the left side of the equation to yield eq 13. The values of $K_{air/w}$ and $K_{glass/air}$ were from literatures, volume of water (V_w) and air (V_{air}), as well as area of glass surface (S_{glass}) were measured in this experiment.

$$D_{i/w} = \left(V_w + K_{air/w} \times V_{air} + K_{air/w} \times K_{glass/air} \times S_{glass}\right) \times \frac{1}{V_i} \times \left(\frac{A_w}{A_{w,\ i}} - 1\right) \quad (13)$$

As shown in Figure 7, BSA binding of neutral 6:2 FTOH, 8:2 FTOH and 10:2 FTOH were measured at four concentrations and there was no significant difference (t-test, $p<0.05$) of log $D_{BSA/w}$ among concentrations. Therefore, their log $D_{BSA/w}$ were calculated from the average values measured at different concentrations (Table 3).

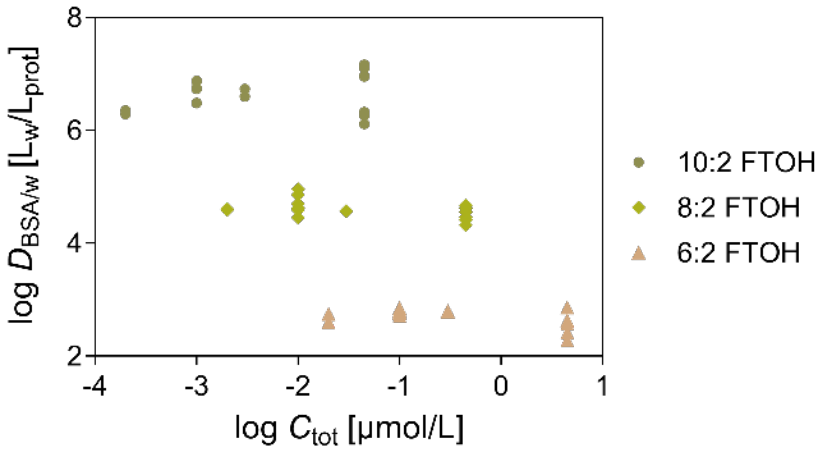

Figure 7. Bovine serum albumin (BSA) binding constants of 3 FTOH measured at different concentrations.

2.1.3 Species difference of human and trout plasma bindings

Binding constants of 16 PFAS between plasma and water (log $D_{plasma/w}$) measured in this thesis are listed in Table 3. Log $D_{plasma/w}$ of 13 non-volatile PFAS were derived from the binding isotherms and 3 semi-volatile FTOH were from average values. There are differences between human and trout plasma binding. Some specific bindings found in human plasma cannot be identified in trout plasma. A comparison of binding isotherms of human and trout plasma is shown in Figure 8. Differences were found in the low concentration ranges of PFBA, PFHxA, PFHpA, PFOA and PFHxS (Figure 8a-d, h). This may be due to lower protein and higher lipid content of trout plasma, where the nonspecific binding of lipids may dominate the affinity of PFAS to the trout plasma already at low concentration ranges. Both plasma binding isotherms were nonlinear for HFPO-DA and PFOS (Figure 2g, i), because they have strong binding affinities to both proteins and lipids in plasmas. PFNA, PFUnA, 6:2 FTSA and PFOSA (Figure 8e, f, j, k) showed slightly concentration-dependence for human plasma binding but almost independent of concentrations for trout plasma binding. These results shown species difference in human and trout plasma bindings of PFAS, which can be explained by the affinities of PFAS to proteins and lipids (chemical characteristics), as well as the protein and lipid contents of the plasmas (species characteristics).

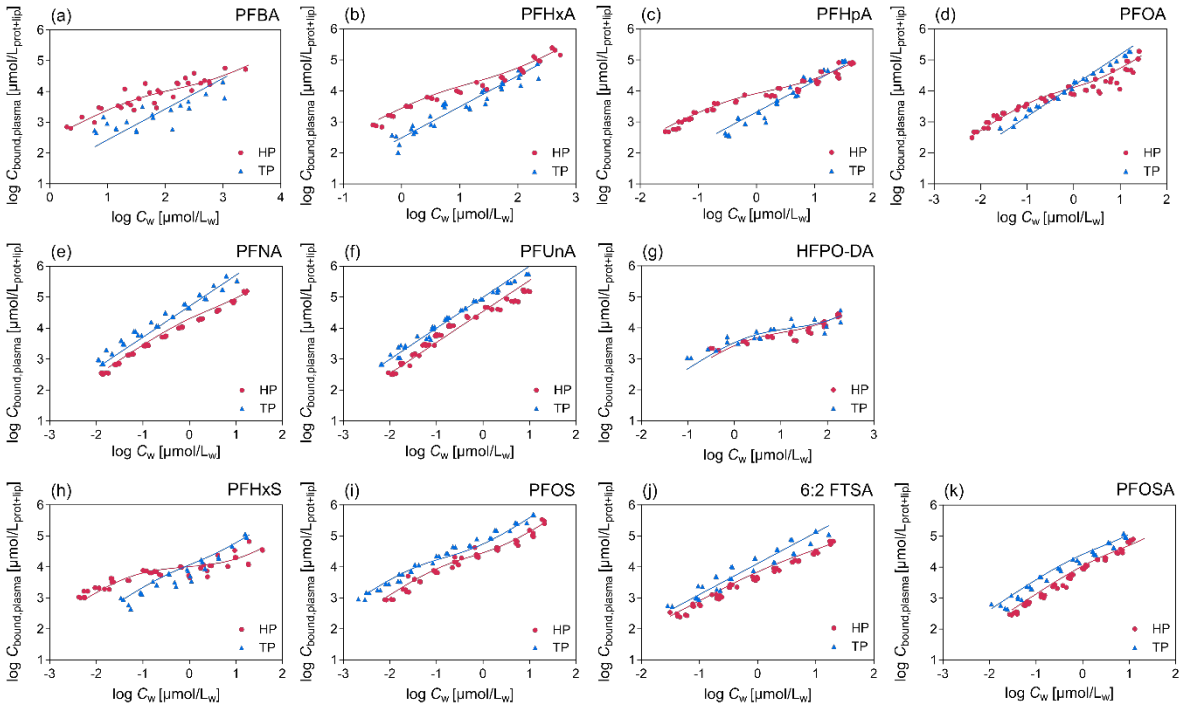

Figure 8. Human plasma (HP) and trout plasma (TP) binding isotherms of 11 anionic PFAS. Curves were fitted linearly with empirical Freundlich-type model (eq 2) or nonlinearly with mechanistic combined binding/partitioning model (eq 8). The selection of models was based on whether the binding isotherms were concentration-dependent (Table 3).

2.2 Binding constants and free concentrations to inform risk assessment with QIVIVE ratios

It is possible to measure the C_{free} of PFAS in various biomaterials with SPME and to derive the binding constants with different binding models. In this subchapter, versatile MBMs are developed to predict the binding constants of $D_{plasma/w}$ in *Publication 1* and *3,* as well as $D_{medium/w}$ and $D_{cell/w}$ in *Publication 1* and *2*. These binding constants are further used to predict the C_{free} of PFAS in human plasma and bioassay medium. The validated MBMs are supposed to serve more chemicals that cannot be measured experimentally.

The free concentrations are more relevant to bioavailability, which is a practical reference for the internal concentration, compared with the concentration predicted from external dose after the mimicking of absorption, distribution, metabolism and excretion process. In a simplified model, the C_{free} (internal concentration) of PFAS is related to binding constants and predictable. A ratio of free concentrations of PFAS in human plasma ($C_{free,plasma}$) and freely effect concentrations of PFAS in cell-based bioassays (EC_{free}), namely $QIVIVE_{free}$ ratio, is expected to make cell-based HTS data widely used to inform risk assessment in a simple way. Detailed information can be found in *Publication 1*.

2.2.1 Mass balance models for binding constants

The binding constants of PFAS with biomaterials were obtained experimentally for plasmas (*Publication 1* and *3*), bioassay media and cell homogenates (*Publication 1* and *2*). Although the components in these biomaterials are complex, PFAS are prone to bind with proteins and lipids, suggesting the complex prediction of binding constants $D_{plasma/w}$, $D_{medium/w}$ and $D_{cell/w}$ (at pH=7.4) can be simplified by MBMs with the distribution of PFAS to proteins and lipids. $D_{plasma/w}$ was further used to predict the $C_{free,plasma}$ of PFAS in the human plasma with epidemiological data from literatures or national health surveys. $D_{medium/w}$ and $D_{cell/w}$ were further used to predict the $C_{free,medium}$ of PFAS in the bioassay medium. A comparison of $C_{free,medium}$ between experimental values or predicted values with $D_{medium/w}$ and $D_{cell/w}$ can verify the accuracy of the MBMs.

It is assumed that proteins and lipids are major sorption phases of PFAS in plasmas, bioassay media and cell homogenates. $D_{plasma/w}$, $D_{medium/w}$ and $D_{cell/w}$ were predicted by eq

14 with protein binding constants $D_{protein/w}$ and lipid binding constants $D_{lipid/w}$, as well as the volume fractions of proteins and lipids in these complex biomaterials.

$$D_{i/w}=D_{protein/w}\times\frac{V_{protein,i}}{V_{protein+lipid,i}}+D_{lipid/w}\times\frac{V_{lipid,i}}{V_{protein+lipid,i}} \quad (14)$$

Notably, the surrogates of $D_{protein/w}$ for protein binding and $D_{lipid/w}$ for lipid binding need to be determined differently according to the components of the biomaterials. $D_{BSA/w}$ is a proxy for all functional plasma protein distribution. Human plasma may contain approximately 40% phospholipids and 60% neutral lipids (Firl et al. 2013; Poulin et al. 2002), where the binding constants of liposome and water $D_{lip/w}$ as a proxy for phospholipid distribution, and binding constants of olive oil and water $D_{oil/w}$ for neutral lipid distribution. $D_{plasma/w}$ can be predicted by eq 14-1.

$$D_{plasma/w}=D_{BSA/w}\times\frac{V_{protein,plasma}}{V_{protein+lipid,plasma}}+D_{lip/w}\times\frac{0.40\times V_{lipid,plasma}}{V_{protein+lipid,plasma}}+D_{oil/w}\times\frac{0.60\times V_{lipid,plasma}}{V_{protein+lipid,plasma}} \quad (14\text{-}1)$$

However, the volume fractions of lipids in medium and cell homogenates were far less than that of proteins, and the lipid types cannot be distinguished. $D_{lip/w}$ is a proxy for all lipid distributions. $D_{medium/w}$ can be predicted by eq 14-2.

$$D_{medium/w}=D_{BSA/w}\times\frac{V_{protein,medium}}{V_{protein+lipid,medium}}+D_{lip/w}\times\frac{V_{lipid,medium}}{V_{protein+lipid,medium}} \quad (14\text{-}2)$$

Since the most abundant proteins in cells are structural proteins (SP), for which muscle proteins are better surrogates than BSA. $D_{cell/w}$ can be predicted by eq 14-3 with $D_{SP/w}$ referring to the binding constants of SP and water.

$$D_{cell/w}=D_{SP/w}\times\frac{V_{protein,cell}}{V_{protein+lipid,cell}}+D_{lip/w}\times\frac{V_{lipid,cell}}{V_{protein+lipid,cell}} \quad (14\text{-}3)$$

The binding constants of 16 PFAS with human and trout plasmas (Table 3) were derived from the binding isotherms (Figure 8) including specific and nonspecific values, as well as the average values. These binding constants can also be predicted by MBMs (eq 14-1). All the predicted log $D_{plasma/w}$ were within a factor of ten compared to the experimental ones for human (Figure 9a) and trout plasmas (Figure 9b). The distribution ratios of 11 PFAS with medium and cells were obtained experimentally at the concentrations that triggered 10% cytotoxicity. The predicted log $D_{medium/w}$ (eq 14-2, Figure 9c) and log $D_{cell/w}$ (eq 14-3, Figure 9d) agreed well with experimental ones.

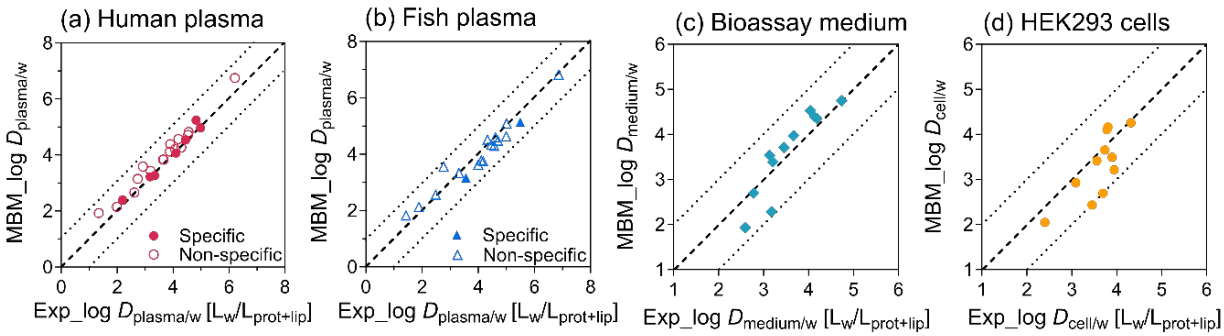

Figure 9. Prediction of binding constants of PFAS with different biomaterials by mass balance models (MBM). The binding constants of plasma and water, log $D_{plasma/w}$ (pH = 7.4) of 16 PFAS with **(a)** human plasma and **(b)** trout plasma were measured experimentally (Exp) and plotted against predicted $D_{plasma/w}$ by eq 14-1. The binding constants of **(c)** medium and water, log $D_{medium/w}$ (pH = 7.4) and **(d)** cell and water, log $D_{cell/w}$ (pH = 7.4) of 11 PFAS were measured experimentally and plotted against predicted $D_{medium/w}$ by eq 14-2 and $D_{cell/w}$ by eq 14-3. Detailed information of plasma binding can be found in *Publication 3*, and medium and cell bindings can be found in *Publication 2*.

2.2.2 Mass balance models for free concentrations in plasma and *in vitro* bioassays

$C_{free,plasma}$ was calculated by eq 15 with the nominal concentration of PFAS in human plasma from the epidemiological investigations.

$$C_{free,\ plasma} = \frac{C_{nom,plasma} \times V_w}{V_w + D_{plasma/w} \times V_{prot+lip,\ plasma}} \quad (15)$$

The $C_{free,medium}$ of PFAS in bioassay medium after 24 h-exposed to cells can be predicted for a serial dilution of concentration as the change of C_{nom} in the bioassays with eq 16. Insertion of $D_{medium/w}$ (eq 14-2) and $D_{cell/w}$ (eq 14-3) yields eq 17.

$$C_{free,medium} = \frac{C_{nom} \times V_{tot}}{V_w + D_{medium/w} \times V_{protein+lipid,medium} + D_{cell/w} \times V_{protein+lipid,cell}} \quad (16)$$

$$C_{free,medium} = \frac{C_{nom} \times V_{tot}}{V_w + D_{BSA/w} \times V_{protein,medium} + D_{lip/w} \times V_{lipid,medium} + D_{SP/w} \times V_{protein,cell} + D_{lip/w} \times V_{lipid,cell}} \quad (17)$$

Meanwhile, the cytotoxicity and cell response of defined targets were measured to derive the concentration-response curves (CRCs), where inhibitory concentration of 10% cytotoxicity (IC_{10}, eq 18) or effect concentration of 10% response of defined targets (EC_{10}, eq 19) can be derived from the linear portions of the CRCs. Both C_{nom} and $\underline{C}_{free,medium}$ are used to develop the CRCs in the bioassays, resulting two concentrations of $IC_{10,nom}$ and $IC_{10,free}$ regarding the cytotoxicity for comparison. Similarly, both $EC_{10,nom}$ and $EC_{10,free}$ are obtained regarding the cell response of defined targets.

$$IC_{10} = \frac{10\%}{\text{Slope (of CRC regarding cytotoxicity)}} \quad (18)$$

$$EC_{10} = \frac{10\%}{\text{Slope (of CRC regarding cell response of defined targets)}} \quad (19)$$

As shown in Figure 10, PFAS are prone to bind with medium components leading lower $C_{free,medium}$ than the associated C_{nom} (Figure 10). As the number of carbons of three perfluoroalkyl carboxylic acid (PFCA) increased, the $C_{free,medium}$ deviated more from the 1:1 line to corresponding C_{nom} (Figure 10a). The relationship between log $C_{free,medium}$ and log C_{nom} was not linear, which was most pronounced for PFHxS and PFOS (Figure 10e) because sulfonic acids were found to have specific binding to protein at low concentration ranges resulting in lower $C_{free,medium}$.

The $C_{free,medium}$ predicted by the MBM (eq 16) with $D_{medium/w}$ and $D_{cell/w}$ agreed well with experimental ones in a concentration-dependent way (Figure 10b-d, f-h, hollow shapes). $C_{free,medium}$ predicted by the MBM (eq 17) with $D_{lip/w}$, $D_{BSA/w}$ and $D_{SP/w}$ were also consistent (Figure 10b-d, f-h, crosses) because the experimental $D_{medium/w}$ were represented well by log $D_{BSA/w}$ and log $D_{lip/w}$ (Figure 9c), as well as the log $D_{cell/w}$ with log $D_{sp/w}$ and log $D_{lip/w}$ (Figure 9d).The IC_{10} (eq 18) were derived with both C_{nom} and $\underline{C}_{free,medium}$ for comparison. A comparison of experimental values and predicted values in Figure 9 and Figure 10 validated the accuracy of MBMs in the prediction of binding constants and free concentration in assay medium.

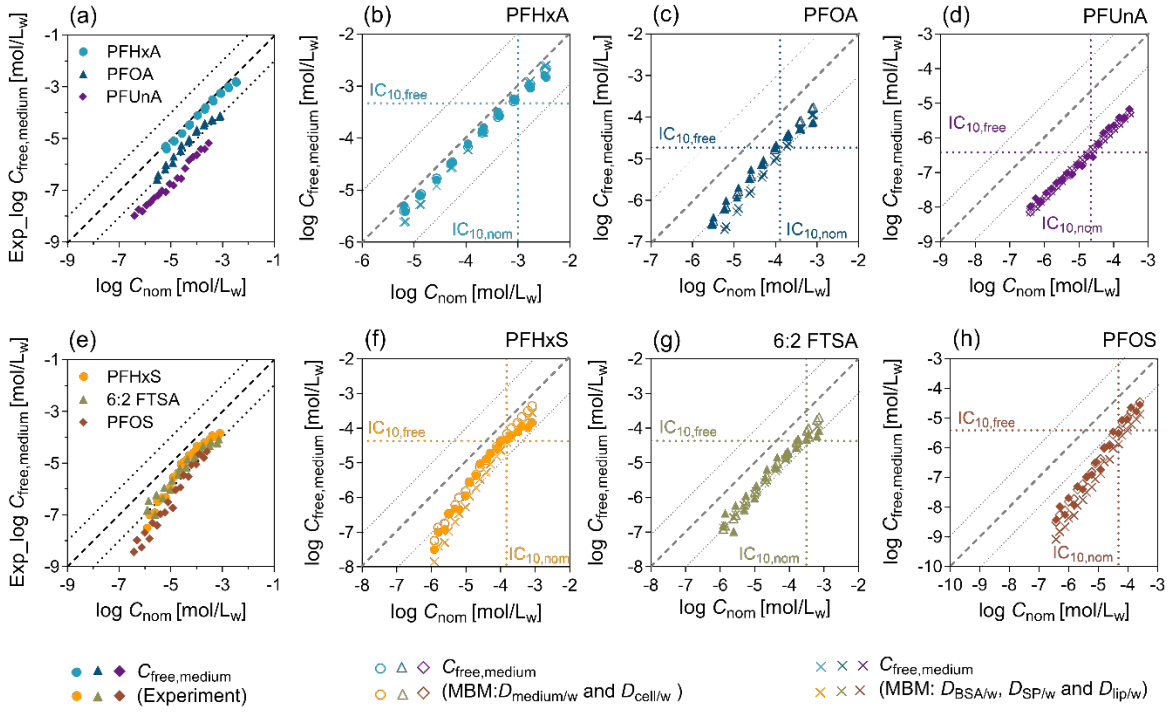

Figure 10. Relationship between nominal (C_{nom}) and measured free ($C_{free,medium}$) concentrations of PFAS in the PPARγ-GeneBLAzer assay. $C_{free,medium}$ were measured experimentally for **(a-d)** three perfluoroalkyl carboxylic acids and **(e-h)** three perfluoroalkyl sulfonic acids. $C_{free,medium}$ were predicted concentration-dependently by the mass balance models (MBMs) from C_{nom} with distribution ratio between medium and water ($D_{medium/w}$) and cell and water ($D_{cell/w}$) measured in this study (eq 16), or with distribution ratio between BSA and water ($D_{BSA/w}$), between structural protein and water ($D_{SP/w}$) and liposome and water ($D_{lip/w}$) (eq 17). Inhibitory concentration $IC_{10,nom}$ or $IC_{10,free}$ were derived from concentration-response curves at 10% cytotoxicity with C_{nom} or measured $C_{free,medium}$. Detailed information can be found in *Publication 2*.

2.2.3 QIVIVE ratios for risk assessment

Risk assessment of chemicals needs to consider both human exposed levels and bio-effective concentrations. To inform a better risk assessment with cell-based HTS data, QIVIVE ratio is defined as eq 20. QIVIVE ratio > 1 indicates *in vitro* effects likely occurred in *in vivo* clinical effects.

$$\text{QIVIVE ratio}=\frac{C_{plasma}}{EC_{bioassay}} \quad (20)$$

As nominal concentrations are widely reported in the epidemiological investigations and in HTS database, $QIVIVE_{nom}$ ratio is easily obtained by eq 20-1.

$$QIVIVE_{nom}\ \text{ratio}=\frac{C_{nom,\ plasma}}{EC_{nom}} \quad (20\text{-}1)$$

The exposure concentrations of PFAS detected in human plasma are usually at nanomolar while the effect concentrations of PFAS in cell-based bioassays are at micromolar. The great difference of the concentrations leads to different binding constants because PFAS bound to proteins of medium and plasma in a concentration-dependent way. The $D_{plasam/w}$ and $D_{medium/w}$ may result in different $C_{free,plasma}$ and $C_{free,medium}$. However, C_{free} is more relevant to bioavailability in both human bodies and bioassays. The $QIVIVE_{free}$ ratio by eq 20-2 is suggested to use to inform potential risk how PFAS exposed in human is relevant to cell response.

$$QIVIVE_{free}\ \text{ratio}=\frac{C_{free,plasma}}{EC_{free}} \quad (20\text{-}2)$$

As an illustrative example, we calculated the QIVIVE ratio with the EC of PFAS in the PPARγ GeneBLAzer assay, as well as C_{plasma} of PFBA, PFOA, PFHxS and PFOS in workers and residents living near fluorochemical plants from Bao et al. (2022) and Gao et al. (2015) or the general population in the US (https://www.cdc.gov/exposurereport/data_tables.html) and Gao et al (2019). As shown in Figure 11, for hydrophilic PFBA, the $QIVIVE_{nom}$ and $QIVIVE_{free}$ ratios was similar, while large differences were found between $QIVIVE_{nom}$ and $QIVIVE_{free}$ ratios for PFOA, PFHxS and PFOS, because their protein bindings are highly concentration-dependent with a high-affinity specific binding at low concentrations and lower nonspecific binding at higher concentrations. Thus, the low concentrations in human plasma are strongly bound to

proteins, while the high concentration needed to trigger effects in *in vitro* bioassays have a higher fraction unbound. $QIVIVE_{free}$ ratios <<1 does not mean it is safe. Proteins and lipids in plasma may act as reservoirs of PFAS, reducing the freely dissolved concentration of PFAS. But a majority of bound PFAS still accumulate in the body and can be remobilized to different tissues and organs via blood circulation. This may result in long-term exposure at low free concentrations, suggesting that chronic toxic effects are more of concern than the acute toxic effects of PFAS on human health.

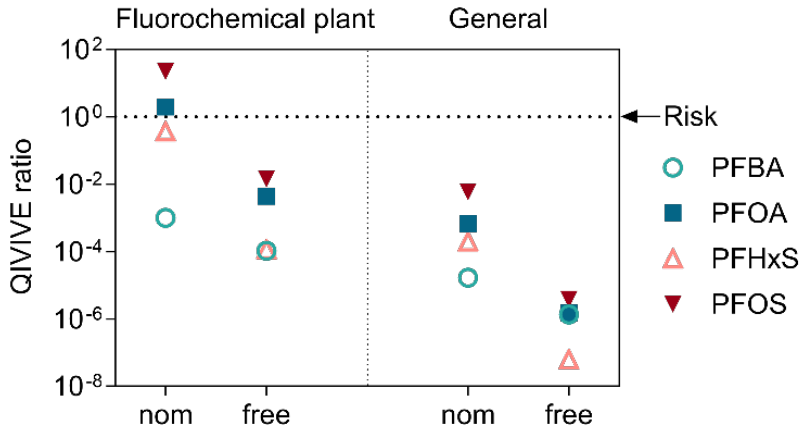

Figure 11. Quantitative *in vitro* to *in vivo* extrapolation (QIVIVE) ratio of PFAS with nominal and free concentrations. QIVIVE ratios for workers and residents living near fluorochemical plants and general population were derived with nominal concentrations (nom, eq 20-1) or free concentrations (free, eq 20-2) of human exposure level and effect concentrations in the PPARγ-GeneBLAzer bioassay. Detailed information can be found in *Publication 1*.

2.3 Baseline toxicity as an anchor to define the specificity level of PFAS in cell-based HTS

Cell-based HTS data can be used not only to inform risk assessment via QIVIVE ratio, but also to develop PFAS-relevant AOPs if the specific responses of MIEs and KEs can be identified in cellular level. In this subchapter, the nonspecific baseline toxicity serves as an anchor to define the specificity degrees of cellular responses of PFAS.

Baseline toxicity prediction models are derived from the validated MBM that links the $IC_{10,membrane,baseline}$ and $IC_{10,free,baseline}$ to $IC_{10,nom,baseline}$ of PFAS in the bioassay medium. The nominal inhibitory concentration of tested chemicals that caused 10% cytotoxicity, $IC_{10,nom}$ is derived from the linear portion of the concentration-cytotoxicity curve, as well as effect concentration of defined targets, $EC_{F,nom}$ is from the concentration-response curve. Ratios of predicted $IC_{10,nom,baseline}$ and experimental $IC_{10,nom}$ or $EC_{F,nom}$ are defied as toxic ratio (TR_{nom}) and specificity ratio (SR_{nom}) to present the potent of cytotoxicity and specificity of cellular responses. A relationship of TR_{nom} and SR_{nom} can be found in Figure 12.

Baseline toxicity prediction models were used in our experimental data of 24 PFAS on four cell-based HTS, including three reporter gene assays targeting PPARγ and the aryl hydrocarbon receptor (AhR) and oxidative stress response of AREc32, as well as an image-based neurotoxicity assay that quantifies inhibition of neurite outgrowth. Baseline toxicity prediction models were also used to re-evaluate literature data of 16 PFAS on five cell-based bioassays targeting human/rat PPARγ, human/rat PPARα and human estrogen receptors (hERs). Detail description can be found in *Publication 2*.

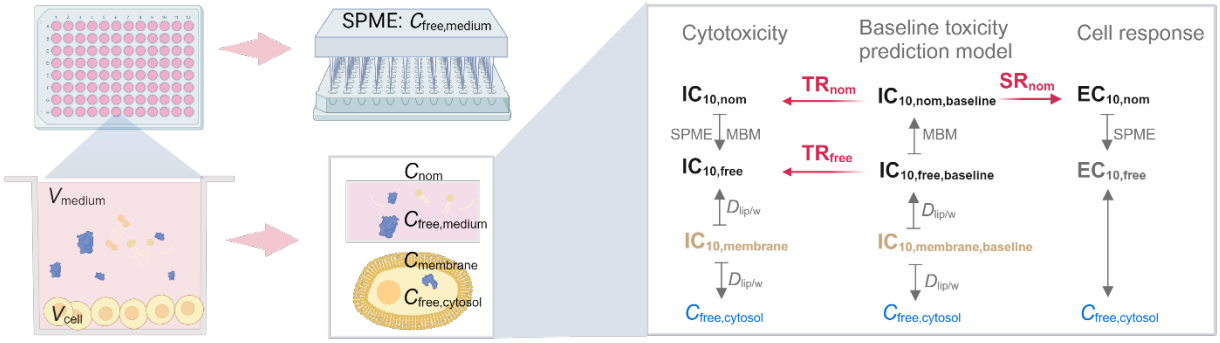

Figure 12. An overview of the dose-metrics and baseline toxicity prediction models for cell-based bioassays. Abbreviation: TR=toxic ratio, SR=specificity ratio, IC=inhibitory concentration, EC=effect concentration, MBM=mass balance model, SPME=solid phase microextraction, nom=nominal concentration, free=free concentration, $D_{lip/w}$=distribution ratio between liposome and water. Detailed information can be found in *Publication 2*.

2.3.1 Baseline toxicity prediction models

Chemicals inevitably accumulate in the membrane during the cellular uptake from medium into cytosol. The partitioning to membrane lipid bilayers can be simulated by phospholipid vesicles, so-called liposomes, $D_{lip/w}$ as eq 21.

$$D_{lip/w} = \frac{C_{lip}}{C_w} \tag{21}$$

Due to the high membrane permeability, passive diffusion has been proven to dominate the cellular uptake of even the anionic PFAS (Ebert et al. 2020). We assumed the free concentration in the cytosol $IC_{10,free,cytosol}$ and in the medium that trigger baseline toxicity $IC_{10,free,baseline}$ are equal at steady state. If C_{lip} is related to a constant cell membrane concentration of baseline toxicants, namely $IC_{10,membrane,baseline}$ of 69 mmol/L_{lip}, the C_w presents the $IC_{10,free,cytosol}$ and $IC_{10,free,baseline}$ of baseline toxicants in the aqueous phase of both cells and medium. Then, $IC_{10,free,baseline}$ can be calculated by transforming eq 21 to eq 22.

$$IC_{10,free,baseline} = \frac{IC_{10,membrane,baseline}}{D_{lip/w}} = \frac{69\ mmol/L_{lip}}{D_{lip/w}} \tag{22}$$

The nominal concentration $IC_{10,nom,baseline}$ can be derived from $IC_{10,free,baseline}$ by inserting eq 22 into eq 17 and moving the $IC_{10,nom,baseline}$ to the left side as eq 23.

$$IC_{10,nom,baseline} = \frac{69\ mmol/L_{lip}}{D_{lip/w}} \times \frac{V_w + D_{BSA/w} \times V_{protein,medium} + D_{lip/w} \times V_{lipid,medium} + D_{SP/w} \times V_{protein,cell} + D_{lip/w} \times V_{lipid,cell}}{V_{tot}} \quad (23)$$

Baseline toxicity usually occurs at high concentrations where the nonspecific protein and lipid bindings dominate. There is a linear relationship between proteins (log $D_{BSA/w}$ or log $D_{SP/w}$) and lipids (log $D_{lip/w}$) for nonspecific binding as eq 24.

$$\log D_{protein/w} = a \times \log D_{lip/w} + b \quad (24)$$

Our experimental data log $D_{protein/w}$ of anionic PFAS were plotted against the log $D_{lip/w}$ as eq 24-1 for functional proteins that BSA is as surrogate, as well as in eq 24-2 for structural proteins.

$$\log D_{BSA/w}(\text{anionic PFAS}) = 0.75 \times \log D_{lip/w} + 1.01\ (R^2 = 0.88) \quad (24\text{-}1)$$

$$\log D_{SP/w}(\text{anionic PFAS}) = 0.46 \times \log D_{lip/w} + 1.50\ (R^2 = 0.85) \quad (24\text{-}2)$$

The relationship of log $D_{BSA/w}$ against log $D_{lip/w}$ for neutral chemicals were derived (Endo et al. 2011b) as eq 24-3, as well as log $D_{SP/w}$ against log $D_{lip/w}$ (Endo et al. 2012) as eq 24-4.

$$\log D_{BSA/w}(\text{neutral}) = 0.70 \times \log D_{lip/w} + 0.34 \quad (24\text{-}3)$$

$$\log D_{SP/w}(\text{neutral}) = 0.72 \times \log D_{lip/w} - 0.47 \quad (24\text{-}4)$$

Inserting eq 24 to eq 23, yields an equation that is only dependent on the log $D_{lip/w}$ and volume fractions of proteins and lipids in bioassay systems. The model can be fitted by an empirical exponential equation to mathematically simplify the equation to reduce to three adjustable parameters (eq 25). Parameters a, b and c are adjusted by inserting bioassay-specific volumes of protein and lipids in cells and medium measured in this thesis.

$$\log \left(\frac{1}{IC_{10,nom,baseline}}\right) = a + b \times (1 - e^{-c \times \log D_{lip/w}}) \quad (25)$$

Notably, anionic PFAS bind more strongly to proteins than comparable neutral chemicals, leading a separate baseline toxicity QSAR for neutral and anionic PFAS. Baseline toxicity prediction models for neutral and anionic PFAS derived from four bioassays are listed in Table 4.

Table 4. Parameters of the empirical baseline toxicity prediction model (eq 25) of neutral and anionic PFAS in four cell-based bioassays and the generic cell.

Assay	Medium	Anionic PFAS			Neutral chemicals (PFAS)		
		a	b	c	a	b	c
PPARγ (HEK293H)	OptiMEM + 2% FBS	1.25	4.76	0.251	1.24	5.47	0.235
AREc32 (MCF7)	DMEM Glutamax + 10 % FBS	1.22	3.78	0.263	1.26	4.43	0.278
AhR (H4IIe)	DMEM Glutamax + 10 % FBS	1.22	3.78	0.263	1.26	4.45	0.277
Neurotoxicity (SH-SY5Y)	Neurobasal medium	1.22	4.07	0.247	1.23	5.61	0.209
Generic cell (6% proteins, 0.1% lipids)	Generic medium (0.3% proteins, 0.001% lipids)	1.22	3.79	0.262	1.26	4.47	0.275

As shown in Figure 13, the models differ because the protein and lipid contents in the assay systems were different, resulting in separated lines of prediction models for anionic PFAS (Figure 13a), as well as for neutral chemicals in general that includes neutral PFAS (Figure 13b). If the baseline toxicity models were used to evaluate literature bioassay data with undisclosed conditions, we assumed a generic cell model condition by using defined experimental conditions as shown in Table 4 for both anionic and neutral PFAS. Two generic models are compared in Figure 13c, where the two lines started to separate at log $D_{lip/w} > 2$. This is due to anionic chemicals having higher affinity to proteins despite baseline toxicity occurs at concentrations, where the protein binding is dominated by nonspecific binding. At log $D_{lip/w} < 2$, $IC_{10,nom}$ of the hydrophilic chemicals are close to their $IC_{10,free}$. Therefore, eq 23 are simplified to eq 26, which is similar to eq 22 and is valid for neutral, anionic and cationic organic chemicals.

$$IC_{10,nom,baseline} \approx IC_{10,free,baseline} = \frac{69\ mmol/L_{lip}}{D_{lip/w}} \quad (26)$$

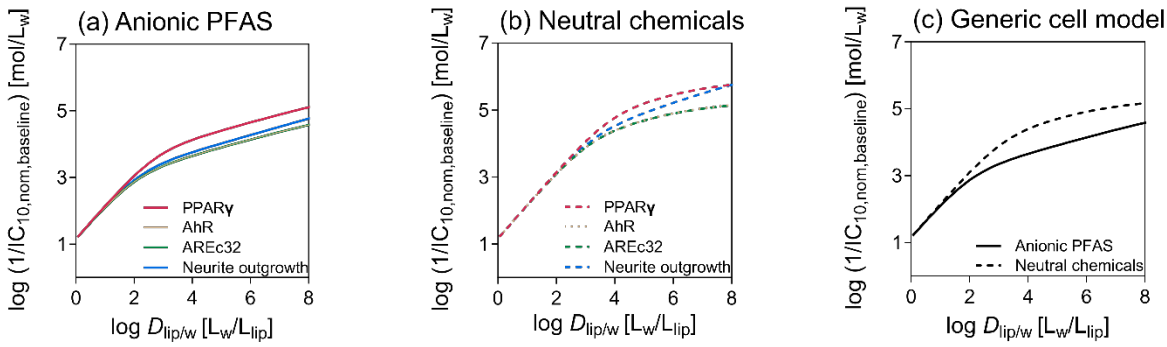

Figure 13. Bioassay-specific baseline toxicity prediction models. Baseline toxicity prediction models for **(a)** anionic PFAS and **(b)** neutral chemicals in general that includes neutral PFAS in four cell-based bioassays: PPARγ-GeneBLAzer (magenta), AREc32 (green), AhR CALUX (gold) and neurotoxicity (blue). **(c)** Baseline toxicity prediction models with the generic cell model for anionic PFAS (solid line) and for neutral chemicals (dashed line).

2.3.2 Specificity of PFAS in cell-based bioassays

The cytotoxicity $IC_{10,nom}$ (eq 18) and the effect concentrations $EC_{10,nom}$ (eq 19) from these assays were compared with $IC_{10,nom,baseline}$ to derive toxic ratios (TR_{nom}, eq 27) and specificity ratios (SR_{nom}, eq 28), which were used to determine if the effects of PFAS are specific.

$$TR_{nom} = \frac{IC_{10,nom,baseline}}{IC_{10,nom}} \quad (27)$$

Chemicals with TR < 10 are classified as baseline toxicants. TR > 10 suggests there may be some specific mode of actions triggering the toxic effects before baseline toxicity occurs (Escher et al. 2020; Maeder et al. 2004).

$$SR_{nom} = \frac{IC_{10,nom,baseline}}{EC_{nom}} \quad (28)$$

SR < 1 suggests the effects on the defined target may be nonspecific. $1 \leq SR < 10$ is considered as moderate specificity with uncertainty. SR > 10 is specific (Escher et al. 2020).

Four cell-based HTS were selected as experimental battery, including three reporter gene assays targeting oxidative stress of AREc32, nuclear receptors of PPARγ and AhR, as well as an image-based neurotoxicity assay that quantifies inhibition of neurite outgrowth of differentiated SH-SYSY cells. Because these targets may be relevant to PFAS according to previous studies, but only several comment PFAS were tested (Li et al. 2018; Long et al. 2013; Ojo et al. 2022; Sun et al. 2018; Yadav et al. 2021). Here, 24 PFAS were tested in 384-well plate format.

As shown in Figure 14, the measured $IC_{10,nom}$ were within a factor of 10 to the $IC_{10,nom,baseline}$ predicted by the four bioassay-specific models and all well within the grey band of $0.1 < TR_{nom} < 10$ of the generic model, indicating that these PFAS did not show specific effects but the cytotoxicity on four cell lines were caused by baseline toxicity.

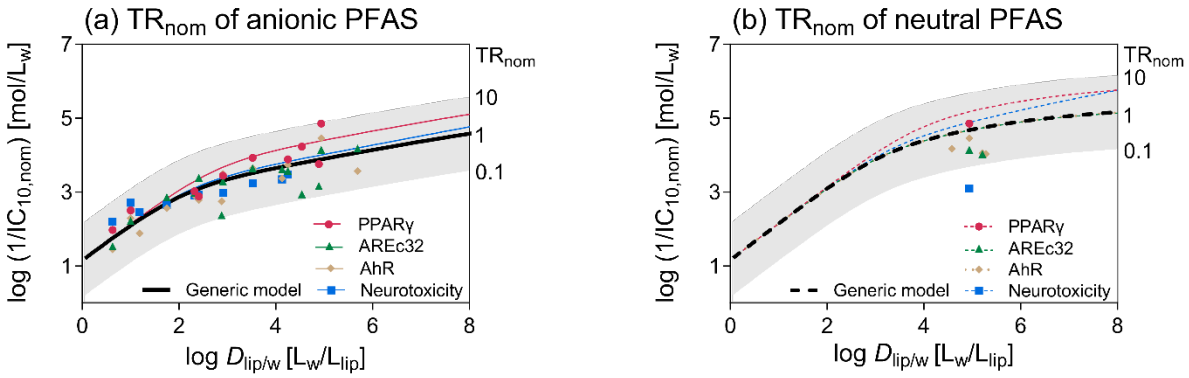

Figure 14. Toxic ratios (TR_{nom}, eq 27) of 24 PFAS in four cell-based HTS assays. **(a)** Nominal inhibitory concentration at 10% cytotoxicity $IC_{10,nom}$ of 16 anionic PFAS in four cell-based bioassays: PPARγ (magenta circle), AREc32 (green triangle), AhR (gold diamond), and neurotoxicity (blue square) and color-matched bioassay-specific baseline toxicity prediction models, as well as the generic model (black line). The grey area depicts the range for baseline toxicity of $0.1 < TR_{nom} < 10$. **(b)** $IC_{10,nom}$ of neutral PFAS in four cell-based bioassays compared with the baseline toxicity prediction models, as well as the generic model (black broken line). All fit parameters of the empirical baseline toxicity prediction model (eq 23) are given in Table 4. Detailed information can be found in *Publication 2*.

As shown in Figure 15a, the measured $EC_{10,nom}$ of the agonistic effects on PPARγ, AREc32, AhR and neurotoxicity, as well as suppression ratio of 20% ($EC_{SPR20,nom}$) of the antagonistic effects on PPARγ were compared with the $IC_{10,nom,baseline}$ from anionic or neutral baseline toxicity prediction models. The SR_{nom} of most PFAS were within 0.1-10, indicating that the effects of PFAS in the tested assays are nonspecific and caused by baseline toxicity. Only HFPO-DA had a SR_{nom} >10 for the agonistic mode of PPARγ assay, indicating HFPO-DA may be a specific PPARγ agonist.

As shown in Figure 15b, Evans et al.(2022) studied agonistic effects of 16 PFAS on five defined targets from human or rat, including hPPARγ, rPPARγ, hPPARα, rPPARα and hER. The $EC_{10,nom}$ were re-calculated from their data and divided by $IC_{10,nom,baseline}$ from the anionic- or neutral-generic models. HFPO-DA, HFPO-DA-AS, PFMOAA showed SR_{nom} > 10, and the other 13 PFAS either had no effects or had 0.1 < SR_{nom}<10 and were therefore classified as baseline toxicants.

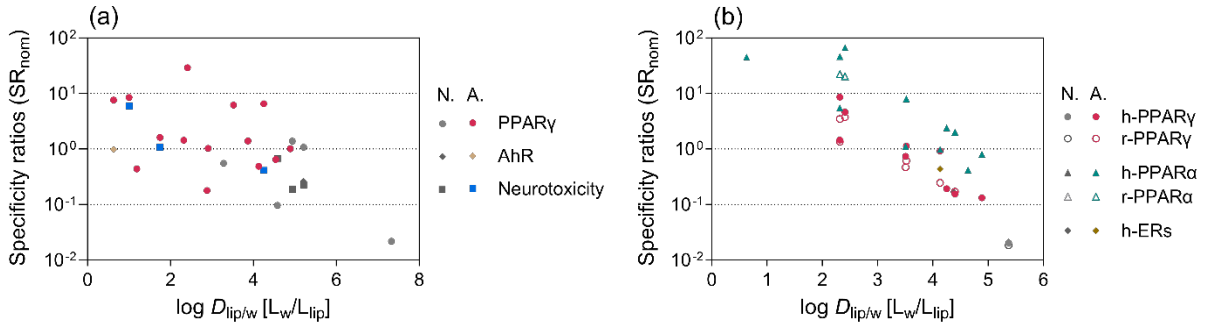

Figure 15. Specificity ratios (SR_{nom}, eq 28) of PFAS in cell-based bioassays. **(a)** SR of 16 anionic (A.) and 8 neutral (N.) PFAS in cell-based bioassays of PPARγ, AhR and neurotoxicity measured in this thesis. **(b)** SR_{nom} of 12 anionic and 4 neutral PFAS in cell-based bioassays of human (h) PPARγ, rat (r) PPARγ, hPPARα, rPPARα and human estrogen receptors (hERs) from Evans et al. (2022). Detailed information can be found in *Publication 2*.

3. Implications of findings

In this chapter, key findings are collected to present the achievement of doctoral study. Implications from these findings are discussed for further applications. A better understanding of bioavailability and species differences of PFAS in cell-based bioassays and human plasma would improve the accuracy of QIVIVE. The identification of specific from nonspecific effects would facilitate risk assessment of PFAS using data from cell-based bioassays.

3.1 Key findings

The SPME methods were developed and optimized in this thesis to study the binding of PFAS to various biomaterials over 3-4 orders of magnitude in concentrations with small sample volumes. Only 180 µL of samples of non-volatile PFAS were needed for C18-SPME and BioSPME combined with LCMS, and 5 mL of samples of semi-volatile FTOHs for head-space SPME combined with GCMS. These volumes are lower than the volumes used in traditional dialysis experiments. The versatile C18-SPME are expected to apply for PFAS with more biomaterials.

The nonlinear binding isotherms of anionic PFAS with proteins and plasmas were characterized by a Freundlich-type model and the specific and nonspecific binding constants were further derived by the combined binding/partitioning model (Table 3). The binding isotherms of PFAS over a wide concentration range depict a broader view to better understand the concentration-dependent protein binding (Figure 6). The binding constants of anionic and neutral PFAS derived by different binding models demonstrated their different binding behaviors.

Differences were found between the binding isotherms of some anionic PFAS with human and trout (fish) plasma in low concentrations (Figure 8), which can be explained by different contents of proteins and lipids. Their binding constants were predicted by MBMs and all the predicted results were within a factor of ten compared to the experimental values for human and trout plasmas (Figure 9a-b), suggesting that the plasma binding across species or between individuals could be predicted if the binding constants of proteins and lipids for PFAS and volume fractions of proteins and lipids in the plasmas are known.

QIVIVE ratios are defined with nominal and free concentrations of chemicals in human plasma and in bioassays. $QIVIVE_{free}$ ratios << $QIVIVE_{nom}$ ratios (Figure 11) can be explained by the concentration-dependent protein bindings of anionic PFAS, where a high-affinity specific binding with plasma proteins at low concentrations and lower nonspecific binding with medium proteins at high concentrations. The free concentrations are bioavailable and can be predicted well with MBMs, which facilitates the realization of using $QIVIVE_{free}$ ratio with cell-based HTS database to inform risk assessment for human beings.

PFAS were found to have toxic effects in cell-based HTS, but the ratios between $IC_{10,nom,baseline}$ of baseline toxicity and $IC_{10,nom}$ of cytotoxicity or EC_{nom} of defined target response, namely TR_{nom} (Figure 14) or SR_{nom} (Figure 15) of most PFAS in this thesis or from literatures were within 0.1-10. This indicates the effects of these PFAS in the tested bioassays were nonspecific and more likely to be caused by baseline toxicity. The bioassay-specific baseline toxicity prediction models are supposed to predict the $IC_{10,nom,baseline}$ that serves a reference to define the cytotoxicity and specificity for more chemicals if more raw data of cell-based HTS are publicly available.

3.2 Species difference in plasma binding

Animal cell lines are widely used because they are easily available and can be derived for disease-specific animal models (Reza Khorramizadeh et al. 2020). Besides, *In vitro* cell responses can be verified by *in vivo* animal studies. Understanding species difference of PFAS in plasma binding would contribute to the effective extrapolation from *in vitro* animal cell model and *in vivo* animal model to potential human adverse outcomes.

Trout (fish) plasma was used as a case study in this thesis because PFAS are widely detected in aquatic environment and the trout is commonly used as a model organism for health assessment of aquatic ecosystems. The trout plasma used in this study contained 1.5 time more lipids than human plasma lipids, while the proteins less than half of the human plasma proteins, leading to the different binding constants of trout and human plasmas. Binding constants are important parameters for the free concentration that is relevant to bioavailability. The binding of PFAS to plasma dependents not only by the affinities to proteins and lipids but also the amount of proteins

and lipids in the plasma. For risk assessment it should also be considered that the amount of proteins and lipids in plasma is influenced by many factors, such as diet, environmental conditions and health status, which exist not only between species but may also exist between individuals.

3.3 Quantitative *in vitro* to *in vivo* extrapolation

The conventional process of QIVIVE is complex because it needs to consider the concentration changes of chemicals in the absorption, distribution, metabolism and excretion, as well as species differences. The simulation involves a series of physiological parameters, which limits the application of QIVIVE. In a simple way, the QIVIVE ratio of plasma concentrations *in vivo* divided by the effect concentrations *in vitro*, directly links the cell-based HTS data to inform risk assessment. Even though many intermediate steps are skipped, the results are still informative if the free concentrations can be used to present the bioavailability (i.e. internal concentrations) of PFAS in plasma and bioassay medium.

As an illustrative example, PFBA, PFOA, PFHxS and PFOS were selected to demonstrate the significance of using free concentrations for the QIVIVE ratio. The $C_{free,plasam}$ and $EC_{free,bioassay}$ can be predicted by MBMs well with the experimental binding constants of $D_{plasma/w}$, $D_{medium/w}$ and $D_{cell/w}$, all of which can be further simplified with distributions of proteins and lipids, where $D_{BSA/w}$ and $D_{lip/w}$ are used. Compared with complex biomaterials, the binding constants of proteins and lipids are easier to measure and predictable with mature experimental and computational methods, yielding reliable $D_{BSA/w}$ and $D_{lip/w}$ for neutral chemicals. But for ionizable chemicals, a concentration-dependent $D_{BSA/w}$ was observed. Still a (more complex) MBM could be developed to predict C_{free}. That means, it will not always be necessary to measure C_{free} of PFAS but existing epidemiological data and cell-based HTS data based on nominal concentrations can be converted to free concentrations using the MBMs for quick assessment of large scale for PFAS and other chemicals.

3.4 Baseline toxicity in cell-based bioassays

Baseline toxicity can be widely used in various cell-based bioassays because it is caused by the nonspecific accumulation of chemicals on membrane exceeding critical membrane burden which is independent of cell lines and chemicals. Baseline toxicity prediction models are derived from MBMs that link the constant critical membrane concentration to the nominal concentrations of chemicals in bioassay medium. This process considers two kinds of factors, namely chemical characteristics of the affinities to proteins and lipids, as well as bioassay-specific conditions of medium and cells.

Four cell-based HTS were used as cases to demonstrate the development process of baseline toxicity prediction models for anionic PFAS and neutral chemicals. The baseline toxicity prediction models can be adapted to any kind of cell-based bioassays if the volume fractions of proteins and lipids in assay medium and cells are known. Otherwise, the generic model developed in this thesis is competent to provide a reference concentration of baseline toxicity to evaluate bioassay data with disclosed conditions. The $D_{lip/w}$ is the only input parameter to predict the $IC_{10,nom,baseline}$ under specific experimental conditions. TR_{nom} and SR_{nom} can help to define the specificity level of cytotoxicity and defined target responses. Such information is useful to screen out individual chemicals with obvious toxic effects for PFAS regulation, as well as to identify the specific MIEs and KEs for the verifications of AOPs related to PFAS.

4. Recommendations for future studies

In the final chapter, some recommendations based on current research are put forth to explore the intricate toxic mechanisms of PFAS-induced adverse outcomes on human and environmental health. A testing strategy that considers the baseline toxicity of PFAS may help to avoid some artifacts of cellular response in the era of high-throughput screening. A conceptual framework of PFAS-AOP networks may serve for single and mixed PFAS in the prediction of toxic mechanisms. Acute and chronic effects of PFAS mixture may better represent the actual exposure of PFAS in human bodies.

4.1 Testing strategy for PFAS in cell-based bioassays

A large number of chemicals in cell-based HTS are usually tested with a constant concentration range using automated pipetting systems and the C_{nom} were used in CRCs to evaluate the bioeffects of tested chemicals in most of case studies. This may underestimate the effects of chemicals or cause artifacts of cell responses.

Chemicals bind to components of bioassay medium and cells leading the C_{free} lower than the C_{nom}, especially for hydrophobic chemicals. The potency of hydrophobic chemicals will be underestimated if a constant range with only C_{nom} were used in CRCs to derive the IC_{nom} or EC_{nom} for all chemicals. Lower concentrations suggest higher potency of chemicals on the cytotoxicity or cell response of defined targets. For example, $IC_{10,free}$ of hydrophilic PFBA (log $D_{lip/w}$ = 1) was 2-time lower than its $IC_{10,nom}$ in the PPARγ-PPARγ-GeneBLAzer reporter gene assays, while the $IC_{10,free}$ of hydrophobic PFOS (log $D_{lip/w}$ = 4.85) was 12-time lower than its $IC_{10,nom}$. It is suggested to use C_{free} in the CRCs to derive the $IC_{10,free}$ or EC_{free} for data evaluation. In addition, a negative artifact may be caused by too low C_{free} to trigger cell response for some hydrophobic chemicals that highly bind to proteins and lipids in the bioassay systems. For example, the hydrophobic PFUnA (log $D_{lip/w}$ = 4.54) had $C_{free,medium}$ up to 90 times lower than C_{nom}. If the dosed concentrations (C_{nom}) were not high enough, there may not be much bioavailable C_{free} for cellular uptake.

The design of concentration range should consider both chemical characteristics and bioassay-specific conditions, which are well integrated into our baseline toxicity prediction models. The highest exposure concentration is suggested to be slightly higher than $IC_{10,nom,baseline}$ if the solubility of chemicals allows, to avoid recording no response

because the dosage was too low. The evaluation of cellular response is suggested to consider a positive artifact if the $IC_{10,nom}$ is near $IC_{10,nom,baseline}$ where cytotoxicity burst may occur when cell are close to death.

A process of experimental design for cell-based HTS:

a) **Model development.** A bioassay-specific baseline toxicity prediction model can be obtained by inserting the volumes of proteins or lipids of the medium and cells to derive system parameters a,b,c in eq 25 via exponential fit.

b) **Baseline toxicity.** $IC_{10,nom,baseline}$ can be predicted with $D_{lip/w}$ of individual chemicals with baseline toxicity prediction models for either anionic or neutral chemicals.

c) **Chemical grouping.** Tested chemicals with similar $IC_{10,nom,baseline}$ are grouped together and a value as the highest dosing concentration is determined for the group, so that all chemicals can be measured in the same concentration ranges under similar operations but avoid artifacts.

d) **Solubility testing.** Chemicals with the highest dosing concentration are prepared in bioassay medium. It is important to make sure the chemical is dissolved well before the exposure. Some acidic or alkaline chemicals require pH adjustment to 7.4 before being checked for their solubility and used for bioassays.

e) **Dilution process.** A dilution factor depends on the highest dosing concentration and the number of concentration points for individual chemicals in one testing plate. It is suggested to develop CRC with a wide range covering 2-3 orders of magnitude in concentrations in order to catch effect concentrations for chemicals with different potencies.

f) **Toxicity evaluation.** $IC_{10,nom,baseline}$ of baseline toxicity serves as a reference to compare with $IC_{10,nom}$ of cytotoxicity and EC_{nom} of selected target responses to define the degree of cytotoxicity and specificity of tested chemicals.

If it is difficult to obtain the bioassay-specific volumes of proteins and lipids in the medium and cells, the generic models that are derived with a general condition using 10% fetal bovine serum in *Publication 2*, can provide $IC_{10,nom,baseline}$ as a reference value. The $D_{lip/w}$ from experiments is given priority, otherwise, it can be predicted by models, such as COSMOtherm (Lampic et al. 2020), poly-parameter linear free energy relationships (PP-LFERs) (Endo et al. 2014) or simple QSARs based on the octanol-water partition constant

(K_{ow}) (Endo et al. 2011a). There are several options to improve the solubilization of the tested chemical in bioassay medium, such as preheating dosing medium to the temperature for the cell incubation (e.g. 37℃), as well as sonication in warm water for 10 min. This does not affect the solubility itself but may speed up the process of solubilization.

$IC_{10,nom,baseline}$ is a reference to design the concentration range for bioassay and it needs to be adjusted according to the cellular responses. The sensitivity of specific targets may be different for the tested chemical. A good concentration-response curve can be obtained after adjusting concentration ranges with suitable dilution factors. For those chemicals with specific effects, especially of the effect occurs in a concentration range far below $IC_{10,nom,baseline}$, the minimum concentration needs to be lower until catching the lowest effect concentration (e.g. 10% cell responses). If there is no effect observed at $IC_{10,nom,baseline}$, the maximum concentration needs to be higher until the limit of solubility, because there may be one order of magnitude of deviation in the baseline toxicity prediction model.

4.2 Specific effects of PFAS in adverse outcome pathways

The AOP concept illustrates how chemical exposure initiate the molecular event and disrupt the key events through the pathway, leading to adverse outcomes in molecule, organs, organisms and ultimately in populations and the ecosystem. PFAS are qualified candidate for a case study due to a big data support in the past decades from globally epidemiological investigations suggesting correlations of PFAS exposed and biomarkers related to specific diseases, as well as various toxicological studies proving signaling pathways mediated by PFAS. The persistence and bioaccumulation of PFAS allow continuously external exposure to human and gradually internal accumulation of PFAS to the levels that may induce adverse outcomes. Validated PFAS-relevant AOPs can inform risk assessment based on intermediate effects without going through the whole pathway, thereby avoiding the need for *in vivo* testing. Since cell responses can serve as early warning signals, new methods targeting the MIE or KEs developed from cell-based bioassays, such as cell-based HTS, enable the next generation risk assessment (NGRA) of chemicals. Some recommendations for the development of AOPs for PFAS are discussed.

(1) Qualitative AOPs based on epidemiological and toxicological studies

Escher et al. (2017) complemented AOP concept with exposome and aggregate exposure pathways (AEP), which allocated the MIEs or KEs to steps from the source of exposure to adverse outcomes. Integrating information of PFAS from environmental monitoring, toxicological and epidemiological studies into the AEP-AOP framework, depicted Figure 16 as an illustrative case, demonstrating a qualitatively causal link at human exposure level of PFAS to the adverse outcome observed, namely qualitative AOPs. There are six categories of PFAS that are widely found in environment media (Ankley et al. 2021). The concentrations of PFAS from different environmental media (Seo et al. 2019) and foods (Mesfin Tefera et al. 2022) were the sum of all the mean values of PFAS in the studies as external exposure. The internal exposure concentrations of plasma, urine and organs were collected from general populations (Cakmak et al. 2022; Jian et al. 2018; Perez et al. 2013), as well as firefighters (Rotander et al. 2015) and workers or residents near the chemical plants (Peng et al. 2021). Many common MIEs, KEs and AOs have been found to be relevant to PFAS according to previous review studies (Fenton et

al. 2021; Guan et al. 2022; Gundacker et al. 2022; Kaiser et al. 2022), and hence the relationship of these bioeffects can present some common pathways for toxic PFAS.

Linear AOPs can be developed by connecting the bioinformatics correlation of the MIE and different KEs, and the AOP network can be further developed by overlaying the same KEs from different linear AOPs. To obtain more detailed information for the AOP network developments, hepatotoxicity was selected as the defined AO. Literature studies related to hepatotoxicity were collected to link PFAS to AOPs (Abe et al. 2017; Beggs et al. 2016; Cwinn et al. 2008; Filgo et al. 2015; Han et al. 2018; Kim et al. 2023; Li et al. 2017; Liu et al. 2017; Minata et al. 2010; O'Brien et al. 2013; Rowan-Carroll et al. 2021; Seacat et al. 2003; Son et al. 2008; Wolf et al. 2008).

These experimental results included molecular interactions, genomics, proteomics, enzyme activities, cellular signal detections, animal histopathology. Integration of these information depicted Figure 17 as an illustrative case. The AOP networks are relevant to hepatotoxicity of PFAS. Since these studies were carried out for different research purposes, the pathways usually started or ended at different levels, but it is obvious that many PFAS shared same MIEs and KEs, leading to similar AOs. A common mechanism of hepatotoxicity is the interactions of PFAS with receptors, which may disrupt the subsequent receptor-mediated signaling pathways, for example the expression of genes that regulate the triglyceride production or metabolism. These signals may further change the cell states or cellular activities, such as fatty acid beta-oxidation and fatty acid trafficking. A long-term accumulation of triglyceride would cause cell inflammation, cell necrosis and even liver steatosis. Notably, Figure 17 is not derived from a systematic literature review or strictly developed as the AOP wiki (https://aopwiki.org/), but the demonstrated case for the rapid development of AOP network based on the common pathways collected from literature studies.

The development from linear AOPs to AOP networks provides a strategy to study toxicity of PFAS from individual to mixture. PFAS share molecular targets that lead to similar outcomes, albeit with different potency. For example, the competitive protein bindings of PFAS with thyroid hormone transport proteins (TTR and TBG) (Ren et al. 2016), peroxisome proliferator activated receptors (PPARs) (Li et al. 2019), membrane G protein-coupled receptor (GPR) 40 (Qin et al. 2020), demonstrated well that the potency in interacting with protein receptors had some relationship with PFAS chain length.

Considering the structural similarity of highly fluorinated PFAS, it is easy to infer PFAS mixtures can act on the same pathway. Besides, individual PFAS can act on multiple targets simultaneously. Therefore, a total concentration of PFAS mixture can be the sum of all individual PFAS measured from the same samples, which is considered as a whole exposome, and then AOP networks can be used to reveal the toxic mechanisms of mixtures via concentration addition, which further explains that low concentrations of individual PFAS in human blood are yet correlated to human diseases (Figure 16).

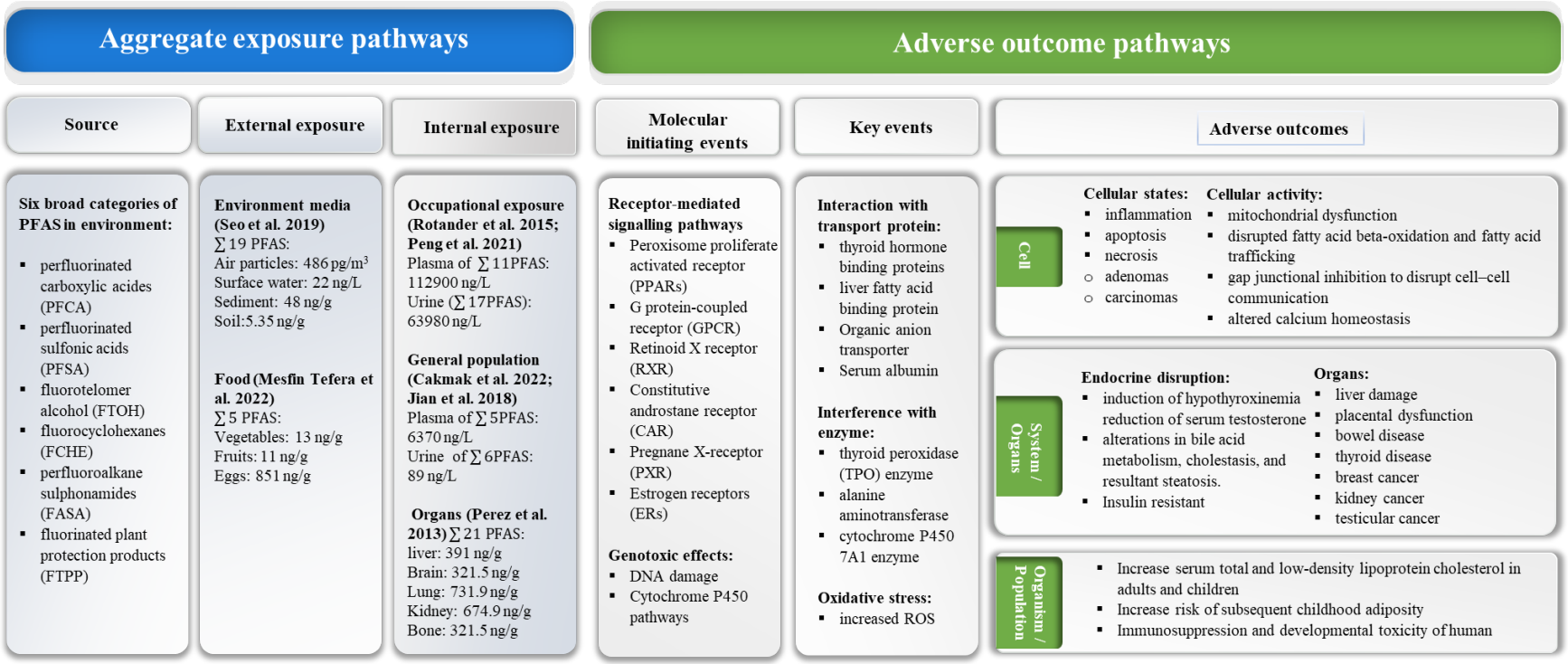

Figure 16. Aggregate exposure pathway and adverse outcome pathway (AEP-AOP) for PFAS. This figure is based on the generic figure in Escher et al. (2017).

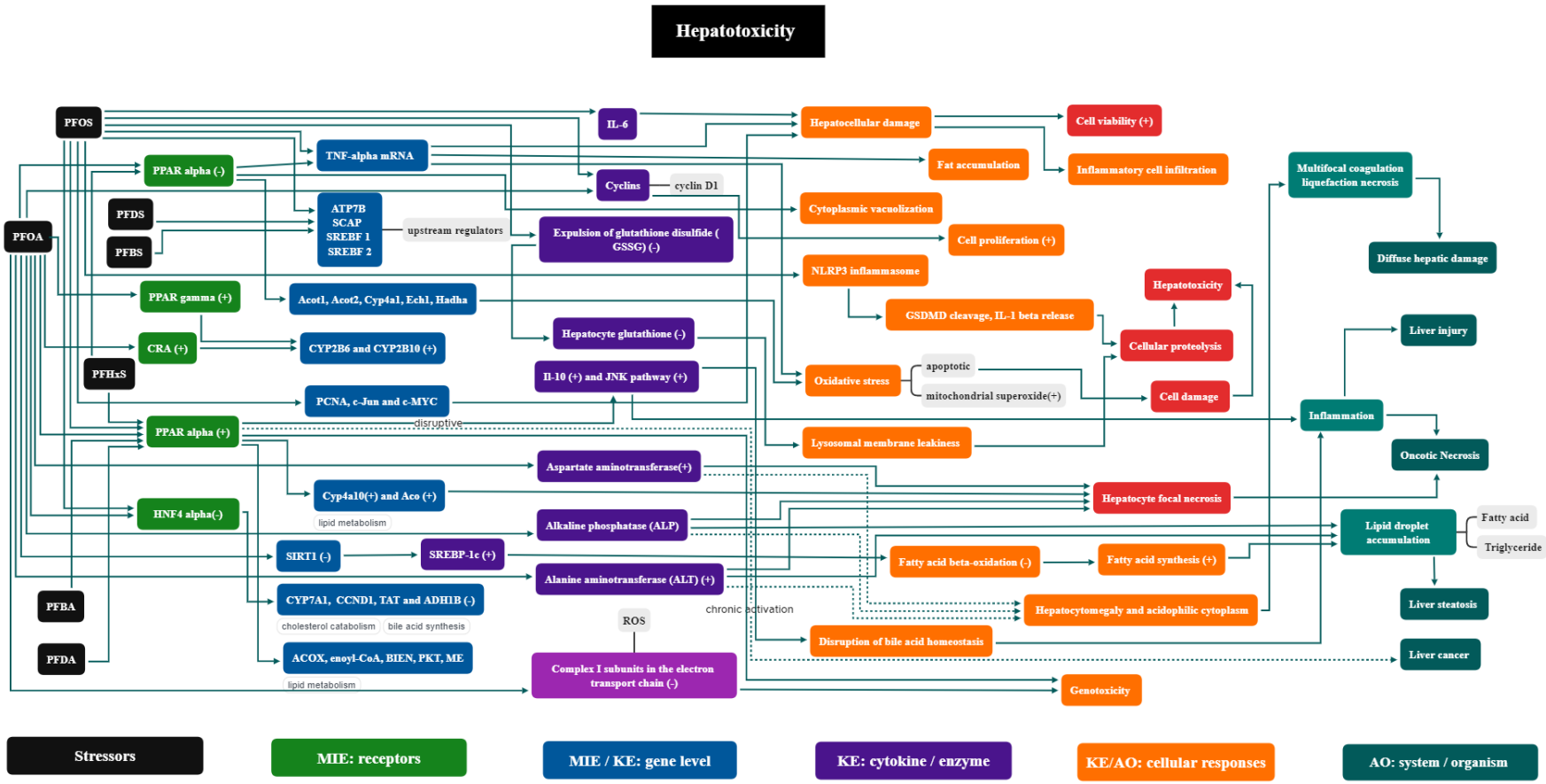

Figure 17. An illustrative case of adverse outcome pathway (AOP) networks for PFAS targeting at hepatotoxicity based on the literature information

(2) Quantitative AOPs with quantified specificity degree

The selectively initiating of PFAS among AOP networks is expected to be characterized by the quantified specificity degree of the MIE and KEs. In general, lower effect concentration of the defined targets stimulated by individual chemicals is related to higher specificity. Although the concentration-response and time-course relationships of the individual KE can be found in many toxicological studies, there is insufficient scientific data or evidence to indicate the response of upstream KE can trigger the occurrence of downstream KE, gradually leading to observed AOs. More authoritative AOPs can be found in the AOP wiki (https://aopwiki.org/), which relies on the collective weight of evidence and consensus of the scientific community. The key event relationship (KERs) is a critical element in AOPs but challenged by intricate interactions between different biological components (genes, proteins, cells, tissues and organs), as well as the limitations of experimental conditions and the variabilities of data evaluations. The development of quantitative AOPs needs continuous efforts.

At present Tox21/ToxCast is performing HTS for 430 PFAS on hundreds of targets (https://comptox.epa.gov/dashboard/chemical-lists/EPAPFASINV), providing an opportunity for the development of PFAS-relevant AOPs. As the case study in subchapter 2.3.2, $IC_{10,nom,baseline}$ from the baseline toxicity prediction model considering the chemical characteristics and bioassay-specific conditions, can be a reference concentration to derive a dimensionless specificity ratio SR_{nom} with effect concentration (e.g. $EC_{10,nom}$) once these screening data become publicly available. It will advance the quantitative AOPs if the SR_{nom} of hundreds of targets be derived for PFAS and allocated appropriately in the AOP networks. As signalling from linear to network, the SR values of junction KEs may act as traffic light to indicate the direction of signal path, leading to different or related outcomes.

A process of PFAS-relevant AOP development:

a) **Qualitative AOPs**: Linear AOP can be developed by integrating information from literatures that are collected and grouped for one specific adverse outcome each time. AOP networks can be developed by converging same and similar KEs from different linear AOPs.

b) **Quantitative AOPs:** Concentration-response and time-course relationships of the KEs with frequent repetition in different AOPs are collected. The effect concentrations of the defined targets need to be converted to equivalent values that can be compared among experiments. For example, a specificity ratio (SR) for cell-based bioassays. The conversion criteria should be designed according to the experimental conditions.
c) **Expansion of AOPs**: Specific effects of defined targets can be identified with the SR value from Tox21/ToxCast database. These targets are integrated into the established AOPs based on their bioinformatics correlations to further upgrade AOP networks.
d) **Prediction potential risk with AOPs**: Human exposure of PFAS are presented by concentrations of individual PFAS and mixture in human blood and urine. Established AOPs link the human exposure concentrations to potential outcomes if the probability of occurrence of individual AOPs can be predicted.

4.3 Mixture effects and concentrations of PFAS

Currently, *in vitro* effect data of 160 PFAS from EPA have been published, including activation on nuclear receptor-mediated signaling pathways (Houck et al. 2021), immunotoxicity (Houck et al. 2023), developmental neurotoxicity (Carstens et al. 2023), thyroid disruption (Stoker et al. 2023). These results indicated bioactivity for less than 30% of the tested PFAS (< 50/160), while a majority of PFAS (> 100/160) was inactive or equivocal. The bioactivation may include the effects from both specific and nonspecific (e.g. baseline toxicity) pathways. If the inactivation of individual PFAS is due to not enough C_{free} to trigger any cell responses, it is still possible that PFAS mixture trigger the effects via concentration addition.

Some ionized PFAS may be actively transported into cells via ion channels or transport proteins, but due to their high membrane permeability, passive diffusion has been proved to dominate the cellular uptake of PFAS from medium into cytosol (Ebert et al. 2020). Some PFAS with high bioactivity may specifically trigger signalling pathways at very low intracellular concentrations, where the cell membrane is still intact and functionable. While most of PFAS that act like baseline toxicants are prone to accumulate in the cell membrane until to induce cytotoxicity by disrupting the membrane functions and even destroy the integrity of membrane. The establishing of mixture concentration-response relationship is important to study the mechanism of mixture effects. Here, two exposure strategies for studying the toxic effects of PFAS mixture are suggested for future studies.

(1) Acute stimulation.

The affinities of PFAS to proteins can vary by orders of magnitude depending on their hydrophobicity. The free concentration of PFAS mixture in protein-rich medium may be significant differences between hydrophilic and hydrophobic ones, and thus difficult to quantify. One strategy is to prepare PFAS mixture in protein-free medium (e.g. no foetal bovine serum) until the highest solubility of mixture, and then to dilute the sample for a series of concentrations. The cells are exposed to the PFAS mixtures for several hours (e.g. 0.5, 1, 2, 4, 6,12 h) to trigger cellular stress response.

This method ensures a sufficiently high C_{free} of the PFAS mixture. The C_{free} is measurable because the matrix is rather simple. The C_{free} can also be predicted by validated MBMs assuming all PFAS dissolved well and negligible loss to other compartments. It is possible to observe some cellular stress response during acute exposure ($\leq$ 24 h) without the obfuscation due to cellular self-repair or adaptation.

(2) Sub-chronic exposure.

The process of PFAS binding to medium protein is usually reversible, which maintains C_{free} at a relatively stable level within the typical exposure time of 24 h. A second strategy can be used to study the long-term effects of PFAS mixture by serially diluting the mixture with protein-containing medium. The cells are exposed to the PFAS mixtures for days (e.g. 1, 2, 3 days) to induce measurable signals.

This method can be used to study some complex AOPs in cellular level, such as receptor-mediated signal pathways. The protein binding would increase the apparent solubility of hydrophobic PFAS in dosing medium, making it possible to study the baseline toxicity of hydrophobic PFAS at high concentrations.

Comprehensive assessment of cellular responses to PFAS mixtures requires a consideration of both acute and chronic changes. Time-course relationship can be obtained by detecting the cellular responses over a designed time period. The C_{free} of PFAS mixtures after exposure can be extracted with SPME and quantified by LCMS to establish the concentration-response curves. Both time-course and concentration-response relationships would contribute to a better understanding of how toxicokinetic and toxicodynamic processes of PFAS are connected.

5. References

Abe, T.; Takahashi, M.; Kano, M.; Amaike, Y.; Ishii, C.; Maeda, K.; Kudoh, Y.; Morishita, T.; Hosaka, T.; Sasaki, T.; Kodama, S.; Matsuzawa, A.; Kojima, H.; Yoshinari, K. Activation of nuclear receptor CAR by an environmental pollutant perfluorooctanoic acid. Arch Toxicol 2017;91:2365-2374

Allendorf, F.; Berger, U.; Goss, K.U.; Ulrich, N. Partition coefficients of four perfluoroalkyl acid alternatives between bovine serum albumin (BSA) and water in comparison to ten classical perfluoroalkyl acids. Environ Sci Process Impacts 2019;21:1852-1863

Ankley, G.T.; Cureton, P.; Hoke, R.A.; Houde, M.; Kumar, A.; Kurias, J.; Lanno, R.; McCarthy, C.; Newsted, J.; Salice, C.J.; Sample, B.E.; Sepulveda, M.S.; Steevens, J.; Valsecchi, S. Assessing the Ecological Risks of Per- and Polyfluoroalkyl Substances: Current State-of-the Science and a Proposed Path Forward. Environ Toxicol Chem 2021;40:564-605

Arp, H.P.; Niederer, C.; Goss, K.U. Predicting the partitioning behavior of various highly fluorinated compounds. Environ Sci Technol 2006;40:7298-7304

Bao, J.; Shao, L.X.; Liu, Y.; Cui, S.W.; Wang, X.; Lu, G.L.; Wang, X.; Jin, Y.H. Target analysis and suspect screening of per- and polyfluoroalkyl substances in paired samples of maternal serum, umbilical cord serum, and placenta near fluorochemical plants in Fuxin, China. Chemosphere 2022;307:135731

Beggs, K.M.; McGreal, S.R.; McCarthy, A.; Gunewardena, S.; Lampe, J.N.; Lau, C.; Apte, U. The role of hepatocyte nuclear factor 4-alpha in perfluorooctanoic acid- and perfluorooctanesulfonic acid-induced hepatocellular dysfunction. Toxicol Appl Pharmacol 2016;304:18-29

Behr, A.C.; Plinsch, C.; Braeuning, A.; Buhrke, T. Activation of human nuclear receptors by perfluoroalkylated substances (PFAS). Toxicol In Vitro 2020;62:104700

Cakmak, S.; Lukina, A.; Karthikeyan, S.; Atlas, E.; Dales, R. The association between blood PFAS concentrations and clinical biochemical measures of organ function and metabolism in participants of the Canadian Health Measures Survey (CHMS). Sci Total Environ 2022;827:153900

Calvert, L.; Green, M.P.; De Iuliis, G.N.; Dun, M.D.; Turner, B.D.; Clarke, B.O.; Eamens, A.L.; Roman, S.D.; Nixon, B. Assessment of the Emerging Threat Posed by

Perfluoroalkyl and Polyfluoroalkyl Substances to Male Reproduction in Humans. Front Endocrinol (Lausanne) 2021;12:799043

Carstens, K.E.; Freudenrich, T.; Wallace, K.; Choo, S.; Carpenter, A.; Smeltz, M.; Clifton, M.S.; Henderson, W.M.; Richard, A.M.; Patlewicz, G.; Wetmore, B.A.; Paul Friedman, K.; Shafer, T. Evaluation of Per- and Polyfluoroalkyl Substances (PFAS) In Vitro Toxicity Testing for Developmental Neurotoxicity. Chem Res Toxicol 2023;36:402-419

Cwinn, M.A.; Jones, S.P.; Kennedy, S.W. Exposure to perfluorooctane sulfonate or fenofibrate causes PPAR-alpha dependent transcriptional responses in chicken embryo hepatocytes. Comp Biochem Physiol C Toxicol Pharmacol 2008;148:165-171

DeWitt, J.C.; Shnyra, A.; Badr, M.Z.; Loveless, S.E.; Hoban, D.; Frame, S.R.; Cunard, R.; Anderson, S.E.; Meade, B.J.; Peden-Adams, M.M.; Luebke, R.W.; Luster, M.I. Immunotoxicity of perfluorooctanoic acid and perfluorooctane sulfonate and the role of peroxisome proliferator-activated receptor alpha. Crit Rev Toxicol 2009;39:76-94

Ebert, A.; Allendorf, F.; Berger, U.; Goss, K.U.; Ulrich, N. Membrane/Water Partitioning and Permeabilities of Perfluoroalkyl Acids and Four of their Alternatives and the Effects on Toxicokinetic Behavior. Environ Sci Technol 2020;54:5051-5061

Endo, S.; Bauerfeind, J.; Goss, K.U. Partitioning of neutral organic compounds to structural proteins. Environ Sci Technol 2012;46:12697-12703

Endo, S.; Escher, B.I.; Goss, K.U. Capacities of membrane lipids to accumulate neutral organic chemicals. Environ Sci Technol 2011a;45:5912-5921

Endo, S.; Goss, K.U. Serum albumin binding of structurally diverse neutral organic compounds: data and models. Chem Res Toxicol 2011b;24:2293-2301

Endo, S.; Goss, K.U. Predicting partition coefficients of Polyfluorinated and organosilicon compounds using polyparameter linear free energy relationships (PP-LFERs). Environ Sci Technol 2014;48:2776-2784

Escher, B.I.; Eggen, R.I.; Schreiber, U.; Schreiber, Z.; Vye, E.; Wisner, B.; Schwarzenbach, R.P. Baseline toxicity (narcosis) of organic chemicals determined by in vitro membrane potential measurements in energy-transducing membranes. Environ Sci Technol 2002;36(9):1971-1979

Escher, B.I.; Glauch, L.; Konig, M.; Mayer, P.; Schlichting, R. Baseline Toxicity and Volatility Cutoff in Reporter Gene Assays Used for High-Throughput Screening. Chem Res Toxicol 2019;32:1646-1655

Escher, B.I.; Hackermuller, J.; Polte, T.; Scholz, S.; Aigner, A.; Altenburger, R.; Bohme, A.; Bopp, S.K.; Brack, W.; Busch, W.; Chadeau-Hyam, M.; Covaci, A.; Eisentrager, A.; Galligan, J.J.; Garcia-Reyero, N.; Hartung, T.; Hein, M.; Herberth, G.; Jahnke, A.; Kleinjans, J.; Kluver, N.; Krauss, M.; Lamoree, M.; Lehmann, I.; Luckenbach, T.; Miller, G.W.; Muller, A.; Phillips, D.H.; Reemtsma, T.; Rolle-Kampczyk, U.; Schuurmann, G.; Schwikowski, B.; Tan, Y.M.; Trump, S.; Walter-Rohde, S.; Wambaugh, J.F. From the exposome to mechanistic understanding of chemical-induced adverse effects. Environ Int 2017;99:97-106

Escher, B.I.; Henneberger, L.; Konig, M.; Schlichting, R.; Fischer, F.C. Cytotoxicity Burst? Differentiating Specific from Nonspecific Effects in Tox21 in Vitro Reporter Gene Assays. Environ Health Perspect 2020;128:77007

Evans, N.; Conley, J.M.; Cardon, M.; Hartig, P.; Medlock-Kakaley, E.; Gray, L.E., Jr. In vitro activity of a panel of per- and polyfluoroalkyl substances (PFAS), fatty acids, and pharmaceuticals in peroxisome proliferator-activated receptor (PPAR) alpha, PPAR gamma, and estrogen receptor assays. Toxicol Appl Pharmacol 2022;449:116136

Evich, M.G.; Davis, M.J.B.; McCord, J.P.; Acrey, B.; Awkerman, J.A.; Knappe, D.R.U.; Lindstrom, A.B.; Speth, T.F.; Tebes-Stevens, C.; Strynar, M.J.; Wang, Z.; Weber, E.J.; Henderson, W.M.; Washington, J.W. Per- and polyfluoroalkyl substances in the environment. Science 2022;375:eabg9065

Fenton, S.E.; Ducatman, A.; Boobis, A.; DeWitt, J.C.; Lau, C.; Ng, C.; Smith, J.S.; Roberts, S.M. Per- and Polyfluoroalkyl Substance Toxicity and Human Health Review: Current State of Knowledge and Strategies for Informing Future Research. Environ Toxicol Chem 2021;40:606-630

Filgo, A.J.; Quist, E.M.; Hoenerhoff, M.J.; Brix, A.E.; Kissling, G.E.; Fenton, S.E. Perfluorooctanoic Acid (PFOA)-induced Liver Lesions in Two Strains of Mice Following Developmental Exposures: PPARalpha Is Not Required. Toxicol Pathol 2015;43:558-568

Firl, N.; Kienberger, H.; Hauser, T.; Rychlik, M. Determination of the fatty acid profile of neutral lipids, free fatty acids and phospholipids in human plasma. Clin Chem Lab Med 2013;51:799-810

Franzosa, J.A.; Bonzo, J.A.; Jack, J.; Baker, N.C.; Kothiya, P.; Witek, R.P.; Hurban, P.; Siferd, S.; Hester, S.; Shah, I.; Ferguson, S.S.; Houck, K.A.; Wambaugh, J.F. High-throughput toxicogenomic screening of chemicals in the environment using metabolically competent hepatic cell cultures. NPJ Syst Biol Appl 2021;7:7

Gao, K.; Zhuang, T.; Liu, X.; Fu, J.; Zhang, J.; Fu, J.; Wang, L.; Zhang, A.; Liang, Y.; Song, M.; Jiang, G. Prenatal Exposure to Per- and Polyfluoroalkyl Substances (PFASs) and Association between the Placental Transfer Efficiencies and Dissociation Constant of Serum Proteins-PFAS Complexes. Environ Sci Technol 2019;53:6529-6538

Gao, Y.; Fu, J.; Cao, H.; Wang, Y.; Zhang, A.; Liang, Y.; Wang, T.; Zhao, C.; Jiang, G. Differential accumulation and elimination behavior of perfluoroalkyl Acid isomers in occupational workers in a manufactory in China. Environ Sci Technol 2015;49:6953-6962

Gluge, J.; Scheringer, M.; Cousins, I.T.; DeWitt, J.C.; Goldenman, G.; Herzke, D.; Lohmann, R.; Ng, C.A.; Trier, X.; Wang, Z. An overview of the uses of per- and polyfluoroalkyl substances (PFAS). Environ Sci Process Impacts 2020;22:2345-2373

Gockener, B.; Weber, T.; Rudel, H.; Bucking, M.; Kolossa-Gehring, M. Human biomonitoring of per- and polyfluoroalkyl substances in German blood plasma samples from 1982 to 2019. Environ Int 2020;145:106123

Goss, K.U.; Bronner, G.; Harner, T.; Hertel, M.; Schmidt, T.C. The partition behavior of fluorotelomer alcohols and olefins. Environ Sci Technol 2006;40:3572-3577

Guan, R.; Luan, F.; Li, N.; Qiu, Z.; Liu, W.; Cui, Z.; Zhao, C.; Li, X. Identification of molecular initiating events and key events leading to endocrine disrupting effects of PFOA: Integrated molecular dynamic, transcriptomic, and proteomic analyses. Chemosphere 2022;307:135881

Gundacker, C.; Audouze, K.; Widhalm, R.; Granitzer, S.; Forsthuber, M.; Jornod, F.; Wielsoe, M.; Long, M.; Halldorsson, T.I.; Uhl, M.; Bonefeld-Jorgensen, E.C. Reduced Birth Weight and Exposure to Per- and Polyfluoroalkyl Substances: A

Review of Possible Underlying Mechanisms Using the AOP-HelpFinder. Toxics 2022;10

Han, R.; Zhang, F.; Wan, C.; Liu, L.; Zhong, Q.; Ding, W. Effect of perfluorooctane sulphonate-induced Kupffer cell activation on hepatocyte proliferation through the NF-kappaB/TNF-alpha/IL-6-dependent pathway. Chemosphere 2018;200:283-294

Henneberger, L.; Huchthausen, J.; Wojtysiak, N.; Escher, B.I. Quantitative In Vitro-to-In Vivo Extrapolation: Nominal versus Freely Dissolved Concentration. Chem Res Toxicol 2021;34:1175-1182

Henneberger, L.; Muhlenbrink, M.; Fischer, F.C.; Escher, B.I. C18-Coated Solid-Phase Microextraction Fibers for the Quantification of Partitioning of Organic Acids to Proteins, Lipids, and Cells. Chem Res Toxicol 2019;32:168-178

Henneberger, L.; Muhlenbrink, M.; Heinrich, D.J.; Teixeira, A.; Nicol, B.; Escher, B.I. Experimental Validation of Mass Balance Models for in Vitro Cell-Based Bioassays. Environ Sci Technol 2020;54:1120-1127

Houck, K.A.; Friedman, K.P.; Feshuk, M.; Patlewicz, G.; Smeltz, M.; Clifton, M.S.; Wetmore, B.A.; Velichko, S.; Berenyi, A.; Berg, E.L. Evaluation of 147 perfluoroalkyl substances for immunotoxic and other (patho)physiological activities through phenotypic screening of human primary cells. ALTEX 2023;40:248-270

Houck, K.A.; Patlewicz, G.; Richard, A.M.; Williams, A.J.; Shobair, M.A.; Smeltz, M.; Clifton, M.S.; Wetmore, B.; Medvedev, A.; Makarov, S. Bioactivity profiling of per- and polyfluoroalkyl substances (PFAS) identifies potential toxicity pathways related to molecular structure. Toxicology 2021;457:152789

Jian, J.M.; Chen, D.; Han, F.J.; Guo, Y.; Zeng, L.; Lu, X.; Wang, F. A short review on human exposure to and tissue distribution of per- and polyfluoroalkyl substances (PFASs). Sci Total Environ 2018;636:1058-1069

Judson, R.; Houck, K.; Martin, M.; Richard, A.M.; Knudsen, T.B.; Shah, I.; Little, S.; Wambaugh, J.; Woodrow Setzer, R.; Kothiya, P.; Phuong, J.; Filer, D.; Smith, D.; Reif, D.; Rotroff, D.; Kleinstreuer, N.; Sipes, N.; Xia, M.; Huang, R.; Crofton, K.; Thomas, R.S. Editor's Highlight: Analysis of the Effects of Cell Stress and Cytotoxicity on In Vitro Assay Activity Across a Diverse Chemical and Assay Space. Toxicol Sci 2016;152:323-339

Kaiser, A.M.; Zare Jeddi, M.; Uhl, M.; Jornod, F.; Fernandez, M.F.; Audouze, K. Characterization of Potential Adverse Outcome Pathways Related to Metabolic Outcomes and Exposure to Per- and Polyfluoroalkyl Substances Using Artificial Intelligence. Toxics 2022;10

Kim, M.; Kim, S.H.; Choi, J.Y.; Park, Y.J. Investigating fatty liver disease-associated adverse outcome pathways of perfluorooctane sulfonate using a systems toxicology approach. Food Chem Toxicol 2023;176:113781

Lampic, A.; Parnis, J.M. Property Estimation of Per- and Polyfluoroalkyl Substances: A Comparative Assessment of Estimation Methods. Environ Toxicol Chem 2020;39:775-786

Lee, J.; Braun, G.; Henneberger, L.; Konig, M.; Schlichting, R.; Scholz, S.; Escher, B.I. Critical Membrane Concentration and Mass-Balance Model to Identify Baseline Cytotoxicity of Hydrophobic and Ionizable Organic Chemicals in Mammalian Cell Lines. Chem Res Toxicol 2021;34:2100-2109

Li, C.H.; Ren, X.M.; Cao, L.Y.; Qin, W.P.; Guo, L.H. Investigation of binding and activity of perfluoroalkyl substances to the human peroxisome proliferator-activated receptor beta/delta. Environ Sci Process Impacts 2019;21:1908-1914

Li, C.H.; Ren, X.M.; Ruan, T.; Cao, L.Y.; Xin, Y.; Guo, L.H.; Jiang, G. Chlorinated Polyfluorinated Ether Sulfonates Exhibit Higher Activity toward Peroxisome Proliferator-Activated Receptors Signaling Pathways than Perfluorooctanesulfonate. Environ Sci Technol 2018;52:3232-3239

Li, K.; Sun, J.; Yang, J.; Roberts, S.M.; Zhang, X.; Cui, X.; Wei, S.; Ma, L.Q. Molecular Mechanisms of Perfluorooctanoate-Induced Hepatocyte Apoptosis in Mice Using Proteomic Techniques. Environ Sci Technol 2017;51:11380-11389

Liu, H.; Wang, J.; Sheng, N.; Cui, R.; Pan, Y.; Dai, J. Acot1 is a sensitive indicator for PPARalpha activation after perfluorooctanoic acid exposure in primary hepatocytes of Sprague-Dawley rats. Toxicol In Vitro 2017;42:299-307

Liu, Y.Z.; Pan, L.H.; Bai, Y.; Yang, K.; Dong, P.P.; Fang, Z.Z. Per- and polyfluoroalkyl substances exert strong inhibition towards human carboxylesterases. Environ Pollut 2020;263:114463

Loizou, G.; McNally, K.; Dorne, J.C.M.; Hogg, A. Derivation of a Human In Vivo Benchmark Dose for Perfluorooctanoic Acid From ToxCast In Vitro Concentration-

Response Data Using a Computational Workflow for Probabilistic Quantitative In Vitro to In Vivo Extrapolation. Front Pharmacol 2021;12:630457

Long, M.; Ghisari, M.; Bonefeld-Jorgensen, E.C. Effects of perfluoroalkyl acids on the function of the thyroid hormone and the aryl hydrocarbon receptor. Environ Sci Pollut Res Int 2013;20:8045-8056

Maeder, V.; Escher, B.I.; Scheringer, M.; Hungerbühler, K. Toxic ratio as an indicator of the intrinsic toxicity in the assessment of persistent, bioaccumulative, and toxic chemicals. Environ Sci Technol 2004;38:3659-3666

Mariussen, E. Neurotoxic effects of perfluoroalkylated compounds: mechanisms of action and environmental relevance. Arch Toxicol 2012;86:1349-1367

Mesfin Tefera, Y.; Gaskin, S.; Mitchell, K.; Springer, D.; Mills, S.; Pisaniello, D. Food grown on fire stations as a potential pathway for firefighters' exposure to per- and poly-fluoroalkyl substances (PFAS). Environ Int 2022;168:107455

Minata, M.; Harada, K.H.; Karrman, A.; Hitomi, T.; Hirosawa, M.; Murata, M.; Gonzalez, F.J.; Koizumi, A. Role of peroxisome proliferator-activated receptor-alpha in hepatobiliary injury induced by ammonium perfluorooctanoate in mouse liver. Ind Health 2010;48:96-107

Mokra, K. Endocrine Disruptor Potential of Short- and Long-Chain Perfluoroalkyl Substances (PFASs)-A Synthesis of Current Knowledge with Proposal of Molecular Mechanism. Int J Mol Sci 2021;22

O'Brien, J.M.; Williams, A.; Yauk, C.L.; Crump, D.; Kennedy, S.W. In vitro microarray analysis identifies genes in acute-phase response pathways that are down-regulated in the liver of chicken embryos exposed in ovo to PFUdA. Toxicol In Vitro 2013;27:1649-1658

Ojo, A.F.; Peng, C.; Ng, J.C. Combined effects of mixed per- and polyfluoroalkyl substances on the Nrf2-ARE pathway in ARE reporter-HepG2 cells. J Hazard Mater 2022;421:126827

Patlewicz, G.; Richard, A.M.; Williams, A.J.; Grulke, C.M.; Sams, R.; Lambert, J.; Noyes, P.D.; DeVito, M.J.; Hines, R.N.; Strynar, M.; Guiseppi-Elie, A.; Thomas, R.S. A Chemical Category-Based Prioritization Approach for Selecting 75 Per- and Polyfluoroalkyl Substances (PFAS) for Tiered Toxicity and Toxicokinetic Testing. Environ Health Perspect 2019;127:14501

Peng, L.; Xu, W.; Zeng, Q.; Cheng, Y.; Zhang, Y.; Guo, Y.; Chen, D.; Jiang, C.; Wang, F. Distribution characteristics of per- and polyfluoroalkyl substances (PFASs) in human urines of acrylic fiber plant and chemical plant. Environ Sci Pollut Res Int 2021;28:69181-69189

Perez, F.; Nadal, M.; Navarro-Ortega, A.; Fabrega, F.; Domingo, J.L.; Barcelo, D.; Farre, M. Accumulation of perfluoroalkyl substances in human tissues. Environ Int 2013;59:354-362

Petriello, M.C.; Mottaleb, M.A.; Serio, T.C.; Balyan, B.; Cave, M.C.; Pavuk, M.; Birnbaum, L.S.; Morris, A.J. Serum concentrations of legacy and emerging per- and polyfluoroalkyl substances in the Anniston Community Health Surveys (ACHS I and ACHS II). Environ Int 2022;158:106907

Poulin, P.; Theil, F.P. Prediction of pharmacokinetics prior to in vivo studies. 1. Mechanism-based prediction of volume of distribution. J Pharm Sci 2002;91:129-156

Qin, W.P.; Cao, L.Y.; Li, C.H.; Guo, L.H.; Colbourne, J.; Ren, X.M. Perfluoroalkyl Substances Stimulate Insulin Secretion by Islet beta Cells via G Protein-Coupled Receptor 40. Environ Sci Technol 2020;54:3428-3436

Rappazzo, K.M.; Coffman, E.; Hines, E.P. Exposure to Perfluorinated Alkyl Substances and Health Outcomes in Children: A Systematic Review of the Epidemiologic Literature. Int J Environ Res Public Health 2017;14

Ren, X.M.; Qin, W.P.; Cao, L.Y.; Zhang, J.; Yang, Y.; Wan, B.; Guo, L.H. Binding interactions of perfluoroalkyl substances with thyroid hormone transport proteins and potential toxicological implications. Toxicology 2016;366-367:32-42

Reza Khorramizadeh, M.; Saadat, F. Animal models for human disease. Animal Biotechnology; 2020

Richard, A.M.; Lougee, R.; Adams, M.; Hidle, H.; Yang, C.; Rathman, J.; Magdziarz, T.; Bienfait, B.; Williams, A.J.; Patlewicz, G. A New CSRML Structure-Based Fingerprint Method for Profiling and Categorizing Per- and Polyfluoroalkyl Substances (PFAS). Chem Res Toxicol 2023;36:508-534

Rotander, A.; Toms, L.M.; Aylward, L.; Kay, M.; Mueller, J.F. Elevated levels of PFOS and PFHxS in firefighters exposed to aqueous film forming foam (AFFF). Environ Int 2015;82:28-34

Rowan-Carroll, A.; Reardon, A.; Leingartner, K.; Gagne, R.; Williams, A.; Meier, M.J.; Kuo, B.; Bourdon-Lacombe, J.; Moffat, I.; Carrier, R.; Nong, A.; Lorusso, L.; Ferguson, S.S.; Atlas, E.; Yauk, C. High-Throughput Transcriptomic Analysis of Human Primary Hepatocyte Spheroids Exposed to Per- and Polyfluoroalkyl Substances as a Platform for Relative Potency Characterization. Toxicol Sci 2021;181:199-214

Seacat, A.M.; Thomford, P.J.; Hansen, K.J.; Clemen, L.A.; Eldridge, S.R.; Elcombe, C.R.; Butenhoff, J.L. Sub-chronic dietary toxicity of potassium perfluorooctanesulfonate in rats. Toxicology 2003;183:117-131

Seo, S.H.; Son, M.H.; Shin, E.S.; Choi, S.D.; Chang, Y.S. Matrix-specific distribution and compositional profiles of perfluoroalkyl substances (PFASs) in multimedia environments. J Hazard Mater 2019;364:19-27

Sipes, N.S., Wambaugh, J. F., Pearce, R., Auerbach, S. S., Wetmore, B. A., Hsieh, J. H., Shapiro, A. J., Svoboda, D., DeVito, M. J. and Ferguson, S. S. An Intuitive approach for predicting potential human health risk with the Tox21 10k Library. Environ Sci Technol 2017;51:10786-10796

Son, H.Y.; Kim, S.H.; Shin, H.I.; Bae, H.I.; Yang, J.H. Perfluorooctanoic acid-induced hepatic toxicity following 21-day oral exposure in mice. Arch Toxicol 2008;82:239-246

Stoker, T.E.; Wang, J.; Murr, A.S.; Bailey, J.R.; Buckalew, A.R. High-Throughput Screening of ToxCast PFAS Chemical Library for Potential Inhibitors of the Human Sodium Iodide Symporter. Chem Res Toxicol 2023;36:380-389

Sun, P.; Nie, X.; Chen, X.; Yin, L.; Luo, J.; Sun, L.; Wan, C.; Jiang, S. Nrf2 Signaling Elicits a Neuroprotective Role Against PFOS-mediated Oxidative Damage and Apoptosis. Neurochem Res 2018;43:2446-2459

Villeneuve, D.L.; Blackwell, B.R.; Cavallin, J.E.; Collins, J.; Hoang, J.X.; Hofer, R.N.; Houck, K.A.; Jensen, K.M.; Kahl, M.D.; Kutsi, R.N.; Opseth, A.S.; Santana Rodriguez, K.J.; Schaupp, C.; Stacy, E.H.; Ankley, G.T. Verification of In Vivo Estrogenic Activity for Four Per- and Polyfluoroalkyl Substances (PFAS) Identified as Estrogen Receptor Agonists via New Approach Methodologies. Environ Sci Technol 2023;57:3794-3803

Wang, S.; Lv, Q.; Yang, Y.; Guo, L.H.; Wan, B.; Zhao, L. Cellular target recognition of perfluoroalkyl acids: in vitro evaluation of inhibitory effects on lysine decarboxylase. Sci Total Environ 2014;496:381-388

Wang, Z.; Buser, A.M.; Cousins, I.T.; Demattio, S.; Drost, W.; Johansson, O.; Ohno, K.; Patlewicz, G.; Richard, A.M.; Walker, G.W.; White, G.S.; Leinala, E. A New OECD Definition for Per- and Polyfluoroalkyl Substances. Environ Sci Technol 2021;55:15575-15578

Wolf, D.C.; Moore, T.; Abbott, B.D.; Rosen, M.B.; Das, K.P.; Zehr, R.D.; Lindstrom, A.B.; Strynar, M.J.; Lau, C. Comparative hepatic effects of perfluorooctanoic acid and WY 14,643 in PPAR-alpha knockout and wild-type mice. Toxicol Pathol 2008;36:632-639

Worley, R.R.; Fisher, J. Application of physiologically-based pharmacokinetic modeling to explore the role of kidney transporters in renal reabsorption of perfluorooctanoic acid in the rat. Toxicol Appl Pharmacol 2015;289:428-441

Xia, X.; Rabearisoa, A.H.; Jiang, X.; Dai, Z. Bioaccumulation of perfluoroalkyl substances by Daphnia magna in water with different types and concentrations of protein. Environ Sci Technol 2013;47:10955-10963

Yadav, A.; Amber, M.; Zosen, D.; Labba, N.A.; Huiberts, E.H.W.; Samulin Erdem, J.; Haugen, F.; Berntsen, H.F.; Zienolddiny, S.; Paulsen, R.E.; Ropstad, E.; Connolly, L.; Verhaegen, S. A human relevant mixture of persistent organic pollutants (POPs) and perfluorooctane sulfonic acid (PFOS) enhance nerve growth factor (NGF)-induced neurite outgrowth in PC12 cells. Toxicol Lett 2021;338:85-96

Yu, C.H.; Riker, C.D.; Lu, S.E.; Fan, Z.T. Biomonitoring of emerging contaminants, perfluoroalkyl and polyfluoroalkyl substances (PFAS), in New Jersey adults in 2016-2018. Int J Hyg Environ Health 2020;223:34-44

6. Thesis publications

Publication 1

Qin, W.; Henneberger, L.; Huchthausen, J.; Konig, M.; Escher, B. I. Role of bioavailability and protein binding of four anionic perfluoroalkyl substances in cell-based bioassays for quantitative in vitro to in vivo extrapolations. Environ Int 2023, 173, 107857. DOI: 10.1016/j.envint.2023.107857.

Publication 2

Qin, W.; Henneberger, L.; Glüge, J.; Konig, M.; Escher, B. I. Baseline Toxicity Model to Identify the Specific and Nonspecific Effects of Per- and Polyfluoroalkyl Substances in Cell-based Bioassays. Sci. Technol. 2024, 58, 13, 5727–5738. https://doi.org/10.1021/acs.est.3c09950.

Publication 3

Qin, W.; Escher, B. I.; Huchthausen, J.; Fu, Q.; Henneberger, L. Species Difference? Bovine, Trout and Human Plasma Protein Binding of Per- and Polyfluoroalkyl Substances. Environ Sci Technol 2024, XXXX, XXX, XXX-XXX. https://doi.org/10.1021/acs.est.3c10824

Publication 1

Role of bioavailability and protein binding of four anionic perfluoroalkyl substances in cell-based bioassays for quantitative *in vitro* to *in vivo* extrapolations

Weiping Qin[1,2], Luise Henneberger[1], Julia Huchthausen[1,2], Maria König[1] and Beate I. Escher[1,2]*

[1] Department of Cell Toxicology, UFZ–Helmholtz Centre for Environmental Research, 04318 Leipzig, Germany

[2] Environmental Toxicology, Department of Geosciences, Eberhard Karls University Tübingen, Schnarrenbergstr. 94-96, DE-72076 Tübingen, Germany

*Corresponding author Beate I. Escher − UFZ−Helmholtz Centre for Environmental Research, 04318 Leipzig, Germany; orcid.org/0000-0002-5304-706X; Email: beate.escher@ufz.de

Published in Environment International, DOI: 10.1016/j.envint.2023.107857.

Environment International 173 (2023) 107857

Contents lists available at ScienceDirect

Environment International

journal homepage: www.elsevier.com/locate/envint

Full length article

Role of bioavailability and protein binding of four anionic perfluoroalkyl substances in cell-based bioassays for quantitative *in vitro* to *in vivo* extrapolations

Weiping Qin [a,b], Luise Henneberger [a], Julia Huchthausen [a,b], Maria König [a], Beate I. Escher [a,b,*]

[a] Department of Cell Toxicology, UFZ–Helmholtz Centre for Environmental Research, 04318 Leipzig, Germany
[b] Environmental Toxicology, Department of Geosciences, Eberhard Karls University Tübingen, Schnarrenbergstr, 94-96, DE-72076 Tübingen, Germany

ARTICLE INFO

Handling Editor: Adrian Covaci

Keywords:
Per- and polyfluoroalkyl substances (PFAS)
Solid phase microextraction (SPME)
Freely dissolved concentration (C_{free})
Peroxisome proliferator-activated receptor gamma (PPARγ)
Quantitative *in vitro* to *in vivo* extrapolation (QIVIVE)

ABSTRACT

Perfluoroalkyl substances (PFAS) are persistent and pose a risk to human health. High throughput screening (HTS) cell-based bioassays may inform risk assessment of PFAS provided that quantitative *in vitro* to *in vivo* extrapolation (QIVIVE) can be developed. The QIVIVE ratio is the ratio of nominal (C_{nom}) or freely dissolved concentration (C_{free}) in human blood to C_{nom} or C_{free} in the bioassays. Considering that the concentrations of PFAS in human plasma and *in vitro* bioassays may vary by orders of magnitude, we tested the hypothesis that anionic PFAS bind to proteins concentration-dependently and therefore the binding differs substantially between human plasma and bioassays, which has an impact on QIVIVE. Solid phase microextraction (SPME) with C18-coated fibers served to quantify the C_{free} of four anionic PFAS (perfluorobutanoate (PFBA), perfluorooctanoate (PFOA), perfluorohexane sulfonate (PFHxS) and perfluorooctane sulfonate (PFOS)) in the presence of proteins and lipid, medium components, cells and human plasma over five orders of magnitude in concentrations. The C18-SPME method was used to quantify the non-linear binding to proteins, human plasma and medium, and the partition constants to cells. These binding parameters were used to predict C_{free} of PFAS in cell bioassays and human plasma by a concentration-dependent mass balance model (MBM). The approach was illustrated with a reporter gene assay indicating activation of the peroxisome proliferator-activated receptor gamma (PPARγ-GeneBLAzer). Blood plasma levels were collected from literature for occupational exposure and the general population. The $QIVIVE_{nom}$ ratios were higher than the $QIVIVE_{free}$ ratios due to the strong affinity to proteins and large differences in protein contents between human blood and bioassays. For human health risk assessment, the $QIVIVE_{free}$ ratios of many *in vitro* assays need to be combined to cover all health relevant endpoints. If C_{free} cannot be measured, they can be estimated with the MBM and concentration-dependent distribution ratios.

1. Introduction

Per- and polyfluoroalkyl substances (PFAS) are used in commercial, industrial and military products for waterproofing, grease- and heat-resistance (Gluge et al., 2020). PFAS are persistent in the environment (Evich et al., 2022), which has led to diffuse worldwide contamination, e.g., in rainwater, that regularly exceed health-based advisory values (Cousins et al., 2022). Epidemiological investigations and toxicological studies have revealed associations between exposure to PFAS and human diseases, caused by endocrine disruption (Mokra 2021), reproductive (Calvert et al., 2021) and developmental toxicity (Rappazzo et al., 2017), neurotoxicity (Mariussen 2012) and immunotoxicity (DeWitt et al., 2009).

Traditional toxicology based on *in vivo* animal testing is expensive and time-consuming, making it impossible to generate safety information for thousands of commercial PFAS. High-throughput screening (HTS) cell-based bioassays proposed by the Tox21 and ToxCast program may inform risk assessment provided that quantitative *in vitro* to *in vivo* extrapolation (QIVIVE) can be developed for HTS (Bell et al., 2018; Sipes et al., 2017). *In vitro* concentration-response curves (CRC) and thereof derived effect concentrations can be converted by QIVIVE models into equivalent *in vivo* concentrations which are further compared to the human exposure levels or translated by reverse dosimetry to external *in vivo* oral exposure (Wetmore 2015).

* Corresponding author.
E-mail address: beate.escher@ufz.de (B.I. Escher).

https://doi.org/10.1016/j.envint.2023.107857
Received 2 September 2022; Received in revised form 24 February 2023; Accepted 25 February 2023
Available online 1 March 2023

Currently, QIVIVE models use nominal concentrations (C_{nom}), but PFAS strongly bind to proteins and lipids in bioassays and blood, which will lower their bioavailability and hence the freely dissolved concentrations (C_{free}) in different ways in bioassays and blood. This problem might be more severe for the anionic PFAS due to their strong and specific binding to proteins.

Effect concentrations in HTS assays are typically based on C_{nom} because there is no routine method available to measure C_{free} in the 1536-well plates used by Tox21 and most reported C_{free} stem from 96-well plates (Huchthausen et al., 2020) or larger formats or were merely predicted (Proenca et al., 2021). Negligible-depletion solid phase microextraction (SPME) has been the choice for quantification of C_{free} of neutral organic chemicals for almost two decades (Heringa et al., 2004; Kramer et al., 2012), and the development of C18-coated fibers and SPME based on mass balances allowed the extension to ionizable chemicals in cell-based bioassay, as well as the experimental quantification of C_{free} of ionizable chemicals in complex bioassay media (Henneberger et al., 2019b; Huchthausen et al., 2020).

If C_{free} cannot be measured directly, it can be predicted with mass balance models (MBM) (Fischer et al., 2017; Proenca et al., 2021). Chemicals may specifically bind or non-specifically partition to medium components and cells, resulting in C_{free} lower than C_{nom} (Henneberger et al., 2019a; 2020). Distribution ratios of chemicals between protein and water ($D_{prot/w}$), lipid and water ($D_{lip/w}$), cell and water ($D_{cell/w}$), and their corresponding volumes ($V_{protein}$, V_{lipid} and V_{cell}) serve as input parameters in these MBM (Fischer et al., 2017). SPME has also been used to measure the binding and partition constants of ionizable chemicals to diverse biological materials and cells (Henneberger et al., 2019a). Anionic chemicals are particularly challenging because they show non-linear binding isotherms to proteins and protein-rich biomaterials (Henneberger et al., 2019a) and while the non-linearity of protein binding of diverse organic ions has been investigated, no such studies exist for anionic PFAS.

PFAS have been reported to cause numerous toxic effects *in vitro* and *in vivo* (Zeng et al., 2019). Specific interactions of PFAS with functional proteins dominate their molecular initiating events, including activation of receptor-mediated signaling pathways (Behr et al., 2020; Qin et al., 2020), interference of activities and functions of enzymes (Liu et al., 2020; Wang et al., 2014) and competitive binding with transport proteins (Ren et al., 2016). Nuclear receptors are universal in HTS testing because reporter gene technology makes the interaction of chemicals with functional proteins measurable. The peroxisome proliferator-activated receptor (PPAR) family comprises endogenous receptors of fatty acids and is involved in the homeostasis of lipid and glucose metabolism. Due to the structural similarity of PFAS and fatty acids, PPARs have been widely proven to be the specific targets for certain PFAS (Vanden Heuvel et al., 2006). A PPARγ reporter gene assay was selected as an example to show how to characterize the difference of C_{nom} and C_{free} of PFAS in HTS cell-based bioassays.

In vitro specific effects of PFAS can be linked to *in vivo* effects via QIVIVE. For example, Loizou et al. (2021) predicted *in vivo* benchmark doses (BMD) of perfluorooctanoic acid (PFOA) from *in vitro* concentration–response curves of the U.S. Environmental Protection Agency (EPA) HTS database using physiologically based pharmacokinetic (PBPK) model-reverse dosimetry. Typical PBPK models use a large group of parameters involving chemical absorption, distribution, metabolism and excretion processes (Loizou et al., 2021; Worley and Fisher, 2015). This greatly limited the application of QIVIVE for the assessments of large numbers of PFAS in screening type assessments. Sipes et al. (2017) developed an intuitive model, a ratio of maximum blood concentration *in vivo* ($C_{max,blood}$) to half-maximum effective concentration (AC50) directly from *in vitro* Tox21-HTS assay. The ratio > 1 indicated that the *in vitro* effect likely also occurred in *in vivo*. In its simplest form, a QIVIVE ratio can be calculated by dividing the plasma concentrations by the effective concentrations *in vitro* (Henneberger et al., 2021).

We selected perfluorobutanoic acid (PFBA), PFOA, perfluorohexane sulfonic (PFHxS), perfluorooctane sulfonic acid (PFOS) as representatives of acidic PFAS. They are fully deprotonated at physiological pH to the corresponding anions, perfluorobutanoate, perfluorooctanoate, perfluorohexane sulfonate and perfluorooctane sulfonate. They were selected because anionic surfactants are known for their non-linear binding to proteins. The four selected anionic PFAS are a special case of anionic surfactants and represent a wide range of hydrophobicity due to the differences in alkyl chain length and two different acid groups. Therefore, they serve for a proof of principle if existing knowledge of anionic organic chemicals can be translated to anionic PFAS.

Typically, the octanol–water partition coefficients (log K_{ow}) are used as measure of hydrophobicity, but they can only be predicted and not measured for surface-active anionic PFAS (Table 1). The octanol–water distribution ratio (log D_{ow}) is strongly dependent on pH and the concentration of counterions (Park et al., 2020) and the predicted log D_{ow} (pH 7.4) cover four orders of magnitude (Table 1). A more suitable predictor of hydrophobicity of surfactants is the distribution ratio between liposomes and water ($D_{lip/w}$). The experimental log $D_{lip/w}$ of PFBA is 1.48, which is considered to be hydrophilic, while other three PFAS with log $D_{lip/w} > 2$ are more hydrophobic (Table 2, data from Ebert et al. (2020), measured with equilibrium dialysis).

The protein binding of PFAS and partitioning to medium and cells, as well as C_{free} in the *in vitro* bioassay were studied by SPME using C18-coated fibers. The measured binding parameters were further used to predict C_{free} by MBM. Literature blood levels of PFAS of workers and residents living near fluorochemical plants (Bao et al., 2022; Gao et al., 2015) and the general population (Gao et al., 2019, https://www.cdc.gov/exposurereport/data_tables.html) were converted to C_{free} in blood with an adjusted blood-MBM using experimental plasma binding constants. An overview of the current approach can be found in Fig. 1. The cytotoxicity and specific effects of PFAS were characterized in a PPARγ reporter gene assay in agonistic and antagonistic model as a proof of principle. For a comprehensive risk assessment, a large set of responsive *in vitro* assays would need to be applied but this study is a demonstration of the importance and impact of nonlinear protein binding of anionic PFAS on QIVIVE.

2. Materials and methods

2.1. Materials

Four PFAS (purity > 98%) were used in this study. Perfluorobutanoic acid (PFBA, CAS. 375-22-4) was purchased from J&K. Perfluorooctanoic acid (PFOA, CAS. 335-67-1), perfluorohexane sulfonate potassium (PFHxS-K, CAS. 3871-99-6) and perfluorooctane sulfonate potassium (PFOS-K, CAS. 2795-39-3) were from Sigma Aldrich. All PFAS were dissolved in methanol as stock solution. Bovine serum albumin (BSA, CAS. 9048-46-8) was from Sigma-Aldrich, Rosiglitazone (CAS. 122320-73-4) and C18-coated fibers (CAT. 5728I-U) were purchased from Sigma-Aldrich. DC™ protein assay kit (CAT. 500-0114) was from Bio-red. GeneBLAzer® FRET Assay kit (LOT. 21972428) was from Invitrogen. GeneBLAzer PPARγ-UAS-bla 293H Cells (HEK293H) were purchased from Thermo Fisher. The GeneBLAzer assay medium contained 98% Opti-MEM (LOT.11058-021, Gibco), 2% charcoal-stripped FBS (cs-FBS, LOT. 2001639, Gibco) and 100 U/mL Penicillin-Streptomycin (LOT. 15140-122, Gibco). Solvents used in the assays were methanol (CAS. 67-56-1, Chemsolute), acetonitrile (CAS. 75-05-8, Chemsolute) and formic acid (CAS. 64-18-6, Honeywell).

2.2. Methods

2.2.1. Method development

Fibers with low C18-coating volume (5 mm coating length, 173 nL coating volume) were used for the hydrophobic PFOS as it showed very strong affinity for the fibers. PFOS samples were incubated at 37 °C using high-speed vortex shaker (DMS-2500, 1200 rpm around a 3.6 mm

Table 1
Predicted octanol-water partition coefficients (log K_{ow}) of the neutral and anionic species, octanol-water distribution ratios (log D_{ow}) at pH 7.4, and experimental data for binding to bovine serum albumin (BSA) of PFBA, PFOA, PFHxS and PFOS. The non-linear binding to BSA was described with a non-linear mechanistic combined binding/partitioning model, where K_d is the dissociation constant and C_{max} corresponds to the number of binding sites Eq. (14). log $K_{specific}$ Eq. (15) and log $D_{non\text{-}specific}$ Eq. (16) refer to the specific and non-specific binding to the BSA according to ν, the molar ratio of PFAS to BSA (mol_{PFAS}/mol_{BSA}, Eq. (13)). The measured bovine serum albumin (BSA) to water distribution ratios (log $D_{BSA/w}$) were also fitted as a function of the aqueous concentration C_w with a Freundlich-type model (Eq. (12)), where the slope corresponds to n_{Fr}-1 and the intercept to the Freundlich constant K_{Fr}.

Chemical	log K_{ow} (neutral species)	log K_{ow} (anionic species)	log D_{ow} (pH7.4)	Mechanistic combined binding/partitioning model					Freundlich-type model	
				K_d [μmol/L_w]	C_{max} [μmol/L_{BSA}]	C_{max} [mol/mol_{BSA}]	log $K_{specific}$ [L_w/L_{BSA}] $\nu \ll 1$	log $D_{non\text{-}specific}$ [L_w/L_{BSA}] $\nu > 1$	log $D_{BSA/w}$ [L_w/L_{BSA}] (C_w in μM)	R^2
PFBA	2.60[a]/2.95[b]	−3.76[b]	−1.22[c]	18.3	9.22×10^3	0.450	2.40	1.63	$\log D_{BSA/w} = -0.391 \times \log C_w + 2.80$	0.67
PFOA	5.68[a]/5.73[b]	−0.585[b]	1.58[c]	0.317	2.54×10^4	1.24	4.60	3.70	$\log D_{BSA/w} = -0.381 \times \log C_w + 4.32$	0.98
PFHxS	3.69[a]/5.29[b]	−1.77[b]	1.65[c]	7.44×10^{-2}	1.88×10^4	0.919	5.10	3.47	$\log D_{BSA/w} = -0.480 \times \log C_w + 4.32$	0.97
PFOS	5.77[a]	−0.153[b]	3.05[c]	6.24×10^{-3}	8.01×10^3	0.391	5.81	4.84	$\log D_{BSA/w} = -0.381 \times \log C_w + 4.91$	0.96

[a] log K_{ow} predicted average by OPERA from https://comptox.epa.gov.
[b] log K_{ow} predicted by COSMOtherm.
[c] log D_{ow} were from Park et al. (2020) and predicted by MarvinSketch from https://chemaxon.com/.

Table 2
Distribution ratios of PFBA, PFOA, PFHxS and PFOS between liposomes and water ($D_{lip/w}$) (Ebert 2020), cells and water ($D_{cell/w}$) (Eq. (11)) and plasma and water ($D_{plasma/w}$). log $D_{plasma/w}$ ($\nu < 1$) refer to the specific binding and were from experiments (Eq. (15)). log $D_{plasma/w}$ ($\nu < 1$) were also predicted by the mass balance model (MBM, Eq. (17)) with log $K_{specific}$ of BSA (Table 1) and log $D_{lip/w}$. Contributions of protein and lipid to the $D_{plasma/w}$ ($\nu < 1$).

	log $D_{lip/w}$ [L_w/L_{lip}]	log $D_{cell/w}$ [$L_w/L_{cell,prot+lip}$]	log $D_{plasma/w}$ [$L_w/L_{prot+lip}$] (experiment) at $\nu < 1$	log $D_{plasma/w}$ [$L_w/L_{prot+lip}$] (MBM) at $\nu < 1$	Contribution of protein binding	Contribution of lipid binding
PFBA	1.61[a]	2.56	2.12	2.36	98.3%	1.68%
PFOA	3.52	3.27	4.60	4.56	99.1%	0.867%
PFHxS	4.13	3.23	5.18	5.06	98.9%	1.12%
PFOS	4.89	4.19	5.96	5.77	98.7%	1.26%

[a] log $D_{lip/w}$ of PFBA was predicted with a linear relationship of log $D_{lip/w}$ and the number of fluorinated carbons of PFBA (Figure A1).

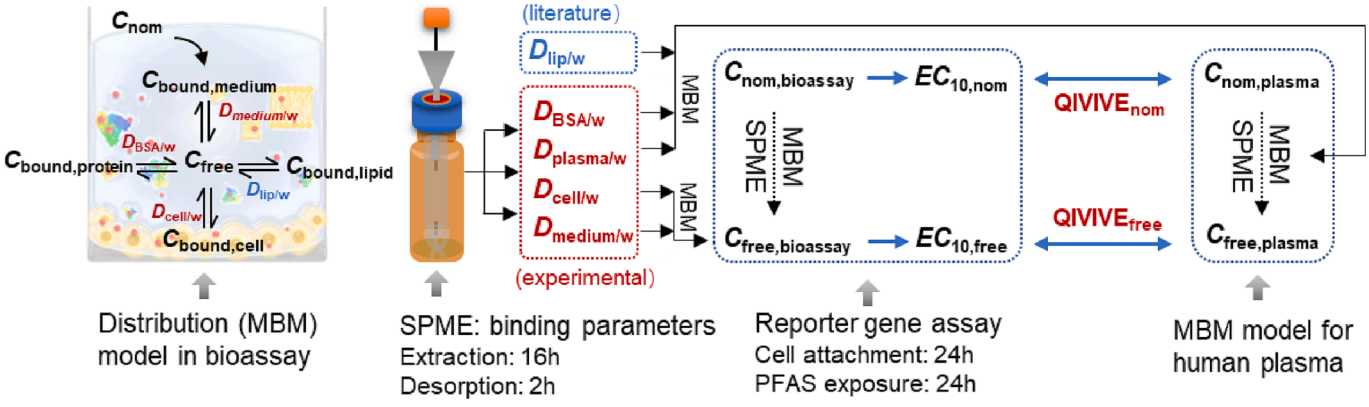

Fig. 1. An overview of the models and experiments needed to derive quantitative *in vitro* to *in vivo* extrapolation ratios (QIVIVE ratio) based on free and nominal (nom) concentrations (C_{free} and C_{nom}). Abbreviations: BSA = bovine serum albumin; $D_{i/w}$ = distribution ratio between i and water; EC = effect concentration; lip = liposome; MBM = mass balance model; SPME = Solid phase microextraction.

orbit) to accelerate adsorption. Pure solvent (100% MeOH) was used to desorb PFOS from fibers. For moderately hydrophobic PFOA, PFHxS and hydrophilic PFBA, fibers with a larger capacity (15 mm coating length, 520 nL coating volume) and a less vigorous shaking on an orbital shaker (MaxQ 6000, 250 rpm around a 19 mm orbit) was used for adsorption, and a mixed solvent (50% MeOH and 50% MilliQ water) was used for desorption. A summary of SPME method is given in Table A1.

There were three steps in the SPME process: adsorption, desorption and sample measurement. According to Henneberger et al. (2019a), C18-coated fibers were conditioned in methanol (2 h) and water (0.5 h) before being inserted to the samples.

2.2.2. Fiber uptake kinetics and sorption isotherm

Methanolic PFAS stock solutions were diluted with phosphate buffered saline (PBS). The concentrations of each PFAS are listed in Table A2. The final percentages of MeOH in samples were < 1%. The pH value of samples was adjusted to pH 7.4 using sodium hydroxide (NaOH) and hydrogen chloride (HCl) before SPME.

For adsorption kinetics, 18 aliquots of 1 mL for each PFAS solution were filled into 1.5 mL HPLC vials (ART. 7,654,554 or 7663230, Labsolute). The initial concentrations of each PFAS are listed in Table A2. The fibers were inserted into the vials individually using blunt cannulas. The samples were incubated at 37 °C using high-speed vortex shaker (1200 rpm) or orbital shaker (250 rpm) for 0.25, 0.5, 1, 2, 4, 6, 24, 48 h.

For sorption isotherm measurements, PFAS stock solutions were diluted with PBS serially with a factor of 2. The concentrations of each PFAS varied by 2–3 orders of magnitude. The concentration ranges are listed in Table A2. Duplicates of 1 mL for each concentration were filled into 1.5 mL HPLC vials. All the samples were shaken with the fibers for 16 h to reach equilibrium for adsorption.

The desorption and measurement were described in 2.2.4. Concentrations of PFAS in PBS and solvent extracts were used to calculate the recovery of the SPME method and distribution ratios of PFAS between fiber and water.

2.2.3. Partitioning to biological materials

The SPME measurement for PFAS partitioning to biological materials (BSA, plasma, medium, cells) were similar as above but different in sample preparations. For determination of protein-water distribution ratios, BSA was dissolved in PBS at a concentration of 5 g/L to aim at a fraction of PFAS bound to protein > 20%. The highest concentrations for PFBA, PFOA, PFHxS and PFOS were 2000, 500, 500 and 166 μmol/L and these concentrations were serially diluted by BSA buffer with a dilution factor of 2 to obtain 10 concentration points (Table A2). The concentration ranges of PFAS were designed to include both concentrations below and above saturation of the primary binding site as ν values (mol_{PFAS} /mol_{BSA}) ranged from 0.01 to 2. All the samples were shaken for 15 min (37 °C, 250 rpm) before aliquoting duplicates of 1 mL PFAS solution into 1.5 mL HPLC vials. The fibers were inserted into vials individually and the samples were shaken for 16 h to reach equilibrium between SPME fibers and all other components.

For determination of plasma-water distribution ratios, human plasma was diluted by PBS buffer to 20% or 4% plasma contents. PFAS solutions were serially diluted in PBS with a dilution factor of 2 to obtain 5 concentration points. 100 μL plasma buffer were transferred to HPLC vials with insert and 100 μL PFAS solution were added. The final plasma contents were then 10% or 2% and highest concentrations of PFBA, PFOA, PFHxS and PFOS were 500, 125, 125 and 50 μmol/L (Table A2). Samples were vortexed for 5 s to mix and then shaken for 15 min (37 °C, 250 rpm) before SPME.

For determination of medium-water distribution ratios, the highest concentrations for PFBA, PFOA, PFHxS and PFOS were 4000, 500, 500 and 200 μmol/L (Table A2) and GeneBLAzer assay medium was used to serially dilute PFAS in a 96-well plate with a dilution factor of 2 to obtain 10 concentration points. The bioassay medium contained 2% cs-FBS, which had proteins and lipids as sorptive phases, and the charcoal stripping (cs) was used to remove hormones and other compounds that would cause a background effect in the bioassay. Nominal PFAS concentrations ranged over 2–3 orders of magnitude while the contents of protein and lipid were constant in the experiments. 180 μL of PFAS solution were transferred from each well to HPLC vials with insert (CAT. 7648146 or 7651116, Labsolute). All the samples were shaken for 15 min (37 °C, 250 rpm) before SPME fibers were inserted.

For determination of cell-water distribution ratios, HEK293H cells were harvested by trypsinization and the number of cells was counted by CASY Counter (Roche Innovatis, Reutlingen, Germany) before centrifugation for a cell pellet. The cell pellet was resuspended with PBS at the density of 2×10^7 cells/mL. 1 mL cell suspension was homogenized by ultrasonic treatment (Sonoplus 2070, Germany) in an ice-water bath for 3×30 s to avoid protein denaturation due to localized overheating. 100 μL of cell homogenate were transferred to HPLC vials with insert and another 100 μL PFAS solution in PBS were added. Samples were vortexed for 5 s to mix and then shaken for 15 min (37 °C, 250 rpm) prior to inserting the SPME fibers.

2.2.4. Desorption and quantification of PFAS

For desorption, fibers were transferred to new vials with 100% MeOH (PFOS) or a mixture of 50% MeOH and 50% MilliQ water (PFOA, PFHxS, PFBA). The volume of samples and desorption solvents for different assays are listed in Table A3. Then, these vials were shaken with vortex or orbital shakers for another 2 h.

PFAS in PBS and all extracts were analyzed by a 1260 Infinity liquid chromatograph (LC) equipped with a Kinetex 1.7 μm, C18, 100 Å, LC column (50 × 2.1 mm) and coupled to 6420 Triple Quad mass spectrometer (MS) from Agilent. Detailed information of LC/MS analysis can be found in Table A4. All samples were diluted to concentrations in the calibration range of PFAS (1–10000 ng/L).

2.2.5. Lipid and protein quantification

Lipid and protein content of medium, cell homogenates, human plasma was determined according to Fischer et al. (2017). Protein and lipid content were quantified with protein assay kit and sulpho-phospho-vanillin reaction, respectively. Samples were diluted with MilliQ water to assure that the protein and lipid contents were within calibration ranges.

2.2.6. PPARγ reporter gene assay

The commercially available GeneBLAzer PPARγ-UAS-bla 293H cells (ThermoFisher) were cultured as described previously (Neale et al., 2017). There were four steps in GeneBLAzer Assay: cell attachment, PFAS exposure, cytotoxicity measurement and reporter protein detection.

2.2.6.1. Cell attachment. HEK293H Cells were harvested by trypsinization and the number of cells was counted by CASY Counter. Cell pellet was resuspended with assay medium at the density of 2.1×10^5 cells/mL. 100 μL of the cell suspension were seeded in each well of the 96-well plates (Corning® BioCoat™ Poly-D-Lysine). After the seeding, the plates were left to rest for 10–30 min at room temperature and incubated at 37 °C and 5% CO_2 and 100% humidity for 24 h to let the cells attach to the plate before dosing with PFAS.

2.2.6.2. PFAS exposure. PFAS stocks were prepared in MeOH. MeOH was evaporated with a gentle stream of nitrogen, leaving only PFAS precipitaties at the bottom of dosing vials. Assay medium contained 2% cs-FBS, which has a low background signal caused by hormone (data not shown), and was added to dissolve the PFAS before being serially diluted with medium in a 96-well plate. 120 μL solution from each well were transferred to previous 96-well plate with adhered cells using a 12-channel pipette. For antagonistic assay, medium containing rosiglitazone (agonist of PPARγ) was used to prepare PFAS solution (Table A2). The dilution process of PFAS was the same as above. The final concentration of rosiglitazone in the cell plate was 7 nmol/L, which was expected to trigger approximately 80% of the maximum effects. An 80% effect level was chosen following the recommendations of Neale et al. (2015) and because some chemicals may have potential weak activation effects at low concentrations. Both agonist and antagonistic effect could be recorded. After PFAS dosing, cell plates were incubated for another 24 h.

2.2.6.3. Cytotoxicity measurement. Cells were imaged non-invasively with the IncuCyte S3 (Essen BioScience) before dosing and the confluency of the cells was calculated by software (IncuCyte S3 v2019A) with details provided in Escher et al. (2019). The confluency of the cells

was measured again by IncuCyte S3 24 h after dosing. The cell viability was determined by comparing the confluency of the exposed and unexposed cells 24 h after dosing.

2.2.6.4. Reporter protein detection. Before the detection of reporter protein, 200 μL of supernatant from each well were transferred to a new 96-well plate and then used for SPME measurement (2.2.3). The activation signal of PPARγ coupled to a reporter gene encoding for β-lactamase was measured by fluorescence after addition of the GeneBLAzer® FRET reagent and additional 2 h incubation. The detailed protocol can be found in Neale et al. (2017).

2.3. Data evaluation

2.3.1. Fiber uptake kinetics

PFAS on the C18-coated fiber were desorbed by solvents and the extract was measured directly by LC/MS. The concentration of PFAS in the fiber (C_f) was calculated from the concentration measured in the extract ($C_{extract}$) and the volume of extract ($V_{extract}$) divided by the volume of fiber coating (V_f) (Eq. (1)).

$$C_f = \frac{C_{extract} \times V_{extract}}{V_f} \quad (1)$$

Adsorption kinetics determine the time required to reach equilibrium. In a single adsorbate system, the rate of adsorption process is expressed based on the amount of chemicals. The amount of PFAS in water as a function of time $n_w(t)$ can be defined by Eq. (2):

$$n_w(t) = n_w(eq) \times \left(1 - e^{-k_1 \times t}\right) + n_w(t_0) \times e^{-k_1 \times t} \quad (2)$$

$n_w(eq)$ and $n_w(t_0)$ are the amounts of PFAS in water at equilibrium and at the start of the experiment. k_1 is the rate constant for kinetic model. Since $n_f(t_0) = 0$, the amount of PFAS in fiber $n_f(t)$ can be fitted by Eq. (3):

$$n_f(t) = n_f(eq) \times \left(1 - e^{-k_2 \times t}\right) \quad (3)$$

The time to reach 95% of equilibrium of fiber absorption ($t_{0.95}$) was derived by Eq. (4).

$$t_{0.95} = \frac{\ln 0.05}{-k_2} \quad (4)$$

The recovery of PFAS during the SPME extraction was calculated by Eq. (5).

$$\text{recovery ratio} = \frac{n_f + n_w}{n_{tot}} \quad (5)$$

2.3.2. Sorption isotherms to the SPME fiber

Sorption isotherms can be used to describe the binding of chemicals to surfaces. The binding of anionic chemicals to C18 fibers is an adsorption process with limited binding sites. In this case the sorption isotherms of C_f against the aqueous concentration C_w are non-linear and experimental sorption data can be fitted with an empirical model, known as Freundlich isotherm (Eq. (6)).

$$C_f = K_{Fr} \times (C_w)^{n_{Fr}} \quad (6)$$

K_{FR} and n_{FR} are Freundlich constant and exponent, which can be deduced from experimental data by the logarithmic form of Eq. (6), which is (Eq. (7)):

$$\log C_f = n_{Fr} \times \log C_w + \log K_{Fr} \quad (7)$$

The apparent distribution ratio of PFAS between fiber and water $D_{f/w}$ Eq. (8) at equilibrium is dependent on the concentrations and can be calculated with K_{FR} and n_{FR} Eq. (9).

$$D_{f/w} = \frac{C_f}{C_w} \quad (8)$$

$$\log D_{f/w} = \left(1 - \frac{1}{n_{Fr}}\right) \times \log C_f + \frac{\log K_{Fr}}{n_{Fr}} \quad (9)$$

2.3.3. Binding of PFAS to biological materials

SPME measurements were used to quantify the aqueous concentration in presence of biomaterials (i = proteins, lipid, human plasma, medium or HEK293H cells) and the mass balance $n_{tot} = n_f + n_w + n_{bound}$ was used to derive the distribution ratios of PFAS between biomaterials i and water. Concentration of PFAS bound to sorptive phases i ($C_{bound,i}$) can be calculated by Eq. (10):

$$C_{bound,i}\left[\frac{\mu mol}{L}\right] = \frac{n_{bound,i}}{V_i} = \frac{n_{tot} - n_f - n_w}{V_i} \quad (10)$$

The distribution ratios of PFAS between phase i and water ($D_{i/w}$) were calculated from experimental data by Eq. (11) for each concentration and experiment.

$$D_{i/w}\left[\frac{L_w}{L_i}\right] = \frac{C_{bound,i}}{C_w} = \frac{\left(\frac{n_{tot}}{n_f} - 1\right) \times D_{f/w} \times V_f - V_w}{V_i} \quad (11)$$

The experimental concentration-dependence of $D_{i/w}$ was fitted with a Freundlich-type model using Eq. (12). The distribution to biomaterials, unlike binding to the SPME fiber, is not a pure surface sorption process but a mix of specific binding to proteins and non-specific partitioning to proteins and lipids. Therefore, Eq. (12) is only a phenomenological fit of the experimental data, and in case of n_{Fr} deviated from 1, a mechanistic model was invoked to describe the non-linear binding. However, the empirical model of the non-linear binding will suffice for developing a mass balance model for the bioassays and to derive the dissolved concentration C_w.

$$\log D_{i/w} = (n_{Fr} - 1) \times \log C_w + \log K_{Fr} \quad (12)$$

2.3.4. Mechanistic model for protein/plasma binding

Protein binding is known to be concentration-dependent and therefore $D_{BSA/w}$ was also modeled with a mechanistic combined binding/partitioning model. PFAS may bind specifically to one or more specific binding sites on proteins at low concentration and partition non-specifically to the protein and lipid at high concentrations. At a ratio ν of bound PFAS molecules to protein molecules (eq. (13), [$mol_{PFAS}/mol_{protein}$]) of $\nu < 1$, a saturation binding model (Eq. (14)) can be used to describe the binding curves of the bound concentration (C_{bound}) as a function of C_w with the dissociation constant K_d and C_{max} as maximum bound concentration. C_{max} reflects the number of binding sites on the protein in case of BSA after the concentrations in [$mol_{PFAS}/L_{protein}$] were converted to [mol_{PFAS}/mol_{BSA}] using the molecular weight of BSA of 66463 Da and a density of 1.36 kg/L (Eq. (13)).

$$\nu = \frac{n_{bound}}{n_{protein}} \quad (13)$$

$$C_{bound,specific} = \frac{C_{max} \cdot C_w}{K_d + C_w} \quad (14)$$

The low-concentration linear range of the binding curves extends approximately to $C_{max}/2$ and can be described by $K_{specific}$ (Eq. (15)).

$$K_{specific} = \frac{C_{max}}{2 \times K_d} \quad (15)$$

After obtaining the K_d and C_{max} from the low-concentration portion of the binding curve ($\nu < 1$) the non-specific distribution constant $D_{non-specific}$ was fitted to the full sorption model by keeping the previously determined K_d and C_{max} constants (Eq. (16)).

$$C_{bound,total} = \frac{C_{max} \cdot C_w}{K_d + C_w} + D_{non-specific} \times C_w \quad (16)$$

2.3.5. Mass balance model for distribution to biomaterials

The biomaterial-water distribution ratio $D_{i/w}$ can also be predicted by a mass balance model (MBM, Eq. (17)) from the concentration-dependent protein binding constants and the concentration-independent distribution to the lipid phases, assuming that protein and lipid are the major sorptive phases in the tested biomaterials (medium, cells, plasma).

$$D_{i/w} = D_{BSA/w} \times \frac{V_{prot}}{V_{prot+lip}} + D_{lip/w} \times \frac{V_{lip}}{V_{prot+lip}} \quad (17)$$

The volume of protein (V_{prot}) and lipid (V_{lip}) in plasma, medium, HEK293H cells were measured for the materials used in this study as described by Fischer et al. (2017).

$D_{BSA/w}$ measured here served as proxy for protein distribution and the liposome (phospholipid vesicles)-water distribution ratio $D_{lip/w}$ from Ebert et al. (2020) as proxy of lipid distribution. The $D_{lip/w}$ of PFBA was predicted from a linear relationship between log $D_{lip/w}$ of perfluorocarboxylic acids and the number of fluorinated carbon (C-F) (Figure A1). The R-squared of this linear regression was 0.95, the slope was 0.476 and intercept was 0.172.

2.3.6. Freely dissolved concentration in the bioassays

The aqueous concentration in the bioassay medium was quantified at the end of the bioassay experiment. Since the SPME extraction leads to a substantial depletion of some of PFAS, one needs to back-calculate to the original aqueous concentration in the bioassay using Eq. (18) (Henneberger et al., 2019b). In *in vitro* toxicology, this aqueous concentration is often termed freely dissolved concentration ($C_{free,bioassay}$) and we use this terminology for consistency. The $D_{f/w}$ used for this conversion was calculated from C_f using the equations given in Table A6.

$$C_{free,bioassay} = \frac{n_{tot}}{D_{f/w} \times \left(\frac{n_{tot}}{C_f} - V_f\right)} \quad (18)$$

$C_{free,bioassay}$ can also be predicted by a mass balance model (Eq. (19)) with the $D_{i/w}$ of different biomaterials i (medium, cells) and their corresponding volume V_i.

$$n_{tot} = n_{free} + n_{bound,i} = C_{free,bioassay} \times \left(V_w + \sum_{i=1}^{n} (D_{i/w} \times V_i)\right) \quad (19)$$

The $C_{free,bioassay}$ can be calculated by rearranging Eq. (19) and introducing the measured $D_{medium/w}$ of GeneBLAzer assay medium and $D_{cell/w}$ of the HEK293H cell line (Eq. (20)).

$$C_{free,bioassay} = \frac{n_{tot}}{(D_{cell/w} \times V_{cell,\ prot+lip} + V_{cell,\ w}) + (D_{medium/w} \times V_{medium,prot+lip} + V_{medium,w})} \quad (20)$$

2.3.7. PPARγ bioassay

Cytotoxicity was expressed as a percentage of reduced cell numbers (confluency) compared to the unexposed cells (eq. (21)). The concentration-cytotoxicity curve, which is typically linear up to 30% reduction of confluency (Escher et al., 2018) was fitted with Eq. (21).

$$\%\text{Cytotoxicity} = 100\% - \frac{\text{confluency(sample)}}{\text{confluency(unexposedcells)}} = \text{slope}_{cytotoxicity} \times \text{concentration} \quad (21)$$

The inhibitory concentration that caused 10% of cytotoxicity (IC_{10}) was calculated from the linear portion of the concentration-cytotoxicity curve below 30% cytotoxicity with Eq. (22) (Escher et al., 2018).

$$IC_{10} = \frac{10\%}{\text{slope}_{cytotoxicity}} \quad (22)$$

The specific effect was the reporter gene activation or suppression of PPARγ. For agonistic effects, effective concentration that triggered 10% of the maximum PPARγ activation induced by the positive control rosiglitazone (EC_{10}, Eq. (23)) was calculated from the linear portion of concentration-effect curve (eq. (23)), at non-cytotoxic concentrations, i.e., at concentrations below IC_{10} and below 30% of maximum effect, with Eq. (24).

$$EC_{10} = \frac{10\%}{\text{slope}_{effect}} \quad (23)$$

$$\%\ \text{of}\quad \text{maximum}\quad PPAR\gamma\quad \text{activation} = \text{slope}_{effect} \times \text{concentration} \quad (24)$$

For antagonistic effects, 7 nM rosiglitazone (agonist of PPARγ) was added in all wells to trigger approximately 80% of the maximum effects and a dilution series of the PFAS was run against that background. The suppression ratio (SPR) of PFAS can be calculated by the reduction of the activation signal of the constant concentration of rosiglitazone (Eq. (25)).

$$SPR = 100\%\text{-}\frac{\text{Activation}_{sample}}{\text{Activation}_{rosiglitazone}} \quad (25)$$

The effective concentration causing a SPR of 20% (EC_{SPR20}, Eq. (26)) was derived from the linear portion of the concentration-suppression curve (similar to Eq. (25)).

$$EC_{SPR20} = \frac{20\%}{\text{slope}} \quad (26)$$

3. Results and discussions

3.1. Fiber uptake kinetics and sorption isotherm of PFAS

To establish a SPME method specifically for PFAS, we performed kinetic uptake and sorption isotherm experiments (Figure A2) to study adsorption characteristics of PFAS to C18-coated fibers. All four PFAS reached equilibrium status within 16 h (Eq. (4), Fig. A2a-d and Table A1) and their average recovery ratios (Eq. (5)) were 95%-120%. Hydrophobic PFHxS, PFOA and PFOS showed strong affinities to fibers in a concentration-dependent way. The sorption isotherm was linear for PFBA but non-linear for the other PFAS with Freundlich exponents n_{Fr} ranging from 0.641 to 0.764 (Eq. (7), Fig. A2e-h, Table A6). The $D_{f/w}$ of PFHxS, PFOA and PFOS hence showed a strong concentration dependence (Eq. (9), Fig. A2j-l and Table A6).

3.2. Binding to proteins

The concentrations of PFAS bound to BSA ($C_{bound,BSA}$) (Eq. (10)) increased non-linearly with C_w (Fig. 2a-d). In the experiment, the volume of BSA was kept constant, while the concentration of PFAS ranged over four to five orders of magnitude. The binding curves of PFOA, PFHxS and PFOS showed three phases. The PFAS appeared to bind to the high-affinity sites of BSA at low concentrations. When these sites gradually saturated, a transition stage in the middle part of curve appeared. At high concentrations, non-specific partitioning was observed. For hydrophilic PFBA, the transition phase was affected by non-specific binding. The binding curves

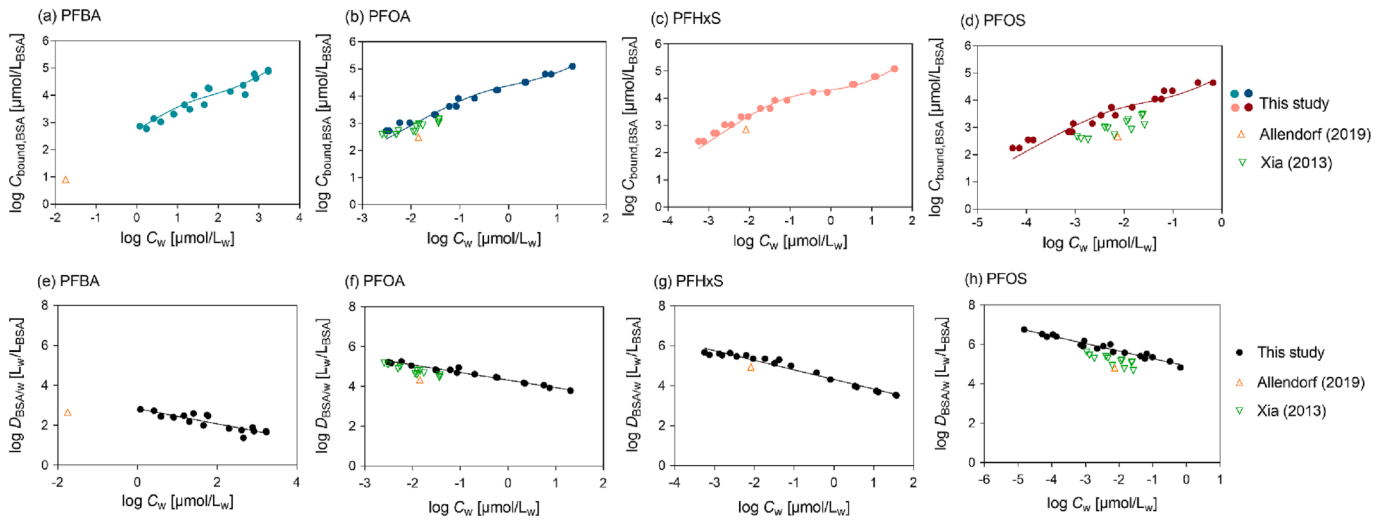

Fig. 2. Protein (BSA) binding curves. The concentrations of (a) PFBA, (b) PFOA, (c) PFHxS and (d) PFOS bound to bovine serum albumin ($C_{bound,BSA}$, circles) were fitted with a mechanistic combined binding/partitioning model (Eq. (16)). Distribution ratios between BSA and water ($D_{BSA/w}$) for (e) PFBA, (f) PFOA, (g) PFHxS and (h) PFOS. log $D_{BSA/w}$ (black circle) was fitted phenomenologically by a Freundlich-type model (Eq. (12)). The experimental data were compared with previous dialysis experiments from Allendorf et al (2019) (orange upward triangles) and Xia et al (2013) (green downward triangles) for comparison. (For interpretation of the references to colour in this figure legend, the reader is referred to the web version of this article.)

were fitted with Eq. (16). The specific saturation binding $K_{specific}$ (Eq. (15)) and the non-specific distribution ratio $D_{non\text{-}specific}$ (Eq. (16), Table 1) were not as distinctly differentiated as for other anionic organics such as naproxen (Henneberger et al., 2019a). The C_{max} of PFBA, PFOA, PFHxS and PFOS were 0.450, 1.24, 0.919 and 0.391 mol_{PFAS}/mol_{BSA}, respectively (Table 1), indicating that there is most likely only one high-affinity binding site for PFAS. PFOS showed the highest potency of specific protein binding with a log $K_{specific}$ of 5.81. The log $D_{non\text{-}specific}$ ($\nu > 1$) (Table 1) were lower than log $K_{specific}$ but were remarkably similar to the log $D_{lip/w}$ for PFBA, PFOA and PFOS (Table 2).

Since PFAS binding to BSA was non-linear, $D_{BSA/w}$ (Eq. (11)) of PFAS were concentration-dependent (Fig. 2e-h). The decrease of experimental $D_{BSA/w}$ with increasing C_w was phenomenologically fitted with Eq. (12) and the resulting Freundlich parameters K_{Fr} and n_{Fr} are listed in Table 1. Note that this very simplified linearization of the three-phasic binding curve does not reflect the complex binding mechanism, but the resulting linear regressions may serve as input function for the MBM.

There are two studies using dialysis experiments to investigate the protein binding of PFAS. Allendorf et al. (2019) measured BSA-water partition coefficients for seven PFAS at one constant concentration. Their experimental data of PFBA, PFOA, PFHxS and PFOS are compared in Fig. 2 with the present binding curves measured with SPME. All are situated at different regions of the binding curves. PFBA (Fig. 2a, orange upward triangle) was measured at very low linear specific binding at concentrations that were two orders of magnitude lower than the concentration range measured here, PFOA (Fig. 2b, orange upward triangle) and PFHxS (Fig. 2c, orange upward triangle) were situated at the linear specific binding concentration range, and PFOS (Fig. 2d, orange upward triangle) at the transition zone, where specific binding was going towards saturation and non-specific binding contributed to the overall binding.

Xia et al. (2013) studied the protein binding of six PFAS with different protein concentrations of BSA and found non-linear binding curves of PFOA and PFOS. Their binding curves for PFOA (Fig. 2b, green downward triangles) were in the range of specific binding and their experimental data from dialysis experiments agreed remarkably well with our data from SPME experiments. PFOS binding was measured at the same concentration range as PFOA but fell into the transition zone between saturation of specific binding and non-specific binding (Fig. 2d, green downward triangles). The present SPME experiment indicated stronger binding in the same concentration range as the dialysis experiment data from Allendorf et al. (2019) and Xia et al. (2013).

Bischel et al. (2010) found up to eight binding sites in PFAS-BSA complexes at $\nu > 4$ (mol_{PFAS}:mol_{BSA}) using Nano-electrospray ionization mass spectrometry. Human serum albumin (HSA) and BSA are 76% conserved in sequences (Theodore 1985) and thus some PFAS showed similar affinity to both BSA and HSA (Bischel et al., 2010). Chen and Guo (2009) further investigated the affinities of PFAS on three binding sites of HSA using site-specific fluorescence. PFBA, PFOA, PFOS had different preferences among these binding sites with orders of magnitude difference in binding constants. If the strongest binding site contributed the most of the PFAS binding to protein, the binding model can be simplified as one high-affinity binding site model as we did here.

Several models have been used in previous studies to analyze how PFAS-protein binding is affected by hydrophobicity, steric limitation and number of fluorinated carbon ($n_{C\text{-}F}$) (Alesio et al. 2022; Almeida et al., 2021; Qin et al., 2020; Ren et al., 2016). Their results suggested that $n_{C\text{-}F}$ plays an important role in PFAS-protein binding because it has positive correlations with chemical hydrophobicity and molecular size (Alesio et al., 2022). In our study, the value of log $D_{non\text{-}specific}$ showed a good relationship with $n_{C\text{-}F}$, PFOS ($n_{C\text{-}F}$:8) > PFOA ($n_{C\text{-}F}$:7) > PFHxS ($n_{C\text{-}F}$:6) > PFBA ($n_{C\text{-}F}$:3), suggesting $n_{C\text{-}F}$ may dominate the non-specific binding of PFAS to protein (Figure A3). Different functional groups (e.g., sulfonic, carboxylic or hydroxy group) were also reported to impact the interactions of PFAS with protein, such as van der Waals interactions, electrostatic interactions and hydrogen bonding (Almeida et al., 2021; Qin et al., 2020; Ren et al., 2016). The higher values of log $K_{specific}$ (Table 1) of PFHxS and PFOS suggest that sulfonic acids may have stronger binding affinity to the ligand binding pockets, which is consistent with previous studies using nuclear protein (e.g., PPARγ), membrane protein (e.g., GPR40) and transport protein (e.g. transthyretin) (Almeida et al., 2021; Qin et al., 2020; Ren et al., 2016).

Overall, the comparison with literature data demonstrates that it is important to measure protein binding at a wide concentration range to assure that all aspects of binding, including specific saturable binding as well as nonspecific partitioning are captured. We extended the concentration range over five orders of magnitude and chose appropriate concentration ranges for each of the tested PFAS to capture all phases of the binding curves. The drawback of literature data was that it was typically measured at a narrower concentration range, which resulted in measurements at different phases of the binding curves, which limits comparisons of the experimental binding constants.

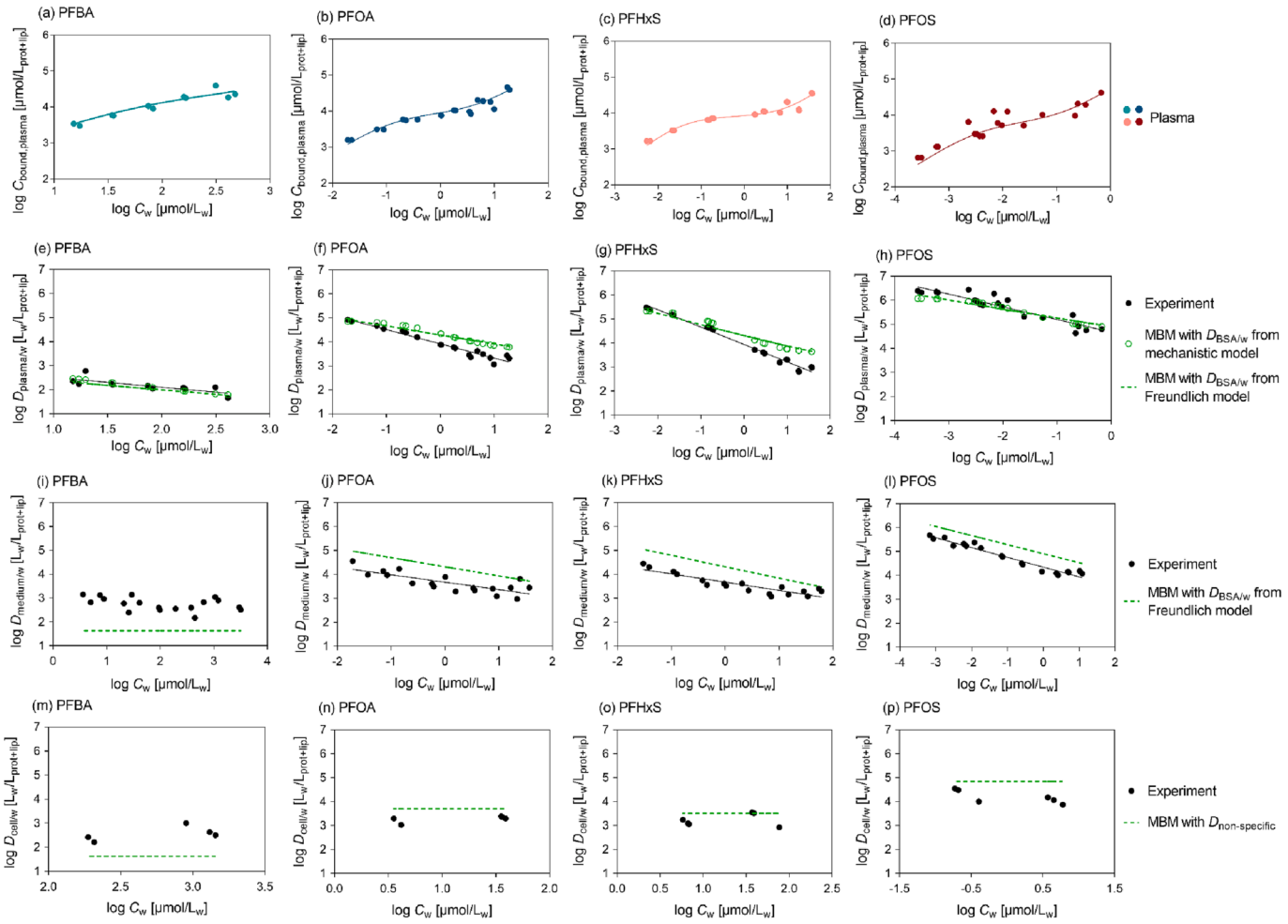

Fig. 3. Partitioning to biological materials (plasma, medium, cells). The concentration of (a) PFBA, (b) PFOA, (c) PFHxS and (d) PFOS bound to plasma ($C_{bound,plamsa}$, circles) were fitted with a mechanistic combined binding/partitioning model (Eq. (16)). Distribution ratios between plasma and water ($D_{plasma/w}$) of (e) PFBA, (f) PFOA, (g) PFHxS and (h) PFOS were fitted phenomenologically by the Freundlich-type model (Eq. (12), black solid line) and predicted by the mass balance model (MBM, Eq. (17)) with concentration-dependent BSA-water distribution ratios, $D_{BSA/w}$ from the Freundlich-type model (Eq. (12), Table 1, green dotted line) or from the mechanistic combined binding/partitioning model (Eq. (16), green hollow circle), and the liposome-water distribution ratio, $D_{lip/w}$ (Table 2). Distribution ratio between medium and water ($D_{medium/w}$) of (i) PFBA, (j) PFOA, (k) PFHxS and (l) PFOS were fitted phenomenologically by the Freundlich-type model (Eq. (12), black solid line) and predicted by the MBM (Eq. (17), green dotted line) with the $D_{BSA/w}$ from the Freundlich-type model (Eq. (12), Table 1) and the $D_{lip/w}$ (Table 2). Distribution ratios between cell and water ($D_{cell/w}$) of (m) PFBA, (n) PFOA, (o) PFHxS and (p) PFOS were calculated by Eq. (11) (black circle) from experiments and predicted by the MBM (Eq. (17), green dotted line) with $D_{non-specific}$ of BSA (Table 1) and $D_{lip/w}$ (Table 2). (For interpretation of the references to colour in this figure legend, the reader is referred to the web version of this article.)

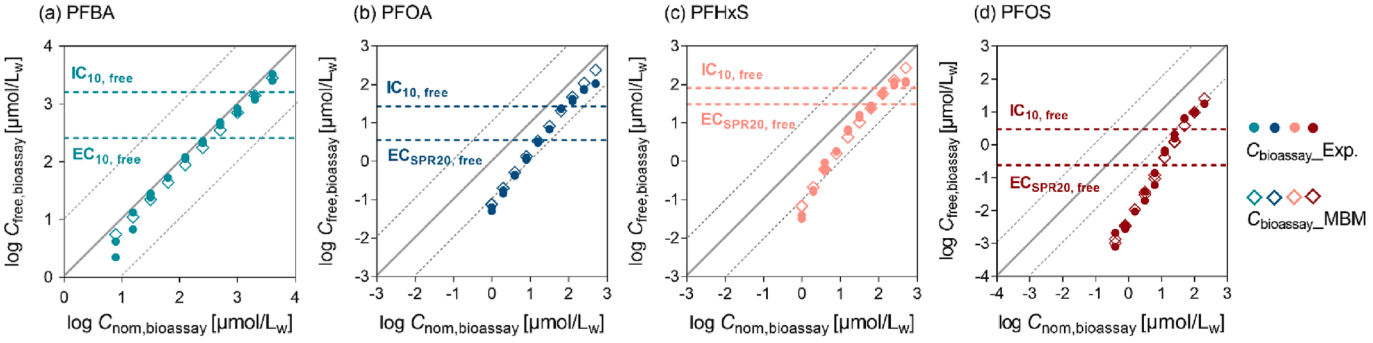

Fig. 4. Freely dissolved concentration of (a) PFBA, (b) PFOA, (c) PFHxS and (d) PFOS in GeneBLAzer medium (220 μL) in presence of 21,000 cells after 24 h cell exposure. log $C_{free,bioassay}$ of PFAS were quantified with SPME (Eq. (18), filled circles) and predicted by mass balance model (MBM, Eq. (20), empty diamond) with the concentration-dependent medium-water distribution ratio, $D_{medium/w}$ (Eq. (12), Table A6) and cell-water distribution ratio, $D_{cell/w}$ (Table 2). Inhibitory concentration (IC_{10}, Eq. (22)) for cytotoxicity and effect concentration (EC_{10} in agonist mode (Eq. (23)) or EC_{SPR20} in antagonistic mode (Eq. (26))) were measured with the PPARγ-GeneBLAzer assays.

3.3. Binding to human plasma

C18-SPME was also used to measure C_{free} in plasma samples and to derive binding curves. As shown in Fig. 3a-e, the plasma binding curves of all four PFAS were also concentration-dependent and could be fitted by the mechanistic combined binding/partitioning model. To align the units, the saturation binding (Eq. (14)) was multiplied by the volume fraction of protein ($V_{prot}/V_{prot+lip} = 0.909$) in the plasma. $D_{plasma/w}$ ($\nu < 1$) in Table 2 refers to the specific binding constant $K_{specific}$ (Eq. (16) and was derived from the low-concentration portion of the binding curves with Eq. (14). $D_{plasma/w}$ ($\nu > 1$) refers to non-specific binding (Eq. (16)). All fit parameters of the mechanistic binding model are listed in Table A7.

The binding curves to BSA and to plasma overlapped for PFBA (Fig. A4a) and PFOS (Fig. A4d), but only overlapped at the low concentration range of protein-specific binding and gradually separated as the concentration increased for PFOA (Fig. A4b) and PFHxS (Fig. A4c). The good agreement is an indication that the plasma binding is dominated by protein binding with a low contribution of the lipids to the overall plasma binding, which justifies the application of the mechanistic combined binding/partitioning model that was derived for BSA.

Despite the non-linearity of plasma binding, we also fitted the experimental $D_{plasma/w}$ with the Freundlich-type model (Eq. (12)) and compared the $\log D_{plasma/w} - \log C_w$ relationship with the prediction by the MBM (Fig. 3e-h, Table 2, and Table A7). There was a decent agreement between the experimental $D_{plasma/w}$ (black circle) and the fit with the Freundlich-type model (black solid lines) and the MBM prediction that was based on the Freundlich model for $D_{BSA/w}$ (green dashed lines) as well as the MBM prediction that were based on the mechanistic protein binding model (green circles) in Fig. 3e-h.

The MBM for plasma based in the mechanistic combined binding/partitioning model for BSA was also used to analyze how lipids and proteins contribute to the bound PFAS. $D_{plasma/w}$ ($\nu < 1$) predicted for realistically low concentrations with $K_{specific\_BSA}$ (Table 1) were comparable to the experimental ones with>98% contribution by protein binding (Table 2). This also rationalizes the overlay of the binding curves to BSA and plasma. $D_{plasma/w}$ ($\nu > 1$) predicted for high concentrations with $D_{non\text{-}specific\_BSA}$ of PFBA, PFOA, PFOS agreed well with the experimental $D_{plasma/w}$ and the contribution of lipid increased from approximately 1% for low concentrations and specific binding (Table 2) to 10% for high concentrations and dominant non-specific binding (Table A7).

Forsthuber et al. (2020) analyzed 11 PFAS bound to albumin and lipoproteins in human blood samples and concluded that albumin was the main carrier in plasma. However, this study only analyzed the blood concentration and did not investigate any binding mechanism. C18-SPME combined with MBM can not only obtain partition constants, but also differentiate the specific and non-specific binding within wide concentration ranges and predict the contribution of lipids and proteins.

3.4. Partitioning in medium

We further studied the partitioning of PFAS in GeneBLAzer assay medium that is commonly used for reporter gene assays in Tox21. Binding curves are depicted in Figure A5. Volume fractions of protein and lipid in the GeneBLAzer assay medium were 0.08% and 0.0007% (Table A5). The $C_{bound,medium}$ of PFAS was also fitted with the combined binding/partitioning model (Eq. (16)). The saturation binding portion of Eq. (14) was multiplied by the volume fraction of protein ($V_{prot}/V_{prot+lip} = 0.992$) in the medium to align the units. Apart from PFOS (Figure A5d), which showed an excellent fit, the other three PFAS did not show the pronounced non-linear binding and a much lower quality of the fit (Figure A5 a-c). The highest concentration of PFOA and PFHxS were excluded from the fit, but the model was still not able to explain the shape of the binding curves. This may be caused by protein denaturation at high concentrations due to the surface-active properties of PFOA and PFHxS, which may have caused unfolding of the protein (MacManus-Spencer et al., 2010).

Since PFAS binding to protein was concentration-dependent and the protein content was 140 times higher than lipid content in the GeneBLAzer assay medium, the $\log D_{medium/w}$ of PFOA, PFHxS and PFOS (Eq. (12)) were also concentration-dependent. The $\log D_{medium/w}$ of PFOA, PFHxS and PFOS predicted with the MBM (Eq. (17), Table A6) showed the same trends as the experimental results but predictions resulted in slightly higher $D_{medium/w}$ than experiments (green dashed line in Fig. 3j-k). For the hydrophilic PFBA, the $\log D_{medium/w}$ was nearly constant over the tested concentration range and the predicted $D_{medium/w}$ of PFBA was lower than experimental ones (Fig. 3i), which might have been caused by the slightly higher recovery of the SPME (95–120%, Eq. (5)), resulting in lower $C_{bound,medium}$ and $D_{medium/w}$ calculated for the MBM (Eqs. (10) and (11)).

3.5. Partitioning to cells

The concentrations of PFAS bound to HEK293H cells ($C_{bound,cell}$, Eq. (10)) were measured at two nominal concentrations that differ by a factor of eight (Table A2). The volume fractions of water, protein and lipid of cells were 91.6%, 8.14% and 0.432% (Table A5), which were comparable to the values determined in previous study (Fischer et al., 2017). $D_{cell/w}$ derived from different concentrations of the same PFAS did not show any statistical difference (Student's t test, $p > 0.05$) and an average value of $\log D_{cell/w}$ for each PFAS is listed in Table 2.

A previous study pointed out that structural proteins (e.g. cytoskeleton) are abundant in mammalian cells and organic acids have lower affinity to structural proteins compared to BSA (Henneberger et al., 2016). Non-specific binding of PFAS to structural protein and lipid may dominate their partitioning to the cells. Based on this assumption, $D_{cell/w}$ was predicted by the MBM (Eq. (17)) with $D_{non\text{-}specific}$ (Table 1) as a surrogate for partitioning to structural proteins and $D_{lip/w}$ (Table 2) for lipid.

The predicted $D_{cell/w}$ (green dashed line in Fig. 3m-p) were not much different from the experimental $D_{cell/w}$ for PFOA, PFHxS and PFOS with discrepancies within 15%. For PFBA, the predicted $D_{cell/w}$ was around 35% lower than the experimental $D_{cell/w}$ similarly to what has been observed for medium. Here, we considered only proteins and lipids of the cell homogenate as the main sorptive phase for $D_{cell/w}$, which is different from Henneberger et al (2019a) where the cells were recognized as an entity containing water, protein and lipid and all of them contributed to cell-water distribution.

3.6. Freely dissolved concentration of PFAS in PPARγ reporter gene assays

In the bioassay, the partitioning of PFAS to medium components and cells inevitably resulted in substantial differences between freely dissolved concentration ($C_{free,bioassay}$) and nominal concentration ($C_{nom,bioassay}$). The $\log D_{f/w}$ in Table A6 were used to derive $C_{free,bioassay}$ in complex assay medium from measured concentrations in the fiber by Eq. (18). As shown in Fig. 4, if $C_{free,bioassay}$ is equal to $C_{nom,bioassay}$, data points fell on the 1:1 diagonal. For the hydrophilic PFBA, $\log C_{free,bioassay}$ and $\log C_{nom,bioassay}$ were almost equal with deviations below 10%, but for hydrophobic PFHxS, PFOA and PFOS, $C_{free,bioassay}$ were up to 100 times lower than $C_{nom,bioassay}$. Our results are consistent with a recent study that hydrophilic chemicals and highly protein-bound chemicals behave differently on C_{free} (Dimitrijevic et al., 2022).

Considering medium components and cells may be contributing to PFAS depletion in bioassays, a MBM (Eq. (20)) with $D_{medium/w}$ and $D_{cell/w}$ for these PFAS (Table A6 and Table 2) was used to predict the values of $C_{free,bioassay}$ of PFAS. The $\log C_{free,bioassay}$ predicted with the MBM agreed well with experimental data (Fig. 4). This means that existing PFAS effect data can be assessed for their freely dissolved effect concentrations in the future by the simple MBM, provided that the distribution ratios ($D_{BSA/w}$ and $D_{lip/w}$) and experimental conditions (lipid and protein content of medium and cells) are available.

Table 3
Nominal and freely dissolved concentration of PFBA, PFOA, PFHxS and PFOS in PPARγ reporter gene assays and human plasma. Quantitative *in vitro* to *in vivo* extrapolation (QIVIVE) ratio for workers and residents living near fluorochemical plants and general population.

	PPARγ reporter gene assay			Workers or residents near fluorochemical plant		General residents	
	Cytotoxicity	PPARγ-activation		Human plasma		Human plasma	
	$IC_{10,nom}$ [μmol/L_w]	Agonism $EC_{10,nom}$ [μmol/L_w]	Antagonism $EC_{SPR20,nom}$ [μmol/L_w]	$C_{nom,plasma}$ [μmol/L]	$QIVIVE_{nom}$ ratio	$C_{nom,plasma}$ [μmol/L]	$QIVIVE_{nom}$ ratio
PFBA	2.20×10^3	316		0.408[a]	1.29×10^{-3}	5.30×10^{-3}[c]	1.68×10^{-5}
PFOA	91.0		18.2	35.8[b]	1.96	1.23×10^{-2}[d]	6.74×10^{-4}
PFHxS	125		70.7	26.4[b]	0.373	1.40×10^{-2}[d]	1.98×10^{-4}
PFOS	29.5		5.54	126[b]	22.7	3.30×10^{-2}[d]	5.95×10^{-3}
	$IC_{10,free}$ [μmol/L_w]	Agonism $EC_{10,free}$ [μmol/L_w]	Antagonism $EC_{SPR20,free}$ [μmol/L_w]	$C_{free,plasma}$ [μmol/L]	$QIVIVE_{free}$ ratio	$C_{free,\ plasma}$ [μmol/L]	$QIVIVE_{free}$ ratio
PFBA	1.61×10^3	259		5.72×10^{-2}	2.21×10^{-4}	7.42×10^{-4}	2.87×10^{-6}
PFOA	27.0		3.64	1.93×10^{-2}	5.31×10^{-3}	6.63×10^{-6}	1.82×10^{-6}
PFHxS	81.6		31.9	3.76×10^{-3}	1.18×10^{-4}	2.00×10^{-6}	6.25×10^{-8}
PFOS	2.98		0.243	2.94×10^{-3}	1.21×10^{-2}	7.71×10^{-7}	3.17×10^{-6}

[c] Data from Gao et al. 2019.
[d] Data from https://www.cdc.gov/exposurereport/data_tables.html.
[a] Data from Bao et al. 2022.
[b] Data from Gao et al. 2015.

3.7. Effect concentrations of PFAS in PPARγ reporter gene assays

All PFAS were cytotoxic at the highest exposure concentrations (Figure A6). Inhibitory concentration that caused 10% of cytotoxicity ($IC_{10,free}$) (Eqs. (21) and (22)) of PFBA, PFOA, PFHxS and PFOS were 1610, 27.0, 81.6 and 2.98 μM respectively (Table 3). To avoid artefacts on the PPARγ activation caused by the cytotoxicity, the cellular effects were evaluated in the non-cytotoxic concentration range below IC_{10}.

Both agonistic and antagonistic effects in the PPARγ-GeneBLAzer reporter gene assay were observed after 24 h exposure to PFAS (Figure A6). PFBA showed agonistic effects up to 30% at lower concentrations and then suppression at higher concentrations, which were already impacted by cytotoxicity (Figure A6a). The effective concentration that triggered 10% of the maximum PPARγ activation ($EC_{10,free}$) (Eqs. (23) and (24)) of PFBA was 259 μM.

PFOA, PFHxS and PFOS showed antagonistic effects on PPARγ (Figure A6b-d), that were measured at a background of 80% activation effect of rosiglitazone. PFHxS suppressed nearly half of the signal from rosiglitazone, and PFOA and PFOS almost eliminated the signal. Suppression ratios (SPR) (Eq. (25)) of 20% of PFHxS, PFOA and PFOS were observed at $EC_{SPR20,free}$ of 3.64, 31.9 and 0.243 μM (Eq. (26), Table 3).

PPARγ-regulated signal pathways have been demonstrated to involve in PFAS disrupting lipid metabolism in many studies (Abbott 2009; Ma et al., 2018; Pan et al., 2021). Some researchers further investigated the interaction of PFAS with PPARγ by using reporter gene assays but their activities on the receptor were inconsistent. For example, no significant activation of PPARγ by PFOA and PFOS were observed on Cos-1 cells (Takacs and Abbott, 2007), which were transfected with plasmid DNA using lipofectamine reagent, while other studies proved they were potential agonists of PPARγ using transient transfected 3 T3-L1 cells (Vanden Heuvel et al., 2006) or HEK293 cells (Li et al., 2019, 2018; Zhang et al., 2014). PFOA, PFHxS and PFOS showed very faint activation effects in the PPARγ GeneBLAzer assay at the low concentration range in absence of rosiglitazone (data not shown) but obvious suppression without prior increase of the rosiglitazone signal when co-exposed with rosiglitazone.

3.8. Freely dissolved concentration of PFAS in human plasma

Many PFAS have been detected at micromolar levels in human plasma of firefighters and workers engaged in PFAS utilization and manufacturing facilities (Costa et al., 2009; Gao et al., 2015; Rotander et al., 2015; Sakr et al., 2007; Wang et al., 2012). For example, the maximum level of PFOA, PFHxS and PFOS of workers from one of the largest PFAS-related producers in China (Henxin Chemical Plant) were 35.8, 26.4 and 126 μmol/L (Table 3) (Gao et al., 2015). The hydrophilic PFBA was seldomly measured in plasma samples, but it was one of the dominant PFAS in urine (Peng et al., 2021). However, some studies applied more sensitive methods and found PFBA in maternal and cord serum (Bao et al., 2022; Gao et al., 2019). The maximum level of PFBA was 0.408 μmol/L among 50 pregnant women living near the fluorochemical industrial plant-Fuxin in China (Bao et al., 2022).

PFAS were also found in the general population at nanomolar level according to national health surveys among developing and developed countries (Cakmak et al., 2022; Gockener et al., 2020; Lin et al., 2019; Petriello et al., 2022; Yu et al., 2020; Zhang et al., 2019). The U.S. Center for Disease Control and Prevention conducted PFAS monitoring of the general U.S. population and their latest results (2017–2018) showed that the maximum concentration of PFHxS, PFOA and PFOS were 12.3, 14.0, 33.0 nmol/L respectively (https://www.cdc.gov/exposurereport/data_tables.html). The maximum concentration of PFBA was 5.30 nmol/L among 132 non-occupationally exposed pregnant women in Beijing, China (Gao et al., 2019).

$C_{free,plasma}$ was calculated with Eq. (27). Since the ν (mol_{PFAS}/$mol_{protein}$) of PFAS in human plasma samples were usually ≪1 and most of PFAS may bind highly specifically to proteins, leading to very low free PFAS concentrations.

$$C_{free,plasma} = \frac{C_{nom,plasma} \times V_w}{V_w + D_{plasma/w} \times V_{prot+lip,plasma}} \quad (27)$$

We derived the log $D_{plasma/w}$ at $\nu < 1$ (Table 2) from the binding curves of PFAS to human plasma (Fig. 3a-d) and used these values to calculate $C_{free,plasma}$ by the MBM (Eq. (27)). As shown in Table 3, $C_{free,plasma}$ was predicted to be lower than $C_{nom,plasma}$ but the ratio was highly chemical-specific. $C_{free,plasma}$ of PFBA was only seven times lower than $C_{nom,plasma}$ but this ratio increased with protein binding affinity to almost 40,000 for PFOS. There was little difference in this ratio for each PFAS between the exposed workers and the general population.

3.9. Quantitative in vitro to in vivo extrapolation

The QIVIVE ratio is the ratio of concentration of PFAS in human plasma and effect concentration EC (EC_{10} or EC_{SPR20}) in the bioassay (Henneberger et al., 2021). The $QIVIVE_{nom}$ ratio was calculated with Eq.

(28). Nominal concentration of PFAS in human plasma samples ($C_{nom, plasma}$) were collected from epidemiological studies and EC_{nom} were measured as illustrative example with the PPARγ GeneBLAzer assay.

$$QIVIVE_{nom}\ ratio = \frac{C_{nom,\ plasma}}{EC_{nom}} \quad (28)$$

The corresponding $QIVIVE_{free}$ ratio was calculated with Eq. (29) from $C_{free,plasma}$ (Eq. (27) and EC_{free} (calculated with Eq. (18)).

$$QIVIVE_{free}\ ratio = \frac{C_{free,plasma}}{EC_{free}} \quad (29)$$

As an illustrative example, we calculated the QIVIVE ratio for plasma concentrations (C_{plasma}) of PFBA, PFOA, PFHxS and PFOS in workers and residents living near fluorochemical plants from Bao et al. (2022) and Gao et al. (2015) or the general population in the US (https://www.cdc.gov/exposurereport/data_tables.html) and Gao et al. (2019), and the EC of PFAS in the PPARγ GeneBLAzer assay (Table 3).

A QIVIVE ratio > 1 would indicate that the particular *in vitro* effect on the PPARγ receptor may have the potential of causing associated adverse outcomes in *in vivo* (Sipes et al., 2017). Notably, this assay is only one example - for a full QIVIVE, one needs to measure many *in vitro* endpoints and evaluate the distributions of QIVIVE ratios. This can be done in the future when more bioassay data become available from HTS studies.

The $QIVIVE_{nom}$ ratios of PFOA and PFOS were 1.96 and 22.7, suggesting PFOA and PFOS might cause an *in vivo* effect after occupational exposure with respect to this particular biological endpoint (Table 3, Fig. 5). In epidemiological studies, associations between decrease of PFOS and PFOA concentrations in serum and low-density lipoprotein cholesterol have been demonstrated (Fitz-Simon et al., 2013), which hints at the relevance of lipid metabolism and hence binding to PPARγ as relevant molecular initiating event.

The $QIVIVE_{free}$ ratio of PFOA and PFOS were reduced to 5.87×10^{-3} and 1.34×10^{-2} (Table 3, Fig. 5), indicating that proteins and lipids in plasma may act as reservoirs of PFAS, reducing the freely dissolved concentration of PFAS. But this does not mean it is safe since a majority of bound PFAS still accumulate in the body and can be remobilized. The large difference between $QIVIVE_{nom}$ and $QIVIVE_{free}$ for anionic PFAS is because protein binding is highly concentration-dependent with a high-affinity specific binding at low concentrations and lower non-specific binding at higher concentrations. Thus, the low concentrations in human plasma are strongly bound to proteins, while the high concentration needed to trigger effects in *in vitro* bioassays have a higher fraction unbound.

Since the concentrations of these PFAS in general population were thousands of times lower than those in workers or residents living near fluorochemical plants, both $QIVIVE_{nom}$ and $QIVIVE_{free}$ ratios of general population were thus calculated to be thousands lower (Table 3, Fig. 5).

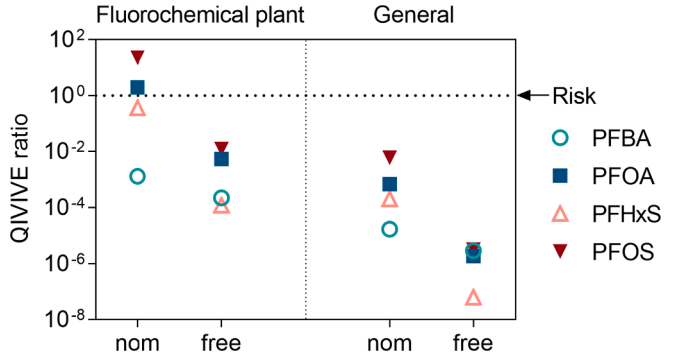

Fig. 5. Quantitative *in vitro* to *in vivo* extrapolation (QIVIVE ratio) for workers and residents living near fluorochemical plants and general population based on nominal concentrations (nom, (Eq. (28)) or free concentrations (free, (Eq. (29)) of human exposure level and effective concentrations in the PPARγ-GeneBLAzer bioassay.

4. Conclusion

The use of PFAS has improved the quality of our life, but their persistence and continued usage perpetuate their adverse impact on humans and the environment. HTS cell-based bioassays can be used to characterize the potential toxicity of PFAS, and the associated QIVIVE ratios allow one rank their relative risk (Bell et al., 2018). This may be a practical strategy to deal with a conflict between commercial needs and environmental health protection.

PFAS bound to proteins in plasma can also be transported to cells or different tissues in bound form with the blood and released at other organs and sites. There is an equilibrium distribution of C_{free} and C_{bound} (Fischer et al., 2018) due to the reversible binding of PFAS to proteins. Receptors with high affinity could trigger the dissociation from serum albumins acting as transporters. Such redistribution can occur in blood and in the *in vitro* bioassays and therefore C_{free} can be considered still a useful parameter from comparisons.

The binding of PFAS to proteins is strongly concentration-dependent. All biomaterials that have much higher protein than lipid content showed also concentration-dependent binding curves, which is a great experimental challenge if many anionic PFAS need to be characterized. Given the small contribution of lipid binding in case of human plasma, it is possible to use $D_{BSA/w}$ as a surrogate for $D_{plasma/w}$ but for plasma of other environmental organisms with higher lipid content, lipid partitioning would need to be included.

The MBM yielded an adequate prediction of C_{free} in cell-based bioassays. Although we demonstrated the validity of the MBM only for four anionic PFAS, one type of bioassay medium and one cell line, previous work on other organic anions has demonstrated that models can be transferred to other bioassay setups if the lipid and protein content has been quantified (Henneberger et al., 2019b; Huchthausen et al., 2020). Again, it must be stressed that the nonlinear binding behavior of anionic PFAS to proteins is not a feature of the perfluorination of the molecules but caused by the deprotonated carboxylic acid or sulfonic acid group of the tested PFAS. Thus, with respect to protein binding, our results and comparison to protein binding of non-fluorinated organic ions demonstrate that the anionic PFAS behave like other organic anions.

The PPARγ reporter gene assay is just one exemplary HTS assay that was included in Tox21. The Tox21 collaboration has employed>60 HTS assays for chemical assessments, including assays for cytotoxicity, cell stress, mitochondrial function and nuclear receptor activation (Sipes et al., 2017). A bioassay test battery that covers a range of relevant modes of action may be used for overall toxicity evaluation for commercially available PFAS. 75 PFAS were selected for high-throughput effect screening (Patlewicz et al., 2019) conducted by researchers of U.S. EPA and the National Toxicology Program (https://www.epa.gov/pfas, accessed January 2023) and the results are still pending. Furthermore, more complex *in vitro* models such as models derived from human induced pluripotent stem cells (Corbett 2019) may serve in the future as a more suitable point of departure for QIVIVE.

As the anionic PFAS have shown such a strong and non-linear binding to proteins, their true internal effect concentrations might be much different from neutral PFAS and the toxic effects of hydrophobic anionic PFAS may be underestimated as compared to the hydrophilic ones. Therefore, $C_{free,bioassay}$ may be a more appropriate dose-metric for comparative effect assessment and QIVIVE of PFAS. The MBM was successfully used to predict $C_{free,bioassay}$ of PFAS in one bioassay, which will greatly improve the accuracy of HTS to identify specific effects and compare effects across bioassay types. It will not always be necessary to measure C_{free} of PFAS but existing HTS effect data based on nominal concentrations can be converted to free effect concentrations using the MBM.

Funding

Weiping Qin received funding through Chinese Scholarship Council

and was supported by the Helmholtz Association under the recruiting initiative scheme, which is funded by the German Ministry of Education and Research, within the Helmholtz POF IV Topic 9 “Healthy Planet-towards a non-toxic environment”.

CRediT authorship contribution statement

Weiping Qin: Conceptualization, Investigation, Validation, Formal analysis, Writing – original draft, Writing – review & editing, Funding acquisition. **Luise Henneberger:** Methodology, Validation, Writing – review & editing. **Julia Huchthausen:** Methodology, Validation, Writing – review & editing. **Maria König:** Investigation, Writing – review & editing. **Beate I. Escher:** Conceptualization, Methodology, Validation, Visualization, Resources, Writing – review & editing, Supervision, Funding acquisition.

Declaration of Competing Interest

The authors declare that they have no known competing financial interests or personal relationships that could have appeared to influence the work reported in this paper.

Data availability

Data will be made available on request.

Acknowledgement

We thank Juliane Glüge of ETH Zürich, Switzerland for helpful discussions and prediction of octanol-water partition constants with COSMOtherm. We thank Xinghui Xia for providing the raw data of their dialysis experiments with BSA (Xia et al., 2013). We gratefully acknowledge access to the platform CITEPro (Chemicals in the Environment Profiler) funded by the Helmholtz Association for bioassay measurements and chemical analysis.

Appendix A. Supplementary material

Supplementary data to this article can be found online at https://doi.org/10.1016/j.envint.2023.107857.

References

Abbott, B.D., 2009. Review of the expression of peroxisome proliferator-activated receptors alpha (PPAR alpha), beta (PPAR beta), and gamma (PPAR gamma) in rodent and human development. Reprod. Toxicol. 27, 246–257.
Alesio, J.L., Slitt, A., Bothun, G.D., 2022. Critical new insights into the binding of poly- and perfluoroalkyl substances (PFAS) to albumin protein. Chemosphere 287, 131979.
Allendorf, F., Berger, U., Goss, K.U., Ulrich, N., 2019. Partition coefficients of four perfluoroalkyl acid alternatives between bovine serum albumin (BSA) and water in comparison to ten classical perfluoroalkyl acids. Environ. Sci. Process Impacts 21, 1852–1863.
Almeida, N.M.S., Eken, Y., Wilson, A.K., 2021. Binding of per- and polyfluoro-alkyl substances to peroxisome proliferator-activated receptor gamma. ACS Omega 6, 15103–15114.
Bao, J., Shao, L.X., Liu, Y., Cui, S.W., Wang, X., Lu, G.L., Wang, X., Jin, Y.H., 2022. Target analysis and suspect screening of per- and polyfluoroalkyl substances in paired samples of maternal serum, umbilical cord serum, and placenta near fluorochemical plants in Fuxin, China. Chemosphere 307, 135731.
Behr, A.C., Plinsch, C., Braeuning, A., Buhrke, T., 2020. Activation of human nuclear receptors by perfluoroalkylated substances (PFAS). Toxicol. In Vitro 62, 104700.
Bell, S.M., Chang, X., Wambaugh, J.F., Allen, D.G., Bartels, M., Brouwer, K.L.R., Casey, W.M., Choksi, N., Ferguson, S.S., Fraczkiewicz, G., Jarabek, A.M., Ke, A., Lumen, A., Lynn, S.G., Paini, A., Price, P.S., Ring, C., Simon, T.W., Sipes, N.S., Sprankle, C.S., Strickland, J., Troutman, J., Wetmore, B.A., Kleinstreuer, N.C., 2018. In vitro to in vivo extrapolation for high throughput prioritization and decision making. Toxicol. In Vitro 47, 213–227.
Bischel, H.N., Macmanus-Spencer, L.A., Luthy, R.G., 2010. Noncovalent interactions of long-chain perfluoroalkyl acids with serum albumin. Environ. Sci. Tech. 44, 5263–5269.
Cakmak, S., Lukina, A., Karthikeyan, S., Atlas, E., Dales, R., 2022. The association between blood PFAS concentrations and clinical biochemical measures of organ function and metabolism in participants of the Canadian Health Measures Survey (CHMS). Sci. Total Environ. 827, 153900.
Calvert, L., Green, M.P., De Iuliis, G.N., Dun, M.D., Turner, B.D., Clarke, B.O., Eamens, A. L., Roman, S.D., Nixon, B., 2021. Assessment of the emerging threat posed by perfluoroalkyl and polyfluoroalkyl substances to male reproduction in humans. Front. Endocrinol. (Lausanne) 12, 799043.
Chen, Y.M., Guo, L.H., 2009. Fluorescence study on site-specific binding of perfluoroalkyl acids to human serum albumin. Arch. Toxicol. 83, 255–261.
Corbett, J.L. and D., S.A. iPSC-Derived Hepatocytes as a Platform for Disease Modeling and Drug Discovery. Front Med (Lausanne) 2019;15:265.
Costa, G., Sartori, S., Consonni, D., 2009. Thirty years of medical surveillance in perfluorooctanoic acid production workers. J. Occup. Environ. Med. 51, 364–372.
Cousins, I.T., Johansson, J.H., Salter, M.E., Sha, B., Scheringer, M., 2022. Outside the Safe Operating Space of a New Planetary Boundary for Per- and Polyfluoroalkyl Substances (PFAS). Environ. Sci. Tech. 56, 11172–11179.
Dimitrijevic, D., Fabian, E., Nicol, B., Funk-Weyer, D., Landsiedel, R., 2022. Toward realistic dosimetry in vitro: Determining effective concentrations of test substances in cell culture and their prediction by an in silico mass balance model. Chem. Res. Toxicol. 35, 1962–1973. https://doi.org/10.1021/acs.chemrestox.2c00128.
DeWitt, J.C., Shnyra, A., Badr, M.Z., Loveless, S.E., Hoban, D., Frame, S.R., Cunard, R., Anderson, S.E., Meade, B.J., Peden-Adams, M.M., Luebke, R.W., Luster, M.I., 2009. Immunotoxicity of perfluorooctanoic acid and perfluorooctane sulfonate and the role of peroxisome proliferator-activated receptor alpha. Crit. Rev. Toxicol. 39, 76–94.
Ebert, A., Allendorf, F., Berger, U., Goss, K.U., Ulrich, N., 2020. Membrane/water partitioning and permeabilities of perfluoroalkyl acids and four of their alternatives and the effects on toxicokinetic behavior. Environ. Sci. Tech. 54, 5051–5061.
Escher, B.I., Glauch, L., Konig, M., Mayer, P., Schlichting, R., 2019. Baseline toxicity and volatility cutoff in reporter gene assays used for high-throughput screening. Chem. Res. Toxicol. 32, 1646–1655.
Escher, B.I., Neale, P.A., Villeneuve, D.L., 2018. The advantages of linear concentration-response curves for in vitro bioassays with environmental samples. Environ. Toxicol. Chem. 37, 2273–2280.
Evich, M.G., Davis, M. J. B., McCord, J. P., Acrey, B., Awkerman, J. A., Knappe, D. R. U., Lindstrom, A. B., Speth, T. F., Tebes-Stevens, C., Strynar, M. J., Wang, Z., Weber, E. J., Henderson, W. M. and Washington, J. W. Per- and polyfluoroalkyl substances in the environment. Science 2022;375:eabg9065.
Fischer, F.C., Cirpka, O. A., Goss, K. U., nneberger, L. and Escher, B. I. Application of experimental polystyrene partition constants and diffusion coefficients to predict the sorption of neutral organic chemicals to multiwell plates in in vivo and in vitro bioassays. Environ Sci Technol 2018;52:13511-13522.
Fischer, F.C., Henneberger, L., Konig, M., Bittermann, K., Linden, L., Goss, K.U., Escher, B.I., 2017. Modeling exposure in the Tox21 in vitro bioassays. Chem. Res. Toxicol. 30, 1197–1208.
Fitz-Simon, N., Fletcher, T., Luster, M.I., Steenland, K., Calafat, A.M., Kato, K., Armstrong, B., 2013. Reductions in serum lipids with a 4-year decline in serum perfluorooctanoic acid and perfluorooctanesulfonic acid. Epidemiology 24, 569–576.
Forsthuber, M., Kaiser, A.M., Granitzer, S., Hassl, I., Hengstschläger, M., Stangl, H., Gundacker, C., 2020. Albumin is the major carrier protein for PFOS, PFOA, PFHxS, PFNA and PFDA in human plasma. Environ. Int. 137, 105324.
Gao, K., Zhuang, T., Liu, X., Fu, J., Zhang, J., Fu, J., Wang, L., Zhang, A., Liang, Y., Song, M., Jiang, G., 2019. Prenatal exposure to per- and polyfluoroalkyl substances (PFASs) and association between the placental transfer efficiencies and dissociation constant of serum proteins-PFAS complexes. Environ. Sci. Tech. 53, 6529–6538.
Gao, Y., Fu, J., Cao, H., Wang, Y., Zhang, A., Liang, Y., Wang, T., Zhao, C., Jiang, G., 2015. Differential accumulation and elimination behavior of perfluoroalkyl acid isomers in occupational workers in a manufactory in China. Environ. Sci. Tech. 49, 6953–6962.
Gluge, J., Scheringer, M., Cousins, I.T., DeWitt, J.C., Goldenman, G., Herzke, D., Lohmann, R., Ng, C.A., Trier, X., Wang, Z., 2020. An overview of the uses of per- and polyfluoroalkyl substances (PFAS). Environ. Sci. Process Impacts 22, 2345–2373.
Gockener, B., Weber, T., Rudel, H., Bucking, M., Kolossa-Gehring, M., 2020. Human biomonitoring of per- and polyfluoroalkyl substances in German blood plasma samples from 1982 to 2019. Environ. Int. 145, 106123.
Henneberger, L., Goss, K.U., Endo, S., 2016. Equilibrium sorption of structurally diverse organic ions to bovine serum albumin. Environ. Sci. Tech. 50, 5119–5126.
Henneberger, L., Huchthausen, J., Wojtysiak, N., Escher, B.I., 2021. Quantitative in vitro-to-in vivo extrapolation: nominal versus freely dissolved concentration. Chem. Res. Toxicol. 34, 1175–1182.
Henneberger, L., Muhlenbrink, M., Fischer, F.C., Escher, B.I., 2019a. C18-coated solid-phase microextraction fibers for the quantification of partitioning of organic acids to proteins, lipids, and cells. Chem. Res. Toxicol. 32, 168–178.
Henneberger, L., Muhlenbrink, M., Heinrich, D.J., Teixeira, A., Nicol, B., Escher, B.I., 2020. Experimental validation of mass balance models for in vitro cell-based bioassays. Environ. Sci. Tech. 54, 1120–1127.
Henneberger, L., Muhlenbrink, M., Konig, M., Schlichting, R., Fischer, F.C., Escher, B.I., 2019b. Quantification of freely dissolved effect concentrations in in vitro cell-based bioassays. Arch. Toxicol. 93, 2295–2305.
Heringa, M.B., Schreurs, R., Busser, F., Van Der Saag, P.T., Van Der Burg, B., Hermens, J. L.M., 2004. Toward more useful in vitro toxicity data with measured free concentrations. Environ. Sci. Tech. 38, 6263–6270.
Huchthausen, J., Muhlenbrink, M., Konig, M., Escher, B.I., Henneberger, L., 2020. Experimental exposure assessment of ionizable organic chemicals in in vitro cell-based bioassays. Chem. Res. Toxicol. 33, 1845–1854.

Kramer, N.I., Krismartina, M., Rico-Rico, A., Blaauboer, B.J., Hermens, J.L., 2012. Quantifying processes determining the free concentration of phenanthrene in Basal cytotoxicity assays. Chem. Res. Toxicol. 25, 436–445.
Li, C.H., Ren, X.M., Guo, L.H., 2019. Adipogenic activity of oligomeric hexafluoropropylene oxide (perfluorooctanoic acid alternative) through peroxisome proliferator-activated receptor gamma pathway. Environ. Sci. Tech. 53, 3287–3295.
Li, C.H., Ren, X.M., Ruan, T., Cao, L.Y., Xin, Y., Guo, L.H., Jiang, G., 2018. Chlorinated polyfluorinated ether sulfonates exhibit higher activity toward peroxisome proliferator-activated receptors signaling pathways than perfluorooctanesulfonate. Environ. Sci. Tech. 52, 3232–3239.
Lin, P.D., Cardenas, A., Hauser, R., Gold, D.R., Kleinman, K.P., Hivert, M.F., Fleisch, A.F., Calafat, A.M., Webster, T.F., Horton, E.S., Oken, E., 2019. Per- and polyfluoroalkyl substances and blood lipid levels in pre-diabetic adults-longitudinal analysis of the diabetes prevention program outcomes study. Environ. Int. 129, 343–353.
Liu, Y.Z., Pan, L.H., Bai, Y., Yang, K., Dong, P.P., Fang, Z.Z., 2020. Per- and polyfluoroalkyl substances exert strong inhibition towards human carboxylesterases. Environ. Pollut. 263, 114463.
Loizou, G., McNally, K., Dorne, J.C.M., Hogg, A., 2021. Derivation of a human in vivo benchmark dose for perfluorooctanoic acid from ToxCast in vitro concentration-response data using a computational workflow for probabilistic quantitative in vitro to in vivo extrapolation. Front. Pharmacol. 12, 630457.
Ma, Y., Yang, J., Wan, Y., Peng, Y., Ding, S., Li, Y., Xu, B., Chen, X., Xia, W., Ke, Y., Xu, S., 2018. Low-level perfluorooctanoic acid enhances 3T3-L1 preadipocyte differentiation via altering peroxisome proliferator activated receptor gamma expression and its promoter DNA methylation. J. Appl. Toxicol. 38, 398–407.
MacManus-Spencer, L.A., Tse, M.L., Hebert, P.C., Bischel, H.N., Luthy, R.G., 2010. Binding of perfluorocarboxylates to serum albumin: a comparison of analytical methods. Anal. Chem. 82, 974–981.
Mariussen, E., 2012. Neurotoxic effects of perfluoroalkylated compounds: mechanisms of action and environmental relevance. Arch. Toxicol. 86, 1349–1367.
Mokra, K., 2021. Endocrine disruptor potential of short- and long-chain perfluoroalkyl substances (PFASs)-A synthesis of current knowledge with proposal of molecular mechanism. Int. J. Mol. Sci. 22.
Neale, P.A., Altenburger, R., Ait-Aissa, S., Brion, F., Busch, W., de Aragao Umbuzeiro, G., Denison, M.S., Du Pasquier, D., Hilscherova, K., Hollert, H., Morales, D.A., Novak, J., Schlichting, R., Seiler, T.B., Serra, H., Shao, Y., Tindall, A.J., Tollefsen, K.E., Williams, T.D., Escher, B.I., 2017. Development of a bioanalytical test battery for water quality monitoring: Fingerprinting identified micropollutants and their contribution to effects in surface water. Water Res. 123, 734–750.
Neale, P.A.a.L., F. D. Considerations when assessing antagonism in vitro: Why standardizing the agonist concentration matters. Chemosphere 2015;135:20-23.
Pan, Z., Miao, W., Wang, C., Tu, W., Jin, C., Jin, Y., 2021. 6:2 Cl-PFESA has the potential to cause liver damage and induce lipid metabolism disorders in female mice through the action of PPAR-gamma. Environ. Pollut. 287, 117329.
Park, M., W.S.M., Lopez, I.J., Chang J.Y., Karanfil T. and Snyder, S.A. Adsorption of perfluoroalkyl substances (PFAS) in groundwater by granular activated carbons: Roles of hydrophobicity of PFAS and carbon characteristics. Water Res. 2020;170: 115364.
Patlewicz, G., Richard, A.M., Williams, A.J., Grulke, C.M., Sams, R., Lambert, J., Noyes, P.D., DeVito, M.J., Hines, R.N., Strynar, M., Guiseppi-Elie, A., Thomas, R.S., 2019. A Chemical Category-Based Prioritization Approach for Selecting 75 Per- and Polyfluoroalkyl Substances (PFAS) for Tiered Toxicity and Toxicokinetic Testing. Environ. Health Perspect. 127, 14501.
Peng, L., Xu, W., Zeng, Q., Cheng, Y., Zhang, Y., Guo, Y., Chen, D., Jiang, C., Wang, F., 2021. Distribution characteristics of per- and polyfluoroalkyl substances (PFASs) in human urines of acrylic fiber plant and chemical plant. Environ. Sci. Pollut. Res. Int. 28, 69181–69189.
Petriello, M.C., Mottaleb, M.A., Serio, T.C., Balyan, B., Cave, M.C., Pavuk, M., Birnbaum, L.S., Morris, A.J., 2022. Serum concentrations of legacy and emerging per- and polyfluoroalkyl substances in the Anniston Community Health Surveys (ACHS I and ACHS II). Environ. Int. 158, 106907.
Proenca, S., Escher, B.I., Fischer, F.C., Fisher, C., Gregoire, S., Hewitt, N.J., Nicol, B., Paini, A., Kramer, N.I., 2021. Effective exposure of chemicals in in vitro cell systems: A review of chemical distribution models. Toxicol. In Vitro 73, 105133.
Qin, W.P., Cao, L.Y., Li, C.H., Guo, L.H., Colbourne, J., Ren, X.M., 2020. Perfluoroalkyl substances stimulate insulin secretion by islet beta cells via G protein-coupled receptor 40. Environ. Sci. Tech. 54, 3428–3436.
Rappazzo, K.M., Coffman, E., Hines, E.P., 2017. Exposure to perfluorinated alkyl substances and health outcomes in children: A systematic review of the epidemiologic literature. Int. J. Environ. Res. Public Health 14.
Ren, X.M., Qin, W.P., Cao, L.Y., Zhang, J., Yang, Y., Wan, B., Guo, L.H., 2016. Binding interactions of perfluoroalkyl substances with thyroid hormone transport proteins and potential toxicological implications. Toxicology 366–367, 32–42.
Rotander, A., Toms, L.M., Aylward, L., Kay, M., Mueller, J.F., 2015. Elevated levels of PFOS and PFHxS in firefighters exposed to aqueous film forming foam (AFFF). Environ. Int. 82, 28–34.
Sakr, C.J., Leonard, R.C., Kreckmann, K.H., Slade, M.D., Cullen, M.R., 2007. Longitudinal study of serum lipids and liver enzymes in workers with occupational exposure to ammonium perfluorooctanoate. J. Occup. Environ. Med. 49, 872–879.
Sipes, N.S., Wambaugh, J.F., Pearce, R., Auerbach, S.S., Wetmore, B.A., Hsieh, J.H., Shapiro, A.J., Svoboda, D., DeVito, M.J., Ferguson, S.S., 2017. An Intuitive approach for predicting potential human health risk with the Tox21 10k Library. Environ. Sci. Tech. 51, 10786–10796.
Takacs, M.L., Abbott, B.D., 2007. Activation of mouse and human peroxisome proliferator-activated receptors (alpha, beta/delta, gamma) by perfluorooctanoic acid and perfluorooctane sulfonate. Toxicol. Sci. 95, 108–117.
Theodore, P.J., 1985. Serum albumin. Adv. Protein Chem. 37, 161–245.
Vanden Heuvel, J.P., Thompson, J.T., Frame, S.R., Gillies, P.J., 2006. Differential activation of nuclear receptors by perfluorinated fatty acid analogs and natural fatty acids: a comparison of human, mouse, and rat peroxisome proliferator-activated receptor-alpha, -beta, and -gamma, liver X receptor-beta, and retinoid X receptor-alpha. Toxicol. Sci. 92, 476–489.
Wang, J., Zhang, Y., Zhang, W., Jin, Y., Dai, J., 2012. Association of perfluorooctanoic acid with HDL cholesterol and circulating miR-26b and miR-199-3p in workers of a fluorochemical plant and nearby residents. Environ. Sci. Tech. 46, 9274–9281.
Wang, S., Lv, Q., Yang, Y., Guo, L.H., Wan, B., Zhao, L., 2014. Cellular target recognition of perfluoroalkyl acids: in vitro evaluation of inhibitory effects on lysine decarboxylase. Sci. Total Environ. 496, 381–388.
Wetmore, B.A., 2015. Quantitative in vitro-to-in vivo extrapolation in a high-throughput environment. Toxicology 332, 94–101.
Worley, R.R., Fisher, J., 2015. Application of physiologically-based pharmacokinetic modeling to explore the role of kidney transporters in renal reabsorption of perfluorooctanoic acid in the rat. Toxicol. Appl. Pharmacol. 289, 428–441.
Xia, X., Rabearisoa, A.H., Jiang, X., Dai, Z., 2013. Bioaccumulation of perfluoroalkyl substances by Daphnia magna in water with different types and concentrations of protein. Environ. Sci. Tech. 47, 10955–10963.
Yu, C.H., Riker, C.D., Lu, S.E., Fan, Z.T., 2020. Biomonitoring of emerging contaminants, perfluoroalkyl and polyfluoroalkyl substances (PFAS), in New Jersey adults in 2016–2018. Int. J. Hyg. Environ. Health 223, 34–44.
Zeng, Z., Song, B., Xiao, R., Zeng, G., Gong, J., Chen, M., Xu, P., Zhang, P., Shen, M., Yi, H., 2019. Assessing the human health risks of perfluorooctane sulfonate by in vivo and in vitro studies. Environ. Int. 126, 598–610.
Zhang, L., Ren, X.M., Wan, B., Guo, L.H., 2014. Structure-dependent binding and activation of perfluorinated compounds on human peroxisome proliferator-activated receptor gamma. Toxicol. Appl. Pharmacol. 279, 275–283.
Zhang, S., Kang, Q., Peng, H., Ding, M., Zhao, F., Zhou, Y., Dong, Z., Zhang, H., Yang, M., Tao, S., Hu, J., 2019. Relationship between perfluorooctanoate and perfluorooctane sulfonate blood concentrations in the general population and routine drinking water exposure. Environ. Int. 126, 54–60.

Publication 2

Baseline Toxicity Model to Identify the Specific and Nonspecific Effects of Per- and Polyfluoroalkyl Substances in Cell-based Bioassays.

Weiping Qin,[1,2] Luise Henneberger,[1] Juliane Glüge,[1,3] Maria König[1] and Beate I. Escher[1,2]*

[1] Department of Cell Toxicology, UFZ–Helmholtz Centre for Environmental Research, 04318 Leipzig, Germany

[2] Environmental Toxicology, Department of Geosciences, Eberhard Karls University Tübingen, Schnarrenbergstr. 94-96, DE-72076 Tübingen, Germany

[3] Institute of Biogeochemistry and Pollutant Dynamics, ETH Zürich, 8092 Zürich, Switzerland.

*Corresponding author Beate I. Escher − UFZ−Helmholtz Centre for Environmental Research, 04318 Leipzig, Germany; orcid.org/0000-0002-5304-706X; Email: beate.escher@ufz.de

Published in Environmental Science & Technology, https://doi.org/10.1021/acs.est.3c09950.

Environmental Science & Technology

pubs.acs.org/est

Article

Baseline Toxicity Model to Identify the Specific and Nonspecific Effects of Per- and Polyfluoroalkyl Substances in Cell-Based Bioassays

Weiping Qin, Luise Henneberger, Juliane Glüge, Maria König, and Beate I. Escher*

Cite This: *Environ. Sci. Technol.* 2024, 58, 5727−5738

Read Online

ACCESS | Metrics & More | Article Recommendations | Supporting Information

ABSTRACT: High-throughput screening is a strategy to identify potential adverse outcome pathways (AOP) for thousands of per- and polyfluoroalkyl substances (PFAS) if the specific effects can be distinguished from nonspecific effects. We hypothesize that baseline toxicity may serve as a reference to determine the specificity of the cell responses. Baseline toxicity is the minimum (cyto)toxicity caused by the accumulation of chemicals in cell membranes, which disturbs their structure and function. A mass balance model linking the critical membrane concentration for baseline toxicity to nominal (i.e., dosed) concentrations of PFAS in cell-based bioassays yielded separate baseline toxicity prediction models for anionic and neutral PFAS, which were based on liposome-water distribution ratios as the sole model descriptors. The specificity of cell responses to 30 PFAS on six target effects (activation of peroxisome proliferator-activated receptor (PPAR) gamma, aryl hydrocarbon receptor, oxidative stress response, and neurotoxicity in own experiments, and literature data for activation of several PPARs and the estrogen receptor) were assessed by comparing effective concentrations to predicted baseline toxic concentrations. HFPO−DA, HFPO−DA-AS, and PFMOAA showed high specificity on PPARs, which provides information on key events in AOPs relevant to PFAS. However, PFAS were of low specificity in the other experimentally evaluated assays and others from the literature. Even if PFAS are not highly specific for certain defined targets but disturb many toxicity pathways with low potency, such effects are toxicologically relevant, especially for hydrophobic PFAS and because PFAS are highly persistent and cause chronic effects. This implicates a heightened need for the risk assessment of PFAS mixtures because nonspecific effects behave concentration-additive in mixtures.

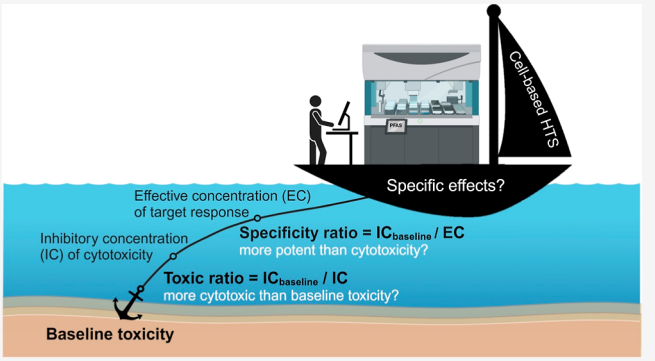

KEYWORDS: *PFAS, membrane concentration, liposome-water distribution ratio, potential adverse outcome pathways, peroxisome proliferator-activated receptors*

INTRODUCTION

The threat that per- and polyfluoroalkyl substances (PFAS) pose to human health has been a great concern for society. The concern has expanded from perfluorooctanoic acid (PFOA) and perfluorooctanesulfonic acid (PFOS) to thousands of PFAS with diverse structures and unclear toxicological effects. The OECD broadened the definition of PFAS to at least one perfluorinated carbon,[1] which implies that there are now more than 14,000 PFAS chemicals in the CompTox Chemistry Dashboard.[2] Traditional methods can no longer cope with the risk assessment of such large numbers of PFAS. New approach methodologies (NAM), especially those based on high-throughput screening (HTS) with cellular assays, provide a strategy of extensive screening for molecular initiating events and key events in adverse outcome pathways (AOP) because cell responses can serve as early warning signals. PFAS may trigger cell responses through several cellular toxicity pathways, including reactive (oxidative stress),[3] specific (receptor-mediated signaling pathways),[4] and nonspecific toxicity.

Baseline toxicity, also known as narcosis, is a common, nonspecific effect caused by an accumulation of chemicals in cell membranes that interfere with membrane function and destroy membrane integrity.[5] Chemicals that act as baseline toxicants can trigger specific effects at critical membrane concentrations. Baseline toxicity does not equate to low toxicity; very hydrophobic chemicals can still be very potent through baseline toxicity, i.e., act in low concentrations. Hence,

Received: November 27, 2023
Revised: February 11, 2024
Accepted: February 12, 2024
Published: February 23, 2024

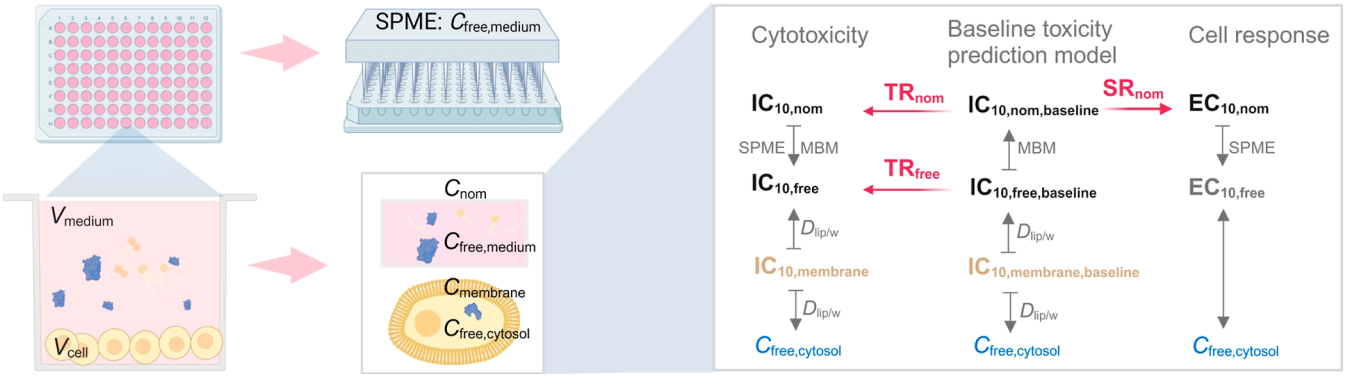

Figure 1. An overview of the dose-metrics and baseline toxicity prediction models for cell-based bioassays. Abbreviation: V_{medium} or V_{cell} = volume of medium or cells, C_{nom} = nominal concentration, C_{free} = free concentration, SPME = solid-phase microextraction, MBM = mass balance model, IC = inhibitory concentration, EC = effect concentration, $D_{lip/w}$ = distribution ratio between liposomes and water, TR = toxic ratio, and SR = specificity ratio.

baseline toxicity may serve as an anchor or reference state to determine the degree of specificity of PFAS in cell-based bioassays because specific effects occur at even lower concentrations.

Baseline toxicity occurs when critical membrane burdens are exceeded. Escher et al.[6] derived the critical membrane concentration of baseline toxicants that causes 10% of cytotoxicity $IC_{10,membrane,baseline}$ as 69 mmol/L_{lip} from eight different cell lines. $IC_{10,membrane,baseline}$ was independent of the cell line and constant for all organic chemicals. As in vitro bioassay responses are reported as nominal (i.e., dosed) concentrations in bioassay medium, one needs to link $IC_{10,membrane,baseline}$ and freely dissolved concentrations ($IC_{10,free,baseline}$) to nominal concentrations ($IC_{10,nom,baseline}$), which can be accomplished by mass balance models (MBM).[7] While $IC_{10,membrane,baseline}$ is constant, $IC_{10,free,baseline}$ is dependent on the partitioning of chemicals into membrane lipid bilayers, which can be simulated by phospholipid vesicles, so-called liposomes. The $IC_{10,free,baseline}$ can vary over many orders of magnitude. Hydrophobic chemicals have much lower $IC_{10,free,baseline}$ values than hydrophilic and charged chemicals. $IC_{10,nom,baseline}$ is determined by the experimental conditions and binding affinities of PFAS to proteins and lipids in the medium and cells. An overview of these metrics can be found in Figure 1.

The inhibitory concentration at 10% cytotoxicity ($IC_{10,nom}$) can be derived from the concentration−cytotoxicity curves using nominal concentrations in the bioassay. The ratio between $IC_{10,nom,baseline}$ and experimental $IC_{10,nom}$ is called the toxic ratio (TR_{nom}).[8,9] At lower, noncytotoxic concentrations, many in vitro bioassays trigger specific effects, such as the activation of receptors or adaptive stress responses. The effect concentration at 10% effect ($EC_{10,nom}$) can be compared to the cytotoxicity $IC_{10,nom,baseline}$ to derive the specificity ratio (SR_{nom}).[9] If TR_{nom} or SR_{nom} are close to 1, cell death or response may be caused by baseline toxicity. A positive artifact due to the so-called cytotoxicity burst may appear when cells are close to death. High TR_{nom} or SR_{nom} values suggest that chemicals specifically trigger cytotoxicity or defined targets at lower concentrations than baseline toxicity.

The specific effects refer to the signals from defined targets, which can be distinguished from the nonspecific baseline toxicity. Here are several cases among the numerous toxicological studies. Oxidative stress is a common mechanism of PFAS-induced cytotoxicity.[3] For example, acute exposure to PFOS induced excessive production of reactive oxidative species, resulting in the apoptosis of mouse islet β-TC-6 cells[10] and human neuroblastoma SH-SY5Y cells.[11] As a cellular defense, PFOS was found to trigger the nuclear factor erythroid 2-related factor 2 (Nrf2)-antioxidant response element (ARE) pathway, which plays a critical role in cellular protection against toxicity and oxidative stress from chemical stressors.[12] Besides, PFAS may disrupt endocrine homeostasis by interacting with receptor-mediated signaling pathways.[4] For example, PFOS promoted adipogenesis via peroxisome proliferator-activated receptors (PPARs) in mouse preadipocyte 3T3-L1 cells;[13] PFDA and PFDoA might disrupt the function of the thyroid hormone system via aryl hydrocarbon receptor (AhR) in rat pituitary GH3 cell;[14] PFOS stimulated insulin secretion via membrane G-protein coupled receptor (GPR) 40 in mouse islet β-TC-6 cells.[15] Neurotoxicity is also of concern; for example, PFOS enhanced nerve growth factor-induced neurite outgrowth in rat pheochromocytoma PC12 cells.[16] To relate the observed effects to baseline toxicity is a way to allow comparison between different test systems and end points and to identify effects that are of particular concern due to high TR_{nom} or SR_{nom}.

Tox21 and ToxCast are programs of multiple federal agencies, including the U.S. Environmental Protection Agency (EPA) and the National Toxicology Program,[17] aiming at efficiently identifying potential AOPs for specified chemicals at molecular, cellular, and organ levels through HTS to facilitate risk assessments of chemicals. Currently, in vitro effect data for 160 PFAS from the EPA have been published.[18−21] Transactivation assays encompassing 81 diverse transcription factors were screened with 142 PFAS to describe the activation of nuclear receptor-mediated signaling pathways.[18] 148 biomarkers relevant to the immune system were measured with 147 PFAS to inform mechanisms of immunotoxicity.[19] A NAM battery for developmental neurotoxicity was developed to evaluate the effects of 160 PFAS on neural network formation and function.[20] Radioactive iodide uptake high-throughput assay was used to test 149 PFAS for potential thyroid disruption.[21] However, data evaluation and ranking scores were done independently with diverse conclusions, which makes it difficult to determine which PFAS are of the highest concern and which in vitro end points are relevant for human health.

In the present study, we systematically assessed the role of PFAS distribution in bioassay systems and how this affected

https://doi.org/10.1021/acs.est.3c09950
Environ. Sci. Technol. 2024, 58, 5727−5738

the different dose-metrics in bioassays (Figure 1). The free concentrations of 10 anionic and one partially charged PFAS in the bioassays run in a 96-well plate format were measured by solid-phase microextraction (SPME) to derive $IC_{10,free}$ from a free concentration−cytotoxicity curve. Experimental $IC_{10,free}$ values were compared with $IC_{10,free}$ predicted by the MBM. A validated MBM was used to link the known critical membrane concentrations for baseline toxicity $IC_{10,membrane,baseline}$ to $IC_{10,nom,baseline}$.

Four cell-based HTS were selected as experimental batteries, including three reporter gene assays targeting oxidative stress (AREc32 assay), nuclear receptors of PPARγ and AhR, as well as an image-based neurotoxicity assay that quantifies inhibition of neurite outgrowth of differentiated SH-SYSY cells, because these targets may be relevant to PFAS according to previous studies.[11−14,16] 24 PFAS were then tested in a 384-well plate format. The cytotoxicity $IC_{10,nom}$ and the effect concentrations $EC_{10,nom}$ from these assays were compared with the $IC_{10,nom,baseline}$ to derive TR_{nom} and SR_{nom}, which were used to determine if the effects of PFAS are specific. We also demonstrated the applicability of the approach to other assays by evaluating the bioassay responses of 16 PFAS from the literature for their degree of specificity.

THEORY

Free Concentrations of PFAS in Bioassays. The nominal concentration (C_{nom}) in a bioassay is the total amount of chemicals (n_{tot}) dosed divided by the total volume of the bioassay system (V_{tot}), which is composed of medium (V_{medium}) and cells (V_{cell}) .

$$C_{nom} = \frac{n_{tot}}{V_{medium} + V_{cell}} = \frac{n_{tot}}{V_{tot}} \quad (1)$$

Fetal bovine serum (FBS) in medium serves as a reservoir of reversibly bound chemical and also facilitates a faster equilibrium of chemical between medium and cells,[22] and thus, the free concentration of PFAS in medium ($C_{free,medium}$) is usually lower than C_{nom}. An MBM that accounts for the binding of chemicals to proteins and lipids in the medium and cells (eq 2) has been developed and validated experimentally for chemicals.[23]

$$n_{tot} = n_{free} + n_{bound,i} = C_{free,medium} \times \left(V_w + \sum_{i=1}^{n} (D_{i/w} \times V_i)\right) \quad (2)$$

$C_{free,medium}$ is related to the C_{nom} by inserting eq 1 in 2 yielding eq 3 with distribution ratios between the medium and water ($D_{medium/w}$) and between the cells and water ($D_{cell/w}$), as well as volumes of protein and lipid ($V_{protein+lipid}$) in cells and medium. The detailed derivation of eq 3 is in Supporting Information Text S1.

$$C_{free,medium} = \frac{C_{nom} \times V_{tot}}{V_w + D_{medium/w} \times V_{protein+lipid,medium} + D_{cell/w} \times V_{protein+lipid,cell}} \quad (3)$$

$D_{medium/w}$ and $D_{cell/w}$ can be measured experimentally or predicted by MBMs with the assumption that proteins and lipids are the main sorption phases in the medium and cells. Bovine serum albumin (BSA) serves as a surrogate for protein binding in medium ($D_{BSA/w}$) and liposomes for partitioning to membrane lipids ($D_{lip/w}$). Then, $D_{medium/w}$ can be predicted by eq 4.

$$D_{medium/w} = D_{BSA/w} \times \frac{V_{protein,medium}}{V_{protein+lipid,medium}} + D_{lip/w} \times \frac{V_{lipid,medium}}{V_{protein+lipid,medium}} \quad (4)$$

The most abundant proteins in cells are structural proteins (SP), for which muscle proteins are better surrogates than BSA.[24] Analogously, $D_{cell/w}$ can be predicted by eq 5 with $D_{SP/w}$ referring to the distribution ratio between SP and water.

$$D_{cell/w} = D_{SP/w} \times \frac{V_{protein,cell}}{V_{protein+lipid,cell}} + D_{lip/w} \times \frac{V_{lipid,cell}}{V_{protein+lipid,cell}} \quad (5)$$

Note that in the previous baseline toxicity model,[7] we had defined the $D_{medium/w}$ and $D_{cell/w}$ by including the water, protein, and lipid volumes in medium and cells, but here only protein and lipid volumes were defined as the sorption phases. $C_{free,medium}$ can be calculated from C_{nom} by inserting eqs 4 and 5 in eq 3.

$$C_{free,medium} = \frac{C_{nom} \times V_{tot}}{V_w + D_{BSA/w} \times V_{protein,medium} + D_{lip/w} \times V_{lipid,medium} + D_{SP/w} \times V_{protein,cell} + D_{lip/w} \times V_{lipid,cell}} \quad (6)$$

Membrane and Free Concentrations Related to Baseline Toxicity. Chemicals inevitably accumulate in the membrane during the cellular uptake from the medium into the cytosol. The partitioning to membrane lipid bilayers can be simulated by phospholipid vesicles, so-called liposomes. The distribution ratio ($D_{lip/w}$ (pH = 7.4)) is the ratio of the concentration of a chemical bound to liposomes (C_{lip}) divided by the free concentration in the water phase (C_w).

$$D_{lip/w} = \frac{C_{lip}}{C_w} \quad (7)$$

Some ionized PFAS may be actively transported into cells via ion channels or transport proteins, but due to their high membrane permeability, passive diffusion has been proven to dominate the cellular uptake of even the anionic PFAS.[25] There is no pH gradient under typical bioassay conditions; thus, even charged organic chemicals reach a steady state in cells within hours.[22] It is safe to assume that free concentrations in cells ($C_{free,cytosol}$) and $C_{free,medium}$ are equal at the steady state.

If C_{lip} is related to a constant cell membrane concentration of baseline toxicants, namely, $IC_{10,membrane,baseline}$ of 69 mmol/

https://doi.org/10.1021/acs.est.3c09950
Environ. Sci. Technol. 2024, 58, 5727−5738

L_{lip},[6] the C_w presents the free concentration of baseline toxicants in the aqueous phase of both medium and cells, $IC_{10,free,baseline}$, which can be calculated by transforming eqs 7 to 8.

$$IC_{10,free,baseline} = \frac{IC_{10,membrane,baseline}}{D_{lip/w}} = \frac{69\ mmol/L_{lip}}{D_{lip/w}} \quad (8)$$

Nominal Concentrations Related to Baseline Toxicity. Combining eqs 6 and 8 yields eq 9, which predicts the nominal baseline toxicity.

$$IC_{10,nom,baseline} = \frac{69\ mmol/L_{lip}}{D_{lip/w}} \times \frac{V_w + D_{BSA/w} \times V_{protein,medium} + D_{lip/w} \times V_{lipid,medium} + D_{SP/w} \times V_{protein,cell} + D_{lip/w} \times V_{lipid,cell}}{V_{tot}} \quad (9)$$

There is a linear relationship between proteins ($\log D_{BSA/w}$ or $\log D_{SP/w}$) and lipids ($\log D_{lip/w}$) for nonspecific binding, as shown in eq 10.

$$\log D_{protein/w} = a \times \log D_{lip/w} + b \quad (10)$$

Inserting eqs 10 to 9 yields an equation that is dependent only on the $\log D_{lip/w}$ and system parameters of the bioassay. The model can be fitted by an empirical exponential equation to mathematically simplify the equation to reduce it to three adjustable parameters (eq 11). Previously, Lee et al.[7] developed an empirical baseline toxicity prediction model for neutral and cationic chemicals. As anionic PFAS bind stronger to proteins than comparable neutral chemicals, the model will need to be updated for anionic PFAS, and there will be a separate baseline toxicity QSAR (quantitative structure−activity relationship) for neutral and anionic PFAS.

$$\log\left(\frac{1}{IC_{10,nom,baseline}}\right) = a + b \times (1 - e^{-c \times \log D_{lip/w}}) \quad (11)$$

Toxic Ratio and Specificity Ratio. The ratio of cytotoxic concentrations (IC_{10}) between predicted baseline toxicity and experimental cytotoxicity is the toxic ratio TR (Figure 1),[8,9] which can be derived from the free (TR_{free}) or the nominal effect concentrations (TR_{nom}) according to eq 12.

$$TR_{free} = \frac{IC_{10,free,baseline}}{IC_{10,free}} \quad \text{or} \quad TR_{nom} = \frac{IC_{10,nom,baseline}}{IC_{10,nom}} \quad (12)$$

In theory, TR_{free} and TR_{nom} are the same, but the empirical values might differ due to different points of departure for their calculations. Chemicals with a TR < 10 are classified as baseline toxicants. TR > 10 suggests that there may be some specific mode of action triggering the toxic effects before baseline toxicity occurs.[8,9]

Any effect concentration (EC) for reporter gene activation or other defined targets can also be related to baseline toxicity by defining a SR, as shown in eq 13.

$$SR_{nom} = \frac{IC_{10,nom,baseline}}{EC_{F,nom}} \quad (13)$$

F is typically 10%, and EC_{10} is defined as the effective concentration triggering 10% of the maximum effect. For antagonism, the suppression ratio SPR of 20% is often used, and in the present study, EC_{SPR20} is the suppression concentration leading to 20% inhibition of the background signal of rosiglitazone on PPARγ.[23] SR < 1 suggests that the effects on defined targets may be nonspecific. One ≤ SR < 10 is considered as moderate specificity with uncertainty. SR > 10 is specific.[9]

MATERIALS AND METHODS

Materials. Eleven PFAS (perfluorobutanoic acid (PFBA), perfluorohexanoic acid (PFHxA), perfluoroheptanoic acid (PFHpA), perfluorooctanoic acid (PFOA), perfluorononanoic acid (PFNA), perfluoroundecanoic acid (PFUnA), perfluoro-2-methyl-3-oxahexanoic acid (HFPO−DA), perfluorohexahexanesulfonic acid (PFHxS), perfluorooctanesulfonic acid (PFOS), 6:2 fluorotelomer sulfonic acid (6:2 FTSA), and perfluorooctane sulfonamide (PFOSA)) were investigated in detail. Their structures are shown in Figure S1. Additional 13 PFAS (10 per- and three polyfluorinated chemicals) were evaluated only in the cell-based assays (Table S1). All PFAS were dissolved in methanol (1428, Chemsolute) as a stock solution (Table S2).

Free Concentration and Cytotoxicity of PFAS in PPARγ-GeneBLAzer Reporter Gene Assays. A detailed description is in Supporting Information text S2, and an experimental workflow is shown in Figure S2. Briefly, on day 1, cells were seeded in a 96-well plate (655946, Greiner) for 24 h of incubation. On day 2, PFAS stock solutions in methanol were pipetted into dosing vials (2214340, Labsolute), and the methanol was blown down gently with nitrogen. The PFAS precipitate at the bottom of each vial was dissolved again with 1000 μL assay medium and serially diluted in a 96-deep-well plate (7696548, Labsolute) with a dilution factor of 2 to obtain 10 concentration points. Then, 120 μL of PFAS dosing medium was transferred from a 96-deep well plate to a cell plate for 24 h of exposure. The concentration exposed to cells is shown in Table S2. On day 3, the cell plate was imaged with the IncuCyte S3 live cell imaging system (Essen BioScience, USA). The cytotoxicity was determined by comparing the confluency of exposed cells and unexposed cells. Then, 200 μL of the supernatant from each well in the cell plate was transferred to a 96-deep-well plate (P-DW-500-C, Labsolute) for SPME to measure the free concentrations of PFAS in the medium. The experimental conditions for Supelco BioSPME 96-Pin Devices (59683-U, Sigma-Aldrich) are listed in Table S3a, and the calculation details for free concentrations of PFAS are as Henneberger et al.[26]

PPARγ-GeneBLAzer Medium Binding of PFAS. A serial dilution of PFAS in a 96-deep well plate (7696548, Labsolute) was prepared as above. A second 96-well plate (655946, Greiner) was filled with 100 μL of fresh assay medium. 120 μL of PFAS dosing medium was transferred from the 96-deep well plate to the second 96-well plate to make the concentrations of PFAS the same as those exposed to cells (Table S2). Then, 200

https://doi.org/10.1021/acs.est.3c09950
Environ. Sci. Technol. 2024, 58, 5727−5738

Table 1. Cytotoxicity of 11 PFAS in the PPARγ-GeneBLAzer Assay and Distribution Ratios of PFAS between Different Biomaterials and Water[a]

	DTXSID	$IC_{10,nom}$ [mol/L]	$IC_{10,free}$ [mol/L]	log $D_{medium/w}$ $[L_w/L_{prot+lip}]$[b]	log $D_{cell/w}$ $[L_w/L_{prot+lip}]$[c]	log $D_{BSA/w}$ $[L_w/L_{prot}]$[b]	log $D_{SP/w}$ $[L_w/L_{prot}]$[c]	log $D_{lip/w}$ $[L_w/L_{lip}]$	TR_{nom}	TR_{free}
PFBA	DTXSID4059916	3.19×10^{-3}	1.78×10^{-3}	2.60	2.40	1.94	2.11	1.00[d]	2.36	3.88
PFHxA	DTXSID3031862	9.95×10^{-4}	4.72×10^{-4}	2.78	3.45	2.70	2.45	2.32[e]	0.49	0.70
PFHpA	DTXSID1037303	3.75×10^{-4}	6.76×10^{-5}	3.21	3.69	3.40	2.65	2.91[e]	0.86	1.26
PFOA	DTXSID8031865	1.30×10^{-4}	1.84×10^{-5}	3.67	3.94	3.98	3.14	3.52[e]	1.32	1.13
PFNA	DTXSID8031863	9.07×10^{-5}	7.72×10^{-6}	4.14	3.74	4.39	3.39	4.25[e]	1.68	0.50
PFUnA	DTXSID8047553	2.16×10^{-5}	3.83×10^{-7}	4.74	3.78	4.75	3.97	4.54[e]	5.04	5.20
HFPO–DA	DTXSID70880215	6.54×10^{-4}	2.20×10^{-4}	3.18	3.09	2.28	2.77	2.41[e]	0.47	1.22
PFHxS	DTXSID3037709	1.46×10^{-4}	4.22×10^{-5}	3.14	3.56	3.52	2.95	4.13[e]	0.17	0.12
PFOS	DTXSID8037706	4.78×10^{-5}	3.89×10^{-6}	4.04	4.32	4.52	3.94	4.89[e]	0.30	0.23
6:2 FTSA	DTXSID6067331	3.07×10^{-4}	4.25×10^{-5}	3.45	3.90	3.71	3.39	3.87[f]	0.25	0.22
PFOSA	DTXSID3038939	7.85×10^{-6}	3.28×10^{-7}	4.18	3.81	4.33	3.52	4.94[f]	2.25	2.43

[a]Nominal and free inhibitory concentrations of PFAS triggering 10% cytotoxicity ($IC_{10,nom}$ and $IC_{10,free}$). Distribution ratios of PFAS between PPARγ-medium and water ($D_{medium/w}$), between HEK293H (PPARγ) cells and water ($D_{cell/w}$), between BSA and water ($D_{BSA/w}$), and structural protein and water ($D_{SP/w}$). Literature and predicted distribution ratios between liposome and water ($D_{lip/w}$). Toxic ratios (eq 12) with free (TR_{free}) and nominal (TR_{nom}) concentrations in the PPARγ-GeneBLAzer assay. [b]The concentration-dependent distribution ratios $D_{medium/w}$ and $D_{BSA/w}$ at $IC_{10,free}$ were derived from the empirical equations given in Table S6. [c]log $D_{cell/w}$ and log $D_{SP/w}$ were measured at PFAS concentrations near $IC_{10,nom}$ (Table S2). [d]log $D_{lip/w}$ were from Droge et al.[31] [e]log $D_{lip/w}$ were from Ebert et al.[25] [f]log $D_{lip/w}$ of 6:2 FTSA and PFOSA was predicted from the linear relationship of experimental log $D_{lip/w}$ from literature[25,31] against the number of fluorinated carbons (Figure S8, eq S10).

μL was transferred to the third 96-deep-well plate (P-DW-500-C, Labsolute) for SPME with a Supel BioSPME 96-Pin device. The distribution ratios of PFAS between medium components and water ($D_{medium/w}$) were determined as described by Qin et al.[23]

Cell Binding of PFAS. The detailed description is in Supporting Information text S3, and the experimental workflow for cell binding experiments is shown in Figure S3. HEK293H cells (modified in the PPARγ-GeneBLAzer reporter gene assay) were homogenized by ultrasonic shattering (Sonoplus 2070, Germany). PFAS stock solutions were diluted with PBS. 100 μL of cell homogenate and 100 μL of PFAS solution were added and vortexed in a 1.5 mL HPLC vial with insert (7648146, 765116, Labsolute). Cell homogenates were derived from approximately 1.25×10^6 cells per experiment, and the concentrations of PFAS are listed in Table S2. We also studied the cell binding of PFAS with the other three cell lines (MCF7, H4lle, and SH-SY5Y), which were used in three cell-based HTS (AREc32, AhR-CALUX, and neurotoxicity). The distribution ratios of PFAS between cells and water ($D_{cell/w}$) were analyzed as described by Qin et al.[23]

Structural Protein Binding of PFAS. The detailed description is in Supporting Information text S4, and the experimental workflow is shown in Figure S4. The structural protein binding assay applied ground powder of chicken breast fillet, which was prepared as described previously.[24] Chicken protein was suspended with PBS by a high-speed vortex. The pH value of the suspension was adjusted to neutral (pH = 7.4). 500 μL of protein suspension and 500 μL of PFAS solution were added and vortexed in a 1.5 mL HPLC vial (7654554, 7663230, Labsolute). The concentration of protein in each sample was 50 mg/mL, and the concentrations of PFAS are listed in Table S2. The binding affinity of PFAS to cells and structural proteins is considered weak,[24] and thus, the C18-SPME fiber (57281-U, Sigma-Aldrich) with a larger volume of C18-particles embedded metal alloy was used. The experimental conditions for the C18-SPME fiber are in Table S3b. The distribution ratios of PFAS between structural protein and water ($D_{SP/w}$) were analyzed according to Qin et al.[23]

Protein and Lipid Content of Medium and Cells. Protein concentrations of assay mediums and cell homogenates for four assays were determined by a Pierce BCA Protein Assay Kit (23228, Thermo Scientific). Their lipid concentrations were determined by the sulfo-phospho-vanillin reaction, as described previously.[27] Units of protein and lipid were converted from mass concentration (mg/L) to volume concentration (mL/L) using a density of protein of 1.36 kg/L and a density of lipid of 1 kg/L.

High-Throughput Screening of PFAS in 384-Well Plates. An experimental workflow for four cell-based bioassays with different targets (PPARγ-GeneBLAzer, AREc32, AhR-CALUX, and neurotoxicity) is shown in Text S5 and Figure S5. These assays were performed in 384-well plates as described previously.[7,28−30] Experimental conditions, including assay medium, cell lines, and cell number, are in Table S4, and PFAS concentrations are in Table S5. Briefly, on day 1, cells were seeded in a 384-well plate by a MultiFlo Dispenser (BioTek,Vermont, USA). On day 2, PFAS stock solutions were prepared with methanol. Defined volumes of PFAS stock were transferred to dosing vials (2214340, Labsolute) and blown down with nitrogen. PFAS were dissolved again in the assay medium. Then, serial concentrations of PFAS in a medium were prepared and dosed to cells by Hamilton Star Robot (Bonaduz, Switzerland). Cell plates were imaged by IncuCyte S3 at the start of exposure. On day 3, cell plates were imaged by IncuCyte S3 again after 24 h of PFAS exposure. The cytotoxicity of three reporter gene cell lines was determined by comparing the confluency of exposed cells and unexposed cells. The cell responses targeting PPARγ, AREc32, and AhR were quantified from the signals of reporter proteins with an Infinite M1000 plate reader (Tecan, USA). The neurite length of differentiated SH-SY5Y cells was quantified by phase-contrast imaging using an IncuCyte S3. Then, Nuclear Green LCS1 (ab138904, Abcam) and propidium iodide (81845, Sigma-Aldrich) were used to stain the total cells and death cells, which were quantified with the IncuCyte S3 to determine the cytotoxicity.

https://doi.org/10.1021/acs.est.3c09950
Environ. Sci. Technol. 2024, 58, 5727−5738

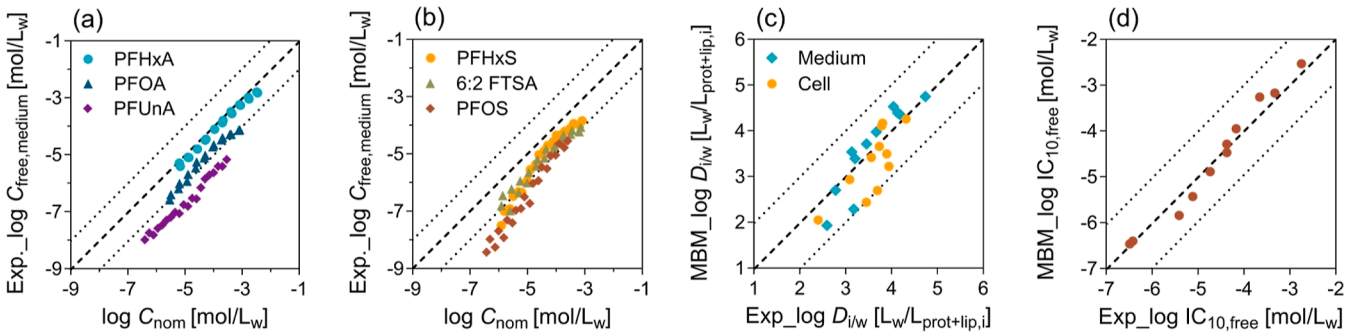

Figure 2. Relationship between nominal (C_{nom}) and free ($C_{free,medium}$) concentrations measured in the PPARγ-GeneBLAzer reporter gene assay for (a) three perfluoroalkyl carboxylic acids and (b) three perfluoroalkyl sulfonic acids. (c) Experimental (Exp) distribution ratios between medium and water ($D_{medium/w}$) and cell and water ($D_{cell/w}$) of 11 PFAS plotted against predicted $D_{medium/w}$ and $D_{cell/w}$. $D_{medium/w}$ was predicted by eq 4 with experimental distribution ratios between BSA and water ($D_{BSA/w}$) and between liposome and water ($D_{lip/w}$) (Table 1). $D_{cell/w}$ values were predicted by eq 5 with distribution ratios between structural protein and water ($D_{SP/w}$) and $D_{lip/w}$ (Table 1). (d) Inhibitory concentration $IC_{10,free}$ values were derived from concentration−cytotoxicity curves at 10% cytotoxicity with measured $C_{free,medium}$. Experimental (Exp) $IC_{10,free}$ plotted against $IC_{10,free}$ predicted by the MBM (eq 6) with $D_{lip/w}$, $D_{BSA/w}$, and $D_{SP/w}$.

RESULTS AND DISCUSSION

Binding to Medium Components, Cells, Liposomes, and Proteins. $D_{medium/w}$ and $D_{cell/w}$ of ten anionic PFAS and the partially anionic PFOSA were determined exclusively with PPARγ-medium and the HEK293H cell line. The $D_{medium/w}$ values of hydrophilic PFBA, PFHxA, and PFHpA and of the hydrophobic PFUnA were independent of concentration (Figure S6) and were used in the MBM (eq 3) to predict the $C_{free,medium}$. In contrast, the $D_{medium/w}$ of seven other PFAS (PFOA, PFNA, HFPO−DA, PFHxS, PFOS, 6:2 FTSA, and PFOSA) were found to be concentration-dependent (Figure S6). PFAS-specific regression equations of log $D_{medium/w}$ against log C_w were derived from the Freundlich-type model (Table S6).[23]

As the protein content in the medium was 64 times higher than the lipid content (Table S7), the concentration-dependent protein binding of anionic PFAS dominated the medium binding.[23] $IC_{10,nom}$ or $IC_{10,free}$ (Table 1) were derived from the concentration−cytotoxicity curve at 10% cytotoxicity with a nominal or free concentration of PFAS in the medium (Figure S7). The log $D_{medium/w}$ at $IC_{10,nom}$ was calculated from the regression eqs (Table S6) with measured C_{free} at $IC_{10,free}$. log $D_{cell/w}$ of HEK293H cells were measured at constant concentrations close to the $IC_{10,nom}$ (Table 1). As the protein and lipid are major sorption phases of the medium component and cells, $D_{BSA/w}$, $D_{SP/w}$, and $D_{lip/w}$ were used as representatives of $D_{medium/w}$ and $D_{cell/w}$ for the MBM (eq 6). Log $D_{BSA/w}$ were calculated with $IC_{10,free}$ from the regression equations listed in Table S6, and log $D_{SP/w}$ were measured at concentrations close to $IC_{10,nom}$. log $D_{lip/w}$ were collected from literature[25,31] or predicted from other experimental descriptors (Figure S8, eqs S9−S11).

Free and Nominal Concentration of PFAS in the PPARγ-GeneBLAzer Reporter Gene Assay. PFAS are considered proteinophilic and lipophilic,[32] and thus, PFAS are prone to bind to components of medium and cells in bioassay systems, indicating $C_{free,medium}$ would be lower than the associated C_{nom}.[33] As the numbers of carbons in the three perfluoroalkane carboxylic acids increased, the $C_{free,medium}$ deviated more from the 1:1 line to the corresponding C_{nom}, but the deviation was independent of the concentration (Figure 2a). The measured $C_{free,medium}$ values of the more hydrophilic PFHxA were close to C_{nom}, while the hydrophobic PFUnA had $C_{free,medium}$ values up to 90 times lower than C_{nom}. The relationship between log $C_{free,medium}$ and log C_{nom} was not linear, which was most pronounced for PFHxS and PFOS (Figure 2b). The difference can be explained because sulfonic acids were found to have specific binding to proteins at low concentration ranges, resulting in a higher deviation of $C_{free,medium}$ from C_{nom} at low concentrations.

The observed differences between $C_{free,medium}$ and C_{nom} can be explained by the MBM. The $C_{free,medium}$ predicted by the MBM (eq 3) with $D_{medium/w}$ (Table S6) and $D_{cell/w}$ (Table 1) agreed well with the experimental ones in a concentration-dependent way (Figure S9). $C_{free,medium}$ predicted by the MBM (eq 6) with $D_{lip/w}$, $D_{BSA/w}$, and $D_{SP/w}$ were also consistent (Figure S9) because the experimental log $D_{medium/w}$ (Table 1) at IC_{10} and were represented well by log $D_{BSA/w}$ at IC_{10} and log $D_{lip/w}$ (eq 4), as well as the log $D_{cell/w}$ with log $D_{sp/w}$ and log $D_{lip/w}$ (eq 5) in Figure 2c. The volume fractions of proteins and lipids in the medium and cells are shown in Tables S7 and S8. Consequently, the experimental and predicted $IC_{10,free}$ values by the MBM (eq 6) also agreed well (Figure 2d).

Toxic Ratios: Baseline Toxicity and Cytotoxicity of PFAS. The toxic ratio TR (eq 12) allows an estimation if PFAS act as baseline toxicants or exert cytotoxicity due to a specific effect. All experimental $IC_{10,free}$ (Table 1) values were close to the $IC_{10,free,baseline}$ values (Table S9) predicted from the critical membrane concentration of 69 mmol/L_{lip} (eq 8). TR_{free} of the 11 PFAS were within the range of baseline toxicants of 0.1−10, suggesting that the cytotoxicity of these PFAS is caused by baseline toxicity (diagonal lines in Figure 3a).

TR_{nom} is more practical than TR_{free} because nominal concentrations are widely reported in the literature. $IC_{10,nom,baseline}$ (Table S9) were predicted from $IC_{10,free,baseline}$ by eqs 3 and 6 with the experimental parameters in Table 1. Consistently, the TR_{nom} of the PFAS was still within the range of 0.1−10 (Figure 3b), confirming that PFAS behave like baseline toxicants in the cytotoxicity endpoint of the PPARγ-GeneBLAzer assay.

Development of a Baseline Toxicity Prediction Model for Nominal Cytotoxicity. Log $D_{BSA/w}$ and log $D_{SP/w}$ are both linearly correlated (eq 10) against log $D_{lip/w}$ (Table 1) for the nine anionic PFAS (Figure S10a,b). 6:2 PFSA and PFOSA were excluded from the regressions in eqs 14 and 15 because

https://doi.org/10.1021/acs.est.3c09950
Environ. Sci. Technol. 2024, 58, 5727−5738

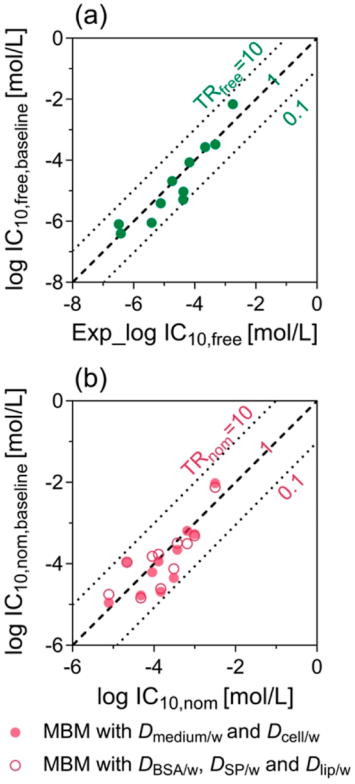

Figure 3. TR (eq 12) of PFAS in the PPARγ-GeneBLAzer assay. (a) Measured free concentration at 10% cytotoxicity $IC_{10,free}$ (Table 1) plotted against the $IC_{10,free,baseline}$ predicted from the critical membrane burden of 69 mmol/L_{lip} (eq 8). The diagonal line depicts the TR_{free} of 1, and the dotted lines represent the range for the baseline toxicity of $10 > TR_{free} > 0.1$. (b) Nominal concentration at 10% cytotoxicity $IC_{10,nom}$ plotted against the $IC_{10,nom,baseline}$ predicted from $IC_{10,free,baseline}$ by eq 3 (filled circle) or eq 6 (empty circle). The diagonal line depicts the TR_{nom} of 1, and the dotted lines represent the range for the baseline toxicity of $10 > TR_{nom} > 0.1$.

their log $D_{lip/w}$ were only predicted, but they are plotted in Figure S10a,b for comparison.

$$\log D_{BSA/w}(\text{non-specific, anionic PFAS}) = 0.75 \times \log D_{lip/w} + 1.01 \quad (R^2 = 0.88) \tag{14}$$

$$\log D_{SP/w}(\text{anionic PFAS}) = 0.46 \times \log D_{lip/w} + 1.50 \quad (R^2 = 0.85) \tag{15}$$

Previously, a relationship of log $D_{BSA/w}$ against log $D_{lip/w}$ for neutral chemicals was derived by Endo and Goss[34] (eq 16, rescaled from K_{ow}). The higher affinity of anionic PFAS for proteins is evident by the larger slope and intercept in eq 14 than in eq 16. The binding of anionic PFAS to structural proteins (eq 15) was also stronger than that of neutral chemicals (eq 17)[35] for log $D_{lip/w} < 5$.

$$\log D_{BSA/w}(\text{neutral}) = 0.70 \times \log D_{lip/w} + 0.34 \tag{16}$$

$$\log D_{SP/w}(\text{neutral}) = 0.72 \times \log D_{lip/w} - 0.47 \tag{17}$$

Insertion of eqs 14 and 15 in eq 9 leads to eq 18 with $sD_{lip/w}$ as the sole input parameter to derive baseline toxicity predictions for anionic PFAS. The volume of cells is much lower than the volume of the medium, and the volume fraction of protein and lipid in the medium is <1% (Tables S7 and S8). Therefore, $V_{tot} \approx V_{medium} \approx V_w$ and the volume fraction (Vf) of protein and lipid in the medium and cells were used to present the distributions of protein and lipid in the baseline toxicity prediction model.

$$IC_{10,nom,baseline}(\text{anionic PFAS}) = \frac{69\ \text{mmol}/L_{lip}}{D_{lip/w}} \times \left(1 + 10^{0.75\times\log D_{lip/w}+1.01} \times Vf_{protein,medium} + D_{lip/w} \times Vf_{lipid,medium} + 10^{0.46\times\log D_{lip/w}+1.50} \times Vf_{protein,cell}\frac{V_{cell}}{V_{medium}} + D_{lip/w} \times Vf_{lipid,cell}\frac{V_{cell}}{V_{medium}}\right) \tag{18}$$

For comparison, a baseline toxicity prediction model for neutral chemicals was developed by the insertion of eqs 16 and 17 into eq 9.

$$IC_{10,nom,baseline}(\text{neutral chemicals}) = \frac{69\ \text{mmol}/L_{lip}}{D_{lip/w}} \times \left(1 + 10^{0.70\times\log D_{lip/w}+0.34} \times Vf_{protein,medium} + D_{lip/w} \times Vf_{lipid,medium} + 10^{0.72\times\log D_{lip/w}-0.47} \times Vf_{protein,cell}\frac{V_{cell}}{V_{medium}} + D_{lip/w} \times Vf_{lipid,cell}\frac{V_{cell}}{V_{medium}}\right) \tag{19}$$

Analogously to Lee et al.,[7] empirical baseline toxicity prediction models for anionic PFAS were derived for all four cell lines by inserting bioassay-specific volumes of protein and lipids in cells and medium measured in the present study (Tables S7 and S8) into eq 18. The models differ because the protein and lipid contents in the assay systems are different. The resulting predictions for anionic PFAS are depicted in Figure 4a. It can be expected that any anionic chemicals behave similarly to anionic PFAS, but as the model was calibrated with anionic PFAS data only, we consider it a PFAS-specific model. The model holds for neutral chemicals (Figure 4b) in general and includes neutral PFAS. These bioassay-specific empirical baseline toxicity models for neutral chemicals and anionic PFAS for the four cell lines were derived by exponential fit (eq 11), and the adjustable parameters a, b, and c are listed in Table 2.

If the baseline toxicity models were used to evaluate literature bioassay data with undisclosed conditions, we assumed the volume fractions of protein and lipid in medium are $Vf_{protein,medium}$ of 3 $mL_{protein}/L_{medium}$ and $Vf_{lip,medium}$ of 0.07 mL_{lipid}/L_{medium} (Table S7), and $Vf_{protein,cell}$ is 30 $mL_{protein}/L_{cell}$ and $Vf_{lip,cell}$ is 5 mL_{lipid}/L_{cell} (Table S8). The volume of medium V_{medium} and volume of cells V_{cell} are dependent on microtiter plates in 96-, 384-, or 1536-well formats, e.g., V_{medium} of 40 μL and V_{cell} of approximately 30 nL for the 384-well plate

https://doi.org/10.1021/acs.est.3c09950
Environ. Sci. Technol. 2024, 58, 5727−5738

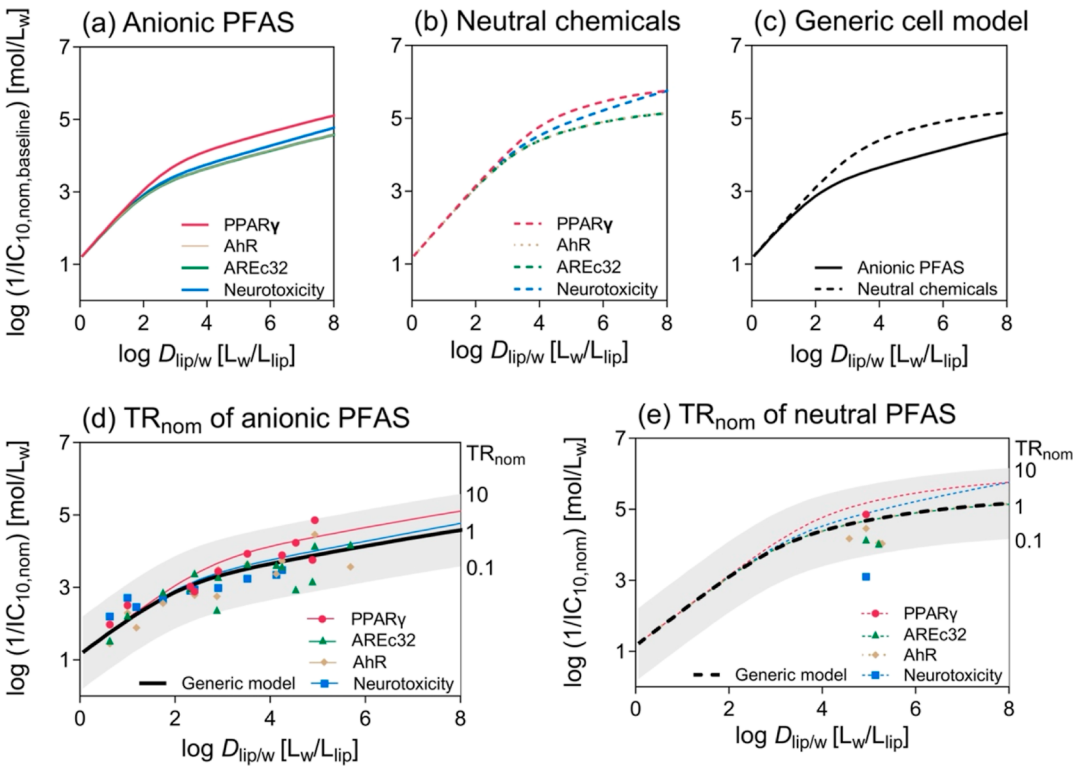

Figure 4. Baseline toxicity prediction models for (a) anionic PFAS (eq 18) and (b) neutral chemicals (eq 19) in four cell-based bioassays: PPARγ-GeneBLAzer (magenta), AREc32 (green), AhR CALUX (gold), and neurotoxicity (blue). (c) Baseline toxicity prediction models with the generic cell model (eqs 18, 19). (d) Nominal inhibitory concentration at 10% cytotoxicity $IC_{10,nom}$ of 16 anionic PFAS in four cell-based bioassays: PPARγ (magenta circle), AREc32 (green triangle), AhR (gold diamond), and neurotoxicity (blue square) and color-matched bioassay-specific baseline toxicity prediction models as well as the generic model (black line). The gray area depicts the range for baseline toxicity of $10 > TR_{nom} > 0.1$. (e) $IC_{10,nom}$ of partially charged and neutral PFAS in four cell-based bioassays compared with the baseline toxicity prediction models as well as the generic model (black broken line). All fit parameters of the empirical baseline toxicity prediction model (eq 11) are listed in Table 2.

Table 2. Parameters of the Empirical Baseline Toxicity Prediction Model (eq 11) of Anionic and Neutral PFAS in Four Cell-Based Bioassays and the Generic Cell Assay

		Anionic PFAS			Neutral PFAS		
assay	Medium	*a*	*b*	*c*	*a*	*b*	*c*
PPARγ (HEK293H)	OptiMEM +2 % FBS	1.25	4.76	0.251	1.24	5.47	0.235
AREc32 (MCF7)	DMEM Glutamax + 10% FBS	1.22	3.78	0.263	1.26	4.43	0.278
AhR (H4IIe)	DMEM Glutamax + 10% FBS	1.22	3.78	0.263	1.26	4.45	0.277
neurotoxicity (SH-SY5Y)	neurobasal medium	1.22	4.07	0.247	1.23	5.61	0.209
generic cell (6% proteins, 0.1% lipids)	generic medium (0.3% proteins, 0.001% lipids)	1.22	3.79	0.262	1.26	4.47	0.275

format. The fit parameters of this generic bioassay model are also listed in Table 2.

These two models are compared in Figure 4c, where the two lines started to separate at $\log D_{lip/w} > 2$. This is due to anionic chemicals having a higher affinity for proteins despite baseline toxicity occurring at concentrations where the protein binding is dominated by nonspecific binding. At $\log D_{lip/w} < 2$ (e.g., PFBA), $IC_{10,nom}$ is close to $IC_{10,free}$ (Table 1 and Figure S9a). Therefore, eqs 18 and 19 are simplified to eq 20, which is similar to eq 8 and is valid for neutral, anionic, and cationic organic chemicals.

$$IC_{10,nom,baseline} = \frac{69\ mmol/L_{lip}}{D_{lip/w}} \quad (20)$$

Sensitivity analysis was performed to study how various parameters contribute to the baseline toxicity prediction model. The protein and lipid contents of these four cell lines were similar (Table S8), and thus, the $D_{cell/w}$ of single PFAS (Table S10) among the four cell lines did not differ much. Besides, the ratio of V_{cell}/V_{medium} is usually <0.001. Therefore, the differences between baseline toxicity prediction models (eqs 18 and 19) with cells and without cells are negligible (Figure S10c).

By contrast, medium components make a difference. Models for AREc32 and AhR CALUX assays were overlaying because the same medium was used in the assays, while less protein and lipid were in the media for PPARγ-GeneBLAzer and neurotoxicity assays (Table S7). The difference is more pronounced as the chemical hydrophobicity increases (Figure 4a,b). The lipid-bound fraction is smaller compared to protein, but it still influences the predicted $IC_{10,nom,baseline}$. For example, if $Vf_{lip,medium}$ changed from 0.07 mL/L to 0, the model for anionic PFAS did not change much because the concentration of anionic PFAS bound to protein is much higher than that bound to lipid, but the model for neutral chemicals deviates for

https://doi.org/10.1021/acs.est.3c09950
Environ. Sci. Technol. 2024, 58, 5727−5738

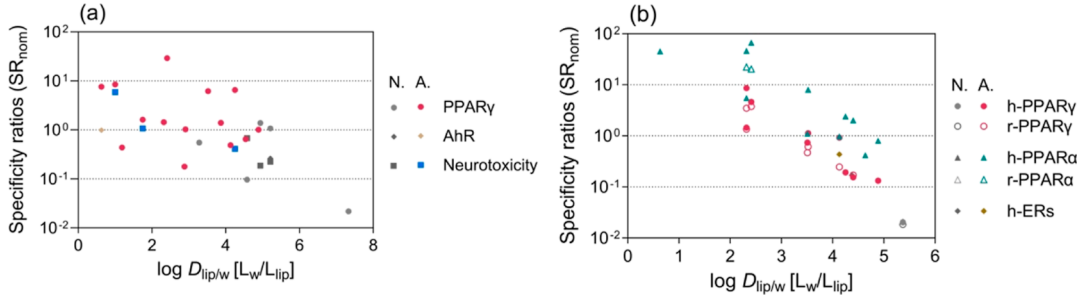

Figure 5. Specificity ratios SR_{nom} (eq 13) of PFAS in cell-based bioassays. (a) SR of 16 anionic (A.) and eight neutral (N.) PFAS in cell-based bioassays of PPARγ, AhR, and neurotoxicity were measured in this study. (b) SR_{nom} of 11 anionic, one partially charged, and four neutral PFAS in cell-based bioassays of human (h) PPARγ, rat (r) PPARγ, hPPARα, rPPARα, and hERs from Evans et al.[36]

chemicals with log $D_{lip/w}$ > 4 (Figure S10d). We recommend to measure the volume fractions of protein and lipid in the medium used for bioassays on a routine basis as they are the main determinants of the model.

Is the Cytotoxicity of PFAS Merely Baseline Toxicity? 24 PFAS (Table S1) were measured in this study. These PFAS have diverse functional groups, including sulfonic acid, carboxylic acid, oxide dimer acid, fluorotelomer alcohol, and sulfonamide, as well as some fluorinated pesticides that contain individual C_nF_{2n}-groups. Their log $D_{lip/w}$ ranges over 6 orders of magnitude (Table S11). Log $D_{lip/w}$ values of these PFAS were used in the baseline toxicity prediction model to derive the $IC_{10,nom,baseline}$ (eq 11).

The $IC_{10,nom}$ of 24 PFAS were measured in four bioassays in 384-well plates (Table S12). The $IC_{10,nom,baseline}$ of 15 anionic PFAS were predicted with eq 18, while $IC_{10,nom,baseline}$ of the other four partially charged and five neutral PFAS were predicted with eq 19. As shown in Figure 4d,e, the measured $IC_{10,nom}$ were within a factor of 10 to the $IC_{10,nom,baseline}$ predicted by the four bioassay-specific models and all well within the gray band of 10 > TR_{nom} > 0.1 of the generic model, indicating that these PFAS did not show specific effects but baseline toxicity was the cause of their cytotoxicity. The generic cell model is adequate to provide $IC_{10,nom,baseline}$ values as a reference for general experimental conditions.

Application of the Baseline Toxicity Prediction Model to Evaluate the Specificity of Effects. The measured $EC_{10,nom}$ values of the agonistic effects on PPARγ, AREc32, AhR, and neurotoxicity, as well as the $EC_{SPR20,nom}$ values of the antagonistic effects on PPARγ, are listed in Table S12, which were derived from the concentration−response curves of the 24 PFAS investigated experimentally in this study (Figure S11). No activation of the oxidative stress response was detected for all 24 PFAS in AREc32 before cytotoxicity started to kick in. A few PFAS showed weak activation of AhR and neurotoxicity. In contrast, PPARγ was a specific target for 19 of the 24 PFAS (Table S12), but the specificity was low. If the $EC_{10,nom}$ or $EC_{SPR20,nom}$ were compared with the $IC_{10,nom,baseline}$ from anionic or neutral baseline toxicity prediction models for PPARγ, AhR, and neurotoxicity (Table 2), as in Figure 5a, SR_{nom} (eq 13) of most PFAS were within 0.1−10, indicating the effects of PFAS in the tested assays are nonspecific and caused by baseline toxicity. Only HFPO−DA had a SR_{nom} > 10 for the agonistic mode of the PPARγ assay, indicating that HFPO−DA may be a specific PPARγ antagonist.

Evaluation of Literature Data for Specificity of Effects. Evans et al.[36] studied the agonistic effects of 16 PFAS (Table S13) on five defined targets from humans or rats, including hPPARγ, rPPARγ, hPPARα, rPPARα, and human estrogen receptors (hER). The $IC_{10,nom,baseline}$ of 16 PFAS was calculated by the generic model (Table 2) from their $D_{lip/w}$ (Table S11). Their $EC_{10,nom}$ were recalculated from a linear portion of concentration−response curves because most of the effects were lower than 50% and the linear model is more suitable to derive 10% effects than a four-parameter logistic model.[37] hPPARα was more likely to be activated than rPPARα (Figure 5b). HFPO−DA, HFPO−DA-AS, and PFMOAA showed SR_{nom} > 10, while the other 13 PFAS either had no effects or had 0.1 < SR_{nom} < 10 and were therefore classified as baseline toxicants. The literature data set showed a clear tendency that SR_{nom} decreased with increasing hydrophobicity (Figure 5b). This phenomenon can be explained by hydrophobic PFAS with strong affinity to membranes, which they may mostly accumulate in the cell membrane before reaching any intracellular-specific target sites. The FTOHs should be excluded from the analysis as they might have escaped from the well-plates or cross-contaminated neighboring wells because they are semivolatile.[6,38,39]

430 PFAS have been selected for a series of bioassay tests in the Tox21/ToxCast program with hundreds of targets (https://comptox.epa.gov/dashboard/chemical-lists/EPAPFASINV). The baseline toxicity prediction model of the present study can be used to evaluate the specificity of different targets once raw data from these bioassays becomes publicly available. Those PFAS with high values of TR and SR on defined targets may provide some hints on initial molecular events and key events, which will facilitate the in vitro to in vivo extrapolation to adverse outcomes and thus promote the development of AOP related to PFAS. However, current results of cell-based HTS from EPA suggest that a majority of 160 PFAS were inactive or equivocal.[18−21]

Although some PFAS showed specific effects on defined targets, their intrinsic specificities appear to be rather low. This does not mean that specific effects are absent. There are many reports about the specific effects of PFAS, but if they are not selective but occur at concentrations similar to baseline toxicity, these effects are easily predictable by the baseline toxicity prediction models derived here. Even if individual PFAS are merely baseline toxicants, their potency can still be of concern because baseline toxicants also cover several orders of magnitude in effect potency.

The biological effects of PFAS were usually detected at the micromolar level in toxicological studies. The blood concentrations of PFAS in some workers and residents living near fluorochemical plants have already reached such levels,[40] even though that in the general population was at a nanomolar

https://doi.org/10.1021/acs.est.3c09950
Environ. Sci. Technol. 2024, 58, 5727−5738

level.[41] PFAS are highly persistent and have been termed "forever chemicals". If their production is not stopped, they will continue to build up over time and may eventually reach levels where they cause effects, especially under chronic exposure, where PFAS are known to adversely affect the immune system[42] and cause liver cancer,[43] as well as other health impacts.[44,45] Baseline toxicants act concentration-additive in mixtures, which means that not only the thousands of PFAS but also all other organic chemicals act together in mixtures. Mixture effects may lead to visible effects even if the individual PFAS' concentrations are below their individual effect threshold.

■ ASSOCIATED CONTENT

Supporting Information

The Supporting Information is available free of charge at https://pubs.acs.org/doi/10.1021/acs.est.3c09950.

Addition of information on chemicals, deviation of equations, experimental procedures and details, volume fractions of proteins and lipids in biomaterials, binding isotherms and binding constants of PFAS between biomaterials and water, a comparison of free and nominal concentrations of PFAS in the bioassay, all results from cell-based HTS assays, and concentration−response curves of 24 PFAS in the PPARγ-GeneBLAzer reporter gene assay (PDF)

■ AUTHOR INFORMATION

Corresponding Author

Beate I. Escher − *Department of Cell Toxicology, UFZ−Helmholtz Centre for Environmental Research, Leipzig 04318, Germany; Environmental Toxicology, Department of Geosciences, Eberhard Karls University Tübingen, Tübingen DE-72076, Germany;* orcid.org/0000-0002-5304-706X; Email: beate.escher@ufz.de

Authors

Weiping Qin − *Department of Cell Toxicology, UFZ−Helmholtz Centre for Environmental Research, Leipzig 04318, Germany; Environmental Toxicology, Department of Geosciences, Eberhard Karls University Tübingen, Tübingen DE-72076, Germany*

Luise Henneberger − *Department of Cell Toxicology, UFZ−Helmholtz Centre for Environmental Research, Leipzig 04318, Germany;* orcid.org/0000-0002-3181-0044

Juliane Glüge − *Department of Cell Toxicology, UFZ−Helmholtz Centre for Environmental Research, Leipzig 04318, Germany; Institute of Biogeochemistry and Pollutant Dynamics, ETH Zürich, Zürich 8092, Switzerland;* orcid.org/0000-0003-1997-2750

Maria König − *Department of Cell Toxicology, UFZ−Helmholtz Centre for Environmental Research, Leipzig 04318, Germany*

Complete contact information is available at: https://pubs.acs.org/10.1021/acs.est.3c09950

Funding

W.Q. received funding through the Chinese Scholarship Council. This study was supported by the Helmholtz Association under the recruiting initiative scheme, which is funded by the German Ministry of Education and Research and was conducted within the Helmholtz POF IV Topic 9 and the Integrated Project "Healthy Planet-towards a non-toxic environment".

Notes

The authors declare no competing financial interest.

■ ACKNOWLEDGMENTS

We gratefully acknowledge access to the platform CITEPro (Chemicals in the Environment Profiler), funded by the Helmholtz Association for chemical analysis and bioassay measurements. We thank Julia Huchthausen for help with the BioSPME measurements, Jungeun Lee for help with the neurotoxicity assay, and Georg Braun for discussions about the dose−response modeling of literature data.

■ REFERENCES

(1) Wang, Z.; Buser, A. M.; Cousins, I. T.; Demattio, S.; Drost, W.; Johansson, O.; Ohno, K.; Patlewicz, G.; Richard, A. M.; Walker, G. W.; White, G. S.; Leinala, E. A New OECD Definition for Per- and Polyfluoroalkyl Substances. *Environ. Sci. Technol.* **2021**, *55* (23), 15575−15578.

(2) Richard, A. M.; Lougee, R.; Adams, M.; Hidle, H.; Yang, C.; Rathman, J.; Magdziarz, T.; Bienfait, B.; Williams, A. J.; Patlewicz, G. A New CSRML Structure-Based Fingerprint Method for Profiling and Categorizing Per- and Polyfluoroalkyl Substances (PFAS). *Chem. Res. Toxicol.* **2023**, *36* (3), 508−534.

(3) Wielsoe, M.; Long, M.; Ghisari, M.; Bonefeld-Jorgensen, E. C. Perfluoroalkylated substances (PFAS) affect oxidative stress biomarkers in vitro. *Chemosphere* **2015**, *129*, 239−245.

(4) Behr, A. C.; Plinsch, C.; Braeuning, A.; Buhrke, T. Activation of human nuclear receptors by perfluoroalkylated substances (PFAS). *Toxicol. In Vitro* **2020**, *62*, 104700.

(5) Escher, B. I.; Eggen, R. I.; Schreiber, U.; Schreiber, Z.; Vye, E.; Wisner, B.; Schwarzenbach, R. P. Baseline toxicity (narcosis) of organic chemicals determined by in vitro membrane potential measurements in energy-transducing membranes. *Environ. Sci. Technol.* **2002**, *36* (9), 1971−1979.

(6) Escher, B. I.; Glauch, L.; Konig, M.; Mayer, P.; Schlichting, R. Baseline Toxicity and Volatility Cutoff in Reporter Gene Assays Used for High-Throughput Screening. *Chem. Res. Toxicol.* **2019**, *32* (8), 1646−1655.

(7) Lee, J.; Braun, G.; Henneberger, L.; Konig, M.; Schlichting, R.; Scholz, S.; Escher, B. I. Critical Membrane Concentration and Mass-Balance Model to Identify Baseline Cytotoxicity of Hydrophobic and Ionizable Organic Chemicals in Mammalian Cell Lines. *Chem. Res. Toxicol.* **2021**, *34* (9), 2100−2109.

(8) Maeder, V.; Escher, B. I.; Scheringer, M.; Hungerbühler, K. Toxic ratio as an indicator of the intrinsic toxicity in the assessment of persistent, bioaccumulative, and toxic chemicals. *Environ. Sci. Technol.* **2004**, *38* (13), 3659−3666.

(9) Escher, B. I.; Henneberger, L.; Konig, M.; Schlichting, R.; Fischer, F. C. Cytotoxicity Burst? Differentiating Specific from Nonspecific Effects in Tox21 in Vitro Reporter Gene Assays. *Environ. Health Perspect.* **2020**, *128* (7), 77007.

(10) Qin, W.; Ren, X.; Zhao, L.; Guo, L. Exposure to perfluorooctane sulfonate reduced cell viability and insulin release capacity of β cells. *J. Environ. Sci.* **2022**, *115*, 162−172.

(11) Sun, P.; Nie, X.; Chen, X.; Yin, L.; Luo, J.; Sun, L.; Wan, C.; Jiang, S. Nrf2 Signaling Elicits a Neuroprotective Role Against PFOS-mediated Oxidative Damage and Apoptosis. *Neurochem. Res.* **2018**, *43* (12), 2446−2459.

(12) Ojo, A. F.; Peng, C.; Ng, J. C. Combined effects of mixed per- and polyfluoroalkyl substances on the Nrf2-ARE pathway in ARE reporter-HepG2 cells. *J. Hazard. Mater.* **2022**, *421*, 126827.

(13) Li, C. H.; Ren, X. M.; Ruan, T.; Cao, L. Y.; Xin, Y.; Guo, L. H.; Jiang, G. Chlorinated Polyfluorinated Ether Sulfonates Exhibit Higher Activity toward Peroxisome Proliferator-Activated Receptors Signal-

ing Pathways than Perfluorooctanesulfonate. *Environ. Sci. Technol.* **2018**, *52* (5), 3232−3239.
(14) Long, M.; Ghisari, M.; Bonefeld-Jorgensen, E. C. Effects of perfluoroalkyl acids on the function of the thyroid hormone and the aryl hydrocarbon receptor. *Environ. Sci. Pollut. Res. Int.* **2013**, *20* (11), 8045−8056.
(15) Qin, W. P.; Cao, L. Y.; Li, C. H.; Guo, L. H.; Colbourne, J.; Ren, X. M. Perfluoroalkyl Substances Stimulate Insulin Secretion by Islet β Cells via G Protein-Coupled Receptor 40. *Environ. Sci. Technol.* **2020**, *54* (6), 3428−3436.
(16) Yadav, A.; Amber, M.; Zosen, D.; Labba, N. A.; Huiberts, E. H. W.; Samulin Erdem, J.; Haugen, F.; Berntsen, H. F.; Zienolddiny, S.; Paulsen, R. E.; Ropstad, E.; Connolly, L.; Verhaegen, S. A human relevant mixture of persistent organic pollutants (POPs) and perfluorooctane sulfonic acid (PFOS) enhance nerve growth factor (NGF)-induced neurite outgrowth in PC12 cells. *Toxicol. Lett.* **2021**, *338*, 85−96.
(17) Patlewicz, G.; Richard, A. M.; Williams, A. J.; Grulke, C. M.; Sams, R.; Lambert, J.; Noyes, P. D.; DeVito, M. J.; Hines, R. N.; Strynar, M.; Guiseppi-Elie, A.; Thomas, R. S. A Chemical Category-Based Prioritization Approach for Selecting 75 Per- and Polyfluoroalkyl Substances (PFAS) for Tiered Toxicity and Toxicokinetic Testing. *Environ. Health Perspect.* **2019**, *127* (1), 14501.
(18) Houck, K. A.; Patlewicz, G.; Richard, A. M.; Williams, A. J.; Shobair, M. A.; Smeltz, M.; Clifton, M. S.; Wetmore, B.; Medvedev, A.; Makarov, S. Bioactivity profiling of per- and polyfluoroalkyl substances (PFAS) identifies potential toxicity pathways related to molecular structure. *Toxicology* **2021**, *457*, 152789.
(19) Houck, K. A.; Friedman, K. P.; Feshuk, M.; Patlewicz, G.; Smeltz, M.; Clifton, M. S.; Wetmore, B. A.; Velichko, S.; Berenyi, A.; Berg, E. L. Evaluation of 147 perfluoroalkyl substances for immunotoxic and other (patho)physiological activities through phenotypic screening of human primary cells. *ALTEX* **2023**, *40* (2), 248−270.
(20) Carstens, K. E.; Freudenrich, T.; Wallace, K.; Choo, S.; Carpenter, A.; Smeltz, M.; Clifton, M. S.; Henderson, W. M.; Richard, A. M.; Patlewicz, G.; Wetmore, B. A.; Paul Friedman, K.; Shafer, T. Evaluation of Per- and Polyfluoroalkyl Substances (PFAS) In Vitro Toxicity Testing for Developmental Neurotoxicity. *Chem. Res. Toxicol.* **2023**, *36* (3), 402−419.
(21) Stoker, T. E.; Wang, J.; Murr, A. S.; Bailey, J. R.; Buckalew, A. R. High-Throughput Screening of ToxCast PFAS Chemical Library for Potential Inhibitors of the Human Sodium Iodide Symporter. *Chem. Res. Toxicol.* **2023**, *36* (3), 380−389.
(22) Fischer, F. C.; Abele, C.; Droge, S. T. J.; Henneberger, L.; Konig, M.; Schlichting, R.; Scholz, S.; Escher, B. I. Cellular Uptake Kinetics of Neutral and Charged Chemicals in in Vitro Assays Measured by Fluorescence Microscopy. *Chem. Res. Toxicol.* **2018**, *31* (8), 646−657.
(23) Qin, W.; Henneberger, L.; Huchthausen, J.; Konig, M.; Escher, B. I. Role of bioavailability and protein binding of four anionic perfluoroalkyl substances in cell-based bioassays for quantitative in vitro to in vivo extrapolations. *Environ. Int.* **2023**, *173*, 107857.
(24) Henneberger, L.; Goss, K. U.; Endo, S. Partitioning of Organic Ions to Muscle Protein: Experimental Data, Modeling, and Implications for in Vivo Distribution of Organic Ions. *Environ. Sci. Technol.* **2016**, *50* (13), 7029−7036.
(25) Ebert, A.; Allendorf, F.; Berger, U.; Goss, K. U.; Ulrich, N. Membrane/Water Partitioning and Permeabilities of Perfluoroalkyl Acids and Four of their Alternatives and the Effects on Toxicokinetic Behavior. *Environ. Sci. Technol.* **2020**, *54* (8), 5051−5061.
(26) Henneberger, L.; Muhlenbrink, M.; Konig, M.; Schlichting, R.; Fischer, F. C.; Escher, B. I. Quantification of freely dissolved effect concentrations in in vitro cell-based bioassays. *Arch. Toxicol.* **2019**, *93* (8), 2295−2305.
(27) Fischer, F. C.; Henneberger, L.; Konig, M.; Bittermann, K.; Linden, L.; Goss, K. U.; Escher, B. I. Modeling Exposure in the Tox21 in Vitro Bioassays. *Chem. Res. Toxicol.* **2017**, *30* (5), 1197−1208.
(28) Neale, P. A.; Altenburger, R.; Ait-Aissa, S.; Brion, F.; Busch, W.; de Aragao Umbuzeiro, G.; Denison, M. S.; Du Pasquier, D.; Hilscherova, K.; Hollert, H.; Morales, D. A.; Novak, J.; Schlichting, R.; Seiler, T. B.; Serra, H.; Shao, Y.; Tindall, A. J.; Tollefsen, K. E.; Williams, T. D.; Escher, B. I. Development of a bioanalytical test battery for water quality monitoring: Fingerprinting identified micropollutants and their contribution to effects in surface water. *Water Res.* **2017**, *123*, 734−750.
(29) Konig, M.; Escher, B. I.; Neale, P. A.; Krauss, M.; Hilscherova, K.; Novak, J.; Teodorovic, I.; Schulze, T.; Seidensticker, S.; Kamal Hashmi, M. A.; Ahlheim, J.; Brack, W. Impact of untreated wastewater on a major European river evaluated with a combination of in vitro bioassays and chemical analysis. *Environ. Pollut.* **2017**, *220* (Pt B), 1220−1230.
(30) Escher, B. I.; Dutt, M.; Maylin, E.; Tang, J. Y.; Toze, S.; Wolf, C. R.; Lang, M. Water quality assessment using the AREc32 reporter gene assay indicative of the oxidative stress response pathway. *J. Environ. Monit* **2012**, *14* (11), 2877−2885.
(31) Droge, S. T. J. Membrane-Water Partition Coefficients to Aid Risk Assessment of Perfluoroalkyl Anions and Alkyl Sulfates. *Environ. Sci. Technol.* **2019**, *53* (2), 760−770.
(32) Conder, J. M.; Hoke, R. A.; Wolf, W. d.; Russell, M. H.; Buck, R. C. Are PFCAs bioaccumulative? A critical review and comparison with regulatory criteria and persistent lipophilic compounds. *Environ. Sci. Technol.* **2008**, *42* (4), 995−1003.
(33) Henneberger, L.; Muhlenbrink, M.; Fischer, F. C.; Escher, B. I. C18-Coated Solid-Phase Microextraction Fibers for the Quantification of Partitioning of Organic Acids to Proteins, Lipids, and Cells. *Chem. Res. Toxicol.* **2019**, *32* (1), 168−178.
(34) Endo, S.; Goss, K. U. Serum albumin binding of structurally diverse neutral organic compounds: data and models. *Chem. Res. Toxicol.* **2011**, *24* (12), 2293−2301.
(35) Endo, S.; Bauerfeind, J.; Goss, K. U. Partitioning of neutral organic compounds to structural proteins. *Environ. Sci. Technol.* **2012**, *46* (22), 12697−12703.
(36) Evans, N.; Conley, J. M.; Cardon, M.; Hartig, P.; Medlock-Kakaley, E.; Gray, L. E., Jr In vitro activity of a panel of per- and polyfluoroalkyl substances (PFAS), fatty acids, and pharmaceuticals in peroxisome proliferator-activated receptor (PPAR) alpha, PPAR gamma, and estrogen receptor assays. *Toxicol. Appl. Pharmacol.* **2022**, *449*, 116136.
(37) Escher, B. I.; Neale, P. A.; Villeneuve, D. L. The advantages of linear concentration-response curves for in vitro bioassays with environmental samples. *Environ. Toxicol. Chem.* **2018**, *37* (9), 2273−2280.
(38) Goss, K. U.; Bronner, G.; Harner, T.; Hertel, M.; Schmidt, T. C. The partition behavior of fluorotelomer alcohols and olefins. *Environ. Sci. Technol.* **2006**, *40* (11), 3572−3577.
(39) Fischer, F. C.; Henneberger, L.; Schlichting, R.; Escher, B. I. How To Improve the Dosing of Chemicals in High-Throughput in Vitro Mammalian Cell Assays. *Chem. Res. Toxicol.* **2019**, *32* (8), 1462−1468.
(40) Gao, Y.; Fu, J.; Cao, H.; Wang, Y.; Zhang, A.; Liang, Y.; Wang, T.; Zhao, C.; Jiang, G. Differential accumulation and elimination behavior of perfluoroalkyl Acid isomers in occupational workers in a manufactory in China. *Environ. Sci. Technol.* **2015**, *49* (11), 6953−6962.
(41) Gockener, B.; Weber, T.; Rudel, H.; Bucking, M.; Kolossa-Gehring, M. Human biomonitoring of per- and polyfluoroalkyl substances in German blood plasma samples from 1982 to 2019. *Environ. Int.* **2020**, *145*, 106123.
(42) Ehrlich, V.; Bil, W.; Vandebriel, R.; Granum, B.; Luijten, M.; Lindeman, B.; Grandjean, P.; Kaiser, A. M.; Hauzenberger, I.; Hartmann, C.; Gundacker, C.; Uhl, M. Consideration of pathways for immunotoxicity of per- and polyfluoroalkyl substances (PFAS). *Environ. Health* **2023**, *22* (1), 19.
(43) Costello, E.; Rock, S.; Stratakis, N.; Eckel, S. P.; Walker, D. I.; Valvi, D.; Cserbik, D.; Jenkins, T.; Xanthakos, S. A.; Kohli, R.; Sisley, S.; Vasiliou, V.; La Merrill, M. A.; Rosen, H.; Conti, D. V.;

https://doi.org/10.1021/acs.est.3c09950
Environ. Sci. Technol. 2024, 58, 5727−5738

McConnell, R.; Chatzi, L. Exposure to per- and Polyfluoroalkyl Substances and Markers of Liver Injury: A Systematic Review and Meta-Analysis. *Environ. Health Perspect.* **2022**, *130* (4), 46001.
(44) Chang, E. T.; Adami, H. O.; Boffetta, P.; Cole, P.; Starr, T. B.; Mandel, J. S. A critical review of perfluorooctanoate and perfluorooctanesulfonate exposure and cancer risk in humans. *Crit. Rev. Toxicol.* **2014**, *44* (sup1), 1−81.
(45) Fenton, S. E.; Ducatman, A.; Boobis, A.; DeWitt, J. C.; Lau, C.; Ng, C.; Smith, J. S.; Roberts, S. M. Per- and Polyfluoroalkyl Substance Toxicity and Human Health Review: Current State of Knowledge and Strategies for Informing Future Research. *Environ. Toxicol. Chem.* **2021**, *40* (3), 606−630.

https://doi.org/10.1021/acs.est.3c09950
Environ. Sci. Technol. 2024, 58, 5727−5738

Publication 3

Species difference? Bovine, Trout and Human Plasma Protein Binding of Per- and Polyfluoroalkyl Substances

Weiping Qin,[1,2] Beate I. Escher,[1,2] Julia Huchthausen,[1,2] Qiuguo Fu[3] and Luise Henneberger[1]*

[1] Department of Cell Toxicology, UFZ–Helmholtz Centre for Environmental Research, 04318 Leipzig, Germany

[2] Environmental Toxicology, Department of Geosciences, Eberhard Karls University Tübingen, Schnarrenbergstr. 94-96, DE-72076 Tübingen, Germany

[3] Department of Analytical Chemistry, UFZ–Helmholtz Centre for Environmental Research, 04318 Leipzig, Germany

*Corresponding author: Luise Henneberger − UFZ−Helmholtz Centre for Environmental Research, 04318 Leipzig, Germany; orcid.org/0000-0002-3181-0044; Email: luise.henneberger@ufz.de

Published in Environmental Science & Technology, https://doi.org/10.1021/acs.est.3c10824.

Environmental Science & Technology

pubs.acs.org/est

Article

Species Difference? Bovine, Trout, and Human Plasma Protein Binding of Per- and Polyfluoroalkyl Substances

Weiping Qin, Beate I. Escher, Julia Huchthausen, Qiuguo Fu, and Luise Henneberger*

Cite This: https://doi.org/10.1021/acs.est.3c10824

Read Online

ACCESS | Metrics & More | Article Recommendations | Supporting Information

ABSTRACT: Per- and polyfluoroalkyl substances (PFAS) strongly bind to proteins and lipids in blood, which govern their accumulation and distribution in organisms. Understanding the plasma binding mechanism and species differences will facilitate the quantitative *in vitro*-to-*in vivo* extrapolation and improve risk assessment of PFAS. We studied the binding mechanism of 16 PFAS to bovine serum albumin (BSA), trout, and human plasma using solid-phase microextraction. Binding of anionic PFAS to BSA and human plasma was found to be highly concentration-dependent, while trout plasma binding was linear for the majority of the tested PFAS. At a molar ratio of PFAS to protein $\nu < 0.1$ $mol_{PFAS}/mol_{protein}$, the specific protein binding of anionic PFAS dominated their human plasma binding. This would be the scenario for physiological conditions ($\nu < 0.01$), whereas in *in vitro* assays, PFAS are often dosed in excess ($\nu > 1$) and nonspecific binding becomes dominant. BSA was shown to serve as a good surrogate for human plasma. As trout plasma contains more lipids, the nonspecific binding to lipids affected the affinities of PFAS for trout plasma. Mass balance models that are parameterized with the protein−water and lipid−water partitioning constants (chemical characteristics), as well as the protein and lipid contents of the plasma (species characteristics), were successfully used to predict the binding to human and trout plasma.

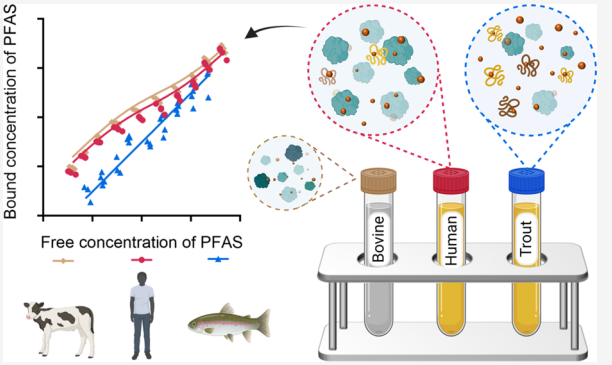

KEYWORDS: *PFAS, solid-phase microextraction, plasma binding mechanism, proteins and lipids, specific and nonspecific protein binding*

1. INTRODUCTION

Blood is one of the major carriers for many per- and polyfluoroalkyl substances (PFAS) in human beings[1] and animal species.[2] The freely dissolved and protein-bound PFAS in blood can be transported with the blood flow to tissues and organs.[3,4] Binding of PFAS to blood components is reversible. Competitive binding between human serum albumin and organ-specific proteins[5] may result in the selective accumulation of PFAS in specific tissues and organs. PFAS accumulate in liver,[6] and even more alarming are detections of PFAS in brain[7,8] and umbilical cord blood,[9,10] indicating that PFAS can cross the blood−brain and placental barrier due to their high cell membrane permeability.[11] Unlike most persistent organic pollutants (POPs) that mainly accumulate in the lipid phase, PFAS have high affinities to both lipids and proteins.[12] Therefore, understanding the binding of PFAS to blood components (e.g., lipids and proteins) is crucial for the prediction of the distribution of PFAS in the body and improving the health risk assessment of PFAS.

The unbound fraction in plasma is an important input parameter for the simulation of the absorption, distribution, metabolism, and excretion (ADME) of PFAS via physiologically based pharmacokinetic (PBPK) modeling.[6,13] The ratio of the bound and free concentrations in plasma is defined by the partition constant between plasma and water ($K_{plasma/w}$). There are now more than 14 000 PFAS chemicals in the CompTox Chemistry Dashboard with different structures and speciation.[14] PFAS may be present as different molecular species at a physiological pH of approximately 7.4. Perfluoroalkyl carboxylic acids (PFCAs) and perfluoroalkyl sulfonic acids (PFSAs) are fully deprotonated and anionic at this pH. The distribution ratio $D_{plasma/w}$ at pH = 7.4 should be used for ionizable PFAS. The unbound fraction of PFAS is available for redistribution or excretion, while the bound fraction of PFAS in tissues and organs has raised concerns about the bioaccumulation and chronic exposure.[13]

To facilitate the quantitative *in vitro*-to-*in vivo* extrapolation (QIVIVE) for PFAS, the concentration−response curves from *in vitro* bioassays should be derived with free concentrations of PFAS to obtain freely dissolved effect concentrations, which can be compared to the actual PFAS levels that human are

Received: December 21, 2023
Revised: May 3, 2024
Accepted: May 14, 2024

exposed to (i.e., freely dissolved concentrations in human plasma).[15−18] Fetal bovine serum (FBS) is typically used as the nutrient supply in an *in vitro* cell-based bioassay, while fish and mice are common *in vivo* animal models. To make the results from the different *in vitro* and *in vivo* models comparable and to allow extrapolation to humans, plasma binding of PFAS among different species needs to be known, but it has not been assessed for PFAS systematically so far.

Human biomonitoring studies suggested that the human blood concentrations of PFAS were at the nanomolar level,[19] while toxicological studies detected the biological effects of PFAS at widely different concentration ranges from upper nano- to millimolar concentrations.[20] For example, a mean value of 40 nmol/L perfluorooctanoic acid (PFOA) in the plasma of breastfed children was associated with reduced antibody responses to childhood vaccines, e.g., production of interferon γ by lymphocytes.[21] A reduction of interferon was found to be regulated via nuclear factor kappa B pathways in zebrafish after a 21 day exposure of PFOA at 2 μmol/L.[22] Other mechanisms of immunotoxicity were proved by *in vivo* animal models after week- or month-administration of PFAS at mg/kg levels, as well as *in vitro* cell models under acute stimulation by PFAS in the μmol/L concentration range.[23] As binding of anionic PFAS to proteins in bioassay medium and human plasma is highly concentration-dependent,[15] the typically large differences between exposure and effect concentrations will have an impact on QIVIVE.

Equilibrium dialysis is widely used to determine the binding of chemicals to BSA and human serum albumin.[24−28] The binding of anionic PFAS to different types of albumin was also identified by ligand blotting,[29] mass spectrometry,[28] and spectroscopy.[24] However, the binding or dissociation constants of PFAS to albumin were derived from single concentrations or limited concentration ranges, which limits an overall understanding of the nonlinear binding behavior of PFAS. Bischel et al.[28] depicted nonlinear binding curves with PFOA and PFNA in a concentration range from 1.6 to 2700 μM, but they only provided specific binding constants at a physiological PFAS:protein molar ratio (ν < 0.001 $mol_{PFAS}/mol_{protein}$). Solid-phase microextraction (SPME) has been used to develop binding isotherms of ionizable chemicals with a small volume of samples over 4 orders of magnitude in concentrations,[30] where the specific and nonspecific binding constants can be differentiated by modeling.[15]

In the present study, we studied the binding mechanism of 16 PFAS to BSA, which was used as a reference for analyzing binding behaviors of PFAS to trout and human plasma. The 16 PFAS covered a wide range of chemical classes including seven PFCAs, two PFSAs, one fluorotelomer sulfonic acid (FTSA), one sulfonamide, three fluorotelomer alcohols (FTOHs), and two fluorinated pesticides with the individual C_nF_{2n} group. Protein and plasma binding isotherms of 13 nonvolatile PFAS were measured in a high-throughput format using a BioSPME 96-Pin Device combined with liquid chromatography mass spectrometry (LCMS).[31] Protein and plasma partition constants of three semivolatile FTOHs were measured with headspace (HS)-SPME combined with gas chromatography mass spectrometry (GCMS). Mass balance models (MBMs) were developed to describe plasma binding from system parameters and chemical-specific parameters. System parameters were volume fractions of proteins and lipids in different plasmas that were experimentally quantified. Chemical-specific parameters were the measured binding constants to the surrogate protein BSA and lipid−water distribution ratios from the literature.

2. MATERIALS AND METHODS

2.1. Materials. Sixteen PFAS (perfluorobutanoic acid (PFBA), perfluorohexanoic acid (PFHxA), perfluoroheptanoic acid (PFHpA), perfluorooctanoic acid (PFOA), perfluorononanoic acid (PFNA), perfluoroundecanoic acid (PFUnA), perfluoro-2-methyl-3-oxahexanoic acid (HFPO−DA), perfluorohexanesulfonic acid (PFHxS), perfluorooctanesulfonic acid (PFOS), 6:2 fluorotelomer sulfonic acid (6:2 FTSA), perfluorooctane sulfonamide (PFOSA), 2-perfluorohexyl-ethanol (6:2 FTOH), 2-perfluorooctyl-ethanol (8:2 FTOH), 2-perfluorodecyl-ethanol (10:2 FTOH), hexaflumuron and flubendiamide) were investigated (Table S1). All PFAS were dissolved in methanol (1428, Chemsolute) as a stock solution. Acetonitrile (34863, Honeywell) and formic acid (Honeywell) were used as eluents for sample measurements. Bovine serum albumin (BSA, 05470, Sigma-Aldrich), trout, and human plasma (S4189, Biowest) were used for protein and plasma binding assays. Rainbow trout (*Oncorhynchus mykiss*) plasma was kindly provided by Pavel Šauer from the University of South Bohemia in České Budějovice, Czech Republic.

Plastic (7696548, Labsolute) and glass-coated (60180-P336, Labsolute) 96-deep-well plates and Supelco BioSPME 96-Pin Devices (59683-U, Sigma-Aldrich) coated with C18 particles were used for 13 nonvolatile PFAS. Headspace crimp vials (20 mL, 762926, Labsolute), a reassembled cover with a magnetic cap (44512, Wicom), and aluminum-coated silicone septa (6086772, Labsolute) and PDMS/DVB fiber (57345-U, Sigma-Aldrich) were used in SPME assays for 3 semivolatile FTOHs. Experiments of uptake kinetics and sorption isotherms were carried out for method development and validations. Experiments of BSA and plasma binding were carried out to derive the binding isotherms and constants.

2.2. Uptake Kinetics of PFAS into C18 Coating of BioSPME. Five or 10 mg of each PFAS was dissolved in 1 mL of methanol as stock solutions. PFAS solution was prepared by diluting the methanolic stock solution with phosphate-buffered saline (PBS) to the concentrations listed in Table S2. The pH value of the PFAS solution was adjusted to 7.4 using sodium hydroxide for each acidic PFAS. The methanol content in the PFAS solution was always ≤1%. Three aliquots of 600 μL were filled in the first 96-deep well plate, and 600 μL of desorption solvents was filled in the second 96-deep well plate. Glass-coated 96-deep well plates were used for hydrophobic PFUnA, PFOSA, hexaflumuron, and flubendiamide to avoid loss due to binding to plastic, and plastic 96-deep well plates were used for the other 9 PFAS (Table S2). The total concentrations of PFAS samples were quantified by a 1260 Infinity liquid chromatograph coupled with a 6420 Triple Quad mass spectrometer (LCMS, Agilent, USA) for mass balance before SPME. The detailed LCMS parameters can be found in Table S3.

The experimental process of BioSPME conditioning, PFAS extraction from the aqueous solution, and desorption of the PFAS from BioSPME were performed automated by a Hamilton Star Robot (Bonaduz, Switzerland) as described by Huchthausen et al.[32] Briefly, the BioSPME 96-Pin Device was conditioned in isopropanol for 20 min and then in Milli-Q water for 10 s. The extraction and desorption processes were performed on a high-speed shaker with a shaking speed of 1000 rpm. The temperature of the shaker was set to 37 °C for

https://doi.org/10.1021/acs.est.3c10824
Environ. Sci. Technol. XXXX, XXX, XXX−XXX

extraction and room temperature (25 °C) for the desorption. The shortest extraction time was 10 min, and the desorption time was always 20 min. After the first cycle, the extracted PFAS solution and desorption solutions were transferred to a third 96-deep well plate for instrumental analysis. The whole process was repeated for different extraction times (20, 40, 80, and 120 min). The experimental device is not airtight, and the extraction time should not be longer than 120 min to avoid the evaporation of the sample. After all of the samples were collected, the PFAS concentrations in the extracted aqueous solution and in the desorption solutions were measured by LCMS.

2.3. Sorption Isotherms for BioSPME. Methanolic stock solutions (10 or 5 mg/mL) containing the individual PFAS were diluted with methanol first to 100 times the desired concentration, and then 50 μL of this solution was further diluted with 4950 μL of PBS (Figure S1). The concentrations of each PFAS (Table S4) were designed according to the distribution ratio of PFAS between the pin coating and water ($D_{pin/w}$). For each PFAS, a 9-step dilution series was prepared from the sample with the highest concentration with a factor of 2 difference between each step (Figure S1). Different volumes of the sample with the highest concentration were added to a new vial, and the respective volume of PBS was added to achieve a final volume of 2 mL for each sample. All samples were vortexed for 30 s. Two aliquots of 600 μL for each concentration were filled in the first 96-deep well plate, and 600 μL of desorption solvents was filled in the second 96-deep well plate. The experimental process for BioSPME was the same as above, and detailed experimental conditions for each PFAS can be found in Table S2 (e.g., extraction time, type of desorption solvent, material of the 96-deep well plate used for desorption and extraction).

2.4. BSA and Plasma Binding Isotherms of 13 Nonvolatile PFAS. BSA solution was prepared by dissolving BSA in PBS. The sample preparation was the same as shown in Figure S1 but using a BSA solution for dilution. The concentrations of PFAS and BSA (Table S5) were designed individually to have bound fractions of PFAS to BSA within a range of 30−90% based on experimental results in the pretests. All PFAS samples with BSA were incubated at 37 °C and shaken at 250 rpm overnight to allow for equilibration of protein binding. On the second day, samples were transferred to a 96-deep well plate for BioSPME.

For human and trout plasma binding assays, the appropriate plasma concentration was prepared by diluting the plasma with PBS. The volumes of human and trout plasma were chosen for each PFAS to keep a similar plasma protein level to that for the BSA binding assays (Table S5). The sample preparation was the same as that in Figure S1 with diluted plasma. PFAS samples with human plasma were incubated at 37 °C, the trout plasma samples were incubated at room temperature (25 °C), and all samples were shaken at 250 rpm overnight for equilibration of plasma binding before BioSPME.

2.5. BSA and Plasma Binding of 3 Semivolatile FTOHs. Ten mg of the individual FTOHs were dissolved in 1 mL of methanol as stock solution. FTOH stock solutions were further diluted with methanol to different concentrations (Figure S2), and then 50 μL of methanolic solution was added to 4950 μL of BSA in PBS in a 20 mL headspace crimp vial. A reassembled cover with a magnetic cap and aluminum-coated silicone septa was secured to the vial immediately using a crimper to form a sealed space to avoid the loss of FTOHs. Samples in the vial were vortexed for 30 s and then incubated at 37 °C and 250 rpm for 2 h. FTOHs were extracted from the headspace using a PDMS/DVB fiber, and the concentrations of FTOHs were quantified by an 8890 gas chromatograph coupled to a 5977B GC/MSD (Agilent, Waldbronn, Germany). Detailed parameters for HS-SPME combined with GCMS are found in Table S6.

For protein and plasma binding assays, 10 mg/mL of BSA was selected to ensure a 30−90% fraction bound for the tested FTOHs (Table S5) according to the pretests. 100 mL/L of plasma was used to keep similar plasma protein levels as for the BSA binding assays. The sample preparation was the same as that in Figure S2 but using PBS-diluted BSA or plasma. FTOH samples with BSA and human plasma were incubated at 37 °C and shaken at 250 rpm for 2 h for equilibration of BSA and plasma binding, while samples with trout plasma were incubated at room temperature (25 °C) and shaken at 250 rpm for 2 h before measurements by HS-SPME combined with GCMS.

2.6. Protein and Lipid Quantification. Plasma was diluted with PBS by a factor of 50 to ensure that the lipid and protein concentrations were within the calibration ranges. Pierce BCA Protein Assay Kit (23228, Thermo Scientific) was used to determine protein concentrations. The sulfophospho-vanillin reaction was used to determine the lipid concentrations as described previously.[33] Units of protein and lipid were converted from mass concentration (mg/L) to volume concentration (mL/L) using a density of protein of 1.36 kg/L and a density of lipid of 1 kg/L.

2.7. Acidity Constant Determination. The pK_a of PFOSA at 25 °C and an ionic strength of 0.15 M KCl was determined with a cosolvent method with methanol according to Yasuda-Shedlovsky,[34,35] and the pK_a values of flubendiamide and hexaflumuron were determined with the UV-metric method,[36] using a Sirius T3 automated titrator (Pion) equipped with a glass Ag/AgCl pH electrode and a UV dip probe. A detailed description can be found in the literature.[37]

3. DATA EVALUATION

3.1. Mass Balance of BioSPME. The method development and validation of the BioSPME for PFAS were similar to C18-SPME using single fibers in our previous study.[15] The amount of PFAS in the water phase (n_w, eq 1) and the coating of the pins (n_{pin}, eq 2) were obtained from the measured concentrations of PFAS in the extracted aqueous phase (C_w) and in the desorption solvent (C_{des}) and their corresponding volumes (V_w and V_{des}). The volume of the C18 pin coating (V_{pin}) was approximately 80 nL.[31] The mass balance (eq 3) was calculated to validate the method

$$n_w = C_w \times V_w \quad (1)$$

$$n_{pin} = C_{pin} \times V_{pin} = C_{des} \times V_{des} \quad (2)$$

$$\text{mass balance}(\%) = \frac{n_{pin} + n_w}{n_{tot}} \quad (3)$$

3.2. Uptake Kinetics into C18 Pin Coating of BioSPME. The equilibration times of PFAS between water and pin coating were determined from first-order kinetics (eqs 4 and 5), where n_w (eq 4) and n_{pin} (eq 5) are the amount of PFAS in the water phase and pin coating at different time points, respectively. n_w (t_0) is the initial amount of PFAS used in the experiment. k_1 is the rate constant for the decrease of the

https://doi.org/10.1021/acs.est.3c10824
Environ. Sci. Technol. XXXX, XXX, XXX−XXX

amount of the chemical in the water phase, and k_2 is the apparent uptake rate constant to the pin coating[30]

$$n_w(t) = n_w(\text{eq}) \times (1 - e^{-k_1 \times t}) + n_w(t_0) \times e^{-k_1 \times t} \quad (4)$$

$$n_{pin}(t) = n_{pin}(\text{eq}) \times (1 - e^{-k_2 \times t}) \quad (5)$$

The time when sorption to the pin coating reached 95% equilibrium ($t_{0.95}$) was calculated from k_2 using eq 6

$$t_{0.95} = \frac{\ln 0.05}{-k_2} \quad (6)$$

3.3. Freundlich-Type Model for Sorption Isotherms. Sorption isotherms of PFAS to the pin coating of the BioSPME, as well as to BSA and plasma proteins and lipids, were fitted with an empirical Freundlich adsorption isotherm by eq 7

$$C_{bound,i} = K_{Fr} \times (C_w)^{n_{Fr}} \quad (7)$$

After a logarithmic transformation, the Freundlich-type model was derived with a linear relationship of the bound concentration, log $C_{bound,i}$ (i = pin coating, BSA, or plasma protein and lipid), against the water concentration (log C_w) by eq 8. The Freundlich constant log K_{Fr} and exponent n_{Fr} were adjusted by a best fit to the experimental data

$$\log C_{bound,i} = n_{Fr} \times \log C_w + \log K_{Fr} \quad (8)$$

Distribution ratios between the sorption phases i and water, log $D_{i/w}$ (eq 9), can be calculated at a given log $C_{bound,i}$ (eq 10) or log C_w (eq 11) with log K_{Fr} and n_{Fr}. The average value of log $D_{i/w}$ is approximately equal to log K_{Fr} when the n_{Fr} is close to 1 canceling the log C_w, suggesting that the log $D_{i/w}$ is independent of concentrations. The standard error (SE) of log K_{Fr} (or log $D_{i/w}$) was derived directly from the model fit. A 95% confidence interval (CI) was obtained as the values 1.96 × SE of either side of log $D_{i/w}$

$$D_{i/w} = \frac{C_{bound,i}}{C_w} \quad (9)$$

$$\log D_{i/w} = \left(1 - \frac{1}{n_{Fr}}\right) \times \log C_{bound,i} + \frac{\log K_{Fr}}{n_{Fr}} \quad (10)$$

$$\log D_{i/w} = (n_{Fr} - 1) \times \log C_w + \log K_{Fr} \quad (11)$$

3.4. Mechanistic Model for BSA and Plasma Binding. The sorption isotherm of some anionic PFAS was concentration-dependent, which can be fitted nonlinearly with a combined binding/partitioning model.[15] A wide range of molar ratios ν of bound PFAS-to-protein (eq 12, $mol_{PFAS}/mol_{protein}$) were used to identify the saturable binding range. A plateau of saturable binding in the range of $\nu < 1$ by eq 13 suggests specific binding of PFAS with proteins

$$\nu = \frac{n_{bound,PFAS}}{n_{protein}} \quad (12)$$

$$C_{bound,specific} = \frac{C_{max} \times C_w}{K_d + C_w} \quad (13)$$

In the saturable binding, where there is only one binding site on the protein, the dissociation constant (K_d) equals the equilibrium concentration of free PFAS (C_w) required to occupy half of the maximum number of binding sites (C_{max}) on the protein. The specific binding constant $D_{specific}$ can be derived with the C_{max} and K_d by eq 14.[15] The SE of $D_{specific}$ was calculated by error propagation using the SE of C_{max} and K_d of the model fit. 95% CI was obtained as the values 1.96 × SE of either side of $D_{specific}$

$$D_{specific} = \frac{C_{bound,specific}}{C_w} = \frac{C_{max}}{K_d + C_w} = \frac{C_{max}}{2 \times K_d} \quad (14)$$

The nonspecific binding constant, $D_{nonspecific}$, was derived by eq 15 with the fixed values of C_{max} and K_d from eq 13. The SE of $D_{nonspecific}$ was derived from the model fitting. 95% CI was obtained as the values 1.96 × SE of either side of $D_{nonspecific}$.

$$C_{bound,total} = \frac{C_{max} \times C_w}{K_d + C_w} + D_{nonspecific} \times C_w \quad (15)$$

Protein and lipid in the plasma are the major sorption phases, with protein binding being highly specific at one binding site,[15] while the nonspecific binding is relevant for proteins and lipids at higher concentrations. Therefore, the plasma binding isotherm was fitted by eq 16 that includes an extra term correcting for the ratio of the volume fraction of protein to protein plus lipid

$$C_{bound,total} = \frac{C_{max} \times C_w}{K_d + C_w} \times \frac{V_{protein,plasma}}{V_{protein+lipid,plasma}} + D_{nonspecific} \times C_w \quad (16)$$

3.5. Mass Balance Model for Protein/Plasma Binding of FTOHs. In a closed headspace vial, the total amount of FTOH (n_{tot}) partitions between water (n_w), air (n_{air}), wet-glass surface (n_{glass}), and biomaterials ($n_{bound,i}$, i = BSA, plasma proteins and lipids)

$$n_{tot} = n_w + n_{air} + n_{glass} + n_{bound,i} \quad (17)$$

Partition constants of FTOHs between air and water ($K_{air/w}$),[38] wet-glass surface and air ($K_{glass/air}$),[39] and biomaterials and water ($D_{i/w}$, i = BSA, plasma) were introduced into eq 17 to derive the concentration of FTOH in the aqueous phase of the PBS samples used as control, C_w (eq 18), as well as the aqueous phase of BSA and plasma samples, $C_{w,i}$ (eq 19)

$$C_w = \frac{n_{tot}}{V_w + K_{air/w} \times V_{air} + K_{air/w} \times K_{glass/air} \times S_{glass}} \quad (18)$$

$$C_{w,i} = \frac{n_{tot}}{V_w + K_{air/w} \times V_{air} + K_{air/w} \times K_{glass/air} \times S_{glass} + D_{i/w} \times V_i} \quad (19)$$

The distribution ratios, $D_{BSA/w}$ and $D_{plasma/w}$, can be derived from the peak areas of GCMS by using HS-SPME as described previously.[40] Given a linear detector response (Figure S3), the GC peak areas of the FTOH from the control samples (A_w, eq 20), BSA, or plasma samples ($A_{w,i}$, eq 21) can be assumed to be linearly related to the concentration of the FTOH in the aqueous phases

$$A_w = \text{slope} \times C_w \quad (20)$$

$$A_{w,i} = \text{slope} \times C_{w,i} \quad (21)$$

https://doi.org/10.1021/acs.est.3c10824
Environ. Sci. Technol. XXXX, XXX, XXX−XXX

Table 1. Distribution Ratios between BSA and Water ($D_{BSA/w}$) and Distribution Ratios between Plasma and Water ($D_{plasma/w}$) of 13 PFAS[a]

	BSA: log $D_{BSA/w}$ [L_w/L_{prot}]	R^2	human plasma: log $D_{plasma/w}$ [$L_w/L_{prot+lip}$]	R^2	trout plasma: log $D_{plasma/w}$ [$L_w/L_{prot+lip}$]	R^2
PFBA	$\log D_{BSA/w} = -0.298 \log C_w + 2.91$	0.60	$\log D_{plasma/w} = -0.402 \log C_w + 2.80$	0.68	1.43	0.74
PFHxA	$\log D_{BSA/w} = -0.271 \log C_w + 3.43$	0.88	$\log D_{plasma/w} = -0.287 \log C_w + 3.29$	0.84	2.49	0.91
PFHpA	$\log D_{BSA/w} = -0.305 \log C_w + 3.95$	0.81	$\log D_{plasma/w} = -0.389 \log C_w + 3.79$	0.89	3.32	0.93
PFOA	$\log D_{BSA/w} = -0.314 \log C_w + 4.38$	0.93	$\log D_{plasma/w} = -0.410 \log C_w + 4.02$	0.86	4.18	0.98
PFNA	$\log D_{BSA/w} = -0.147 \log C_w + 4.52$	0.61	$\log D_{plasma/w} = -0.183 \log C_w + 4.13$	0.91	4.71	0.98
PFUnA	4.75	0.96	4.54	0.95	4.99	0.98
HFPO−DA	$\log D_{BSA/w} = -0.493 \log C_w + 3.44$	0.86	$\log D_{plasma/w} = -0.633 \log C_w + 3.41$	0.95	$\log D_{plasma/w} = -0.646 \log C_w + 3.20$	0.97
PFHxS	$\log D_{BSA/w} = -0.472 \log C_w + 4.28$	0.92	$\log D_{plasma/w} = -0.677 \log C_w + 3.95$	0.96	$\log D_{plasma/w} = -0.236 \log C_w + 3.96$	0.68
PFOS	$\log D_{BSA/w} = -0.379 \log C_w + 4.74$	0.92	$\log D_{plasma/w} = -0.336 \log C_w + 4.46$	0.85	$\log D_{plasma/w} = -0.303 \log C_w + 4.91$	0.92
6:2 FTSA	$\log D_{BSA/w} = -0.092 \log C_w + 3.86$	0.54	$\log D_{plasma/w} = -0.144 \log C_w + 3.66$	0.71	4.11	0.91
PFOSA	$\log D_{BSA/w} = -0.105 \log C_w + 4.28$	0.50	$\log D_{plasma/w} = -0.103 \log C_w + 3.87$	0.52	$\log D_{plasma/w} = -0.164 \log C_w + 4.26$	0.60
hexaflumuron	3.96	0.97	4.29	0.94	4.61	0.91
flubendiamide	3.98	0.96	3.88	0.99	4.46	0.97

[a]Regression equations between log $D_{BSA/w}$ and log $D_{plasma/w}$ against log C_w were derived using a Freundlich-type model (eq 11). The concentration unit of PFAS in the water phase (C_w) is micromolar [μmol/L].

The slope is the response factor of the GC measurement, which cancels out if the ratio of peak areas ($A_w/A_{w,i}$) is calculated. Insertion of eqs 18−20 and eqs 19−21 also cancels out the n_{tot} for control samples and BSA and plasma samples. $D_{i/w}$ was moved to the left side of the equation to yield eq 22. The SE of $D_{i/w}$ was calculated from the standard deviation of samples measured with different concentrations. 95% CI was obtained as the values 1.96 × SE of either side of mean $D_{i/w}$. The derivation of eq 22 and detailed information about the $K_{air/w}$, $K_{glass/air}$ (Table S7), and S_{glass} can be found in Supporting Information Text S1

$$D_{i/w} = (V_w + K_{air/w} \times V_{air} + K_{air/w} \times K_{glass/air} \times S_{glass}) \times \frac{1}{V_i} \times \left(\frac{A_w}{A_{w,i}} - 1\right) \quad (22)$$

3.6. Plasma Binding Prediction. The distribution ratios of neutral PFAS ($D_{plasma/w}$, pH = 7.4) between plasma proteins and lipids and water can be predicted by eq 23. $D_{BSA/w}$ measured in the present study served as a proxy for protein distribution, as well as the distribution ratio of liposome and water $D_{lip/w}$ for phospholipid distribution and olive oil and water $D_{oil/w}$ as a proxy for neutral lipid distribution. The ratio of phospholipids to neutral lipids in human plasma is approximately 2:3 according to previous reports.[41,42] The differentiation between phospholipids and neutral lipids is necessary because anionic chemicals showed high affinities to phospholipid[43] but do not partition to neutral bulk lipids. Predictions of $D_{plasma/w}$ for anionic PFAS can therefore be simplified by neglecting the third term in eq 23

$$D_{plasma/w} = D_{BSA/w} \times \frac{V_{protein,plasma}}{V_{protein+lipid,plasma}} + D_{lip/w} \times \frac{0.40 \times V_{lipid,plasma}}{V_{protein+lipid,plasma}} + D_{oil/w} \times \frac{0.60 \times V_{lipid,plasma}}{V_{protein+lipid,plasma}} \quad (23)$$

3.7. Statistical Analysis. Results were analyzed by Microsoft Excel and GraphPad Prism 10.0. The Freundlich-type model and combined binding/partitioning model were fitted with Graphpad Prism 10.0. The SE of the parameters derived from the model fitting is used to calculate the 95% confidence interval of the binding constants. Differences among testing concentrations were evaluated by Student's t test. Results were considered as statistically significant if the p value was <0.05.

4. RESULTS

4.1. Validation of BioSPME Method. The average mass balance of 13 PFAS measured by BioSPME was between 92 and 115% (eq 3, Table S2) in the kinetic uptake experiments, suggesting that the loss of chemicals to other compartments (e.g., plate or pin material) was less than 10%. As shown in Figure S4, 95% of equilibrium between pin coating and water (eq 6) was reached within 30 min for hydrophilic PFAS, while hydrophobic PFAS needed a longer time (max 58 min). Other experimental conditions, such as desorption solvents, desorption time, and plate materials, were determined for each PFAS according to their mass balance in the assays. Detailed information can be found in Table S2.

Sorption isotherms to the pin coating were fitted with a Freundlich-type model (eq 8). The isotherm curves of 8 anionic PFAS were found to be concentration-dependent, and thus, their log $D_{pin/w}$ were fitted against log $C_{bound,pin}$ (eq 10) and are listed in Table S4. The log $D_{pin/w}$ were determined by setting n_{Fr} = 1 (eq 10) for long-chain PFNA, PFUnA, and PFOSA, as well as complex hexaflumuron and flubendiamide (Table S4), because their sorption isotherms were weakly dependent on concentrations (0.90 < n_{Fr} < 1) or independent of concentrations ($n_{Fr} \geq 1$). Log C_{pin} of PFHpA was presented in a concentration-dependent way, although its n_{Fr} was 0.93, because the chain length of PFHpA is between PFHxA and PFOA, for which log C_{pin} was concentration-dependent.

4.2. BSA Binding Isotherms. The BSA binding isotherms of the 13 PFAS were first fitted using the Freundlich-type model (eq 8, see Figure 1a,e for HFPO−DA and PFNA; for all other chemicals, see Figure S5). The log $D_{BSA/w}$ were plotted against the log C_w (eq 11) and were concentration-dependent for HFPO−DA and PFNA (Figure 1b,f) and other 8 PFAS, and results of all PFAS are listed in Table 1. The BSA binding isotherm of PFUnA (0.90 < n_{Fr} < 1) was weakly dependent on concentrations, and the BSA binding isotherm of hexaflumuron and flubendiamide was independent of concentrations ($n_{Fr} \geq$

https://doi.org/10.1021/acs.est.3c10824
Environ. Sci. Technol. XXXX, XXX, XXX−XXX

Table 2. Distribution Ratios of PFAS between Lipids, Proteins, Plasma, and Water[a,b]

				BSA: log $D_{BSA/w}$ [L_w/L_{prot}]		human plasma: log $D_{plasma/w}$ [$L_w/L_{prot+lip}$]		trout plasma: log $D_{plasma/w}$ [$L_w/L_{prot+lip}$]	
	number of C−F	log $D_{lip/w}$ [L_w/L_{lip}]	log $D_{oil/w}$ [L_w/L_{oil}]	specific	nonspecific or average*	specific	nonspecific or average*	specific	nonspecific or average*
PFBA	3	1.00[c]	n/a	*2.44 (2.10−2.63)*	1.97 (1.90−2.04)	2.20 (0.87−2.49)	1.35 (1.23−1.44)	n/a	1.43 (1.28−1.58)*
PFHxA	5	2.32[d]	n/a	3.26 (2.98−3.42)	2.69 (2.66−2.72)	3.19 (3.01−3.31)	2.61 (2.56−2.66)	n/a	2.49 (2.41−2.57)*
PFHpA	6	2.91[d]	n/a	4.12 (3.87−4.27)	3.47 (3.42−3.52)	4.10 (3.98−4.20)	3.20 (3.15−3.24)	n/a	3.32 (3.25−3.39)*
PFOA	7	3.52[d]	n/a	4.58 (4.47−4.67)	3.88 (3.86−3.90)	4.45 (4.34−4.54)	3.65 (3.59−3.70)	n/a	4.18 (4.14−4.21)*
PFNA	8	4.25[d]	n/a	n/a	4.61 (4.56−4.65)*	n/a	4.19 (4.14−4.24)*	n/a	4.71 (4.65−4.76)*
PFUnA	10	4.54[d]	n/a	n/a	4.75 (4.71−4.80)*	n/a	4.54 (4.49−4.59)*	n/a	4.99 (4.96−5.03)*
HFPO−DA	5	2.41[d]	n/a	3.31 (2.95−3.50)	2.17 (2.05−2.26)	3.35 (2.77−3.58)	1.99 (1.93−2.04)	3.56 (3.08−3.78)	1.89 (1.67−2.04)
PFHxS	6	4.13[d]	n/a	5.02 (4.90−5.11)	3.58 (3.50−3.64)	4.98 (4.80−5.11)	2.92 (2.78−3.03)	n/a	4.00 (3.91−4.10)*
PFOS	8	4.89[d]	n/a	5.27 (4.84−5.48)	4.17 (4.14−4.20)	4.82 (4.41−5.03)	4.07 (4.04−4.11)	5.49 (4.88−5.74)	4.57 (4.54−4.60)
6:2 FTSA	6	3.87[e]	n/a	n/a	3.87 (3.84−3.90)*	n/a	3.67 (3.63−3.70)*	n/a	4.11 (4.04−4.19)*
PFOSA	8	4.94[e]	4.61[h]	n/a	4.32 (4.28−4.37)*	n/a	3.90 (3.86−3.93)*	n/a	4.33 (4.27−4.40)*
hexaflumuron	2	4.58[f]	5.19[h]	n/a	3.96 (3.93−4.00)*	n/a	4.29 (4.24−4.35)*	n/a	4.61 (4.53−4.69)*
flubendiamide	3	3.28[f]	4.91[h]	n/a	3.98 (3.93−4.02)*	n/a	3.88 (3.85−3.91)*	n/a	4.46 (4.42−4.50)*
6:2 FTOH	6	4.38[g]	3.81[g]	n/a	2.67 (2.54−2.77)*	n/a	2.73 (2.49−2.89)*	n/a	2.77 (2.49−2.94)*
8:2 FTOH	8	5.85[g]	4.55[g]	n/a	4.61 (4.48−4.72)*	n/a	4.55 (4.49−4.61)*	n/a	5.01 (4.90−5.10)*
10:2 FTOH	10	7.73[e]	6.03[e]	n/a	6.72 (6.44−6.89)*	n/a	6.21 (6.11−6.28)*	n/a	6.86 (6.68−6.99)*

[a]n/a: not available. [b]Distribution ratios between membrane lipids (liposomes) or neutral lipids and water (log $D_{lip/w}$ or log $D_{oil/w}$) were from the literature or predicted. Distribution ratios between bovine serum albumin and water (log $D_{BSA/w}$) and between human or trout plasma and water (log $D_{plasma/w}$) were measured in this study. Average log $D_{i/w}$ were calculated with the Freundlich-type model (eq 11). log $D_{i/w}$ of specific and nonspecific binding were derived with the combined binding/partitioning model (eqs 13, 15, 16). In parentheses are the 95% confidence intervals. [c]log $D_{lip/w}$ were from Droge et al.[44] [d]log $D_{lip/w}$ were from Ebert et al.[11] [e]log $D_{lip/w}$ of 6:2 FTSA and PFOSA were predicted from the linear relationship of experimental log $D_{lip/w}$ against the number of fluorinated carbons (Figure S10) by eq S12. log $D_{lip/w}$ of 10:2 FTOH were predicted by eq S13. log $D_{oil/w}$ of 10:2 FTOH were predicted by eq S14. [f]log $D_{lip/w}$ were predicted with COSMOtherm.[45] [g]log $D_{lip/w}$ and log $D_{oil/w}$ (olive oil) were from Endo et al.[46] [h]log $D_{oil/w}$ approximated by the ionization-corrected octanol−water partition constant log D (pH 7.4) (ACD/percepta 14.51.0).

https://doi.org/10.1021/acs.est.3c10824
Environ. Sci. Technol. XXXX, XXX, XXX−XXX

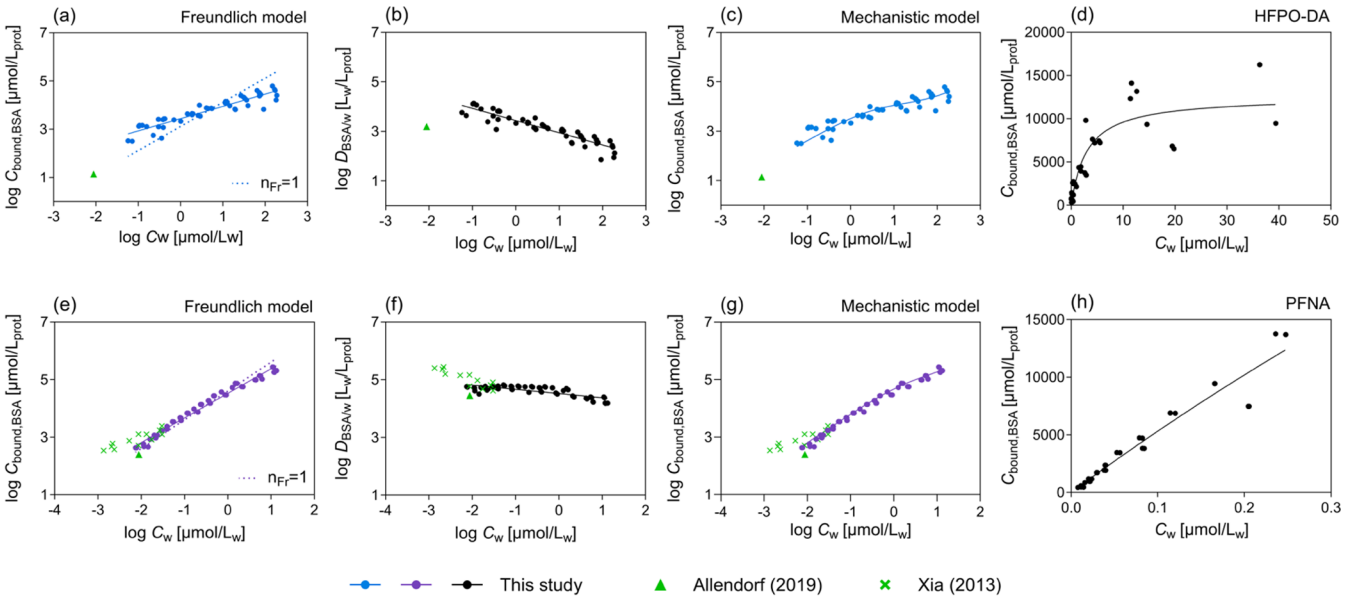

Figure 1. Bovine serum albumin (BSA) binding of (a−d) HFPO−DA and (e−h) PFNA. (a, e) Data points were fitted linearly with the Freundlich-type model (eq 8, solid line); the dotted line refers to fixed n_{Fr} = 1 for comparison. (b, f) The concentration-dependent distribution ratios between BSA and water, log $D_{BSA/w}$, were fitted linearly (eq 11). (c, g) Experimental data points were fitted nonlinearly with the combined binding/partition model (eq 15). (d, h) The saturable specific binding in the low concentration range was derived with eq 13. Results of this study were compared with literature data[25,26] (green triangle and crosses).

1) (Table S8); therefore, their average log $D_{BSA/w}$ were obtained by setting the n_{Fr} = 1 (eq 11).

For nonlinear binding isotherms (n_{Fr} < 0.9), a combined binding/partitioning model was used to derive the specific and nonspecific log $D_{BSA/w}$ (Figure 1c,g). If a plateau of $C_{bound,BSA}$ was found in the low concentration range (ν < 1, eq 13), e.g., for HFPO−DA (Figure 1d), specific binding applies in this concentration range and the specific $D_{BSA/w,specific}$ (eq 14) was derived. The nonspecific log $D_{BSA/w,nonspecific}$ was subsequently derived from the overall fit of the isotherm (eq 15). Similarly, the specific and nonspecific log $D_{BSA/w}$ (Table 2) could be derived for PFBA, PFHxA, PFHpA, PFOA, PFHxS, and PFOS from the concentration-dependent binding isotherms (Figure S5).

However, for some PFAS such as PFNA (Figure 1h), 6:2 FTSA, and PFOSA (Figure S5h,i), no specific binding could be identified because there was no plateau of $C_{bound,BSA}$ in saturable binding curves. An average log $D_{BSA/w}$ was obtained for them by setting n_{Fr} = 1 (eq 11). This may be due to sensitivity limitations of the SPME method and instrumental analysis. All values of specific and nonspecific log $D_{BSA/w}$ for 7 anionic PFAS, as well as average log $D_{BSA/w}$ of other 6 PFAS, are listed in Table 2.

BSA binding isotherms of PFBA, PFOA, and PFHxS measured in the present study were compared with our previous results with C18-SPME using single fibers.[15] Because the data from the two methods were almost overlapping (Figure S6a−c), all data were fitted together to derive $D_{BSA/w}$ (Tables 2 and S9). The specific binding of PFOS measured with C18-SPME was a bit higher. However, 5 mg/mL of BSA was used for the C18-SPME, resulting in a bound fraction of PFOS > 99% in the low concentration range. The bound fraction reduced to 40−90% after adjusting BSA to 0.1 mg/mL in this study (Figure S6d and Table S10). log $D_{BSA/w}$ of PFOS were also fitted with data from two methods, but several points in the low concentrations were excluded. Detailed information can be found in Supporting Information Text S2.

4.3. Acidity Constants. The BSA binding isotherm of PFOSA was slightly concentration-dependent (Figure S5i). We therefore measured its acidity constant. PFOSA was found to be an N-acid with a pK_a value of 8.77 ± 0.27, which means that 4.1% of PFOSA is anionic at pH 7.4. Sulfonamide pharmaceuticals typically have pK_a > 9, but the perfluorinated alkyl chain possibly stabilizes the anion and reduces the pK_a value. As binding of the anion is higher and usually specific, we can explain the observed nonlinearity of the sorption isotherm by the speciation of PFOSA. We also measured the pK_a of hexaflumuron and flubendiamide with the values of 9.11 ± 0.143 and 9.03 ± 0.10, which means these chemicals are 98% neutral and 2% anionic at pH = 7.4. The pK_a values of anionic PFAS and neutral FTOHs were not measured since they are 100% anionic or neutral at physiological pH = 7.4.

4.4. Protein and Lipid Contents of Human and Trout Plasma. The human plasma contained 42.25 mL/L of protein, almost 10 times higher than the lipid content of 4.46 mL/L. The trout plasma had a lower protein content of 15.46 mL/L and more lipids of 7.08 mL/L compared with the human plasma (Table 3).

4.5. Plasma Binding Isotherms. Similar to BSA binding, the human plasma binding of 10 PFAS was concentration-dependent (Table 1), but specific and nonspecific log $D_{plasma/w}$ could be distinguished for only 7 anionic PFAS (Table 2). Average values of log $D_{plasma/w}$ for PFNA, PFUnA, 6:2 FTSA, PFOSA, hexaflumuron, and flubendiamide were derived with

Table 3. Volume Fractions (Vf) of Proteins and Lipids in Human and Fish Plasma

	$Vf_{protein}$ [mL/L]	Vf_{lipid} [mL/L]
human plasma	42.25	4.46
fish plasma	15.46	7.08

https://doi.org/10.1021/acs.est.3c10824
Environ. Sci. Technol. XXXX, XXX, XXX−XXX

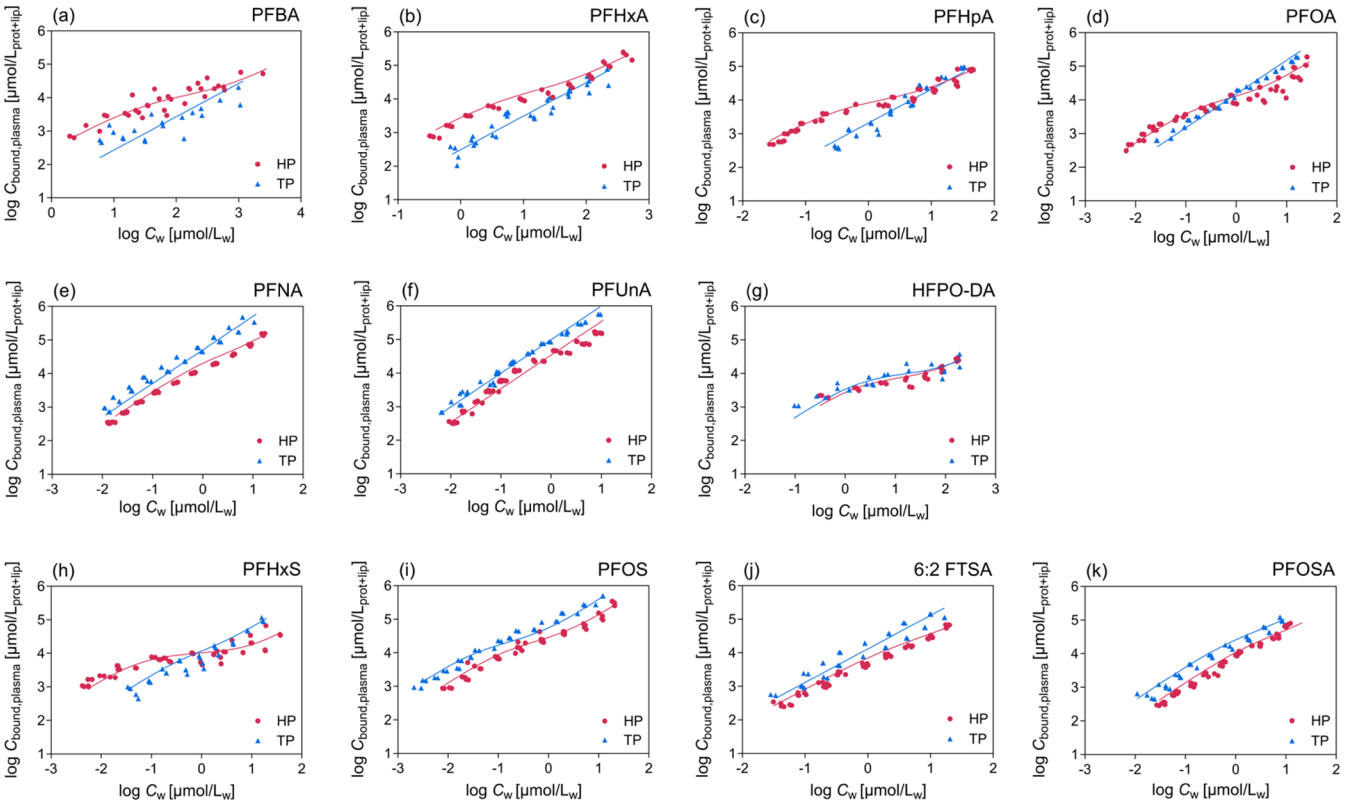

Figure 2. Human plasma (HP) and trout plasma (TP) binding isotherms of 11 anionic PFAS. Curves were fitted linearly with the Freundlich-type model (eq 8) or nonlinearly with the combined binding/partitioning model (eq 16). The selection of models was based on whether the binding isotherms were concentration-dependent (Table 1).

fixed $n_{Fr} = 1$ (Table 2). The volume fraction of proteins was 10 times higher than that of lipids; therefore, proteins are expected to dominate the human plasma binding. Differently, HFPO−DA, PFHxS, PFOS, 6:2 FTSA, and PFOSA ($n_{Fr} <$ 0.90, Table S8) were found to have concentration-dependent binding isotherms for trout plasma, but only for HFPO−DA and PFOS, the specific binding could be fitted (Table 2).

Human and trout plasma binding isotherms were directly compared for 11 of the 13 tested PFAS in Figure 2. Differences were observed between trout and human plasma binding in the low concentration ranges of PFBA, PFHxA, PFHpA, PFOA, and PFHxS, while the isotherms overlapped at high concentrations (Figure 2a−d,h) because the nonspecific lipid binding ($\log D_{lip/w}$) is similar to the nonspecific protein binding ($\log D_{BSA/w}$) (Table 2). The difference at low concentrations is due to the higher protein content of human plasma which led to dominance of strong specific binding. The trout plasma had lower protein content and higher lipid content and lipid binding may have masked the specific protein binding. For PFHxS and PFOA, trout plasma binding gradually surpassed the human plasma binding at high concentrations (Figure 2d,h), suggesting that lipid binding may dominate the plasma binding at high concentrations where their $\log D_{lip/w}$ were higher than the nonspecific $\log D_{BSA/w}$. For PFNA and 6:2 FTSA, trout plasma binding was linear, but slightly concentration-dependent for human plasma, indicating that specific protein binding was relevant but partially masked by nonspecific binding (Figure 2e,j). PFOSA showed a rather weak concentration dependence for both types of plasma (Figure 2k). Both plasma binding isotherms were linear for PFUnA (Figure 2f), hexaflumuron, and flubendiamide (Figure S7).

4.6. Comparison of BSA and Plasma Binding of Neutral FTOHs and Anionic PFAS. BSA binding of neutral 6:2 FTOH, 8:2 FTOH, and 10:2 FTOH was measured at four concentrations, and there was no significant difference (t test, $p < 0.05$) of $\log D_{BSA/w}$ among concentrations (Figure S8). Therefore, their $\log D_{BSA/w}$ values were calculated from the average values measured at different concentrations (Table 2). Similarly, the average values of $\log D_{plasma/w}$ of human and trout plasma were calculated for those chemicals that did not show any specific binding (Table 2). The $\log D_{plasma/w}$ of the FTOHs for trout plasma were higher than that of human plasma because FTOHs bind stronger to lipids compared to proteins (Table 2) and the volume fraction of lipids was higher in trout plasma than in human plasma. Both human and fish plasma binding constants of neutral FTOHs and anionic PFAS were chain-length-dependent (Figure S9).

The acidic functional groups have an impact on the specific binding of PFAS to BSA. Carboxylic and sulfonic acids deprotonate to anionic carboxylates and sulfonates and bind to proteins via electrostatic interaction, which may lead to the specific protein binding of PFBA, PFHxA, PFHpA, PFOA, HFPO−DA, PFHxS, and PFOS (Table 2). The BSA binding of 6:2 FTOH was 10 times lower than that of PFOA, PFHxS, and 6:2 FTSA, which have the same number of perfluorinated carbons, because the neutral alcohols bind to proteins mainly via van der Waals forces with contribution of hydrogen bonds by the alcohol groups. However, as the number of C−F increases, the hydrophobicity increases and consequently the nonspecific portion of binding dominated, where the specific

https://doi.org/10.1021/acs.est.3c10824
Environ. Sci. Technol. XXXX, XXX, XXX−XXX

binding of PFNA and PFUnA cannot be distinguished from the nonspecific binding (Figures 1h and S5e). Also, the impact of hydrophobicity may surpass that of the functional groups. For example, the log $D_{BSA/w}$ (nonspecific or average) of PFNA, PFOS, PFOSA, and 8:2 FTOH with eight perfluorinated carbons were similar despite the different head groups. The log $D_{BSA/w}$ of 10:2 FTOH were higher than that of PFUnA, both of which carry 10 perfluorinated carbons, presumably due to the combined effect of the extra ethane moiety (C_2H_4) of 10:2 FTOH and the different head groups of an anionic carboxylate versus a neutral hydroxy group (Table 2).

Linear regressions were developed for log $D_{BSA/w}$ (nonspecific or average) against the number (n) of C−F for PFCAs and FTOHs (Figure 3) to study how the chain length may

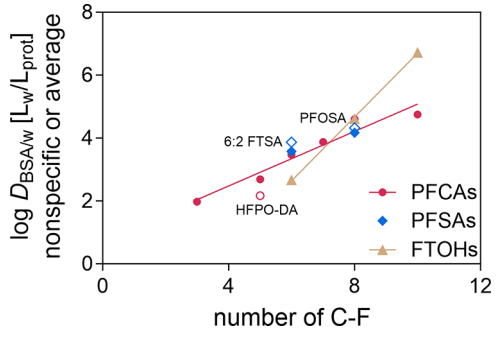

Figure 3. Nonspecific or average BSA binding, log $D_{BSA/w}$ (pH = 7.4) of perfluoroalkyl carboxylic acids (PFCAs, magenta circle), sulfonic acids (PFSAs, blue diamond), and average BSA binding of fluorotelomer alcohols (FTOHs, gold triangle). log $D_{BSA/w}$ of HFPO−DA (empty circle), 6:2 FTSA, and PFOSA (empty diamond) were excluded from the regression but plotted for comparison.

affect their binding constants (eqs 24 and 25). The relationship for PFSAs is missing because two values of log $D_{BSA/w}$ of PFHxS and PFOS are not enough to fit an exclusive line for PFSAs. However, as shown in Figure 3, values of log $D_{BSA/w}$ of PFHxS and PFOS overlapped with the regression of PFCAs. At high concentrations, hydrophobicity dominates the BSA binding of PFAS and the number of C−F has a more significant impact on the BSA binding than the functional groups of carboxylic and sulfonic acids. log $D_{BSA/w}$ (nonspecific) of HFPO−DA, 6:2 FTSA, and PFOSA are excluded from the regression since their structures are different from PFCAs and PFSAs

$$\text{PFCAs: } \log D_{BSA/w}(\text{nonspecific or average}) = 0.434 \times n - 0.743 \ (R^2 = 0.942) \quad (24)$$

$$\text{FTOHs: } \log D_{BSA/w}(\text{nonspecific or average}) = 1.01 \times n - 3.44 \ (R^2 = 0.999) \quad (25)$$

4.7. Prediction of Plasma Binding. Plasma binding of PFAS can be predicted by eq 23 by assuming that proteins and lipids in the plasma are the major sorption phases. Input parameters for the model are chemical properties ($D_{BSA/w}$, $D_{lip/w}$, and log $D_{oil/w}$, Table 2), as well as volume fractions of proteins and lipids in different types of plasmas (Table 3).

Experimental values of $D_{lip/w}$ and $D_{oil/w}$ of PFCAs, PFSAs, and FTOHs were from the literature[11,44,46] and are used to develop regression relationships of log $D_{lip/w}$ or log $D_{oil/w}$ against the number of C−F (Figure S10), which were further used to predict the log $D_{lip/w}$ for 6:2 FTSA, FTOSA (eq S12), as well as log $D_{lip/w}$ (eq S13) and log $D_{oil/w}$ (eq S14) for 10:2 FTOH. The log $D_{lip/w}$ of hexaflumuron and flubendiamide were predicted by COSMOtherm 2020[45] because of their very different structures. For the partially charged PFOSA, flubendamide, and hexaflumuron (>95% neutral), we used the ionization-corrected octanol−water partition constant predicted with ACD as a proxy of log $D_{oil/w}$. For the fully anionic PFAS, the partitioning to a neutral lipid was neglected.

The specific log $D_{plasma/w}$ at low concentrations were predicted with log $D_{BSA/w}$ (specific), and the nonspecific log $D_{plasma/w}$ at high concentrations were predicted with log $D_{BSA/w}$ (nonspecific or average). As shown in Figure 4, all of the predicted results were within a factor of 10 compared to the experimental ones for human and trout plasmas.

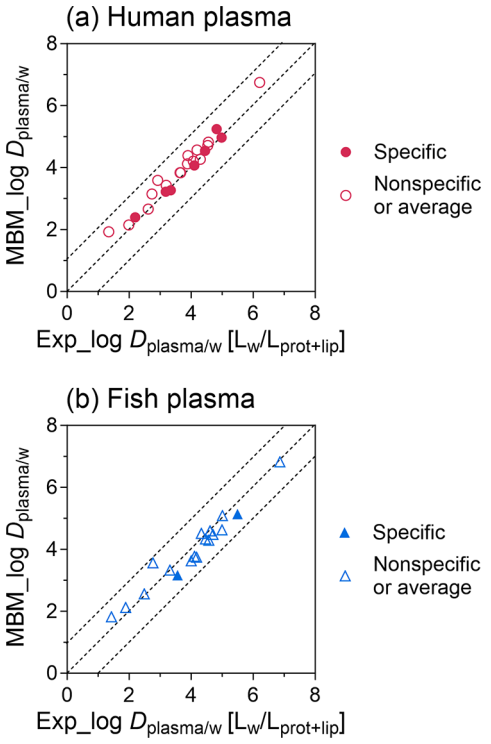

Figure 4. Prediction of plasma−water distribution ratios, log $D_{plasma/w}$ (pH = 7.4), of 16 PFAS. log $D_{plasma/w}$ of (a) human plasma or (b) trout plasma were measured experimentally (Exp) and compared with the $D_{plasma/w}$ predicted by a mass balance model (MBM) from protein binding constants, log $D_{BAS/w}$ (pH = 7.4) and lipid binding constants, log $D_{lip/w}$ and log $D_{oil/w}$, as well as the volume fractions of proteins and lipids in plasmas (eq 23).

5. DISCUSSION

5.1. Methods for Measuring BSA and Plasma Binding of PFAS. Serum albumin binding of PFAS has been measured by various methods in the past decades.[47] Specific binding of PFAS to defined binding sites on certain proteins was identified in competition assays by using site-specific probes[48] and probe-labeled proteins.[49] Here, we compared binding constants of 9 PFAS measured by traditional dialysis,[25,26] with the BSA binding isotherms measured in the present study (Figures 1 and S5). Literature data, which initially looked inconsistent, turned out to be located in different regions of the binding isotherms, reconciling results from different

https://doi.org/10.1021/acs.est.3c10824
Environ. Sci. Technol. XXXX, XXX, XXX−XXX

methods. The extensive binding isotherms derived in the present study depict a broader view of the binding behavior of these anionic PFAS.

The bound fraction affected the binding constants in this and previous studies.[24,25,27] However, under actual physiological concentration, the molar ratio of PFAS to protein is low, suggesting that more than 99% PFAS would be bound in 100% plasma.[28] It cannot be ruled out that the binding constants derived under the *in vitro* experimental conditions in the present study with a low plasma content may underestimate the bound fraction of some chemicals with very high affinities to proteins in the bloodstream *in vivo*. However, extrapolation from, e.g., 10% plasma should still be more accurate than measuring free concentrations at close to 100% bound fraction, which would be technically challenging to impossible.

Blood is a favorable matrix for an internal exposure assessment. Although plasma and serum are major fractions of the whole blood, the different components (e.g., blood cells, fibrinogen, platelet, and others) may affect the detected frequencies, concentrations, or distributions of PFAS.[50] High-purity serum albumin is used in most mechanistic binding studies, while we compared the binding isotherms of BSA and plasma in the present study in order to further demonstrate the binding behavior of PFAS in real life. Plasma contains most of the proteins and also other components of blood after the removal of cells and clotting factors. Although proteins dominate the specific binding of plasma, the role of nonspecific binding to lipids cannot be ignored, especially for plasma with high lipid fraction like trout plasma.

5.2. Implications of Plasma Binding of PFAS for Organ-Specific Accumulation. Plasma binding of PFAS is chain-length-dependent (Figure S9), and log $D_{plasma/w}$ > 4 were determined for PFOA, PFNA, PFUnA, PFHxS, and PFOS, indicating that they may accumulate in plasma and be transported in a bound form through the whole body. This can explain why middle- and long-chain PFAS were widely found in tissues and organs of humans,[3] trouts,[4] whales,[43] and finless porpoises.[51]

The binding of PFAS to plasma components is reversible, and the free PFAS in plasma may redistribute to tissues and organ-specific proteins.[11] The liver and brain have a higher metabolic demand and thus receive substantial blood flows. A competitive binding between human serum albumin and liver fatty acid-binding protein (hL-FABP) was found to correlate with the ratio of blood to liver concentration of PFAS.[52] Differences in lipid homeostasis perturbation between mice and humans may also be partially related to (dose-dependent) differences in binding affinity.[52]

PFAS also have high affinities to transthyretin,[53,54] which is primarily produced in the liver and also expressed in the choroid plexus of the brain.[55] Competitive binding of PFAS between plasma components and transthyretin might also lead to the selective accumulation of PFAS in the liver and the brain.

Protein binding does not only affect internal distribution but also affect toxicokinetics, in particular, the elimination kinetics and mechanism. Their persistence, together with the high affinity to proteins in general and specifically liver fatty acid-binding proteins in the liver, can lead to slower clearance and consequently long half-lives (>1 year) of PFAS.[56−58] Human urinary excretion was found to decrease with the chain length of PFCAs because only freely dissolved PFAS may be excreted via urine.[59] Long-chain PFCAs are strongly bound and can only be eliminated via the bile to feces.[59] With enterohepatic circulation and recycling of bile acids, PFCAs can also be reabsorbed back,[52,59,60] slowing the elimination rate. Furthermore, it needs to be considered that half-lives of PFAS also depend on the activity of renal transporters and therefore knowledge of plasma protein binding alone is not sufficient to correctly predict PFAS half-lives.[61]

Although the values of $D_{plasma/w}$ of FTOHs are noteworthy, especially 8:2 and 10:2 FTOH, their concentrations in human samples were very low or not detected[61] because FTOHs can be metabolized to PFCAs (e.g., PFHxA, PFHpA, PFOA, PFNA).[62,63]

5.3. Species Difference? Distributions of Protein and Lipid Binding in Plasma. Depending on their structure, PFAS have different affinities to proteins and lipids (Table 2), suggesting that predictive models for plasma binding need to consider the volume fractions of proteins and lipids in plasma. Han et al.[29] demonstrated that there was no difference between PFOA bound to rat or human serum protein by using ligand blotting. The differences between trout and human plasma of PFBA, PFHxA, PFHpA, PFOA, and PFHxS were obvious in the present study, and the different lipid contents of the two types of plasma are the main cause of the observed species difference, which was also confirmed by the MBMs.

Protein binding of PFAS dominated their binding in human plasma[64] but not in fish plasma.[65] PFBA, PFHxA, PFHpA, PFOA, and PFHxS are specifically bound to protein at low concentrations ($\nu < 1$), resulting in specific $D_{BSA/w}$ or $D_{plasma/w}$ almost 10 times higher than their $D_{lip/w}$. The volume fraction of lipids in the trout plasma was only half of that of the protein, which was similar to the values reported in a previous study[65] and decreased the contribution of the specific binding in trout plasma. In contrast to the anionic PFAS, lipid binding was more relevant than protein binding for the neutral FTOHs.

A recent study demonstrated that differences of albumin and globulin contents in human blood affected the free concentrations of PFAS across individuals.[58] Besides proteins, we also considered the distribution of PFAS to lipids in order to simulate actual plasma conditions. The $D_{plasma/w}$ measured in this study can be used in PBTK models to calculate the free PFAS in plasma. For risk assessment, it should also be considered that the amount of proteins and lipids in plasma is influenced by many factors, such as diet, environmental conditions, and health status, which exist not only between species but may also exist between individuals.

■ ASSOCIATED CONTENT

Supporting Information

The Supporting Information is available free of charge at https://pubs.acs.org/doi/10.1021/acs.est.3c10824.

Additional information on chemical structures; derivation of equations; experimental details; binding isotherms and binding constants; and linear relationship of binding constants against the number of perfluorinated carbons (PDF)

■ AUTHOR INFORMATION

Corresponding Author

Luise Henneberger − *Department of Cell Toxicology, UFZ—Helmholtz Centre for Environmental Research, 04318*

https://doi.org/10.1021/acs.est.3c10824
Environ. Sci. Technol. XXXX, XXX, XXX−XXX

Leipzig, Germany; orcid.org/0000-0002-3181-0044; Email: luise.henneberger@ufz.de

Authors

Weiping Qin − *Department of Cell Toxicology, UFZ—Helmholtz Centre for Environmental Research, 04318 Leipzig, Germany; Environmental Toxicology, Department of Geosciences, Eberhard Karls University Tübingen, DE-72076 Tübingen, Germany*

Beate I. Escher − *Department of Cell Toxicology, UFZ—Helmholtz Centre for Environmental Research, 04318 Leipzig, Germany; Environmental Toxicology, Department of Geosciences, Eberhard Karls University Tübingen, DE-72076 Tübingen, Germany;* orcid.org/0000-0002-5304-706X

Julia Huchthausen − *Department of Cell Toxicology, UFZ—Helmholtz Centre for Environmental Research, 04318 Leipzig, Germany; Environmental Toxicology, Department of Geosciences, Eberhard Karls University Tübingen, DE-72076 Tübingen, Germany;* orcid.org/0000-0003-4916-1174

Qiuguo Fu − *Department of Environmental Analytical Chemistry, UFZ—Helmholtz Centre for Environmental Research, 04318 Leipzig, Germany;* orcid.org/0000-0002-4227-5948

Complete contact information is available at: https://pubs.acs.org/10.1021/acs.est.3c10824

Funding

W.Q. received funding through the Chinese Scholarship Council. This study was supported by the Helmholtz Association under the recruiting initiative scheme, which was funded by the German Ministry of Education and Research and was conducted within the Helmholtz POF IV Topic 9 and the Integrated Project "Healthy Planet- towards a non-toxic environment".

Notes

The authors declare no competing financial interest.

■ ACKNOWLEDGMENTS

The authors gratefully acknowledge access to the platform CITEPro (Chemicals in the Environment Profiler) funded by the Helmholtz Association for chemical analysis and bioassay measurements. The authors thank Pavel Šauer from the University of South Bohemia in České Budějovice for kindly providing the trout plasma, Georg Braun for help with the LCMS measurement of HFPO−DA, Sandra Jäsch and Anne Röhrig for assistance with the headspace GCMS measurement of FTOHs, and Kai-Uwe Goss and Satoshi Endo for discussion about the partition constants of FTOHs. The authors also thank Juliane Glüge of ETH Zürich for the COSMOtherm prediction of the D_{lipw} of hexaflumuron and flubendiamide.

■ REFERENCES

(1) Jian, J. M.; Chen, D.; Han, F. J.; Guo, Y.; Zeng, L.; Lu, X.; Wang, F. A short review on human exposure to and tissue distribution of per- and polyfluoroalkyl substances (PFASs). *Sci. Total Environ.* **2018**, *636*, 1058−1069.

(2) Numata, J.; Kowalczyk, J.; Adolphs, J.; Ehlers, S.; Schafft, H.; Fuerst, P.; Muller-Graf, C.; Lahrssen-Wiederholt, M.; Greiner, M. Toxicokinetics of seven perfluoroalkyl sulfonic and carboxylic acids in pigs fed a contaminated diet. *J. Agric. Food Chem.* **2014**, *62* (28), 6861−6870.

(3) Pérez, F.; Nadal, M.; Navarro-Ortega, A.; Fabrega, F.; Domingo, J. L.; Barcelo, D.; Farre, M. Accumulation of perfluoroalkyl substances in human tissues. *Environ. Int.* **2013**, *59*, 354−362.

(4) Goeritz, I.; Falk, S.; Stahl, T.; Schafers, C.; Schlechtriem, C. Biomagnification and tissue distribution of perfluoroalkyl substances (PFASs) in market-size rainbow trout (Oncorhynchus mykiss). *Environ. Toxicol. Chem.* **2013**, *32* (9), 2078−2088.

(5) Jia, Y.; Zhu, Y.; Xu, D.; Feng, X.; Yu, X.; Shan, G.; Zhu, L. Insights into the Competitive Mechanisms of Per- and Polyfluoroalkyl Substances Partition in Liver and Blood. *Environ. Sci. Technol.* **2022**, *56* (10), 6192−6200.

(6) Baumert, B. O.; Fischer, F. C.; Nielsen, F.; Grandjean, P.; Bartell, S.; Stratakis, N.; Walker, D. I.; Valvi, D.; Kohli, R.; Inge, T.; et al. Paired Liver:Plasma PFAS Concentration Ratios from Adolescents in the Teen-LABS Study and Derivation of Empirical and Mass Balance Models to Predict and Explain Liver PFAS Accumulation. *Environ. Sci. Technol.* **2023**, *57* (40), 14817−14826.

(7) Di Nisio, A.; Pannella, M.; Vogiatzis, S.; Sut, S.; Dall'Acqua, S.; Rocca, M. S.; Antonini, A.; Porzionato, A.; De Caro, R.; Bortolozzi, M.; et al. Impairment of human dopaminergic neurons at different developmental stages by perfluoro-octanoic acid (PFOA) and differential human brain areas accumulation of perfluoroalkyl chemicals. *Environ. Int.* **2022**, *158*, No. 106982.

(8) Cao, Y.; Ng, C. Absorption, distribution, and toxicity of per- and polyfluoroalkyl substances (PFAS) in the brain: a review. *Environ. Sci.: Processes Impacts* **2021**, *23* (11), 1623−1640, DOI: 10.1039/D1EM00228G.

(9) Cai, D.; Li, Q. Q.; Chu, C.; Wang, S. Z.; Tang, Y. T.; Appleton, A. A.; Qiu, R. L.; Yang, B. Y.; Hu, L. W.; Dong, G. H.; Zeng, X. W. High trans-placental transfer of perfluoroalkyl substances alternatives in the matched maternal-cord blood serum: Evidence from a birth cohort study. *Sci. Total Environ.* **2020**, *705*, No. 135885.

(10) Hanssen, L.; Dudarev, A. A.; Huber, S.; Odland, J. O.; Nieboer, E.; Sandanger, T. M. Partition of perfluoroalkyl substances (PFASs) in whole blood and plasma, assessed in maternal and umbilical cord samples from inhabitants of arctic Russia and Uzbekistan. *Sci. Total Environ.* **2013**, *447*, 430−437.

(11) Ebert, A.; Allendorf, F.; Berger, U.; Goss, K. U.; Ulrich, N. Membrane/Water Partitioning and Permeabilities of Perfluoroalkyl Acids and Four of their Alternatives and the Effects on Toxicokinetic Behavior. *Environ. Sci. Technol.* **2020**, *54* (8), 5051−5061.

(12) Conder, J. M.; Hoke, R. A.; De Wolf, W.; Russell, M. H.; Buck, R. C. Are PFCAs bioaccumulative? A critical review and comparison with regulatory criteria and persistent lipophilic compounds. *Environ. Sci. Technol.* **2008**, *42* (4), 995−1003.

(13) Chou, W. C.; Lin, Z. Bayesian evaluation of a physiologically based pharmacokinetic (PBPK) model for perfluorooctane sulfonate (PFOS) to characterize the interspecies uncertainty between mice, rats, monkeys, and humans: Development and performance verification. *Environ. Int.* **2019**, *129*, 408−422.

(14) Richard, A. M.; Lougee, R.; Adams, M.; Hidle, H.; Yang, C.; Rathman, J.; Magdziarz, T.; Bienfait, B.; Williams, A. J.; Patlewicz, G. A New CSRML Structure-Based Fingerprint Method for Profiling and Categorizing Per- and Polyfluoroalkyl Substances (PFAS). *Chem. Res. Toxicol.* **2023**, *36* (3), 508−534.

(15) Qin, W.; Henneberger, L.; Huchthausen, J.; Konig, M.; Escher, B. I. Role of bioavailability and protein binding of four anionic perfluoroalkyl substances in cell-based bioassays for quantitative in vitro to in vivo extrapolations. *Environ. Int.* **2023**, *173*, No. 107857.

(16) Li, C.; Jiang, L.; Zhang, D.; Qi, Y.; Wang, X.; Jin, Y.; Liu, X.; Lin, Y.; Luo, J.; Xu, L.; et al. Human health risk assessment of 6:2 Cl-PFESA through quantitative in vitro to in vivo extrapolation by integrating cell-based assays, an epigenetic key event, and physiologically based pharmacokinetic modeling. *Environ. Int.* **2023**, *173*, No. 107846.

(17) Fragki, S.; Louisse, J.; Bokkers, B.; Luijten, M.; Peijnenburg, A.; Rijkers, D.; Piersma, A. H.; Zeilmaker, M. J. New approach methodologies: A quantitative in vitro to in vivo extrapolation case study with PFASs. *Food Chem. Toxicol.* **2023**, *172*, No. 113559.

(18) Loizou, G.; McNally, K.; Dorne, J. C. M.; Hogg, A. Derivation of a Human In Vivo Benchmark Dose for Perfluorooctanoic Acid From ToxCast In Vitro Concentration-Response Data Using a Computational Workflow for Probabilistic Quantitative In Vitro to In Vivo Extrapolation. *Front. Pharmacol.* **2021**, *12*, No. 630457.
(19) Fenton, S. E.; Ducatman, A.; Boobis, A.; DeWitt, J. C.; Lau, C.; Ng, C.; Smith, J. S.; Roberts, S. M. Per- and Polyfluoroalkyl Substance Toxicity and Human Health Review: Current State of Knowledge and Strategies for Informing Future Research. *Environ. Toxicol. Chem.* **2021**, *40* (3), 606−630.
(20) Zeng, Z.; Song, B.; Xiao, R.; Zeng, G.; Gong, J.; Chen, M.; Xu, P.; Zhang, P.; Shen, M.; Yi, H. Assessing the human health risks of perfluorooctane sulfonate by in vivo and in vitro studies. *Environ. Int.* **2019**, *126*, 598−610.
(21) Abraham, K.; Mielke, H.; Fromme, H.; Volkel, W.; Menzel, J.; Peiser, M.; Zepp, F.; Willich, S. N.; Weikert, C. Internal exposure to perfluoroalkyl substances (PFASs) and biological markers in 101 healthy 1-year-old children: associations between levels of perfluorooctanoic acid (PFOA) and vaccine response. *Arch. Toxicol.* **2020**, *94* (6), 2131−2147.
(22) Zhang, H.; Shen, L.; Fang, W.; Zhang, X.; Zhong, Y. Perfluorooctanoic acid-induced immunotoxicity via NF-kappa B pathway in zebrafish (Danio rerio) kidney. *Fish Shellfish Immunol.* **2021**, *113*, 9−19, DOI: 10.1016/j.fsi.2021.03.004.
(23) Ehrlich, V.; Bil, W.; Vandebriel, R.; Granum, B.; Luijten, M.; Lindeman, B.; Grandjean, P.; Kaiser, A. M.; Hauzenberger, I.; Hartmann, C.; et al. Consideration of pathways for immunotoxicity of per- and polyfluoroalkyl substances (PFAS). *Environ. Health* **2023**, *22* (1), 19.
(24) Alesio, J. L.; Slitt, A.; Bothun, G. D. Critical new insights into the binding of poly- and perfluoroalkyl substances (PFAS) to albumin protein. *Chemosphere* **2022**, *287*, No. 131979.
(25) Allendorf, F.; Berger, U.; Goss, K. U.; Ulrich, N. Partition coefficients of four perfluoroalkyl acid alternatives between bovine serum albumin (BSA) and water in comparison to ten classical perfluoroalkyl acids. *Environ. Sci. Process Impacts* **2019**, *21* (11), 1852−1863.
(26) Xia, X.; Rabearisoa, A. H.; Jiang, X.; Dai, Z. Bioaccumulation of perfluoroalkyl substances by Daphnia magna in water with different types and concentrations of protein. *Environ. Sci. Technol.* **2013**, *47* (19), 10955−10963.
(27) Bischel, H. N.; Macmanus-Spencer, L. A.; Zhang, C.; Luthy, R. G. Strong associations of short-chain perfluoroalkyl acids with serum albumin and investigation of binding mechanisms. *Environ. Toxicol. Chem.* **2011**, *30* (11), 2423−2430.
(28) Bischel, H. N.; Macmanus-Spencer, L. A.; Luthy, R. G. Noncovalent interactions of long-chain perfluoroalkyl acids with serum albumin. *Environ. Sci. Technol.* **2010**, *44* (13), 5263−5269.
(29) Han, X.; Snow, T. A.; Kemper, R. A.; Jepson, G. W. Binding of perfluorooctanoic acid to rat and human plasma proteins. *Chem. Res. Toxicol.* **2003**, *16* (6), 775−781.
(30) Henneberger, L.; Muhlenbrink, M.; Fischer, F. C.; Escher, B. I. C18-Coated Solid-Phase Microextraction Fibers for the Quantification of Partitioning of Organic Acids to Proteins, Lipids, and Cells. *Chem. Res. Toxicol.* **2019**, *32* (1), 168−178.
(31) Roy, K. S.; Nazdrajic, E.; Shimelis, O. I.; Ross, M. J.; Chen, Y.; Cramer, H.; Pawliszyn, J. Optimizing a High-Throughput Solid-Phase Microextraction System to Determine the Plasma Protein Binding of Drugs in Human Plasma. *Anal. Chem.* **2021**, *93* (32), 11061−11065.
(32) Huchthausen, J.; Escher, B. I.; Grasse, N.; Konig, M.; Beil, S.; Henneberger, L. Reactivity of Acrylamides Causes Cytotoxicity and Activates Oxidative Stress Response. *Chem. Res. Toxicol.* **2023**, *36* (8), 1374−1385.
(33) Fischer, F. C.; Henneberger, L.; König, M.; Bittermann, K.; Linden, L.; Goss, K. U.; Escher, B. I. Modeling Exposure in the Tox21 in Vitro Bioassays. *Chem. Res. Toxicol.* **2017**, *30* (5), 1197−1208.
(34) Yasuda, M. Dissociation Constants of Some Carboxylic Acids in Mixed Aqueous Solvents. *Bull. Chem. Soc. Jpn.* **1959**, *32* (5), 429−432.
(35) Shedlovsky, T. The Behaviour of Carboxylic Acids in Mixed Solvents. In *Electrolytes*; Pesce, B., Ed.; Pergamon Press, 1962; pp 146−151.
(36) Allen, R. I.; Box, K. J.; Comer, J. E. A.; Peake, C.; Tam, K. Y. Multiwavelength spectrophotometric determination of acid dissociation constants of ionizable drugs. *J. Pharm. Biomed. Anal.* **1998**, *17* (4), 699−712.
(37) Niu, L.; Henneberger, L.; Huchthausen, J.; Krauss, M.; Ogefere, A.; Escher, B. I. pH-Dependent Partitioning of Ionizable Organic Chemicals between the Silicone Polymer Polydimethylsiloxane (PDMS) and Water. *ACS Environ. Au* **2022**, *2* (3), 253−262.
(38) Goss, K. U.; Bronner, G.; Harner, T.; Hertel, M.; Schmidt, T. C. The partition behavior of fluorotelomer alcohols and olefins. *Environ. Sci. Technol.* **2006**, *40* (11), 3572−3577.
(39) Arp, H. P. H.; Niederer, C.; Goss, K. U. Predicting the partitioning behavior of various highly fluorinated compounds. *Environ. Sci. Technol.* **2006**, *40* (23), 7298−7304.
(40) Geisler, A.; Endo, S.; Goss, K. U. Partitioning of polar and nonpolar neutral organic chemicals into human and cow milk. *Environ. Int.* **2011**, *37* (7), 1253−1258.
(41) Firl, N.; Kienberger, H.; Hauser, T.; Rychlik, M. Determination of the fatty acid profile of neutral lipids, free fatty acids and phospholipids in human plasma. *Clin. Chem. Lab. Med.* **2013**, *51* (4), 799−810, DOI: 10.1515/cclm-2012-0203.
(42) Poulin, P.; Theil, F. P. Prediction of pharmacokinetics prior to in vivo studies. 1. Mechanism-based prediction of volume of distribution. *J. Pharm. Sci.* **2002**, *91* (1), 129−156.
(43) Dassuncao, C.; Pickard, H.; Pfohl, M.; Tokranov, A. K.; Li, M.; Mikkelsen, B.; Slitt, A.; Sunderland, E. M. Phospholipid Levels Predict the Tissue Distribution of Poly- and Perfluoroalkyl Substances in a Marine Mammal. *Environ. Sci. Technol. Lett.* **2019**, *6* (3), 119−125.
(44) Droge, S. T. J. Membrane-Water Partition Coefficients to Aid Risk Assessment of Perfluoroalkyl Anions and Alkyl Sulfates. *Environ. Sci. Technol.* **2019**, *53* (2), 760−770.
(45) Glüge, J.; Scheringer, M. Evaluation of Physicochemical Property Data in the ECHA Database. *J. Phys. Chem. Ref. Data* **2023**, *52* (4), 043101 DOI: 10.1063/5.0153030.
(46) Endo, S.; Goss, K. U. Predicting partition coefficients of Polyfluorinated and organosilicon compounds using polyparameter linear free energy relationships (PP-LFERs). *Environ. Sci. Technol.* **2014**, *48* (5), 2776−2784.
(47) Liu, X.; Fang, M.; Xu, F.; Chen, D. Characterization of the binding of per- and poly-fluorinated substances to proteins: A methodological review. *TrAC, Trends Anal. Chem.* **2019**, *116*, 177−185, DOI: 10.1016/j.trac.2019.05.017.
(48) Chen, Y. M.; Guo, L. H. Fluorescence study on site-specific binding of perfluoroalkyl acids to human serum albumin. *Arch. Toxicol.* **2009**, *83* (3), 255−261.
(49) Shao, X.; Ji, F.; Wang, Y.; Zhu, L.; Zhang, Z.; Du, X.; Chung, A. C. K.; Hong, Y.; Zhao, Q.; Cai, Z. Integrative Chemical Proteomics-Metabolomics Approach Reveals Acaca/Acacb as Direct Molecular Targets of PFOA. *Anal. Chem.* **2018**, *90* (18), 11092−11098.
(50) Poothong, S.; Thomsen, C.; Padilla-Sanchez, J. A.; Papadopoulou, E.; Haug, L. S. Distribution of Novel and Well-Known Poly- and Perfluoroalkyl Substances (PFASs) in Human Serum, Plasma, and Whole Blood. *Environ. Sci. Technol.* **2017**, *51* (22), 13388−13396.
(51) Zhang, B.; He, Y.; Yang, G.; Chen, B.; Yao, Y.; Sun, H.; Kannan, K.; Zhang, T. Legacy and Emerging Poly- and Perfluoroalkyl Substances in Finless Porpoises from East China Sea: Temporal Trends and Tissue-Specific Accumulation. *Environ. Sci. Technol.* **2022**, *56* (10), 6113−6122.
(52) Fragki, S.; Dirven, H.; Fletcher, T.; Grasl-Kraupp, B.; Bjerve Gutzkow, K.; Hoogenboom, R.; Kersten, S.; Lindeman, B.; Louisse, J.; Peijnenburg, A.; et al. Systemic PFOS and PFOA exposure and disturbed lipid homeostasis in humans: what do we know and what not? *Crit. Rev. Toxicol.* **2021**, *51* (2), 141−164.
(53) Ren, X. M.; Qin, W. P.; Cao, L. Y.; Zhang, J.; Yang, Y.; Wan, B.; Guo, L. H. Binding interactions of perfluoroalkyl substances with

https://doi.org/10.1021/acs.est.3c10824
Environ. Sci. Technol. XXXX, XXX, XXX−XXX

thyroid hormone transport proteins and potential toxicological implications. *Toxicology* **2016**, *366*−*367*, 32−42.
(54) Weiss, J. M.; Andersson, P. L.; Lamoree, M. H.; Leonards, P. E.; van Leeuwen, S. P.; Hamers, T. Competitive binding of poly- and perfluorinated compounds to the thyroid hormone transport protein transthyretin. *Toxicol. Sci.* **2009**, *109* (2), 206−216.
(55) Gião, T.; Saavedra, J.; Cotrina, E.; Quintana, J.; Llop, J.; Arsequell, G.; Cardoso, I. Undiscovered Roles for Transthyretin: From a Transporter Protein to a New Therapeutic Target for Alzheimer's Disease. *Int. J. Mol. Sci.* **2020**, *21* (6), 2075 DOI: 10.3390/ijms21062075.
(56) Drew, R.; Hagen, T. G.; Champness, D.; Sellier, A. Half-lives of several polyfluoroalkyl substances (PFAS) in cattle serum and tissues. *Food Addit. Contam.: Part A* **2022**, *39* (2), 320−340, DOI: 10.1080/19440049.2021.1991004.
(57) Rosato, I.; Bonato, T.; Fletcher, T.; Batzella, E.; Canova, C. Estimation of per- and polyfluoroalkyl substances (PFAS) half-lives in human studies: a systematic review and meta-analysis. *Environ. Res.* **2024**, *242*, No. 117743.
(58) Fischer, F. C.; Ludtke, S.; Thackray, C.; Pickard, H. M.; Haque, F.; Dassuncao, C.; Endo, S.; Schaider, L.; Sunderland, E. M. Binding of Per- and Polyfluoroalkyl Substances (PFAS) to Serum Proteins: Implications for Toxicokinetics in Humans. *Environ. Sci. Technol.* **2024**, *58* (2), 1055−1063.
(59) Fujii, Y.; Niisoe, T.; Harada, K. H.; Uemoto, S.; Ogura, Y.; Takenaka, K.; Koizumi, A. Toxicokinetics of perfluoroalkyl carboxylic acids with different carbon chain lengths in mice and humans. *J. Occup. Health* **2015**, *57* (1), 1−12. (acccessed 2024/05/02)
(60) Loccisano, A. E.; Campbell, J. L., Jr.; Andersen, M. E.; Clewell, H. J., 3 Evaluation and prediction of pharmacokinetics of PFOA and PFOS in the monkey and human using a PBPK model. *Regul. Toxicol. Pharmacol.* **2011**, *59* (1), 157−175, DOI: 10.1016/j.yrtph.2010.12.004.
(61) Jin, H.; Mao, L.; Xie, J.; Zhao, M.; Bai, X.; Wen, J.; Shen, T.; Wu, P. Poly- and perfluoroalkyl substance concentrations in human breast milk and their associations with postnatal infant growth. *Sci. Total Environ.* **2020**, *713*, No. 136417.
(62) Chen, D.; Zhao, Y.; Xu, W.; Pan, Y.; Wei, Q.; Xie, S. Biotransformation and tissue bioaccumulation of 8:2 fluorotelomer alcohol in broiler by oral exposure. *Environ. Pollut.* **2020**, *267*, No. 115611.
(63) Kabadi, S. V.; Fisher, J.; Aungst, J.; Rice, P. Internal exposure-based pharmacokinetic evaluation of potential for biopersistence of 6:2 fluorotelomer alcohol (FTOH) and its metabolites. *Food Chem. Toxicol.* **2018**, *112*, 375−382.
(64) Henneberger, L.; Kluver, N.; Muhlenbrink, M.; Escher, B. Trout and Human Plasma Protein Binding of Selected Pharmaceuticals Informs the Fish Plasma Model. *Environ. Toxicol. Chem.* **2022**, *41* (3), 559−568.
(65) Escher, B. I.; Cowan-Ellsberry, C. E.; Dyer, S.; Embry, M. R.; Erhardt, S.; Halder, M.; Kwon, J. H.; Johanning, K.; Oosterwijk, M. T.; Rutishauser, S.; et al. Protein and lipid binding parameters in rainbow trout (Oncorhynchus mykiss) blood and liver fractions to extrapolate from an in vitro metabolic degradation assay to in vivo bioaccumulation potential of hydrophobic organic chemicals. *Chem. Res. Toxicol.* **2011**, *24* (7), 1134−1143.

https://doi.org/10.1021/acs.est.3c10824
Environ. Sci. Technol. XXXX, XXX, XXX−XXX